Mobility and Separation of Knotted Polymers

Elena Boniolo

H. H. Wills Physics Laboratory
University of Bristol

A thesis submitted to the University of Bristol in
accordance with the requirements of the degree of
Ph.D. in the Faculty of Science

School of Physics, March 2020

Word count: 52600

Abstract

Knotting happens naturally in biological polymers, such as proteins and DNA, and plays a role in the basic mechanisms of cell functioning and replicating.

For this reason, recently there has been increasing interest in studying knots in long macromolecules and in understanding the role of topology in their behaviour.

One interesting problem is how to separate molecules according to their knot type, all the other characteristics being the same.

Inspired by the widely-used laboratory tool, agarose-gel electrophoresis, I present a minimal model of knotted macromolecular chains moving through a suspension and the results of simulations performed with my own code. I show that with a medium of small spheres at the vertices of a regular lattice, the topology has an effect on the rate of diffusion. Specifically, in the absence of a driving force more complex knots tend to move more slowly than simpler knots, while the opposite happens in the presence of a sufficiently strong field.

Additionally, I present a more biologically-oriented system, with longer molecules modelled after DNA, moving in a suspension of random spheres of comparable size to the radius of gyration of the chains, and I show the results of simulations performed with the molecular-dynamics program LAMMPS. I show that in the presence of a driving force and if the suspension spheres are in random motion, the rate of mobility increases linearly with the complexity of the knot.

Finally, I explore the possibility of phase separating a binary mixture of molecules according to their knot type. With the simulations performed so far, it has not been possible to show any evidence of phase separation, but the results can be used to establish limits on the parameters of the problem, and I have made some suggestions about possible future research in this area.

Acknowledgements

I would like to start by thanking the two most important people who have guided and helped me in my work: my supervisors Simon Hanna and Annela Seddon. Thank you for all your advice and support throughout the years.

I would also like to thank my former supervisor and lead of the SPOCK (Scientific Properties of Complex Knots) group in Bristol Mark Dennis for his guidance and endless enthusiasm, as well as the Leverhulme Trust for funding this PhD (Research Programme Grant No. RP2013-K-009).

I am grateful to all the SPOCK group and theory group for advice and fruitful discussion during these PhD years, in particular Michael Berry, Martin Gradhand, Alexander Taylor and David Foster. I would also like to thank Stu Whittington from the University of Toronto, for his kindness and for our chats about knots.

It was great to meet and work alongside my PhD colleagues: Teuntje Tijssen, Danica Sugic, Benjamin Bode, Keith Alexander, Alexander Houston, Lauren Scanlon, and our visiting colleague from China, Xi Peng. Thanks for being there!

A very special thanks is due to Davide Michieletto from the University of Edinburgh, for his priceless help with the work presented in Chapter 4 and Chapter 5 of this thesis. In particular, the idea and starting point of the simulations in Chapter 5 came from him. If it were possible, I would build you a statue in Bristol city centre.

Other people who were important to my life at the University of Bristol through these years have been Emma Creasey, Walther Schwarzacher, Briony Spraggon, Paddy Royall and Massimo Antognozzi. Thank you for your support and encouragement.

Last but not least among my colleagues, I want to thank the ACRC (Advanced Computing Research Centre) group of the University, especially Christopher Edsall, for their very beneficial guidance in all things computational.

Among family and friends, I want to thank my parents for encouraging me to start this PhD, and my friends Floss and Alex, Becci, Gareth and William, Gabri and Davide, Raffaella, John, and all of Martin's family for encouraging me to

stay with it.

Finally, big thanks goes to Martin himself, for putting up with my more stressful moments and, in general, for keeping me alive and fed in these last few difficult months.

I cannot finish without thanking my cutest little friend: Cotton the hamster, full-time Provider of Cuddles. I'll pay you back with a life-long supply of peanuts.

This thesis was written in LaTeX, with pictures created or adapted by means of the software programs gnuplot, VMD, POV-Ray and the Gimp. All calculations not included in my own programs were implemented in gnuplot. The simulations were performed by means of the computational facilities of the Advanced Computing Research Centre of the University of Bristol.

Author's Declaration

I declare that the work in this dissertation was carried out in accordance with the requirements of the University's *Regulations and Code of Practice for Research Degree Programmes* and that it has not been submitted for any other academic award. Except where indicated by specific reference in the text, the work is the candidate's own work. Work done in collaboration with, or with the assistance of, others, is indicated as such. Any views expressed in the dissertation are those of the author.

SIGNED: Elena Boniolo DATE: 29/09/2020

Contents

List of Tables

List of Figures

Acronyms

ACN Average Crossing Number
AFM Atomic Force Microscopy
BD Brownian Dynamics
DNA Deoxyribonucleic acid
LAMMPS Large-scale Atomic/Molecular Massively Parallel Simulator
MCN Minimal Crossing Number
MD Molecular Dynamics
MSD Mean Square Displacement
NVE fixed Number, Volume, Energy
NVT fixed Number, Volume, Temperature
NPT fixed Number, Pressure, Temperature
NPH fixed Number, Pressure, Enthalpy
RMS Root Mean Square (displacement)
SEM Scanning Electron Microscopy
SONO ShrinkOnNoOverlaps
VMD Visual Molecular Dynamics

1 Introduction and background

1.1 Introduction

Knots and links have been part of the human culture for millennia. They have various important practical purposes, sailors and fishermen's knots being among the most famous examples, but they can also have a decorative function, like in Chinese or Celtic artwork, or a symbolic connotation, such as the endless knot in Buddhism or the Borromean rings, a widespread-through-the-ages representation of strength in unity.

Knotting also happens naturally in long biological polymers, and has been found both in proteins and DNA, which are at the very foundation of all living cells. This is easily understandable, as we can see knotting happen commonly in everyday life when long threads are involved, for example, when we leave earphones in a pocket for some time. Rigorous studies have shown that knotting occurs in long ball chains when shaken (Hickford et al., 2006), and the probability of knot formation in polymers increases with length until the chance for a very long polymer not to be knotted becomes exponentially small (Orlandini and Whittington, 2007). It is no wonder, then, if the approximately two metres of DNA present in a human diploid cell, confined to a nucleus only a few micron wide (Alberts et al., 2002), are normally in a knotted state. And no wonder the cell has evolved specific enzymes able to disentangle DNA, when it is needed for replication (see below Section 1.4.2). Not all knotting is disadvantageous, though, as it may facilitate ejection of viral DNA into the host or play an important role in the function of a protein (Section 1.4.1). Either way, knots are present and abundant in the basic components of life, and the living cell is able to deal with them and even take advantage from them.

For this reason, in recent years there has been increasing interest in studying

how knotting affects the properties of long polymers. Among the many possible questions, there is the problem of being able to separate and distinguish between the different knots present in a biological sample. In the case of circular DNA, a very wide-spread method to separate knots in molecules of the same molecular weight is by electrophoresis in agarose gels (Section 1.5). While this is now a very reliable tool and the experimental results are straightforward to interpret, the intrinsic, microscopic mechanisms underlying this process are still unclear, as it becomes apparent when the parameters used in the experiments are non-standard (Section 1.5.1).

In this context, modelling a possible structure for the gel matrix and testing specific assumptions *in silico* is proving very effective in helping understand the physical problem (Section 1.7). The purpose of this thesis will be to give a contribution to this research and test the effect of a suspension, modelled in as simple a way as possible, on the mobility of knotted chains. In addition, preliminary tests will be presented on the possible phase separation of molecules due to their different knotted topologies.

1.2 Some knot concepts

While the first analytical studies of knots date back to Alexandre-Théophile Vandermonde (Vandermonde, 1771) and Johann Carl Friedrich Gauss (see Bühler (2012)), the real momentum started in the second half of the 19$^{\text{th}}$ century, when Lord Kelvin theorised that atoms were knots in the fabric of what was then believed to be the substrate permeating all space, ether, and Peter Guthrie Tait painstakingly created the first table of the simplest knots. It was suggested that studying the different kinds of knots would mean understanding the physical properties of the elements.

Kelvin's theory of atoms as knots in the ether was subsequently proven to be incorrect, and even ether was shown not to exist, but by then knot theory had been born.

1.2.1 Classical knot theory

Knot theory is the mathematical field that deals with the classification and properties of knots. From the mathematical point of view, a *knot* is defined as a closed, non-self intersecting curve embedded in three dimensions which cannot be unravelled to form a simple loop (that is, the *unknot*).

In this sense, a typical everyday knot, such as those we all commonly tie in our shoe laces, is not a knot according to the mathematical meaning. Any open curve can be untangled, easily or not, and, topologically, it is not possible to consider it a knot. Moreover, knots that may appear different at a first examination, may actually be topologically the same knot, as two knots are topologically equivalent if they can be transformed into each other by deforming the thread without cutting it.

Knots, as defined, are exclusively three-dimensional objects. No crossing is obviously possible in two dimensions, and all knots can be untangled in four or higher dimensions, by having the strands pass each other in the fourth direction. Nonetheless, it is possible and convenient to represent them with two-dimensional diagrams as long as at each crossing it is made clear whether a strand passes over or under the other. Any such representation is called a *projection* of the knot.

There may be many (infinitely so) projections of the same knot (Fig. 1.1). The minimal number of crossings that is possible to count in the simplest projection(s) of a knot is called the *Minimal Crossing Number (*MCN) and it is an invariant of the knot. Except for the simplest knots, the trefoil and the figure-of-eight, more than one topologically distinct knot exists for each minimal crossing number. For this reason, traditionally, each knot is designated by the minimal crossing number and a subscript indicating its conventional position in the knot table. Therefore, for example, the three six-crossing knots are denoted by 6_1, 6_2 and 6_3.

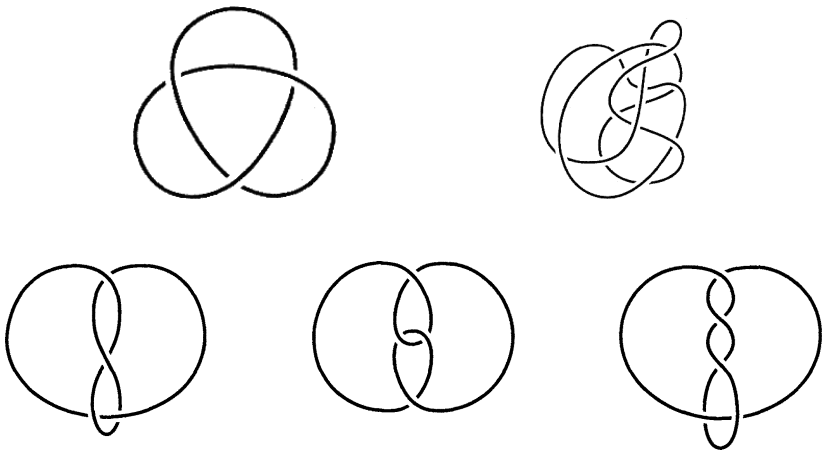

Figure 1.1: Projections of simple knots. Top: a standard and a non-standard diagram for the trefoil knot (3_1). Bottom: three different diagrams for the figure-of-eight knot (4_1). Pictures from Adams (1994).

In order to decide if two projections represent the same knot or two topologically different objects, it is possible to rearrange the strands in space as long as they are not allowed to pass through each other. Some of these rearrangements will not change the relations between the crossings in a two-dimensional projection, while some will. Three ways to change such relations which do not however change the topology of the original knot are the Reidermeister moves, which are illustrated in Fig. 1.2.

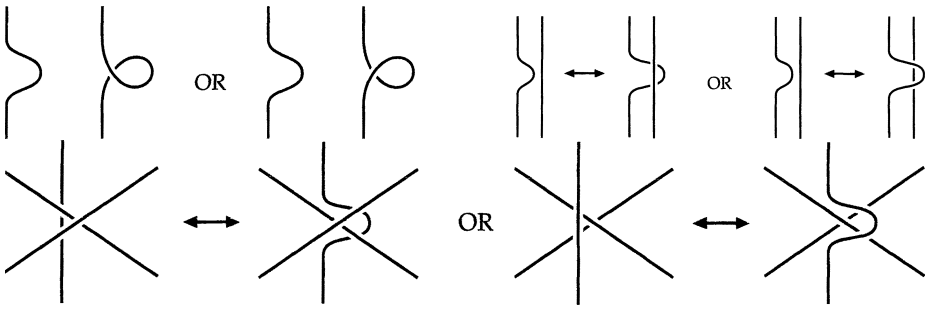

Figure 1.2: Reidermeister moves. Top left: Type-I Reidemeister move, addition or removal of a twist. This removes a crossing, but leaves the knot type unchanged. Top right: Type-II Reidemeister move, addition or removal of two crossings. These moves correspond to sliding a bend in a strand away from another strand in the same area of the projection, or vice-versa, to move it over or under another strand. Bottom: Type-III Reidemeister move, shifting of a strand from one side to the other of a crossing. All these moves change the number of crossing in a projection, but, at a further look, do not change the 3D relations between the strands of the knot. Pictures from Adams (1994).

When the knot is too complex to be recognised visually, other mathematical invariants than the MCN can be computed from a projection in order to have a polynomial formula of the knot. Among such polynomials, there are the Alexander, Jones and HOMFLY polynomials, the first one being at the moment the most widely used for its simplicity in computational terms. Unfortunately, no complete invariant has been found yet, that is, no unique quantity able to distinguish the specific knot, but a combination of invariants can be used in ambiguous cases.

Knot theory is now highly developed, and knots have been classified according to many characteristics. Among these characteristics, some knots may have a specific chirality, or we can distinguish composite knots, if they are the composition of two or more non-trivial knots, from prime knots, if they are not.

An important class of knots are *torus knots*, that is those which lie on the surface of an (unknotted) torus. These have particular mathematical properties

and, as we will see in Section 2.6.1, a three-dimensional representation can be easily generated through parametric equations.

In this thesis, only prime knots up to minimal crossing number nine will be considered, and no distinction will be made between a knot and its mirror image. In fact, the interest will be mainly on the effects of knotting on the geometry, especially size and shape, of ring polymers, while any mathematical property not relevant to the point at issue will be neglected.

For more information about knot theory in general and knot invariants, see for example Adams (1994) and Sossinsky (2002). A method to practically compute the Alexander polynomial can be found in Orlandini and Whittington (2007).

1.2.2 Ideal knots and Average Crossing Number

The historical classification of knots through the minimal crossing number and their position on the knot table corresponds to the mathematical (topological) fact that all configurations of a certain mathematical knot are equivalent as long as they can be deformed into each other without strand crossing. The particular geometry of a knot does not play a role and is not taken into consideration in the classic knot table, where knots with the same minimal crossing number are ordered according to when they were added to the table rather than to any physical or mathematical property.

More recently, a different approach has been suggested that focuses on some physical characteristics of particular configurations of knots (Katritch et al., 1996). This different point of view does not change the type of available knots and, for example, a trefoil will still be a trefoil and will be different from a cinquefoil, but every knot will be classified according to particular quantities related to a specific geometric configuration.

This specific geometric configuration is called the *ideal form* and corresponds to the shape having the highest ratio of volume to surface area. This is independent of the particular scale considered and can be quantified through the length-to-diameter ratio: if we consider a piece of string with a fixed-diameter cross section, the ideal configuration for a particular knot type will be the one that minimises the length, that is, the *tightest* possible knot. Different types of knot will require different lengths to be tied, with more complex knots requiring longer lengths. Or equivalently, for a given length, more complex knots will

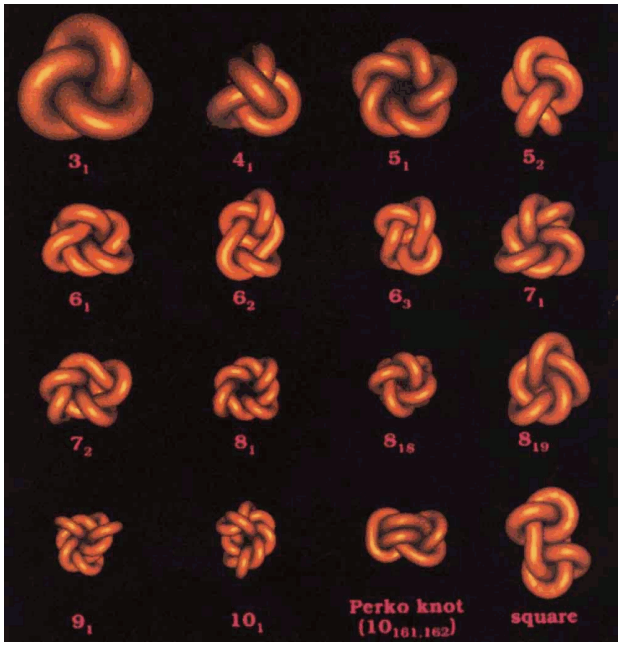

Figure 1.3: Examples of ideal geometrical representations of knots. As the total length of the rope is the same for all the shapes, the overall dimensions decrease with the complexity of the knot (From Katritch et al. (1996)).

have to be represented by thinner tubes. Ideal configurations of some simple knots can be seen in Fig. 1.3.

A new interesting quantity can also be calculated from these ideal forms. This is the *Average Crossing Number (*ACN) of the ideal representation of a knot. In the same way as the minimal crossing number is defined as the number of crossings in the simplest possible two-dimensional representation of the knot (Section 1.2.1), the average crossing number is defined as the average number of crossings over all the possible projections. That is, the average is taken over all the directions from which the knot can be looked at. This is therefore a real number rather than an integer like the MCN. Different knots that have the same minimal crossing number, such as the three six-crossing knots for example, will have different ACNs which will depend on the particular shape of the ideal forms of the corresponding topology and which can be used to distinguish between the different topologies.

Finding the ideal conformation of a knot is not a straightforward mathematical problem. Instead, it relies on simulating the tightening of a rope until no shorter configuration is possible, while ensuring that this minimum is global and not a local one. The values of the ACN used in this thesis were taken from

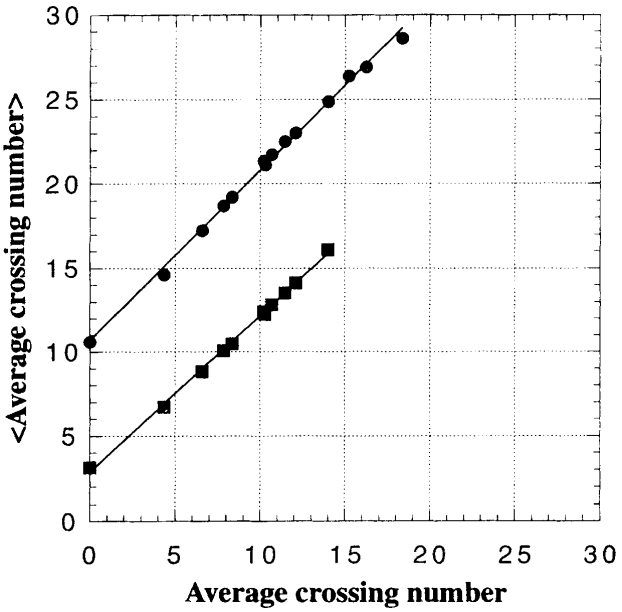

Figure 1.4: Relation between ACNs of ideal configurations and the mean of the ACNs of simulated knotted DNA chains distorted by thermal motion. On the x axis we have the ACN of the ideal configurationsn of some of the simplest knots, as calculated from the configurations obtained with the SONO algorithm. On the y axis, $\langle$ Average crossing number $\rangle$ indicates the mean of the ACN of ensembles of simulated configurations of knotted DNA molecules. Filled squares: 1800 base pairs; filled circles: 5400 base pairs (from Katritch et al. (1996)).

those obtained with the ShrinkOnNoOverlaps (SONO) algorithm (Pierański, 1998) and published in Stasiak et al. (1998).

Average crossing number of ideal representations and real-life molecules

An interesting characteristic of the ACN of ideal representations is its relevance to real-life knotted molecules. In fact, computer simulations have shown that the ACNs calculated for same-length loosely-knotted polymers in thermal motion in a good solvent are linearly dependent on the ACNs of the ideal representations. In addition, although longer chains have more random crossings than shorter ones, the slope of the correlation is close to 1 regardless of the length of the considered polymers (Fig. 1.4).

The value of the ACN is linked to the compactness of the knots and it is inversely proportional to the radius of gyration (Piili et al., 2013). For this reason, knots with the same minimal crossing number can have very different average crossing numbers. For example, the 8_{19} knot has a very compact configuration

and its ACN is more similar to the 7_1 than the 8_1.

1.3 Basic concepts of polymer physics

Before discussing the phenomenology of knots in biological polymers, a short review is presented about some basic results of polymer physics which are relevant to all polymers and which will inform the design of the simulations and the discussion of the results presented in this thesis.

A polymer is a long molecule constituted of a great number of elementary units, called monomers, joined together by chemical bonds. They can occur naturally, like rubber, or be synthesised artificially. Polymers are found in every living cell, as biological macromolecules like proteins or DNA belong to this category.

This brief introduction will be limited to linear polymers, as these are ultimately the type which form closed loops when knotted. Also, in this thesis, the focus will be mainly on on the dynamics of single chains in suspensions. Therefore, it will be possible to neglect the interactions between various molecules in a polymer material. The only exception will be the system examined in Chap. 5, which will be treated separately in the relative chapter.

1.3.1 Isolated polymer molecules

Ideal chains

The simplest model for a polymer is that of an *ideal chain*. In an ideal chain we assume that the interactions between different sections of the molecule are either negligible or extend only to a limited distance along the chain.

If we consider the end-to-end vector $\mathbf{R}$, that is, the vector joining one end of a linear chain to the other, this quantity can be considered as a measure of the size of the polymer. If the chain is ideal and there is no correlation between the directions of the different segments $\mathbf{r_n}$, it can be shown (Doi, 1996) that on average the end-to-end distance is the same as a random walk:

$$\langle \mathbf{R}^2 \rangle = \sum_{n=1}^{N} \langle \mathbf{r_n}^2 \rangle = Nb^2, \tag{1.1}$$

where N is the number of bonds and b is the length of a bond.

This equation shows that for this model, the size of a polymer is proportional to $N^{1/2}$.

If interactions are present, but limited to a short distance, the same equation holds, with the provision that b represents an effective bond length b_{eff} which depends on the interactions.

This model can be made more complex by adding energy terms linked to the angles between the bonds. If these terms are absent, the chain is said to be *freely jointed*, otherwise if a determined angle between the segments is favoured due to the specific chemical bond, the chain is said to be *freely rotating*. Finally, if an energy term associated with torsional angles is present, a hindered-rotation model needs to be applied.

In particular, freely-rotating chains are characterised by a quantity called the *persistence length*, which quantifies its bending stiffness. The persistence length is the range over which the directions of the bonds lose all correlation and can be considered independent. In the case of double-stranded DNA, for example, such length has been measured to be approximately 50 nm.

Radius of gyration

Another commonly-used measure for the size of a polymer is the *radius of gyration*, R_G (Doi, 1996):

$$R_G^2 := \frac{1}{2N^2}\sum_{n=1}^{N}\sum_{m=1}^{N}\langle(\mathbf{R}_n - \mathbf{R}_m)^2\rangle = \frac{1}{N}\sum_{n=1}^{N}\langle(\mathbf{R}_n - \mathbf{R}_{CM})^2\rangle \tag{1.2}$$

where $\mathbf{R}_{CM}$ are the coordinates of the center of mass.

This is a more convenient quantity than the end-to-end-vector length, as it can be calculated for any kind of polymer, not necessarily linear, and it can be measured directly in experiments.

For an ideal chain, the radius of gyration is directly linked to the end-to-end-vector length by the relation $R_G^2 = \frac{1}{6}\langle\mathbf{R}^2\rangle$.

Real chains

Ideal chains are allowed to bend back onto themselves, and two strands can in theory occupy the same point in space. Real chains have a volume associated with each segments which prevent them from overlapping. This volume is called the *excluded volume*, and forces the chain to move like a self-avoiding walk, rather than a simple random walk. As a consequence, the whole chain will occupy a bigger volume in space than the corresponding ideal chain. It can be

shown (Doi, 1996) that in this case the radius of gyration is of the order

$$R_G \approx N^{\nu} b \tag{1.3}$$

where the exponent ν has been found in simulations to be $\nu \approx 0.588$, which also corresponds to the value calculated theoretically (Flory, 1953; De Gennes, 1979).

1.3.2 Diffusion of polymers in diluted solutions

A particle in a solvent is subject to a Brownian force due the constant bombardment from the particles of the solvent. The resulting motion of the particle follows Einstein's diffusion equation (Einstein, 1905):

$$\frac{\partial}{\partial t} P(x,t) = \frac{\partial^2}{\partial x^2} P(x,t), \tag{1.4}$$

whose solution in one dimension is a Gaussian PDF:

$$P(x,t) = \frac{1}{\sqrt{4\pi D t}} e^{-\frac{x^2}{4Dt}}, \tag{1.5}$$

from which:

$$\langle x^2(t) \rangle = \int_{-\infty}^{\infty} x^2 P(x,t) \mathrm{d}x = 2Dt, \tag{1.6}$$

D being the *diffusion coefficient.*

In n dimensions, this becomes

$$\langle x^2(t) \rangle = 2nDt. \tag{1.7}$$

If we want this to be a physical model, the probability distribution has to be equal to the equilibrium Boltzmann distribution. This is achieved if the diffusion coefficient D obeys the Einstein relation (Doi, 1996):

$$D = \frac{k_B T}{\zeta}, \tag{1.8}$$

where ζ is an "inverse mobility", $\zeta = \frac{1}{\mu}$.

1.3.3 Anomalous diffusion

When the motion is no longer Brownian, due for example to the presence of a turbulent flow (Richardson, 1926) or of different particles in the medium, Eq. 1.7 is no longer valid, and it is replaced by a power law:

$$\text{MSD} = \langle x^2(t) \rangle \simeq D_\alpha t^\alpha, \tag{1.9}$$

with α the anomalous-diffusion exponent and D_α the generalised diffusion coefficient.

In regimes where $0 < \alpha < 1$, we talk about *subdiffusion*. On the contrary, when $\alpha > 1$ the system is undergoing *superdiffusion*. The three types of diffusion are shown in Fig. 1.5.

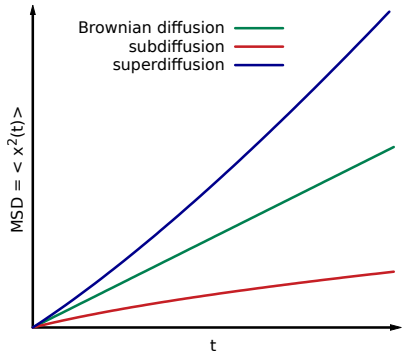

Figure 1.5: Mean squared displacement $\langle x^2(t) \rangle$ for different types of diffusion. Brownian diffusion: $\langle x^2(t) \rangle \propto Dt$. Superdiffusion: $\langle x^2(t) \rangle \propto t^\alpha$, $\alpha > 1$. Subdiffusion: $\langle x^2(t) \rangle \propto t^\alpha$, $\alpha < 1$.

Subdiffusion is common in crowded environments (Weiss et al., 2004; Sokolov, 2012), while superdiffusion has been observed for example in the atmosphere (Richardson, 1926), in the internal environment of the cell, where we can have facilitated diffusion (Campagnola et al., 2015; Reverey et al., 2015; Samanta and Thirumalai, 2019), or with particles moving through hydrogels (Castiglione et al., 2019).

Subdiffusion can depend on the time scale considered, and it may appear only as a transient condition before the behaviour becomes diffusive (Ernst et al., 2017; Berezhkovskii et al., 2014).

1.3.4 Diffusion with an applied field

When diffusion takes place in the presence of an applied field, the resulting velocity in the direction parallel to the field will depend on the characteristics of the fluid and the shape of the particle, as well as the strength of the field. If we define the *Reynolds number* (Sommerfeld, 1909) as the ratio of inertial forces to viscous forces a particle is subjected to in a fluid flow, in the limit

of low Reynolds number (that is, for small particles), and in the presence of a driving force F, a particle of mass m is subject to an acceleration a and, due to the presence of the viscous fluid, will reach a terminal velocity v_t in the direction of the field:

$$v_t = s\,a = s\,\frac{F}{m}, \tag{1.10}$$

where s is the *sedimentation coefficient* of the particle.

As seen in Section 1.3.2, the diffusion coefficient can be written as $D = \frac{k_B T}{\zeta} = k_B T \cdot \mu$ (Eq. 1.8). In the presence of a driving force, the mobility μ represents the ratio between the terminal velocity v_t and the force F applied to the particle in the fluid:

$$D = k_B T \mu = k_B T \frac{v_t}{F}, \tag{1.11}$$

which means that the sedimentation coefficient s and the diffusion constant D are linearly proportional:

$$s = m\frac{v_t}{F} = m\frac{D}{k_B T}. \tag{1.12}$$

In this thesis, either quantity will be used as a measure of the mobility of a particle or molecule.

Typically, the applied field may be gravity, a centrifugal force, or, in the case of electrophoresis (as we will see below in Section 1.5), an electric-potential difference.

1.4 Knots in biology

Knots are present in many biological systems, among which those of greater practical interest at this moment are biopolymers like DNA and proteins.

The study of knots and the mechanisms by which the cell deals with them has become increasingly important over the last decades, as knotted proteins important in bio-medicine have been discovered, such as the ubiquitin hydrolase UCH-L1, related to Parkinson's disease (Das et al., 2006), which contains very complex knots. In addition to this, the comprehension of how the two families of topoisomerase enzymes (see Section 1.4.2) function has led to the development of new drugs capable of interfering with this mechanism, so hindering the replication of bacteria and cancerous cells (Froelich-Ammon and Osheroff, 1995; Deweese and Osheroff, 2009; Levine et al., 1998; Tse-Dinh, 2007).

1.4.1 Knots in proteins

As noted, in some instances proteins have been found to be knotted. Indeed, after translation, proteins must fold into a 3D structure in order to be able to perform their tasks, and according to a recent study (Sułkowska et al., 2012), about 1 percent of proteins in the Protein Data Bank (PDB), show the presence of knots or slipknots in the polypeptide backbone. The most frequent knot is the trefoil, but also figure-of-eight, cinquefoil and Stevedore's (6_1) knots have been observed.

However, knots in proteins seem to appear much less frequently than it would be expected from random polymers with similar characteristics, and this can be explained by the fact that knotted structures are subject to more kinetic difficulties and for this reason they are an evolutionary disadvantage which has in part been eliminated over time.

For this reason, when a knot is indeed present in a protein, this disadvantage is likely to be balanced by some kind of functional advantage for the cell. This is confirmed by an analysis of the protein structures in the PDB (Sułkowska et al., 2012), which shows that the same knotting patterns appear in several different protein families that play similar roles in the activity of the cell, although their sequences differ considerably.

It has been proposed that knots may provide a stabilising function, and the same can be said about slipknots, as protein subchains surround other subchains (Sułkowska et al. (2008); Sayre et al. (2011); Virnau et al. (2006)).

Research is very active on this front. However, in this thesis the focus will be mainly on knotted polymer systems similar to DNA moving in gels, which will be given more coverage in the rest of this chapter, while other kinds of molecules like proteins will not be considered further.

1.4.2 Structure and topology of DNA

An extensive overview of DNA topology can be found in Buck (2009), which will be followed in the next paragraphs. Also, an interesting historical account (in French) appears in Weber (1995).

DNA (Deoxyribonucleic Acid) is the molecule that contains the information required to build a new living organism.

The primary structure of DNA consists of pairs of units called *nucleotides*, each consisting of a phosphate group and a sugar, to which one of four bases

(Adenine, Thymine, Guanine or Cytosine) is linked. These nucleotides form a ladder, where the bases occupy the interior and are linked to each other in fixed couples (A with T, and G with C) through hydrogen bonds.

This ladder has a natural twist and chemical orientation due to the different links formed by the sugar with the adjacent phosphates. This "double helix" represents the secondary structure of the molecule. Schematic representations of the primary and secondary structures of DNA are shown in Fig. 1.6.

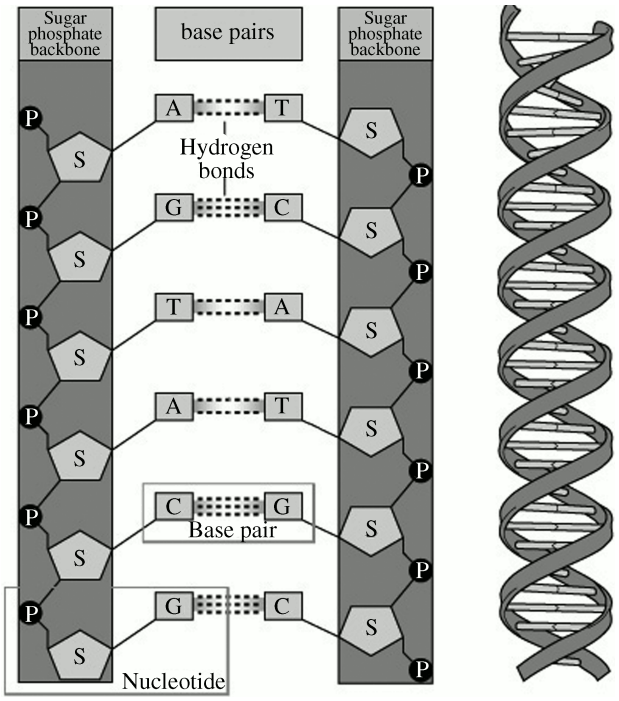

Figure 1.6: Primary and secondary structure of DNA. (Image from Buck (2009))

The tertiary structure consists in the coiling of the axis of the molecule in space (Shure and Vinograd, 1976). This "supercoiled DNA" is the native state in almost all cells (Cozzarelli et al., 1990) because it has important consequences: it compactifies the molecule, it makes it easier to access the base pairs and to separate the two strands when necessary, and it has energetic implications for the chemical reactions within the cell. A schematic representation of the tertiary structure of DNA and the formation of supercoiling is shown in Fig. 1.7.

The DNA axis is often linear, but it may also be circular, and, in this case, can show the presence of knots and links (the latter known as *catenanes*, in biological literature).

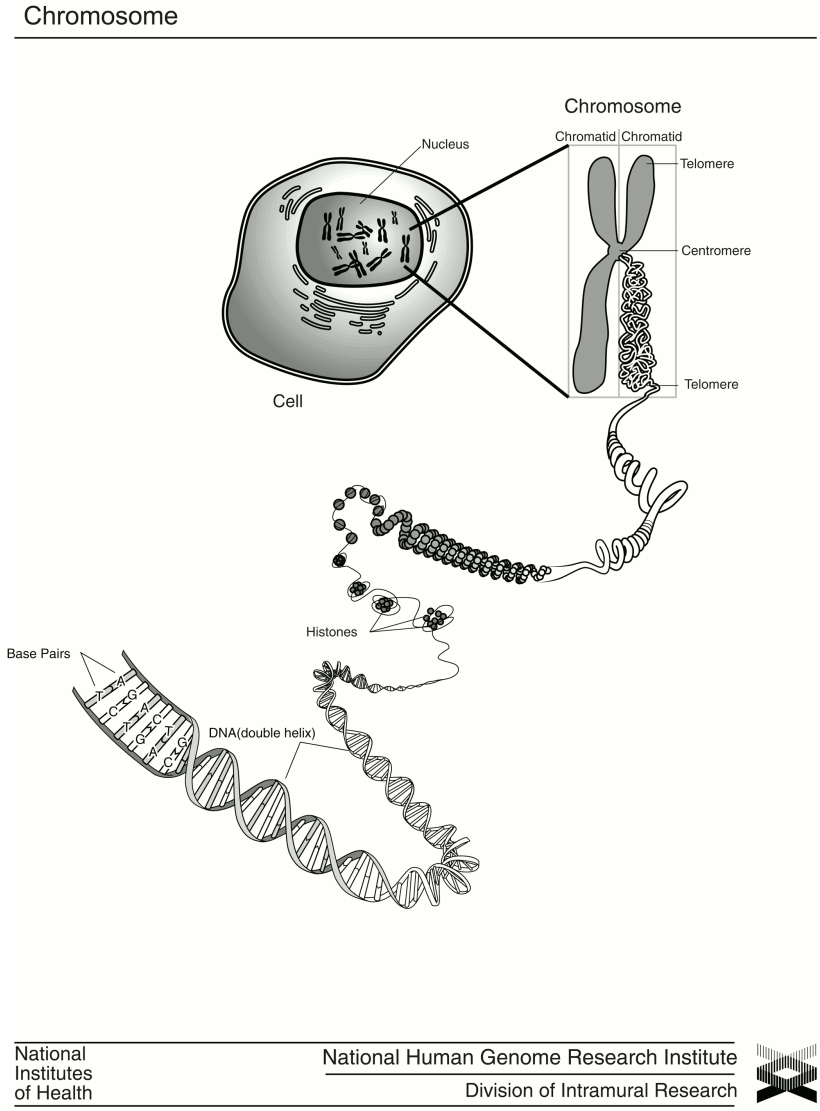

Figure 1.7: Compactifying and tertiary structure of DNA, which shows the formation of supercoiling. Image by National Human Genome Research Institute, from Buck (2009).

Since the past century, the combined efforts of mathematicians and biologists have led to many important outcomes, such as, for example, the Călugăreanu-White-Fuller theorem, which links topology and geometry in DNA molecules, seen as topological ribbons (Călugăreanu, 1961; White, 1969; Fuller, 1971).

For the purpose of this thesis only the type of knot present in a molecule, and only prime knots, will be considered. Links, supercoiled molecules, composite

knots, or twist and writhe will not be examined. It is important, however, to acknowledge that this is a very active field where research is prolific and ongoing.

How the cell deals with knots in DNA

Two DNA molecules that have the same sequence of bases but different linking numbers are called *topoisomers*. One topoisomer can be converted into another by the action of enzymes called *topoisomerases*, which are classified in two types according to their topological effects.

Type-I topoisomerases cleave a single strand of DNA so it can pass through the other strand, and then rejoin it. The effect of this process is to relax supercoils.

Type-II topoisomerases cleave both strands allowing them to pass through another segment of DNA, and then rejoin them. The primary effect is to change (usually simplify) the knot or link type of the molecule, but some can change the number of supercoils as well.

Both types are found in every cell and are essential to its life, in particular when the helix has to be opened during cellular replication. In addition, these enzymes can be mixed with DNA molecules *in vitro* in order to generate knotted molecules to be used in laboratory experiments.

Another mechanism through which the topology of DNA can be changed is called *site-specific recombination*. Actually, the main result of this process is to change the DNA sequence by deleting, inverting or inserting fragments of DNA, but these reactions can give rise to a change in the knot or link type as a by-product. The kinds of knots and links that can occur in this case can be predicted by a topological model developed by Buck and Flapan (2007).

Role of knotting in viral DNA ejection

Knotting of DNA does not necessary have a harmful effect on the activity of biological organisms. On the contrary, DNA densely packed in the capsids of bacteriophages, a kind of viruses that infect bacteria, has been shown to be naturally knotted, and it has been suggested that the resulting spatial structure, which is similar to a spool, facilitates the quick ejection of viral DNA into the cytosol of the host. In fact, knots in phages have been among the first to ever be isolated (Liu et al., 1981b,a).

Computer simulations suggest that due to the high density, DNA is able to reach an ordered configuration in which the topology, and in particular cholesteric interactions, knotting and twisting, play a fundamental role in determining how fast the ejection can happen (Spakowitz and Wang, 2005; Rollins et al., 2008; Marenduzzo et al., 2009, 2013).

By taking advantage of the tendency of phage DNA to form knots when restricted to the small space of a capsid, it is also possible to artificially produce knotted DNA to be used in subsequent laboratory studies. In fact, the molecules obtained by cosmid circularisation after forcing the DNA into phage capsids are knotted with high probability and show the presence of knots of various types (Trigueros and Roca, 2007).

1.4.3 Experimental resolution of knots in DNA

Traditionally, there are two main ways to determine experimentally the kind of knots featured in DNA: *agarose gel electrophoresis* and *Scanning Electron Microscopy* (SEM) imaging.

The first method is the most widespread in biological laboratories, and will be very important in this thesis. This procedure will be described below in Section 1.5, but, as a brief introduction, it consists in pipetting the DNA into one end of a slab of agarose gel placed in an aqueous bath through which an electric current is run. As DNA is negatively charged, it will migrate towards the positive end of the gel, with velocity proportional to the compactness of the molecule and so to the minimal crossing number of the knot. This will result in a separation of the knots in a series of bands; however, it is not sufficient to identify a particular knot among all the others with the same MCN.

The SEM method, on the contrary, is very reliable on this distinction, as it gives clear images of the knot (Liu et al. (1981b,a); Wasserman et al. (1985)). However, it is a very complex procedure and the molecule needs to be coated with the protein RecA before it can be observed. For this reason it is often used in conjunction with gel electrophoresis in order to select and reduce the number of molecules to observe.

More recently, a third method, *Atomic Force Microscopy* (AFM) has been applied to the distinction of knots in DNA (Valle et al., 2005). This procedure allows the examination of the molecules in an aqueous medium, and has the advantage of permitting the operator to interact with the sample and verify directly whether a strand is passing over or under another strand. However,

this still requires expensive equipment and, unlike gel electrophoresis, can only examine one molecule at a time.

Examples of images obtained with scanning electron microscopy and atomic-force microscopy are shown in Fig. 1.8.

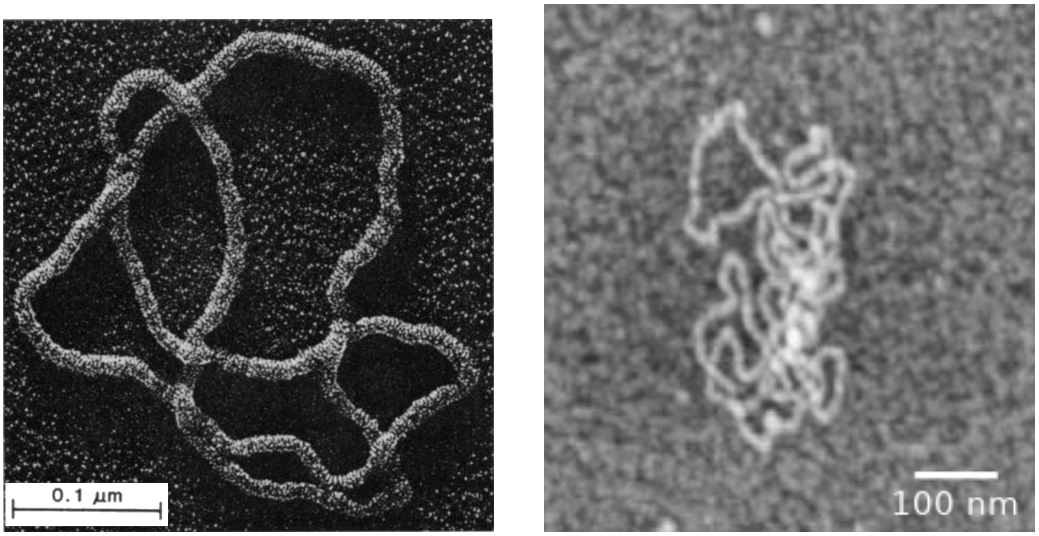

Figure 1.8: Imaging of knotted DNA. Left: electron micrograph of six-noded knot (from Wasserman et al. (1985)). Right: atomic-force microscopy image of DNA knots adsorbed onto AP-mica (from Valle et al. (2005)).

1.5 Agarose-gel electrophoresis

Electrophoresis is the process of applying an electric field at the two ends of a sample in order to separate the particles present in the sample, typically proteins or nucleic acids, with respect to their electrical-charge density, their size and their conformation. The addition of a solid support in the form of a gel slab increases the effects of size and shape in the separation (Serwer, 1983). Many materials can be used to form the gel, for example starch (Smithies, 1955) or polyacrylamide (Alberts et al., 2002), but, as explained below, the most commonly-used with DNA molecules is agarose gel.

Nucleic acids can be stained with ethidium bromide, which makes them fluorescent under UV light and more easily visualised. The sample is then inserted in a well in the gel slab, and the electric field is applied, forcing the motion of charged molecules through the gel. In this way, the sample is separated into bands according to the different kinds of molecules present (Fig.1.9). After a

given time (depending on the system), the slab is removed and the position and composition of the bands can be examined.

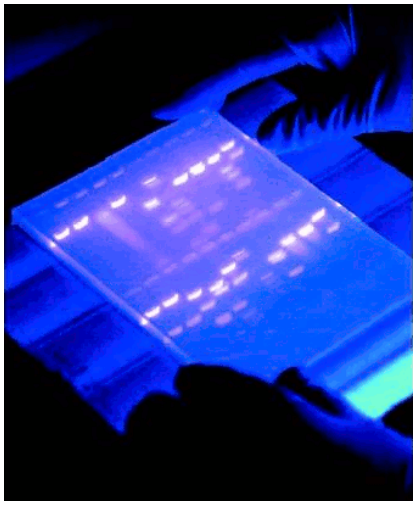

Figure 1.9: An electrophoresis gel (image from the website www.biologyreference.com).

Electrophoresis is usually performed in direct current, but reversing pulses are also possible and can be useful to suppress trapping of larger molecules (Levene and Zimm, 1987; Turmel et al., 1990). In this thesis, when electrophoresis is mentioned, it will be assumed to be in direct current.

Agarose gel

An agarose is a polysaccharide polymer material, generally extracted from seaweed. It is dissolved at the required concentration in a buffer, and cast in the shape of a slab. When it cools down it forms a three-dimensional matrix made of helical agarose molecules in supercoiled bundles that are aggregated into three-dimensional structures. This matrix has channels and pores through which biomolecules can pass. We can roughly picture this structure as a sponge. Although clear images of this structure in aqueous solution are difficult to obtain, some images in liquid water have been taken through AFM (Pernodet et al., 1997; Maaloum et al., 1998), while a graphical representation and a picture of dried agarose are shown in Fig. 1.10.

The higher the concentration of agarose, the smaller the pores. For example, the pore size of a 3% gel has been estimated to be around 300 nm (Pernodet et al., 1997).

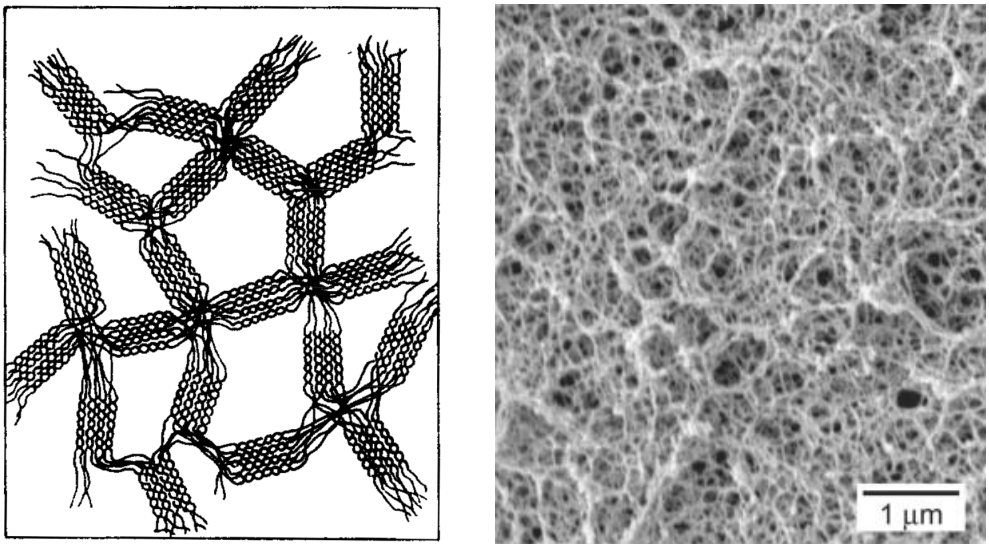

Figure 1.10: The structure of agarose gel. Left: schematic representation of the agarose-gel network (from Arnott et al. (1974)). Right: SEM image of dried agarose gel (from Wang et al. (2007)).

Gels as weak as 0.15% concentration can be used to form slabs for electrophoresis and their low cost and ease of use currently make them the preferred choice for the separation of particles of dimensions larger than 5–10 nm (Serwer, 1983). For this reason, agarose gels are often the choice in the case of DNA and larger protein molecules. However, electrophoresis of DNA can be also performed in other media, such as uncross-linked polymer solutions (Barron et al., 1993) or synthetic lattices microlithographically constructed as a 2D array of posts (Volkmuth and Austin, 1992; Volkmuth et al., 1994). A review of the effects of matrices of different nature on DNA electrophoretic mobility can be found in Stellwagen and Stellwagen (2009).

1.5.1 Two-dimensional agarose-gel electrophoresis

The size resolution that is possible to obtain depends strongly on the pore size of the matrix. In fact, different gel concentrations and different voltages allow us to fine-tune the separation of the different kind of molecules. Roughly speaking, lower concentrations mean bigger pore size and allow the motion of larger (or less compact) fragments, but at the same time reduce separation of smaller molecules, while higher concentrations stop bigger molecules altogether, but increase resolution of smaller (or more compact) fragments. For this reason, in order to have good resolution for both small and large fragments, it is possible

to run electrophoresis in two separated steps, the first with a low-concentration gel and the second with a high-concentration gel and electric field applied in the orthogonal direction. This results in increased sensitivity, and spots clearly separated in the gel. It is also possible to vary the voltage between the two steps and analyse the dependence on that parameter.

1.6 Separation of knotted DNA molecules through agarose-gel electrophoresis

Agarose-gel electrophoresis has been used for decades to separate DNA molecules by size or conformation. It would not be possible to separate DNA through electrophoresis by sedimentation in a simple solution, due to the fact that the charge associated to a piece of DNA is proportional to its size. Since the rate of migration through the medium is directly proportional to charge and inversely proportional to size, the two effects balance each other. The presence of some kind of matrix is therefore necessary for separation (Urbach and Waring, 2005). This has been confirmed experimentally for DNA of a wide range of molecular weights (Olivera et al., 1964).

Various experimental and theoretical studies have focused on the separation of linear or circular DNA molecules (among others, Lumpkin and Zimm (1982); Lumpkin et al. (1985); Noolandi et al. (1987); Deutsch (1988); Cole and Åkerman (2003)).

Similarly, agarose-gel electrophoresis has also a long history of being used to separate knotted DNA molecules according to their topology. Among the first to do so, Dean et al. (1985) showed that DNA knots produced by Escherichia coli Topoisomerase I would separate into bands according to knot type, with more complex knots travelling further than simpler knots in the gel (Fig. 1.11). The molecules in the samples were analysed through electron microscopy in order to determine the knot type.

Stasiak et al. (1996) and Vologodskii et al. (1998) analysed experimental data from Kanaar et al. (1990) and Crisona et al. (1994), the former, and Crisona et al. (1994) again the latter, to show how the displacement was linearly dependent on the average crossing number of the ideal representation of the knots (as defined above in Section 1.2.2). A schematic representation of this behaviour can be seen in Fig. 1.12.

The reason for this behaviour is commonly attributed to the fact that the

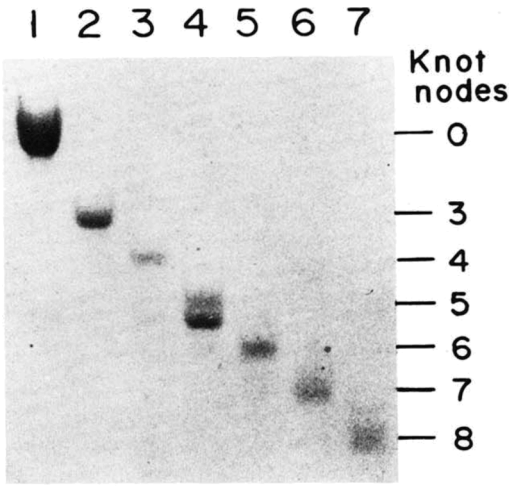

Figure 1.11: Electrophoresis of purified knots in E. coli DNA. The crossing number indicated on the right was assigned via electron microscopy (from Dean et al. (1985)).

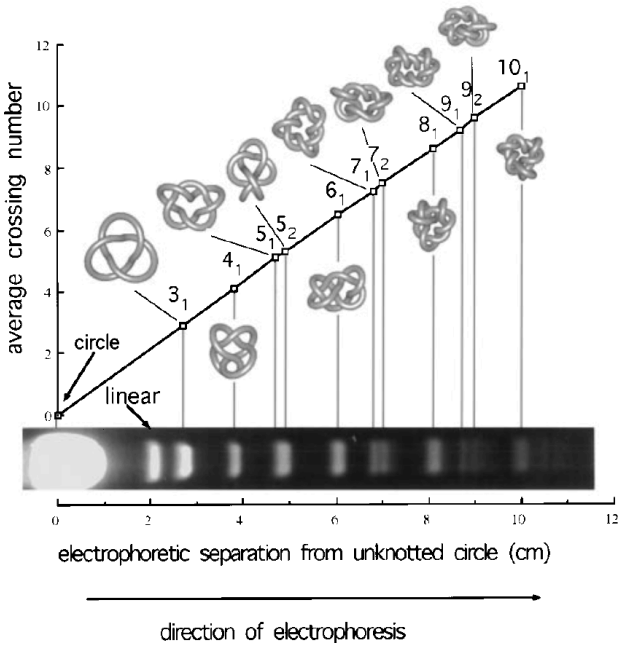

Figure 1.12: Agarose-gel electrophoresis of knotted DNA. Linear relationship between mobility and ACN (From Vologodskii et al. (1998), with experimental data from Crisona et al. (1994)).

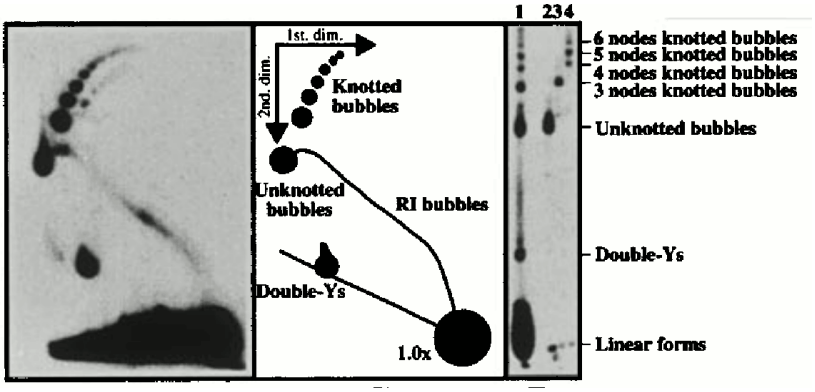

Figure 1.13: Two-dimensional electrophoresis of knotted replication bubbles of pHH5.8 plasmids (From Sogo et al. (1999)).

compactness of the molecules increases linearly with the complexity of the knot, as quantified by the average crossing number (see also below Section 1.7.1).

1.6.1 Two-dimensional agarose-gel electrophoresis of knotted DNA molecules

Depending on the gel electrophoresis parameters, it is possible to see different behaviours of the diffusion of differently-knotted molecules.

Inversion of the mobility

During DNA replication, the two strands of the molecule must unwind and separate so that the sequence can be copied. This open region of DNA where replication occurs is called a *replication bubble*. In an article from 1999, Sogo et al. (Sogo et al., 1999) characterised the knots formed *in vivo* in partially replicated DNA molecules in bacterial plasmids. They both separated the knotted replication bubbles via two-dimensional agarose-gel electrophoresis and analysed the topology in the different bubbles by electron microscopy of Rec-A-coated molecules.

The electrophoresis is performed at 1 V/cm in the first dimension, and at 5 V/cm in the second (Weber et al., 2006). In Fig. 1.13 it is possible to see that at the lower voltage more complex knots travel a longer distance than simpler knots, while the opposite is true for the higher voltage.

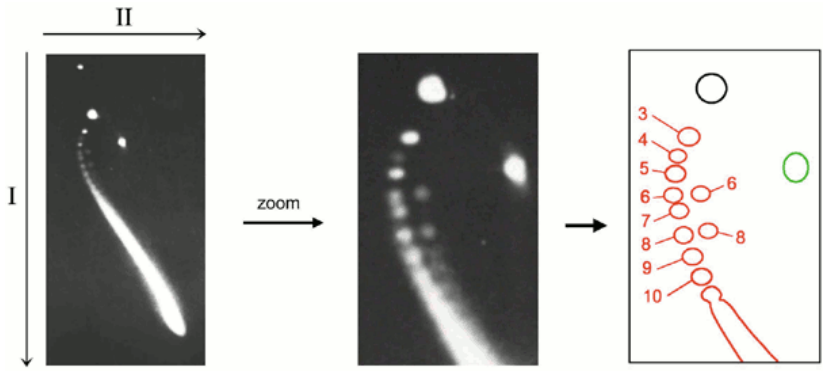

Figure 1.14: Two-dimensional electrophoresis of knotted P4 phage DNA. Left: the full sample results; center: magnification of the area containing the first simplest knots; right: identification of the topology in the different populations – knotted molecules in red, linear molecules in green and unknotted molecules in black (From Trigueros et al. (2001)).

More complex behaviour: arc pattern

Along similar lines, in more recent years other experiments with different values of the electrophoretic parameters were performed in order to better determine the unusual behaviour of knotted DNA molecules.

Among these, Trigueros et al. (2001) showed an interesting non-monotonic pattern in the distribution of the knotted molecules after 2D electrophoresis. The DNA used had been isolated from bacteriophage P4 capsids. These molecules are convenient because they are known to present various types of knots and they do not present supercoiling as they are not covalently closed. The electrophoresis was performed in 0.4% agarose gel at 0.8 V/cm in the first direction and 3.4 V/cm in the second and the results are shown in Fig. 1.14. In the first dimension at lower voltage, more complex knots travel faster than simpler knots as is expected due to their smaller size (Section 1.6). However, in the second direction at higher voltages, some simpler knots travel faster than other slightly more complex ones, giving rise to a characteristic arc pattern where the six-crossing knot appears to move more slowly than any other knot type. The explanation proposed by the authors attributes this behaviour to the reduced flexibility of knotted molecules, which would take longer to change shape and adapt to the pore size of the gel.

A similar arc pattern was also found by Cebrián et al. (2015) in both knotted molecules and catenanes. They used Escherichia Coli plasmid DNA prepared in samples containing various knot and link types, nicked to release any torsional

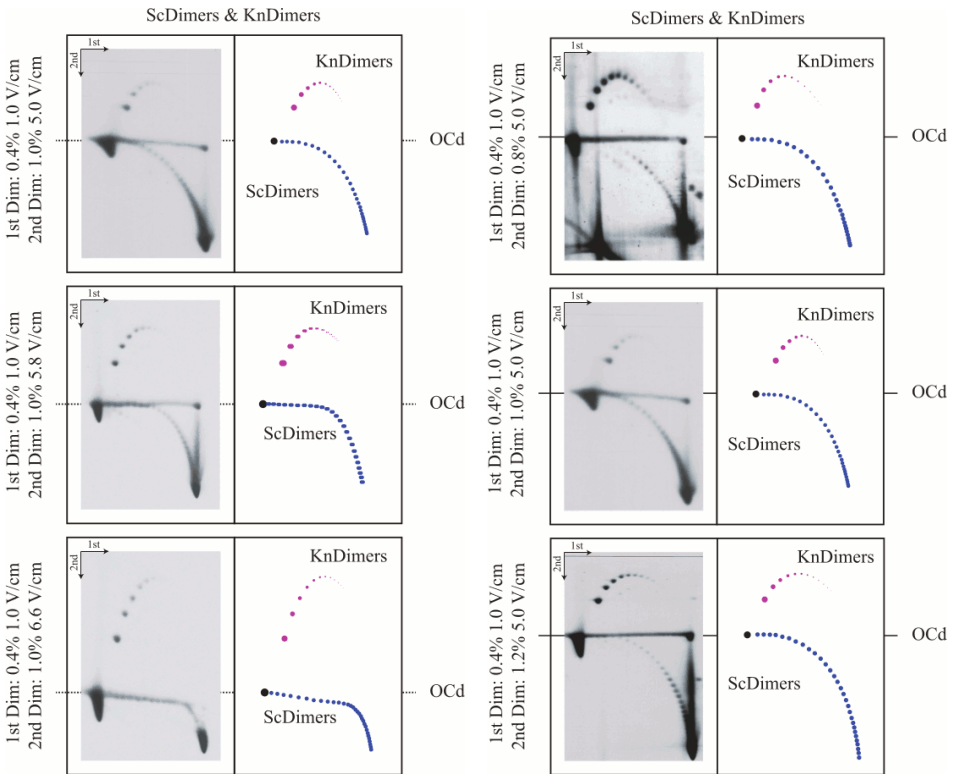

Figure 1.15: Two-dimensional electrophoresis of knotted dimers and supercoiled DNA dimers. Left: the second dimension is run at 0.1% gel concentration and different voltages. Right: the second dimension is run at the same voltage of 5.0 V/cm with gels of different concentrations. Interpretative diagrams are also shown to the right of each picture. (From Cebrián et al. (2015)).

stress. At the same time, unknotted supercoiled molecules were present in the sample. They kept the parameters for the first dimension of electrophoresis constant at a 0.4 % concentration of agarose and 1.0 V/cm electric field, while they tested the second dimension with various strengths of the electric field at fixed agarose concentrations or, vice versa, with various concentrations at a fixed electric field. Focusing on the knotted molecules only, if we look at Fig. 1.15 we can see that in all cases the knotted molecules show an arc pattern comparable to the one found by Trigueros et al. (2001). The explanation suggested by the authors associates the lower mobility of complex knots to the higher number of regions that need to be bent in order to squeeze through the smaller pores. The arc pattern, rather than a simple inversion, would be due to the fact that for complex knots above a certain ACN knotting itself causes a strong bending of the molecules that helps them pass through the pores.

1.7 Previous computational models

The reasons for the behaviour of knotted DNA molecules in agarose-gel electrophoresis have been the focus of much research. Since such behaviour varies according to the parameters used in the experiments, different models have been proposed in order to explain the different experimental results.

1.7.1 Linear relation with ACN

As we have seen (Section 1.6), in most experiments of agarose-gel electrophoresis in standard conditions (low-concentration gel and low electric field), the mobility of the knotted DNA molecules is linearly dependent on the complexity of the knot, as measured by the average crossing number. The typical argument to explain this behaviour relies on the analogy with the motion of a spherical particle in a viscous fluid, where the radius of gyration of the DNA molecules plays the part of the hydrodynamic radius r in the Stoke's law $F^{drag} = 6\pi\eta r$.

Numerical simulations of sedimentation with full hydrodynamics interactions

Based on this analogy, Piili et al. (2013) simulated the sedimentation of knotted polymers taking into full account hydrodynamic interactions by modelling the solvent as consisting of point-like particles and using a Navier-Stokes integrator called stochastic rotation dynamics (SRD) (Malevanets and Kapral, 1999). They found that, like in the experiments with gel, the sedimentation coefficient was linearly dependent on the average crossing number of the corresponding ideal form of the knot and inversely proportional to the radius of gyration, which can be considered, as well as the ACN, a good measure of the complexity of the knot.

Rigid ideal knots in a Stokes fluid

Hydrodynamic interactions play an important role also in the model studied in Gonzalez et al. (2004). They examined the dynamics of a generic rigid body in a viscous fluid under a uniform external force, by studying a three-dimensional system of ordinary differential equations determined by the hydrodynamic mobility properties of the system. Their showed that steady states correspond to screw motions with the centre of mass moving along a helical path while the body spins around the direction of the force. They applied their results to rigid filaments, in particular in the shape of ideal knots, and showed that, both

in simulations based on their equations and by computing the speed directly from the mobility matrix, the sedimentation speed is approximately in linear relationship with the average crossing number.

Experiments with macroscopic rigid knots

The relation between shape of the knots in their ideal form and mobility has also been tested with macroscopic models made of resin (Weber et al., 2013). The samples were manufactured through stereolithography in the shape of ideal knots in such a way that that they were all made of tubes of the same length (30 cm) and diameter (0.5 cm). They were then left to fall under gravity inside transparent plexiglass tanks filled with either water or viscous silicon oil and the sedimentation velocity measured. Also in this case, with filaments of macroscopic size and a length-to-diameter ratio more than ten times smaller than DNA, a linear relation was observed between ACN and mobility of the knots.

It has to be noted that this experiment measures sedimentation of macroscopic knots, without the presence of a gel. In the same way, the two mathematical models just described study sedimentation in the absence of a gel and solely rely on hydrodynamic interactions within the fluid. It is nonetheless interesting that the type of dependence of the mobility on the average crossing number is the same as knotted DNA molecules in agarose gel, as it can give an indication of the role of shape and hydrodynamics in the problem.

1.7.2 Inversion

In order to explain the inversion of mobility found in Sogo et al. (1999) (Section 1.6.1), Weber et al. (2006) propose lattice Monte Carlo simulations which are in good accord with the experimental results. In these simulations, the knots are represented by closed self-avoiding walks on a three-dimensional lattice. The gel, instead, is represented by a two-dimensional grid, shifted with respect to the knot lattice so that the points of the knot cannot lie on the gel, and perpendicular to the direction of the electric field. The knots move according to the BFACF algorithm (Berg and Foester (1981); Aragão De Carvalho et al. (1983), see Fig. 1.16), which preserves the knot type. In addition, if a proposed move would cause the knot to cross a gel fibre, that move is prohibited.

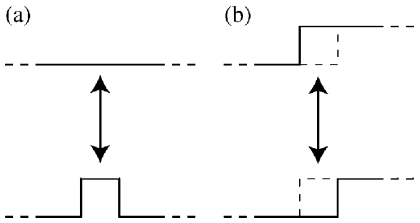

Figure 1.16: BFACF elementary moves: (a) handle creation or destruction; (b) corner flip (From Weber et al. (2006)).

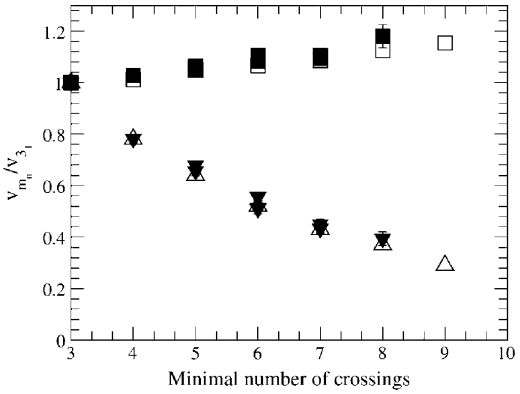

Figure 1.17: Simulated and experimental velocities as a function of the minimal crossing number of the knots in the simulations by Weber et al. Squares are for low and triangles for high electric field. Open symbols are for experimental results and solid symbols for simulation results. Values normalised to the value for the respective trefoil knot (From Weber et al. (2006), with experimental data from Sogo et al. (1999)).

For low electric fields, they found that the smaller size of more complex knots means they encounter the fibres of the gel less frequently and this is sufficient for them to move faster. On the contrary, in the presence of high electric fields, the self-avoidance condition makes it more difficult for complex knots with respect to simpler knots, to move around the gel fibre and free themselves. With this model they were able to see an inversion behaviour and replicate the results in Sogo et al. (1999) (see Fig. 1.17). However, this model does not seem to predict the possibility of an arc pattern, as seen in Section 1.6.1.

1.7.3 Arc pattern

A model that specifically aims at explaining the arc pattern as seen in two-dimensional electrophoresis experiments has been proposed by Michieletto, Marenduzzo and Orlandini (Michieletto et al., 2015). They use Brownian-dynamics simulations to reproduce the motion of knotted DNA chains through

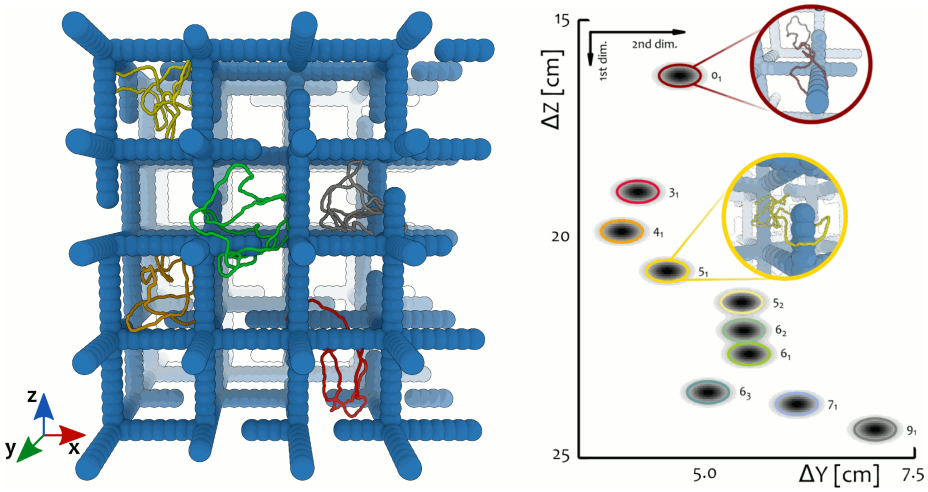

Figure 1.18: Agarose gel as an imperfect cubic mesh in the simulations by Michieletto et al. Left: snapshot of the model gel with some examples of knotted chains. Right: results of the *in silico* 2d gel electrophoresis with electric field $E \approx 50$ V/cm in the first direction and $E \approx 150$ V/cm in the second direction (from Michieletto et al. (2015)).

a gel in the presence of electric fields of various strength and direction. As shown in Fig. 1.18, left, the gel is modelled as an imperfect cubic mesh where some of the bonds have been cut to simulate the presence of open strands as it is expected to find in agarose gels (Section 1.5).

According to their results, the non-regularity of the gel is what causes the anomalous behaviour observed experimentally. In fact, they show that under a strong electric field, knotted molecules get trapped by these open strands and the time needed to free themselves increases with a quantity, the Average Entanglement Number (AEN), which they define as a measure of complexity and which can be calculated for each knot type. The AEN increases linearly with the ACN, and the competing effects of these long entrapment times and the Stokes drag give rise to the non-monotonic distribution of the mobilities (the arc pattern). They also show that if they remove the irregularities in the mesh, the arc pattern disappears and a linear relationship re-emerges.

As part of their simulations, they performed a set of runs with low-intensity electric field in their irregular gel and, like in the first dimension of agarose-gel electrophoresis, the mobility of the knots increased linearly with the ACN (Fig. 1.19, left).

Additionally, as briefly mentioned, in order to show that the imperfections were key to the appearance of the arc pattern, they tested their system at high

electric field, but with a regular mesh without dangling ends. Also in this case, the trend that they found was a linear increase of mobility with the ACN (Fig. 1.19, right).

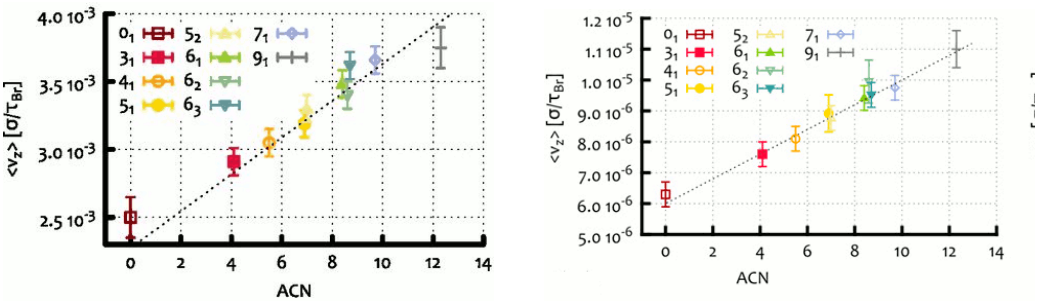

Figure 1.19: Linear mobility as particular cases in the model by Michieletto et al. Left: average velocity of different knot types with weak electric field. Right: average velocity of different knot types with a regular mesh. This trend only emerges if the gel is dense (spacing of 200 nm); for sparser gels (spacing of 500 nm) no trend emerges.

1.8 Outline of the thesis

In this Chapter, I have motivated the interest in the study of the mobility and separation of knotted polymers, and I have introduced basic concepts of knot theory, polymer theory, and knots in biology. Finally, I have summarised the main previous theoretical and computational models of gel electrophoresis of knotted DNA molecules found in the literature.

In Chapter 2, I will describe the methods used in the simulations presented in the rest of the thesis. In particular, I will define the characteristics of the Brownian-dynamics method which will be the basis of all the simulations, both performed through my own software program and with the molecular-dynamics program LAMMPS. All the parameters used in the simulations will also be explained.

In Chapter 3, I will present the results of the simulations, performed with my own program written in the C language, of a minimal model of short knotted chains in a suspension of spheres arranged at the vertices of a small regular cubic lattice with varying densities. I will show that the presence of such a medium has an influence on the molecule that depends both on the suspension and the type of knot.

In Chapter 4, I will present the results of simulations performed with LAMMPS of the mobility of knotted molecules, with characteristics based on double-stranded DNA, subjected to a driving force that pushes them through a suspension of random monodisperse spherical particles of comparable size to the radius of gyration of the chains. I will show that, if the spheres of the suspension are allowed to move in space, the mobility of the chains increases linearly with the ACN of the knot, like in standard experiments of agarose-gel electrophoresis.

In Chapter 5, I will move away from isolated chains to look at phase separation in blends of different types of knots. I will create a blend of ring molecules where half will not be knotted and half will present a nine-crossing knot. I will change the density and the temperature to explore the conditions for the two topologies to phase separate. I will show that, within the limits of the parameters tested so far, no phase separation has been found.

Finally, in Chapter 6, I will present my conclusions and possible outlook of the research presented in this thesis.

2 Methods

2.1 Introduction

In this chapter the simulation methods used in the remainder of the thesis are introduced and explained in detail.

In Chapter 3, the system under study is a minimal model for the mobility of a knotted chain in a suspension, and to that aim, the structure is stripped to the bare minimum and only the features essential to describe it are included. This model was developed according to coarse-graining principles as a bead-spring chain as explained below (Section 2.2). In order to have total control over all the characteristics of the simulations, a program in the C language was specially written. This allowed for better computational speed, but limited the complexity of the system that was reasonably achievable compared with more sophisticated molecular-dynamics software.

On the other hand, in Chapters 4 and 5, the systems analysed tend to be more similar to a particular kind of molecule, namely DNA. This implies longer polymers than those in Chapter 3 and the ability to introduce more complex features, such as the persistence length. For these reasons, a molecular-dynamics simulator was used, specifically Large-scale Atomic/Molecular Massively Parallel Simulator (LAMMPS) from Sandia National Laboratories [Sandia National Laboratories (2004 – present)]. This software allows the user to choose the kind of forces involved and set all the necessary variables associated to the particles and the environment through a script, which is then loaded and run by the main software. The script also specifies the results of interest, which can then be analysed.

Although the second approach includes more details than the first, the two models describe similar systems and follow the same fundamental principles

and common coarse-graining assumptions. Therefore the methods used in all the simulations performed in this thesis share the same general core elements, although the particular choices that were made in the two cases differ according to the structure described.

2.2 Bead-spring model

2.2.1 Introduction: coarse-graining principles

Before modern high-speed computers were available, testing theories for the rheology of polymer solutions computationally was only possible in greatly simplified forms. In recent years, on the contrary, the advances and specialisation of modern clusters of computer have made it possible to directly solve the equation of motion of particles in the presence of well-defined forces with such speed that it is possible to utilise them to investigate complex polymer models.

However, when the properties of long-time-scale dynamics of non-trivial molecules are of interest, it is neither possible nor useful to focus on an exactly atomistic description of the system. In this case it is necessary to use a "coarse-graining" approximation, that is, to ignore the fine details and the small-scale dynamics while concentrating on coarse-grain elements of the system, provided all the parameters that can have an effect on the dynamics are taken into consideration.

A commonly used approach to determine the coarse graining of a polymer chain is to consider a section of the chain long enough so that the internal microscopic characteristic, such as the position of the atoms and the angles or rigidity of the single bonds, can be ignored and the section can be modelled as a bead (frictional drag centres) and a freely-rotating rod. In this way, the succession of beads and rods will form a freely-jointed chain. The length of one rod is called a *Kuhn step* and it is denoted as b_K.

The original polymer and the resulting bead-rod chain will be very different, but they will share the physical characteristics needed to represent the motion if b_K and the number of steps N_K in the new chain are chosen appropriately. In fact, the two chains will have the same equilibrium mean-square end-to-end length $\langle R^2 \rangle_0$ and the same total extended length L as long as b_K and N_K are chosen so that $b_K^2 N_K = \langle R^2 \rangle_0$ and $b_K N_K = L$. The particular values will depend on the material and the solvent.

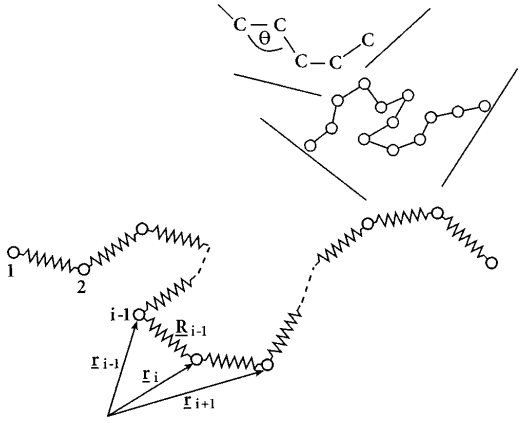

Figure 2.1: Coarse-graining mapping of real polymer chain. The original chain is made of a C-C backbone, with the carbon atoms at a fixed dihedral bond angle as described by Larson (2005). A section is turned into a bead-and-rod element and a number of bead and rods can be represented as a bead and a spring, as explained in Section 2.2. Image from Larson (2005)

This approximation is still very detailed, and simulating the dynamics in this way is computationally very expensive. However, if we consider a small section of the chain, the rapid internal fluctuations in the motion of the rods in this section will be much faster than the dynamics of the polymer on the whole and they can be averaged as a resulting spring force. The number of connected rods in each of these springs is denoted as $N_{K,s}$, and can be chosen so that the total number of springs $N_s = N_K/N_{K,s}$ is convenient for the type of simulations performed.

The physical origin of this spring force is due to entropic reasons. In fact, the individual monomers composing the section of the polymer considered are subjected to thermal fluctuations which constantly change their microscopic state. As entropy tends to be maximised, the resulting macroscopic state from this process will be the one that maximises the number of all the possible configurations of these microscopic states. If we model this chain of monomers as an ideal chain, it can be shown (see, for example, Treloar (1975)) that the number of microscopic states compatible with a shorter length is higher than the number of microscopic states compatible with a longer length, so resulting in a force that tends to compress the chain, similar to the restoring force of a spring.

A schematic representation of the bead-rod and bead-spring models can be seen in Fig 2.1, taken from Larson (2005).

2.2.2 The bead

As seen, a bead represents the physical position of a section of the polymer. The forces acting on that section are seen as applied to the centre of mass of the bead. The quantities associated with a bead are: mass, hydrodynamic radius, electric charge and excluded-volume radius.

2.2.3 Bonding potential: types of spring

The elasticity of the bond between the i-th and the j-th bead, i and j sequential in the chain, is given by a bonding potential, which, as explained earlier in Section 2.2.1, can be imagined like a spring connecting the two beads.

Linear spring

The simplest model for this kind of force is the linear, or Hookean, spring, described by the equation:

$$F^{\text{spring}}(R) = HR, \tag{2.1}$$

where H is the linear-spring constant and R is the extension of the spring.

While the restoring force increases with the extension, this force is not bounded and the spring can extend indefinitely. This law is adequate to describe the simple harmonic oscillation of a spring near its equilibrium position, but it is not suitable for bonds of defined maximum length, as in a physical molecule.

FENE model

As mentioned, simple linear springs are not adequate for the physical systems considered in this work. Therefore, in order to represent the elasticity of the chain, but with the physical constraint that the length of bond cannot exceed the length of the section of molecule considered, we use the FENE (Finite Extensible Non-linear Elasticity) model (Warner Jr, 1972). In this model, although the return force is linear with the displacement for small extensions of the bond, like a linear spring, it increases and eventually becomes asymptotically high as the length approaches the full extension of the bond.

$$F_{ij}^{\text{spring}}(R_{ij}) = \frac{H}{1 - \left(\frac{R_{ij}}{L_s}\right)^2} R_{ij}, \tag{2.2}$$

where $H = \frac{3k_BT}{N_{k,s}b_k^2}$, with $N_{k,s}$ and b_k as explained in Section 2.2.1, L_s is the length of a spring and R_{ij} is the distance between the two beads.

The value of the spring constant H depends on the temperature and on the equilibrium mean-square end-to-end length $\langle R^2\rangle_0$ of the portion of the original polymer represented by the spring (as seen in Section 2.2.1, $\langle R^2\rangle_0 = b_K^2 N_K$).

2.2.4 Excluded volume

Excluded-volume interactions are due to the repulsive forces between different objects which keep them from occupying the same region of space. Therefore, an excluded-volume force $\mathbf{F}^{\text{ev}}$ due to the presence of each bead in a specific position and by the proximity of connected beads is what can stop the chain from crossing itself.

The excluded volume is represented by a repulsive force given as the gradient of a potential $U^{ev}(\mathbf{R})$:

$$\mathbf{F}_i = -\sum_j \frac{\partial}{\partial \mathbf{r}_i} U^{ev}(\mathbf{r}_i - \mathbf{r}_j), \tag{2.3}$$

where F_i is the force acting on the i-th bead and $U^{ev}(\mathbf{R})$ depends on the system and the approximations considered.

In this thesis, the focus of the research is on the topology of the chains, and it is essential that molecules that are generated as knotted in a certain way retain the type of knot for the duration of the simulation. The excluded-volume force, along with a sensible choice of the bond length, need always to be considered carefully and chosen in such a way as to prevent the strands from crossing each other.

Lennard-Jones excluded-volume potential

The Lennard-Jones model (Lennard-Jones, 1924) aims to describe the binding energy of neutral atoms or molecules with the equation:

$$V_{\text{LJ}}(r) = 4\varepsilon\left[\left(\frac{\sigma}{r}\right)^{12} - \left(\frac{\sigma}{r}\right)^{6}\right]. \tag{2.4}$$

This potential is repulsive at short separation distances, while it becomes attractive for larger separations, due to London forces. The potential is zero at distance σ, σ representing the diameter of the atom or molecule, while the equilibrium distance is $r_{min} = 2^{\frac{1}{6}}\sigma \approx 1.122\sigma$. At the minimum, the potential function has the value -ε.

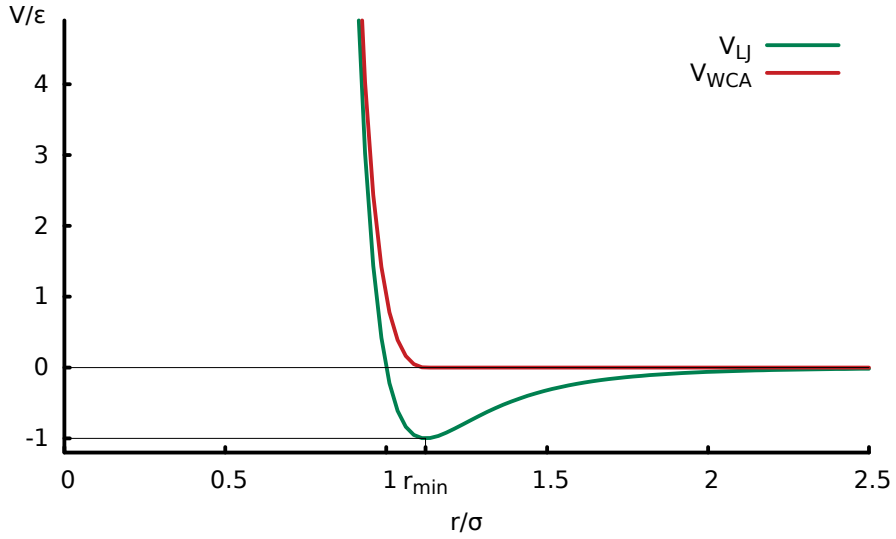

Figure 2.2: A graph of strength versus distance for the Lennard-Jones and the Weeks-Chandler-Andersen potentials. Both provide a strong repulsion for particles appoaching distance σ. The L-J becomes attractive at longer distances, with r_{min} equilibrium distance, while the W-C-A potential is purely repulsive and has no action for $r \geq 2^{\frac{1}{6}}\sigma$.

If we want to model the excluded volume of a hard sphere, that is, an impenetrable potential at short determined distance, but no attraction, it is possible to consider only the repulsive part of the interaction by introducing a cut-off as in the Weeks-Chandler-Andersen potential (Weeks et al., 1971):

$$V_{\mathrm{WCA}}(r) = \begin{cases} 4\varepsilon\left[\left(\frac{\sigma}{r}\right)^{12} - \left(\frac{\sigma}{r}\right)^{6}\right] + \varepsilon & \text{for } r < 2^{\frac{1}{6}}\sigma \\ 0 & \text{for } r \geq 2^{\frac{1}{6}}\sigma \end{cases} \tag{2.5}$$

The W-C-A potential is also considerably faster than the plain L-J to calculate computationally, as it only intervenes at distances comparable with the size of the beads.

The two potentials are shown in the graph in Fig. 2.2.

This kind of potential has the advantage of producing a strong repulsion force at small distances, so the particles are virtually impenetrable. This means that, as long as the separation (spring) length between the beads is chosen sensibly, crossing of strands is not possible, and topology is almost certainly conserved. However, as it increases exponentially with decreasing distances, numerical integration can can only be performed with small time steps.

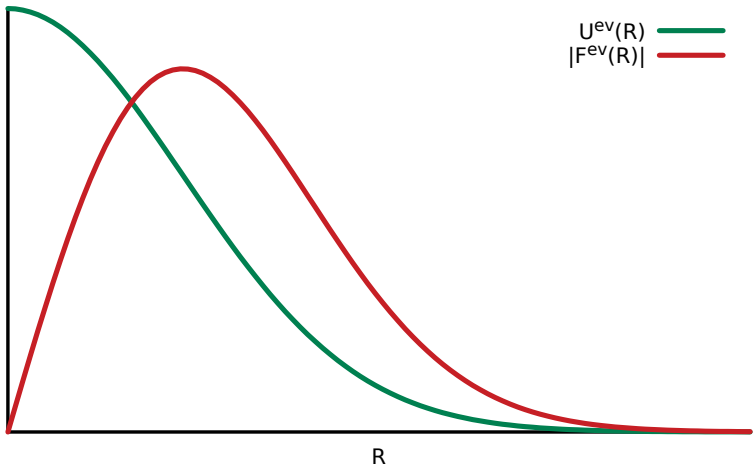

Figure 2.3: A graph of strength versus distance for soft excluded-volume potential and the corresponding force. The parameter A in Eq. 2.6 determines the height of the curve, while B affects the width.

Soft excluded-volume potential

Another possible choice for the excluded-volume potential is a soft potential, that is, a potential that decays exponentially with the distance (see Larson (2005), p.18, Jendrejack et al. (2002)).

$$U^{ev}(\mathbf{R}) = A\, e^{-B\,|\mathbf{r}_i - \mathbf{r}_j|^2}, \tag{2.6}$$

where the parameters A and B depend on the system.

This allows for a longer time step in simulations compared to a hard potential, and it has the advantage of remaining bounded at all distances.

In this case, the force acting on the i-th bead is of the form:

$$\mathbf{F}_i^{\text{ev}} = -\sum_{\substack{j=1 \\ j\neq i}}^{N} a\, e^{-b\,|\mathbf{r}_i - \mathbf{r}_j|^2}\,(\mathbf{r}_i - \mathbf{r}_j), \tag{2.7}$$

with $a = 2\,A\,B$ and $b = B$. A graph of this type of potential and the resulting force is shown in Fig. 2.3.

A potential of this type has been introduced for example by Jendrejack et al. (2002) with parameters as (see also Larson (2005)):

$$U^{ev}(R) = \frac{1}{2} v k_b T N_{K,s}^2 \left(\frac{9}{2\pi R_s^2}\right)^{\frac{3}{2}} e^{-\frac{9R^2}{2R_s^2}}, \tag{2.8}$$

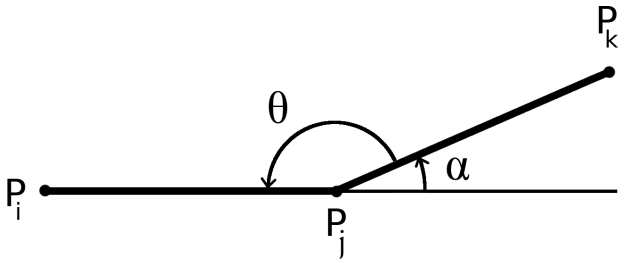

Figure 2.4: The bond angle associated with the bending rigidity. The energy is zero if two bonds are aligned. For $\theta \approx \pi$, i.e. $\alpha \approx 0$, we have $1 + \cos\theta = 1 + \cos(\pi - \alpha) \approx \frac{\alpha^2}{2}$.

where $R_s^2 = b_K^2 N_K = \langle R^2 \rangle_0$, equilibrium mean-square end-to-end length of a spring as seen in Section 2.2, and the *interaction volume* v is proportional to the microscopic volume of a Kuhn step of the chain.

As the time step used in the simulations can be longer, this type of excluded-volume force allows longer periods of time to be simulated in the same computer time. However, the chains are somehow penetrable, and strand crossing is not impossible. In this case, the force needs to be tuned so that crossing only happens occasionally, if ever, and the topology needs to be checked during and after the run to ascertain that the knot type has not changed.

2.2.5 Bond angles

In order to better describe one particular kind of polymer and consider its stiffness as well, it is possible to add a potential that depends on the angle between two consecutive bonds.

A simple way of modelling the rigidity is to consider the energy as depending on the cosine of the angle θ between two consecutive bonds (LAMMPS documentation, 2019a):

$$E = K(1 + \cos\theta), \tag{2.9}$$

where K is an energy coefficient associated with the bending rigidity and θ is the angle between two adjacent bonds, as shown in Fig. 2.4.

Torsional angles

If simulations aim to be fully atomistic, it is necessary to consider all energy terms, including the one associated with torsional (dihedral) angles between three successive bonds. However, a standard approach in these kind of simula-

tions is to consider the freely-rotating chain model (as defined in Section 1.3.1) and to neglect the torsional term.

2.3 Brownian dynamics

The motion of a bead is determined by the sum of the forces acting on it. When dealing with molecules the size of the order of a micron or less, such as colloidal particles or proteins, the inertial effects are much lower that the viscous forces, so that, for sufficiently long time steps, the term $m\mathbf{a} = m\frac{d\mathbf{v}}{dt}$ can be neglected. In this case the motion is said to be *overdamped* and we can write the equation:

$$\mathbf{F}_i^{\text{drag}} + \mathbf{F}_i^{\text{spring}} + \mathbf{F}_i^{\text{rand}} + \mathbf{F}_i^{\text{ev}} + \mathbf{F}_i^{\text{angle}} + \mathbf{F}_i^{\text{med}} + \mathbf{F}_i^{\text{electric}} = 0, \tag{2.10}$$

where the forces depend on the particular setting.

2.3.1 Thermal noise

As mentioned in Section 1.3.2, a stochastic (Brownian) force is present due to the motion of the solvent particles. Indeed the molecules that make up the solvent are in constant motion in no particular direction with average velocity depending on the temperature, and they put the polymer through a steady bombardment from all possible directions.

This happens on a time-scale of picoseconds, which is extremely small compared to the motion of the beads (μs). So, over the time scale normally considered in computer simulations, the net force due to the Brownian motion averages to zero, and can be described as a Wiener process with zero mean and non-zero variance (Ibáñez-García and Hanna, 2009).

In the model described in Chap. 3, this random force can be written as

$$\mathbf{F}_i^{\text{rand}} = \sqrt{\frac{6k_BT\zeta}{dt}}\,\mathbf{n}_i, \tag{2.11}$$

where $\mathbf{n}_i$ is a three-dimensional vector with initial point at the origin and terminal point uniformly distributed on the surface of a unit sphere.

This expression depends on the inverse of the squared root of the time step, as we are averaging noise, and on the factors k_bT and ζ according to the *fluctuation-dissipation theorem* that connects drag force and Brownian motion.

2.3.2 Viscous drag

The chain is moving in a solvent, so that each bead is subject to a frictional force opposing the motion due to the viscosity of the medium.

$$\mathbf{F}_i^{\text{drag}} = -\zeta \frac{d\mathbf{r}_i}{dt}, \tag{2.12}$$

with drag coefficient $\zeta = 6\pi\eta r$ (η viscosity of the solvent; r hydrodynamic radius of the bead).

2.3.3 Hydrodynamic interactions

Hydrodynamic interactions are due to long-ranged flows caused by the particles moving in the fluid and interacting, through these flows, with each other and with the walls of the container. Due to their nature, modelling these interactions is only feasible for simple, well-known systems, such as, for example, a single particle in a container with straight walls. The models described in this thesis involve chains made of multiple beads and a medium composed of numerous curved surfaces (spheres). For this reason, and as is customary in these kind of simulations (Michieletto et al., 2015), hydrodynamic interactions are not considered in any of the models in this thesis.

2.3.4 External forces

As the initial inspiration of this work was the behaviour of knotted DNA molecules during agarose-gel electrophoresis, and as we need some kind of external influence to help make the properties of the systems apparent, we apply a constant field of different strengths to our systems in Chapters 3 and 4.

The effect of this field is to apply a constant force $\mathbf{F}_i^{\text{electric}}$ to each bead of the chain. There are no electrostatic forces acting between the beads, because they are considered as effectively screened for distances greater than a few nm.

2.3.5 The Langevin equation

When all the forces in the system are known, it is possible to highlight the drag term $\mathbf{F}_i^{\text{drag}} = -\zeta \frac{d\mathbf{r}_i}{dt}$ (Eq. 2.12) and write the resulting equation of motion for each bead. This is given by a *Langevin equation*:

$$\frac{d\mathbf{r}_i}{dt} = \frac{1}{\zeta}\left(\mathbf{F}_i^{\text{spring}} + \mathbf{F}_i^{\text{rand}} + \mathbf{F}_i^{\text{ev}} + \mathbf{F}_i^{\text{angle}} + \mathbf{F}_i^{\text{med}} + \mathbf{F}_i^{\text{electric}}\right). \tag{2.13}$$

Numerically, it is possible to integrate Eq. 2.13, with $\mathbf{F}_i^{\text{rand}}$ as in Eq. 2.11, via a time-stepping algorithm (Section 2.3.6), using a series of values for the coordinates of each $\mathbf{n}_i$ provided by a random number generator. This yields the time evolution of the positions of the beads (Larson, 2005).

2.3.6 Time-stepping

The Euler method

The Langevin Equation is a first order first degree differential equation. A very simple method to solve this kind of equation numerically is the Euler method, named after Leonhard Euler who first introduced it in 1768 (Euler, 1768-1770).

If we have a one-dimensional ordinary differential equation (ODE) of the form

$$\frac{dx}{dt} = v(x,t), \tag{2.14}$$

the idea is to consider, instead of the differential, arbitrarily small, but finite, differences in t and x: $dt \to \Delta t$; $dx \to \Delta x$. In this way, if the initial values (t_0, x_0) are known, it is possible to calculate the values of the coordinates after a step Δt as

$$\begin{cases} x \approx x_0 + \Delta t\, v(x_0, t_0); \\ t = t_0 + \Delta t. \end{cases} \tag{2.15}$$

The Verlet algorithm

Another widely-used method for integrating the equation of motion, and slightly more sophisticated than the Euler method, is the Verlet algorithm (Verlet, 1967). The starting point for the calculations is a Taylor expansion of the equation up to the third power:

$$\begin{cases} \mathbf{x}(t+\Delta t) = \mathbf{x}(t) + \mathbf{v}(t)\Delta t + \frac{\mathbf{a}(\mathbf{x}(t))}{2}\Delta t^2 + \frac{\mathbf{b}(t)}{3!}\Delta t^3 + O(\Delta t^4), \\ \mathbf{x}(t-\Delta t) = \mathbf{x}(t) - \mathbf{v}(t)\Delta t + \frac{\mathbf{a}(\mathbf{x}(t))}{2}\Delta t^2 - \frac{\mathbf{b}(t)}{3!}\Delta t^3 + O(\Delta t^4). \end{cases} \tag{2.16}$$

If we sum up these two equations, we obtain the integration step for the position, where the approximation is treated as an equality:

$$\mathbf{x}(t+\Delta t) = 2\mathbf{x}(t) - \mathbf{x}(t-\Delta t) + \mathbf{a}(\mathbf{x}(t))\Delta t^2 \tag{2.17}$$

The velocities are not required to calculate the time evolution, but if needed (for example to calculate energies), they can be obtained by subtracting the two

equations in 2.16:

$$\mathbf{v}(t) = \frac{\mathbf{x}(t+\Delta t) - \mathbf{x}(t-\Delta t)}{2\Delta t}. \tag{2.18}$$

A modified version of this method is the *Velocity-Verlet algorithm*, first introduced in Swope et al. (1982). It is derived as above, but it explicitly includes the velocities in the computation of the steps. It is straightforward to see that Eq. 2.17 and Eq. 2.18 are equivalent to the following:

$$\mathbf{x}(t+\Delta t) = \mathbf{x}(t) + \mathbf{v}(t)\Delta t + \frac{\mathbf{a}(\mathbf{x}(t))}{2}\Delta t^2, \tag{2.19}$$

and

$$\mathbf{v}(t+\Delta t) = \mathbf{v}(t) + \frac{\mathbf{a}(\mathbf{x}(t+\Delta t)) + \mathbf{a}(\mathbf{x}(t))}{2}\Delta t. \tag{2.20}$$

These equations give us a simple way of implementing thermal noise into the algorithm, as the effect of a stochastic collision can be included in the value of $\mathbf{v}(t)$ before $\mathbf{x}(t+\Delta t)$ is computed.

2.3.7 Boundary conditions

All the systems studied in this work use periodic boundary conditions in a three-dimensional cubic box. This means that the particles being simulated are moving in a cubic box and whenever one exits from one wall, it reappears with the same position and velocity at the inside of the opposite wall. With respect to open boundary conditions, this allows for an infinitely-wide system by using just a finite number of particles, so keeping it computationally easy to manage.

In the case of the minimal model in Chap. 3 and the longer molecules in Chap. 4, the number of polymer chains in a single simulation is either one or four, and the box is big enough that there is virtually no interaction between them in any case. The suspension in Chap. 3 is a regular cubic lattice, so periodic boundary conditions are a natural choice. The suspension in Chap. 4 is a series of randomly-generated spheres whose aim is to interfere with the motion of the chains, therefore it is of no consequence if it repeats itself after the chain has gone through each periodic box.

2.4 Dynamic models for polymers in diluted solutions

The basic concepts of molecular motion of polymers in diluted solutions has been introduced in the previous chapter in Section 1.3.2. Having better specified the characteristics of the systems under study in this chapter, two models for

the mobility of polymer chains are described here. They will be useful as a comparison with the results found for the mobility of the chains presented in the following chapters.

2.4.1 The Rouse model

A bead-spring model as described in Section 2.2, with dynamics expressed through the Langevin Equation (Eq. 2.13), was first proposed by Prince E. Rouse in 1953 (Rouse Jr, 1953). In this model, excluded-volume forces and hydrodynamic interactions are neglected. As a result, the mean square displacement of the centre of mass of a molecule can be calculated to be (Doi, 1996):

$$\langle(\mathbf{R}_{CM}(t) - \mathbf{R}_{CM}(0))^2\rangle = \frac{6k_BT}{N\zeta}t, \tag{2.21}$$

which means that the diffusion constant associated with the centre of mass is inversely proportional to the number of beads:

$$D_{CM} = \frac{k_BT}{N\zeta} \propto \frac{1}{N}. \tag{2.22}$$

Equation 2.22 is valid for an ideal chain and for short chains (below the entanglement length) in a polymer melt, but does not agree with experiments where large hydrodynamic interactions are present and reptation starts being significant. In fact, in these systems, the motion of each bead is affected by the motion of the others through the presence of the solvent. The Zimm model aims to solve this problem.

2.4.2 The Zimm model

The Zimm model is still a bead-spring model, but with equation of motion modified as to include hydrodynamic interactions. When these are considered, the equation becomes (Doi, 1996):

$$\frac{d\mathbf{r}_i}{dt} = k\sum_j \mathbf{H}_{ij}\cdot(\mathbf{r}_{j+1} + \mathbf{r}_{j-1} - 2\mathbf{r}_j) + \mathbf{F}_i^{\text{rand}}, \tag{2.23}$$

where the tensor $\mathbf{H}_{ij}$, corresponding to the mobility matrix, includes hydrodynamic interactions and depends on $\mathbf{r}_i$. Being a non-linear equation, Eq. 2.23 is very difficult to solve.

In the Zimm model, $\mathbf{H}_{ij}$ is replaced by its equilibrium average value $\langle\mathbf{H}_{ij}\rangle_{eq}$. This approximation is possible due to hydrodynamic interaction being long

range, and gives rise to the following relation between the diffusion constant of the centre of mass and the number of beads:

$$D_{CM} \propto \frac{1}{\sqrt{N}}. \tag{2.24}$$

This kind of dependence is more accurate and has been shown to hold in experiments of polymers in solutions at the Θ temperature.

2.5 Parameter choice

2.5.1 Minimal model

Coarse graining

The polymers are modelled as coarse-grained bead-spring chains of N beads, following the standard methods described in Section 2.2.

The system was tested for various values of N, and the value $N = 40$ was chosen for the bulk of the simulations. The reason for this choice was to keep chain as short as possible, both for simplicity and for computational economy, and $N = 40$ was the minimum number of beads which still allowed a certain conformational flexibility of the chain. However, as discussed in Chap. 3, in the case of more complex knots, due to the choice of the excluded-volume radius of the beads, the resulting chains resulted to be more rigid than expected and this may have affected the mobility of the chain.

In this model, each bead represents $N_{k,s} = 10$ Kuhn steps, each Kuhn step b_k being 132 nm, as in double-stranded DNA (Larson, 2005), so that the maximum length of the springs, $L_s = N_{k,s} b_k$, is $L_s = 1.32\mu$m. By considering a relatively large number of Kuhn steps per bead it is therefore possible to ignore the bending rigidity of the molecule and consider the bonds free to take any direction consistent with the excluded-volume constraints.

Drag

The drag considered is as in Eq. 2.12 with $\eta = 1.002$ mPa·s, viscosity of the water, and $r = 0.64\, b_k (N_{k,s}/6)^{1/2} = 0.1091\mu$m, hydrodynamic radius, following Jendrejack et al. (2002).

The hydrodynamic radius is therefore compatible with DNA molecules, unlike the excluded-volume radius which, as explained below had to be made considerably bigger. Consequently, the two radii have very different values.

Excluded-volume potential

For computational reasons, as explained in Section 2.2.4, a soft potential as in Eq. 2.6 is used. The parameters are chosen as $a = 10\frac{\sqrt{2}\,3k_BT}{b_k} \cdot \frac{2}{10b_k} \cdot e^{1.5} = 8.92 \cdot 10^{-6}$Nm and $b = \frac{1.5}{(L_s/2)^2} = 3.44 \cdot 10^{12}\text{m}^{-2}$.

This force is greater than usually found in literature, as in this work not only is it important to reproduce the dynamics, but it is also vital to ensure that the chain does not cross itself and the topology is conserved. For this reason, while keeping the shape of the force unchanged, the parameters were adjusted until the knot types were found to be conserved during the simulations. In particular, the parameters a and b were chosen to represent the smallest possible bead, consistent with being large enough to prevent the random force from overcoming the excluded volume in a single time step. The resulting excluded-volume radius of the beads is 0.54 μm.

Electric field

The systems were tested both with and without an electric field.

The charge associated with each bead is one quarter of the charge of one electron (q_e) per base pair (bp). This aims to take into account the screening due to counter ions, which are not otherwise present in the model. Each bead has therefore a charge of $q_b = \frac{1}{4} \cdot 1.32\mu\text{m} \cdot \frac{1\text{bp}}{0.34\text{nm}} q_e = 1.55 \cdot 10^{-16}$C.

The range of values considered for the electric field are between 0.25 and 1.50 V/cm, consistent with gel electrophoresis, so giving forces in the range $3.89 \cdot 10^{-3} - 2.33 \cdot 10^{-2}$ pN per bead. In particular, the values tested are: E={0, 0.12, 0.25, 0.50, 0.75, 1.00, 1.50} V/cm.

Timestep

The timestep considered was $dt = 10^{-5}$ s. This value was chosen so that all the forces considered would keep within the same approximate range of each other. This would allow the simulations to run smoothly and give physically-consistent result while keeping the chains from breaking.

Table of parameters

All the values of the parameters used, apart from E, are listed in Tables 2.1, 2.2 and 2.5.

N	number of beads	40	
$N_{k,s}$	Kuhn steps per spring (Larson, 2005, p. 33)	10.0	
λ	persistence length	$6.6{\cdot}10^{-8}$	m
b_k	$= 2\lambda$ Kuhn length	$1.32{\cdot}10^{-7}$	m
L_s	$= N_{k,s}b_k$ length of one spring	$1.32{\cdot}10^{-6}$	m
L	$= L_s N$ total length of the chain	$52.8{\cdot}10^{-6}$	m
L_{bp}	distance between each base pair in DNA	$3.4{\cdot}10^{-10}$	m
dt	timestep	10^{-5}	s
η	viscosity of the medium (water)	$1.002{\cdot}10^{-3}$	Pa·s
T	temperature	296.0	K
r	$= C_a b_k (N_{k,s}/6)^{1/2}$; Stokes radius	$1.091{\cdot}10^{-7}$	m
Ca	constant of proportionality (Jendrejack et al., 2002, p. 7758)	0.64	
ζ	$= 6\pi\eta r$ drag coefficient	$2.060{\cdot}10^{-9}$	Pa·s·m
$\lVert\mathbf{F}_i^{\text{rand}}\rVert$	$= \sqrt{\frac{6k_BT\zeta}{dt}}$ random force (Larson, 2005, p. 13)	$2.247{\cdot}10^{-12}$	N
H	$= \frac{3k_BT}{N_{k,s}b_k^2}$ spring constant (Larson, 2005, p. 11)	$7.036{\cdot}10^{-8}$	N·m^{-1}
q_{bead}	$= \frac{1}{4}\frac{L_s}{L_{\text{bp}}}\, q_{\text{e}}$ electric charge of one bead	$1.555{\cdot}10^{-16}$	C

Table 2.1: Values of the parameters used in the simulations for the minimal model.

Theoretical values of the parameters for the excluded-volume force:

a	$= \frac{1}{2}\nu k_BT N_{k,s}^2 \left(\frac{9}{2\pi R_s^2}\right)^{\frac{3}{2}}$	$1.11{\cdot}10^{-20}$	N·m
b	$= \frac{9}{2R_s^2}$	$2.58{\cdot}10^{13}$	m^{-2}
$2ab$	$= \left(\frac{9}{5R_s}\right)^{5/2} \pi^{-3}\nu k_BT N_{k,s}^2$	$5.73{\cdot}10^{-7}$	N/m

where
$\nu = b_k^3$ volume associated with one bead
$R_s^2 = N_{k,s}b_k^2$ mean square end-to-end length of a spring

Our values for the parameters:

a	$= \frac{\sqrt{2}\, e^{1.5}}{6}\, 3k_BT\, N_{k,s}^2$	$1.30{\cdot}10^{-18}$	N·m
b	$= \frac{1.5}{(L_s/2)^2}$	$3.44{\cdot}10^{12}$	m^{-2}
$2ab$	$= 10 \cdot \frac{\sqrt{2}\, 3k_BT}{b_k} \cdot \frac{2}{10b_k} \cdot e^{1.5}$	$8.92{\cdot}10^{-6}$	N/m

Table 2.2: Values of the parameters for the excluded-volume force between the beads of the chain: theoretical values and the values actually used in the simulations for the minimal model.

2.5.2 Longer molecules with LAMMPS

As in the previous model, these are still molecular-dynamics simulations, which allows much liberty in the choice of the level of coarse-grain details described. Like in the previous case, the interest is on the long-term behaviour of long chains in a medium while subject to an external field. Therefore microscopic interactions, which would be slow to compute, are ignored, instead focusing on a few key elements that are important in the motion of the polymers. These elements will be: the length of the chains, the persistence length, which measures the rigidity of the simulated polymer, and the bonding and excluded-volume forces needed to keep the chains together and to avoid the different strands crossing each other. This last requirement is, like in the previous case, particularly important, as it is essential that the topology, that is, the type of knot, does not change during the simulation.

Lennard-Jones system units

In the scripts used for the simulations with LAMMPS, the excluded-volume potential is a Lennard-Jones potential with cut off at a distance $2^{\frac{1}{6}}\sigma$. This is equivalent to a W-C-A potential (Eq. 2.5), as potentials are defined to within an arbitrary additive constant. The choice of parameters is expressed in terms of dimensionless quantities related to the choice of the fundamental quantities in the model. This simplifies the way both starting configurations and results of the simulations are written, as all the figures easily compare with the typical sizes of the system under study.

In this system, distances will be measured in terms of σ, where σ is the chosen diameter of the bead and the distance at which the Lennard-Jones potential (Eq. 2.4) is zero. Similarly, masses will be given in terms of the mass m of the bead, energies in units of ε (cf. Eq. 2.4) and times in terms of the *Lennard-Jones time*, defined as $\tau_{LJ} := \sigma\sqrt{\frac{m}{\varepsilon}}$.

Also, in these units, temperatures are given in terms of $\frac{\varepsilon}{k_B}$ and forces in terms of $\frac{\varepsilon}{\sigma}$.

It is conventional to further simplify the expressions by setting the Lennard-Jones reduced units as $\sigma = m = \varepsilon = k_B = 1$, which also gives $\tau_{LJ} = 1$.

An important time scale for the system is the *Brownian time*. This represents the time needed for a particle to diffuse a distance of the order of its size. As the diffusion coefficient D for a spherical particle through a viscous fluid is given by

the Stokes-Einstein equation (as seen in Section 1.3.2):

$$D = \frac{k_B T}{3\pi\eta\sigma} = \frac{k_B T}{\zeta}, \tag{2.25}$$

and the mean squared displacement is proportional to the diffusion coefficient, the Brownian time τ_B can be defined as (Michieletto, 2016):

$$\tau_B = \frac{\sigma^2}{D} \tag{2.26}$$

In addition, in LAMMPS, it is possible to set a damping parameter $\gamma = \frac{m}{\zeta}$. In the simulations presented in this thesis, γ is set to coincide with the Lennard-Jones time, $\gamma = \tau_{LJ}$. With this choice, the Brownian time coincides with the Lennard-Jones time, $\tau_{Br} = \tau_{LJ}$, and they are both equal to one in the reduced units.

Coarse graining and relation with real units

Following Michieletto (2016), for the chains in Chap. 4 and Chap. 5, the value chosen for σ is $\sigma = 2.5$ nm, which aims to be comparable to the diameter of double-strand DNA molecules in physiological conditions (e.g., the effective diameter d_{eff} at 0.15 M of NaCl is $d_{eff} \approx 5$nm, see Rybenkov et al. (1993)).

The elasticity is modelled with a FENE spring (Section 2.2.3) of maximum length $1.6\sigma = 4$ nm.

As for the bending rigidity, the factor K in Eq. 2.9 is taken to be 20 in units of σ, so as to model the persistence length of double-stranded DNA $\lambda = 50$ nm (see Section 1.3.1).

The length of the chains is typically 500 beads, that is $500\sigma = 1.25\mu$m.

The chains are moving in water (viscosity $\eta = 1cP = 10^{-3}$ kg $\cdot$ m$^{-1} \cdot$ s^{-1}) at a temperature of 300 K. This gives a Brownian time of $\tau_{Br} \approx 36$ ns.

The time step for the integration is $dt = 0.01\tau_{Br}$.

The system is moving in a cubic box with side $L_{box} = 200\sigma$ with periodic boundary conditions (see Section 2.3.7). This is large compared to the average radius of gyration R_G of the molecules, which is typically between 20 and 30 σ.

Electric field

The force representing the electric field is constant at $F^{electric} = 0.001$ in Lennard-Jones units, which corresponds to $1.66 \cdot 10^{-3}$pN. Different intensities of the electric force were tried, and it was found that for values of $F^{electric} = 0.1$ and

$F^{electric} = 0.01$, with a suspension of fixed random spheres as described below (Section 2.7.2), the pushing force was so strong that if two adjacent spheres were very close to each other, the chains would often get caught between them and were not able to free themselves for the rest of the simulation, leading to uninteresting results. $F^{electric} = 0.001$ was found to be a suitable value that would lead to good mobility while allowing the movement of the chains to be disrupted by the suspension, but not stopped altogether (trapping will be discussed at length in Chap. 4).

All the values of the parameters, both in reduced and real units, are reported in Table 2.3.

Values of the parameters used in the simulations with LAMMPS

Parameter	**LJ reduced units**	**Real units**
σ	1	2.5 nm
L_s	1.6	4 nm
L	500	1.25 μm
R_G	20 - 30	50-75 nm
λ	20	50 nm
$T = \frac{\varepsilon}{k_B}$	1	300 K
$\eta = \frac{\zeta}{3\pi\sigma}$	$\frac{1}{3\pi}$	$1 \cdot 10^{-3}\text{kg} \cdot \text{m}^{-1} \cdot \text{s}^{-1}$
$\tau_{LJ} = \tau_{Br} = \frac{m}{\zeta} = \sigma\sqrt{\frac{m}{\varepsilon}} = \frac{3\pi\eta\sigma^3}{k_bT}$	1	36 ns
dt	0.01	$3.6 \cdot 10^{-10}$ s
$F^{electric}$	0.001	$1.66 \cdot 10^{-3}$pN
L_{box}	200	500 nm

Table 2.3: Values of the parameters for the chains used in the simulations with LAMMPS.

Statistical-mechanics ensembles

In LAMMPS, the time integration can be performed so that it creates a system trajectory consistent with a specific statistical-mechanics state. This can be determined by fixing a specific parameter in the script. Among the most standard choices, we can have:

- *NVE*: the number of molecules, the volume and the energy are fixed. This corresponds to the microcanonical ensemble.
- *NVT*: the number of molecules, the volume and the temperature are fixed. This corresponds to the canonical ensemble.
- *NPT*: the number of molecules, the volume and the pressure are fixed (isothermal-isobaric ensemble).

– *NPH*: the number of molecules, the pressure and the enthalpy are fixed (isenthalpic ensemble).

Time integration

All of the simulations described in Chap. 4 were performed in the *NVE* (microcanonical) ensemble. This is used in conjunction with a Langevin thermostat to perform Brownian dynamics (LAMMPS documentation, 2019b).

The numerical integration is carried out through a velocity-Verlet integrator as described in Section 2.3.6, with timestep $dt = 0.01\tau_{LJ}$.

2.6 Initial configurations of the knotted molecules

The molecules in the simulations were created as knotted, and as the number of knots is infinitely large, a selection had to be made. All the knots with minimal crossing number up to six (unknot, 3_1, 4_1, 5_1, 5_2, 6_1, 6_2 and 6_3) were considered and, in addition to these, the 7_1, 8_1, 8_{19} and 9_1.

2.6.1 Methods

Two different ways were used to generate the initial configurations of the knotted chains.

Equations for torus knots

If available in a suitable form, we generate the starting configurations from the mathematical equations of the knots. Typically, (p, q)-torus knots (see Section 1.2.1) can be parametrised with the equations (adapted from, e.g., Soret and Ville (2015)):

$$\begin{cases} x = (\cos(q\phi) + 2) \cdot \cos(p\phi); \\ y = (\cos(q\phi) + 2) \cdot \sin(p\phi); \\ z = -\sin(q\phi), \end{cases} \tag{2.27}$$

where $0 < \phi < 2\pi$, and p and q as in Table 2.4

Although it is not a torus knot, the figure-of-eight (4_1) can be drawn through a similar three-dimensional parametric equation:

Knot	p	q
3_1	2	3
5_1	2	5
7_1	2	7
8_{19}	3	4
9_1	2	9

Table 2.4: Values of the parameters p and q for the torus knots used in the simulations.

$$\begin{cases} x = (\cos(2\phi) + 2) \cdot \cos(3\phi); \\ y = (\cos(2\phi) + 2) \cdot \sin(3\phi); \\ z = \sin(4\phi), \end{cases} \tag{2.28}$$

for $0 < \phi < 2\pi$.

If the chain is supposed to be made of N beads, in order to have a three-dimensional knot, it is sufficient to divide the interval $[0, 2\pi)$ into $N-1$ equal parts, take the value of ϕ at those points and substitute into the equation. When the strands in the resulting knots were found to be very close to each other, the z coordinate was expanded by a small amount (e.g. multiplied by 1.5), so as to give a more open configuration.

Afterwards, the coordinates of the points need to be resized in such a way as to have a total length which corresponds with the chain in the model.

The three-dimensional distances between the beads, that is, the springs, will be shorter than the corresponding one-dimensional segments in the parameter ϕ, and they will not be of uniform length, due to the different curvature around the various beads. For this reason, before starting the actual simulations, it is important to have a short transition time to let the chains assume a shape in equilibrium with themselves and with the surrounding medium. After this transition time, it is necessary to verify that the bonds have not broken and that the type of knot has not changed (see below Section 2.9.4).

An example of the three-dimensional parametric equation and a resulting knotted chain with 40 beads is shown in Fig. 2.5.

When used, the linear chain was created simply as the unknot, but with a missing bond.

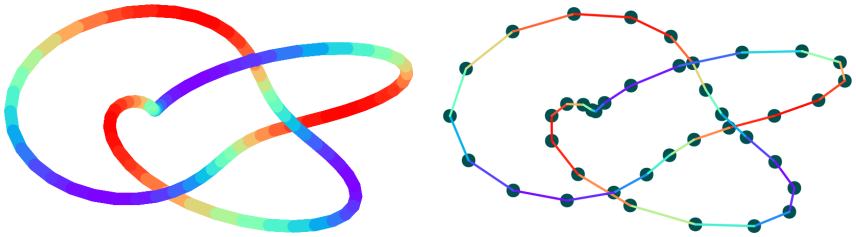

Figure 2.5: Starting configuration from the parametric equation for the trefoil (3_1) knot. Left: plot of the three dimensional equation. Right: resulting coordinates of the beads.

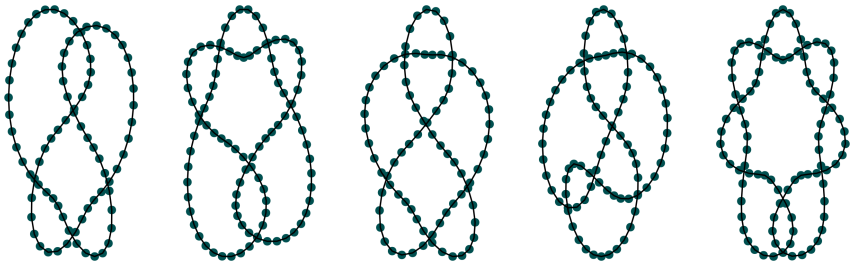

Figure 2.6: Example of initial configurations for some knots, 5_2, 6_1, 6_2, 6_3, 8_1, from coordinates available from The Knot Server (2003). The number of points has to be adapted according to the requirements of the specific simulation.

Knot server for other knots

If an equation for the knot is not available, it is possible to consider sets of points representing the knot taken from various freely-accessible sources on the Internet and adapt them for the number of beads considered. The sources utilised in this work are the Knot Server (The Knot Server, 2003) and a database of ideal knots (Cantarella, 2012) (for ideal knots, see Section 1.2.2). An example of configurations obtained from sets of points taken from the Knot Server is shown in Fig. 2.6

In order to adjust the number of points, if the number of beads in the starting knot exceeds the number of beads required, it is possible to simply select the coordinates for the correct number from the existing ones, taking care of doing so uniformly. If, on the contrary, the number of points is not sufficient, it is possible to add the coordinates of as many intermediate points as necessary and then uniformly select the required number. In practice, if we want to multiply the number of beads by M, we can create $M-1$ new sets of coordinates for every

Figure 2.7: Initial configurations for some torus knots: 0_1, 3_1, 5_1, 7_1, and 8_{19}. Top: the knots tied with 40 beads. Bottom: the same knots tied with 500 beads.

pair of existing, adjacent, points, by interpolation:

$$\begin{cases} x_j = x_i + \frac{j}{M}(x_{i+1} - x_i); \\ y_j = y_i + \frac{j}{M}(y_{i+1} - y_i); \\ z_j = z_i + \frac{j}{M}(z_{i+1} - z_i), \end{cases} \tag{2.29}$$

for $i = (1, \ldots, M-1)$.

Also in this case the distances will not be uniform, and an equilibration time and a subsequent check of the knot type will be necessary.

2.6.2 Example configurations

As an example of initial configurations used in this work, the torus knots up to 8 crossings generated with 40 beads and with 500 beads are shown in Fig. 2.7.

2.7 The suspension

Two different models of the suspension were tested in the simulations: a regular lattice of spheres of different size and stiffness for the minimal model in Chap. 3, and a series of randomly distributed hard spheres of fixed size for the model in Chap. 4.

2.7.1 Regular lattice

The porous medium considered for the minimal model in Chap. 3 is a network of spheres distributed on the vertices of a regular lattice with spacing 1 μm. It is worth noticing that this lattice spacing is small compared to the polymer contour length, and of the same order of magnitude as the excluded-volume size of the chain beads. Therefore the spheres are inside and around the chain, and interfere with the motion of the molecule. It may be easier to picture the network as a thick, permeating medium, rather than an external structure (Fig. 2.8).

The shape of the interaction due to the medium is the same as the excluded volume used for the beads of the polymer, but with parameters chosen as in Eq. 2.30 and depending on the radius R_{sphere} of the sphere we want to simulate. R_{sphere} will be determined by the density ρ of the medium, and will vary between 0 (no medium) and half the lattice spacing for $\rho = 1$.

$$\mathbf{F}_i^{\text{med}} = - \sum_{\text{all spheres}} A(R_{\text{sphere}})\, e^{-B \frac{|\mathbf{r}_i - \mathbf{r}_{\text{sphere}}|^2}{R_{\text{sphere}}^2}} (\mathbf{r}_i - \mathbf{r}_{\text{sphere}}) \tag{2.30}$$

where

$$A(R_{\text{sphere}}) = \frac{\sqrt{2}\, 3k_B T}{b_k} \cdot e^{1.5} \cdot \frac{h}{R_{\text{sphere}}} = 5.887 \cdot 10^{-13} \cdot \frac{h}{R_{\text{sphere}}}$$

and $B = 1.5$; with $R_{\text{sphere}} = 0.5 \cdot \rho \cdot c_l$; $c_l = 1\mu$m, lattice spacing; $\rho = \{0.0, 0.2, 0.4, 0.6, 0.8.1.0\}$.

The additional parameter, h, is used to tune the intensity of the force, as shown in Fig. 2.9. In our simulations, h takes the values $h = \{1.0, 2.5, 5.0, 10.0\}$.

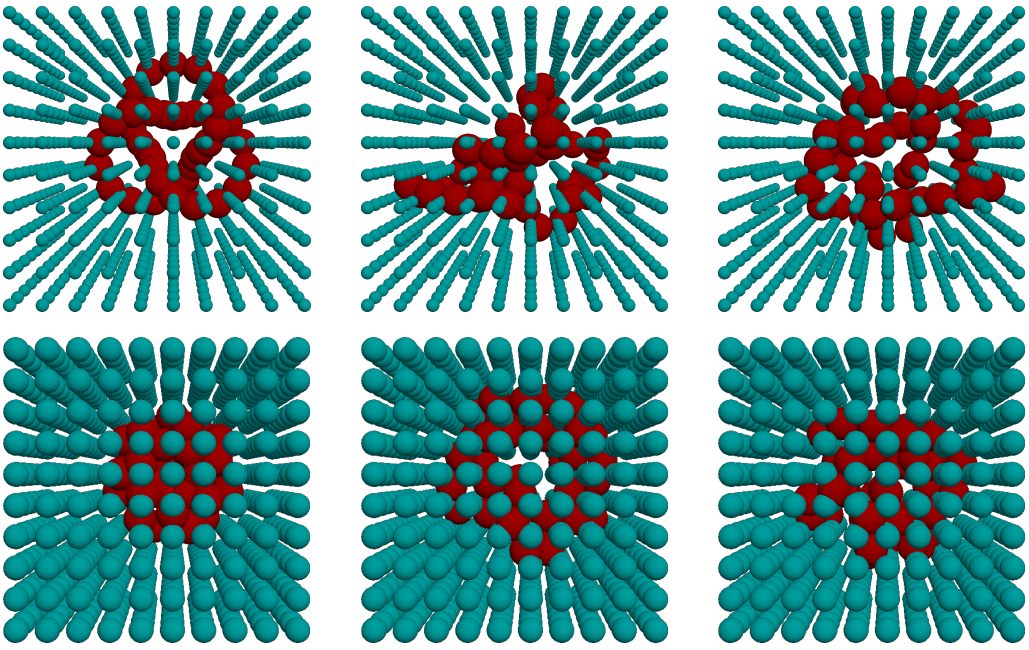

Figure 2.8: Schematic representation of two sample knotted chains immersed in the suspension during a simulation. From left to right, the shape at the beginning of the simulation, after 50 s and after 100 s. Top: a trefoil knot in a thin suspension. Bottom: a 7_1 knot in a thick suspension. The picture is for illustrative purpose only, as the spheres of the suspension are soft, that is, they do not have a well-defined surface that can be easily represented graphically.

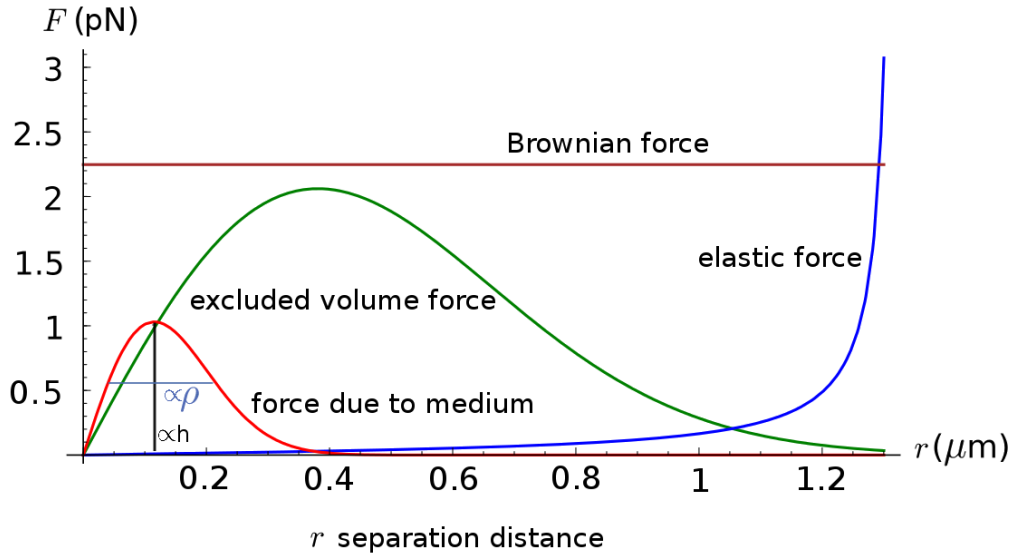

Figure 2.9: Graph of the forces applied to the beads, included (in bright red) the force due to the medium. Parameters h and ρ can be tuned to simulate media of different densities. In the picture, $h = 5$ and $\rho = 0.4$.

Values of the parameters for the force due to the medium in Eq. 2.30:

$$B = 1.5$$

$$A(R_{\text{sphere}}) = \frac{\sqrt{2}\,3k_BT}{b_k} \cdot e^{1.5} \cdot \frac{h}{R_{\text{sphere}}} = 5.887 \cdot 10^{-13} \cdot \frac{h}{R_{\text{sphere}}}$$

where

$R_{\text{sphere}} = 0.5 \cdot \rho \cdot c_l$

$c_l = 10^{-6}$ m, lattice spacing

$\rho = \{0.0, 0.2, 0.4, 0.6, 0.8.1.0\}$

$h = \{1.0, 2.5, 5.0, 10.0\}$

Table 2.5: Values of the parameters for the force due to the medium used in the simulations for the minimal model.

2.7.2 Randomly-distributed spheres

The suspension in the model simulated with LAMMPS in Chap. 4 is a set of 100 hard spheres of diameter $D = 30\sigma$ generated randomly in a cubic simulation box with side $L = 200\sigma$. The size of a sphere is comparable with the radius of gyration of the molecules as this is between 20 and 30 σ, depending on the type of knot. The size of the box is much larger than both the spheres and the knotted chains.

Two sets of otherwise equivalent simulations were performed. In one, the

spheres are generated randomly and, after a short time in which the system reaches a suitable configuration, that is with no overlapping of spheres between each other or with the beads, the spheres are kept fixed for the entire duration of the simulation. In the second set of simulations, the spheres are always able to move in random directions due to thermal motion.

The parameters of the suspension are summarised in Table 2.6.

Size of the simulation box:	200σ
Number of spheres in the box:	100
Diameter of the spheres:	30σ
Mass of a sphere:	$m_S = 10$
Damping factor for the spheres:	$\gamma_S = 0.03333$
Volume occupied by the spheres:	$\frac{4}{3}\pi(15\sigma)^3 \cdot 100 = 1.41 \cdot 10^6\sigma^3 = 17.7\%$ of the box
Average space between spheres:	$\left(\frac{200^3}{100}\right)^{\frac{1}{3}} - 30 = 13.1$

Table 2.6: Characteristics of the suspension used in the simulations in Chap. 4. Sizes are given in Lennard-Jones units.

2.8 Simulation setup

2.8.1 Minimal model

We generate the starting configuration of the chains as described in Section 2.6.1.

We then compute the motion of the beads step by step, by integrating the Langevin equation 2.13 with the Euler method (Section 2.3.6).

Each combination of type of knot, electric field and suspension is run for 10^8 timesteps, with the timestep being $dt = 10^{-5}$s, that is, for a total 1000 s. For the first 0.5 s, only the elastic and excluded-volume forces are active, to allow the beads of the polymer to reach an equilibrium position, as explained above in Section 2.6.1; the random force is then activated for a further 0.5 s. After this time, the electric force is switched on and the dynamics are simulated for the rest of the simulation time.

The knot type is checked at the beginning of the simulation, after a third and two thirds of the time steps, and at the end, using Knot ID analysis tools (Taylor and other SPOCK contributors, 2017) in case of chain crossings. If the knot type has changed, we discard the data.

The results are analysed as described below in Section 2.9.1 and discussed in Chap. 3.

2.8.2 Longer molecules with LAMMPS

The system is created and run in LAMMPS according to the scripts described below in Section 2.10.2. The integration of the equation of motion for the beads is performed according to the choice of potentials and parameters set up in the script.

In each simulation, four knotted molecules are pushed through a random-sphere suspension by a fixed force for 1–2 $\cdot 10^8$ time steps. The topology of the knotted molecules is checked at the end of the preparation run and at the end of the actual longer run to verify that the knot type has not changed. The results are written by the software as a series of coordinates of both the beads of the chains and the suspension spheres, with a frequency determined in the script. The same data is also saved in one file formatted so as to be viewed in VMD as a video of the simulation. A sample snapshot from one such video is shown in Fig. 2.10.

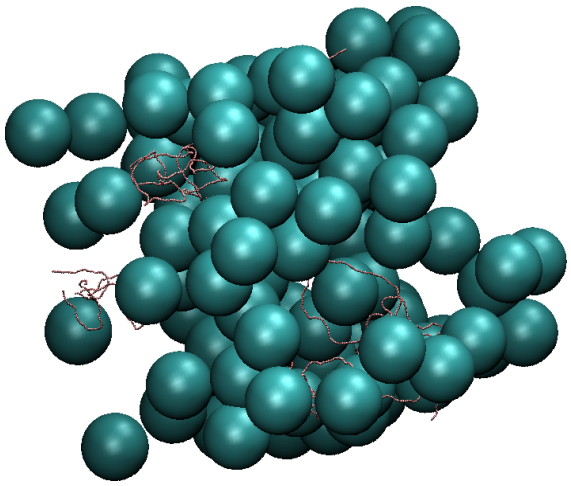

Figure 2.10: Snapshot of a typical simulation with random spheres.

2.8.3 Knotted blends with LAMMPS

The simulations for the systems described in Chap. 5 are performed in LAMMPS with similar parameters to the simulations in Chap. 4 described above. The main differences are the absence of the spheres modelling a gel, the absence of a driving force and the presence of a large number of molecules in a smaller cubic box, as the aim is to have a dense system of chains interacting with each

other.

The system is, again, described in terms of Lennard-Jones units and is prepared in the following way.

In a cubic box with side of 100 σ, two knotted molecules are generated as described in Section 2.6.1. These can be made of either 500 or 250 beads each and they will be one unknot and one 9_1. The box is then duplicated and resized several times in the three spatial directions until there are 128 molecules in the case of 500 beads per molecule, or 256 molecules in the case of 250 beads per molecule. This means a total of 64000 beads in both cases. The final box can be set to the required size as explained in Chap. 5. As before, the boundary conditions are set to be periodic.

2.9 Data Analysis

The main quantity that is analysed in all the simulations is the displacement of the centre of mass of the molecules.

The results in Chap. 3 are given in terms of the time-averaged displacement, as calculated on one long simulation run per set of parameters.

The results in Chap. 4 are given as an average over 4 knots per simulation in 28 separate simulations per set of parameters. The values of the average crossing numbers of the ideal configurations of knots used as the x axis to plot the values have been taken from Stasiak et al. (1998).

2.9.1 Time-averaged MSD

The simulations performed for the minimal model in Chap. 3 were analysed in terms of time-averaged MSD.

For each 1000-s simulation, we discard the first 10 seconds in order to ignore any transient behaviour, and we compute the time-averaged root-mean-squared (RMS) displacement of the center of mass versus time.

This corresponds to a single-particle tracking as first described by Perrin (Perrin, 1908) and Nordlund (Nordlund, 1914).

The recorded time series $x'(t)$ is evaluated in terms of the time-averaged MSD:

$$\langle x^2(\Delta)\rangle = \frac{1}{t-\Delta}\int_0^{t-\Delta}[x(t'+\Delta)-x(t')]^2\mathrm{d}t' \tag{2.31}$$

This average is computed over multiple time origins, with Δ taking values of multiples of 10^{-1} s. It has to be noted that these displacements are overlapping for any $\Delta = n \cdot 10^{-1}$ s with $n > 1$, and, as a consequence, they are not statistically independent.

2.9.2 Shape of the polymers

It is possible to qualitatively examine the shape of the polymers during a simulation by saving the configuration of the beads at regular intervals and visualise the resulting snapshot or video with the molecular dynamics viewer VMD (Humphrey et al. (1996)).

In order to have a more quantitative understanding, the radius of gyration of the molecules has been analysed. The square radius of gyration can be calculated as follows (also see Section 1.3.1):

$$R_G^2 = \frac{1}{N_{\text{beads}}} \sum_{m=1}^{N_{\text{beads}}} \langle (x_m - x_{CM})^2 + (y_m - y_{CM})^2 + (z_m - z_{CM})^2 \rangle, \tag{2.32}$$

which highlight the contributions due to the three orthogonal directions. These can be isolated by calculating, for example in the direction Z:

$$(R_G^2)_Z = \frac{1}{N_{\text{beads}}} \sum_{m=1}^{N_{\text{beads}}} \langle (z_m - z_{CM})^2 \rangle. \tag{2.33}$$

If a big proportion of the value of R_G^2 is due to $(R_G^2)_Z$, by definition this means that the chain is elongated in the Z direction.

Therefore, the component of the radius of gyration due to the directions parallel and perpendicular to the electric field have been measured and the results are shown and discussed in Sections 3.4.1 and 4.2.

2.9.3 Curvature of the molecules

A characteristic that depends on the knot type and may affect the mobility of the chains is its rigidity. As explained in Section 2.5.1, in the case of the minimal model in Chap. 3, 40 beads was chosen as the minimal number of beads that would allow the chains to be tied in knots up to 9 crossings and still ensure some flexibility. However, in spite of not having any bending rigidity, more complex knots tend to be more rigid simply due to excluded volume reasons (see Fig. 2.11 for an example), and this may play a role in the dynamics of the system. As a quantity related to this kind of stiffness, the total curvature of the chains was

analysed. This is defined as the sum of all the angles between adjacent beads, for different numbers of beads N (Fig. 2.12):

$$\text{Total curvature} = \sum_{i=1}^{N} \theta_i = \sum_{i=1}^{N} \arccos\left[\frac{\mathbf{r}_i \cdot \mathbf{r}_{i+1}}{|\mathbf{r}_i| \cdot |\mathbf{r}_{i+1}|}\right] \tag{2.34}$$

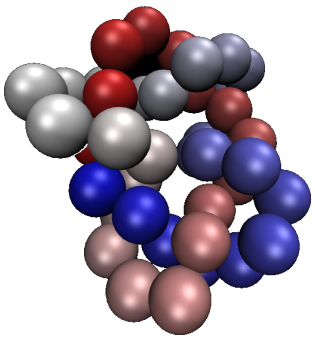

Figure 2.11: Example of a complex knot (a 7_1) tied with 40 beads.

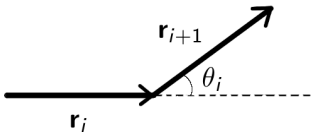

Figure 2.12: Angles used to calculate the total curvature of the chains.

This is particularly important for short molecules with relatively large beads, as in the minimal model in Chap. 3. The values of the curvature in this case is reported and analysed in the corresponding chapter.

2.9.4 Knot type

The knot type is analysed regularly during the simulations and at the end, as it is essential that the polymers under study maintain the topology at all time. The programs used to that aim are The Knot ID analysis tools (Taylor and other SPOCK contributors, 2017) for the simulations in Chap. 3 and the program KymoKnot (Tubiana et al., 2018, 2011b,a) for the simulations in Chapters 4 and Section 5.

2.9.5 LAMMPS simulations

Multiple simulations of the same system were performed with the scripts described below (Section 2.10.2). The trajectories and other quantities, such as the radius of gyration of the molecules, were analysed separately and the velocities subsequently averaged as explained in Section 2.10.2. The results for the different systems were then compared as discussed in Chap. 4.

2.10 Software

2.10.1 Outline of C-code function for the minimal model

The program used for the simulation of the minimal model in Chap. 3 is called "knotInSuspension.c". This was developed *ad hoc* for the simulations of the minimal model described earlier in this chapter and whose results are discussed in Chap. 3. This program is run in the command line where the parameters of the different simulations can be set. In particular, the combination of type of knot, electric force and the two parameters ρ and h defining the suspension change for each run.

The program creates the required knot as explained in Section 2.6 and a cubic box with sides measuring 10 μm and occupied by a regular lattice of 10 by 10 by 10 points which represent the centres of the spheres composing the medium. At every time step, the integration is performed with the Euler method with forces calculated as seen in Section 2.5.1.

A random-number generator is needed to provide a series of values for the coordinates of each $\mathbf{n}_i$ in the expression of the force $\mathbf{F}_i^{\text{rand}}$ in Eq. 2.11. The random-number generator used in this program is an implementation of the *Mersenne Twister* (Matsumoto and Nishimura, 1998), together with the method by Marsaglia (Marsaglia, 1972) for sampling on the surface of a sphere.

At regular intervals, as determined by the user, the software writes a set of files with the quantities of interest, including the coordinates of the center of mass, the radius of gyration and a file with the coordinates of all the beads that can be visualised in VMD.

Analysis scripts and programs

For each simulation, the coordinates of the centre of mass of the molecule are used to calculate the time-averaged MSD. This is done by another ad-hoc

program written in C. The resulting data is then plotted in *gnuplot* (Williams et al., 1986 – present).

In order to give the mobility of the chain in function of the topology, for a fixed combination of E, ρ and h, the value at particular fixed times is extracted and plotted against the ACN of the knot.

2.10.2 Outline of LAMMPS scripts for longer molecules

The simulations with LAMMPS were run in two phases. In the first script, called "crowdersPrep.lam", the initial configuration is generated, while the actual run is performed in the second script, called "crowdersRun.lam".

For every type of knot, 28 different starting configurations are created and then simulated. Every configuration includes four knotted molecules (with the same knot type) and a set of suspension spheres.

The simulations were performed with the version of LAMMPS released on 17th August 2017. For each type of knot, the respective 28 processes are run in parallel through the MPI technology.

Preparation run

Initially, a knotted molecule is generated as described in Section 2.6.1 and resized to be made up of 500 beads, with bead separation of approximately σ. This chain is then loaded in LAMMPS, duplicated twice and the four molecules are placed in the top section of a rectangular box of size 200 by 200 by 300 σ.

At this point, 100 spheres (crowders) are generated randomly in the lower part of the box so as to only occupy an area of size 200 by 200 by 200 below the region where the knotted chains are located. These spheres are initially created small and associated with a soft potential. The radius and the rigidity of the spheres are then gradually increased while they are allowed to change position due to the presence of the other spheres and thermal motion, but they are not allowed to access the area where the chains are. At the end of this process, the crowders are non-overlapping Lennard-Jones hard spheres.

Finally, the chains are pulled downwards by a force and enter the area where the crowders are. The box is then resized to a cubic box of size 200 by 200 by 200 and the system is left to equilibrate for 10^5 time steps. The final configuration is saved into a file which is then used for the actual run with the second script.

Actual run

The second script loads the final configuration from the first one and allows the system to relax for a further 50000 time steps.

After this, in half the simulations the spheres are left free to move due to thermal motion, while in the other half the spheres are kept fixed from this point onwards.

Finally, a constant pulling force, which in the following will be denoted with E, is added and the simulation is performed for either $1 \cdot 10^8$ or $2 \cdot 10^8$ time steps.

Each simulation saves both a series of files with the coordinates of each bead and suspension sphere and one large file with similar information in a format that can be opened in VMD and visualized as a video of the motion.

Analysis scripts and programs

The files with the coordinates are loaded in a script and then analysed one by one with a C++ program initially developed by Davide Michieletto and his colleagues at the University of Edinburgh, and subsequently modified for the simulations in this work. The output is the trajectory and the value of the radius of gyration of each molecule. The former is then loaded in the mathematical and graphing utility *gnuplot* (Williams et al., 1986 – present) through a script that calculates the velocities, their average and standard error for each given type of molecule, and, finally, draws a graph of comparison of the results for all the knots.

2.10.3 Hardware and run times

The simulations were performed on the supercomputer owned by the University of Bristol called BlueCrystal, currently in its fourth incarnation as BlueCrystal Phase 4.

The Linux login nodes allow the users to run jobs on the compute nodes through the Slurm job scheduler. There are 525 Lenovo nx360 m5 compute nodes available, each with two 14 core 2.4 GHz Intel E5-2680 v4 (Broadwell) CPUs, and 128 GiB of RAM. Extra RAM and GPUs are available, but they were not used for the simulations in this thesis.

Typically the simulations performed for this thesis with LAMMPS were run in parallel on 28 processors (corresponding to 1 compute node) and required 500–1000 MB of RAM per processor. Their duration varied between a few days

and two weeks, depending on the length of the molecules simulated and the number of timesteps.

The simulations performed with my own code in C run on a single processor each, with a duration of approximately three days per run.

3 A minimal model for knotted polymers in a suspension

3.1 Introduction

As we saw in Section 1.5, the most wide-spread laboratory tool used to separate different kinds of knotted DNA molecules is agarose-gel electrophoresis. In typical laboratory conditions, the mobility of knotted DNA molecules passing through a gel is, with very good approximation, linearly dependent on the ACN of the knot, as long as the lengths of the knotted DNA strands are the same. This is hardly surprising, as we have seen (Section 1.2.2) that the ACN can be considered as a measure of the compactness of the knot and it is not particularly remarkable that, all other parameters being the same, a smaller knot may experience less friction from the surrounding gel.

However, as we saw in Section 1.6.1, experiments (Sogo et al., 1999; Trigueros et al., 2001) have shown that when the system is put under a strain, with a higher-density gel and a stronger electric field, the relation between ACN and mobility is no longer linear: something else must take place, a different process that is at least as important as the compactness of the molecules and depends on the type of knot in a different way. Interestingly, in spite of various efforts, a definitive explanation of this behaviour has not yet been found, which indicates that the mechanisms underlying this technique are not yet fully understood.

In this context, as we saw in Section 1.7, modelling a possible structure for the gel matrix and testing specific assumptions in silico is proving very effective in helping understand the physical problem and has given good results in specific conditions.

Inspired by this question, I have been looking at a simpler structure, a class of "toy models", for a polymer moving through a series of obstacles. I aim to represent the minimal model for the chain, and a very simple range

of media, consisting of small spheres positioned at the vertices of a regular three-dimensional cubic lattice, with different densities. By keeping the model simple, and comparing the results for different knot types, all other parameters for the chain being kept fixed, I want to assess the role of the topology in the diffusion rate of the chain in the different media.

To this aim, I preset numerical results from simulations performed by means of an ad-hoc code written in the C programming language. As this is a basic model, the physical parameters used in my simulations do not claim to represent real DNA molecules, as the thickness of the chains is not compatible with actual DNA, and the length is not as typically used in experiments. However, we will see that even with molecules of this kind and a simple medium consisting of spheres on the vertices of a regular lattice, the mobility of the chain is still affected by its topology. In particular, we show that in the absence of a driving force more complex knots tend to move more slowly than simpler knots, while the opposite is true when a constant force is applied to each bead in the chain.

In this chapter, I also describe the particular characteristics of the diffusion of the chains in this model, and I compare this model with the previous work by the other groups as mentioned in Section 1.7 and with laboratory experiments of agarose-gel electrophoresis (Section 1.6).

3.2 Results

The techniques used to perform these simulations have been explained at length in Chap. 2.

As we saw in Section 2.5.1, the chains are made of 40 beads and they are constructed closed and knotted with different knot types up to a Minimal Crossing Number (MCN) of 9.

The suspension is a regular lattice of spheres with lattice spacing small compared to the size of the molecules. All the excluded-volume forces are soft, therefore the dimensions of the spheres are indicative as these are not impenetrable. Two parameters characterize the suspension: the density of the spheres, indicated by the symbol ρ, which varies between 0 and 1, and a parameter h that will be called “firmness”, which is a multiplying constant in the excluded-volume force associated with the spheres and expresses how strong the repulsion is. The parameter h takes the values 1, 2.5, 5 and 10, and its meaning can be better understood by looking at Fig. 2.9 in the previous chapter.

I single out and describe the results for a particular value of the parameter h, that is, $h = 1$, which corresponds to a soft perturbation of the medium. The motion of the chains is affected by this obstruction, but the beads can still overcome it and pass through.

I subsequently describe the effect of increasing the value of the parameter h, up to the value $h = 10$, which corresponds to making the spheres harder and harder to get past.

As noted in Section 1.3.3, for thick media, we found that, as expected, the chains exhibit anomalous diffusion. In order to be able to compare results for different regimes, we chose to consider the value of the displacement after 10 seconds for all simulations (1 second in the absence of an electric field) and we plot it against the ACN of the ideal representation (Section 1.2.2) for each knot type.

3.2.1 Mobility for $h = 1$ (lesser firmness)

In this section I show the results for firmness $h = 1$ at different values of the density ρ, plotted against the ACN of the knots, for different values of the external field $E = \{0, 0.25, 0.75, 1.5\}$ V/cm. The forces in this system are as shown in Fig. 3.1.

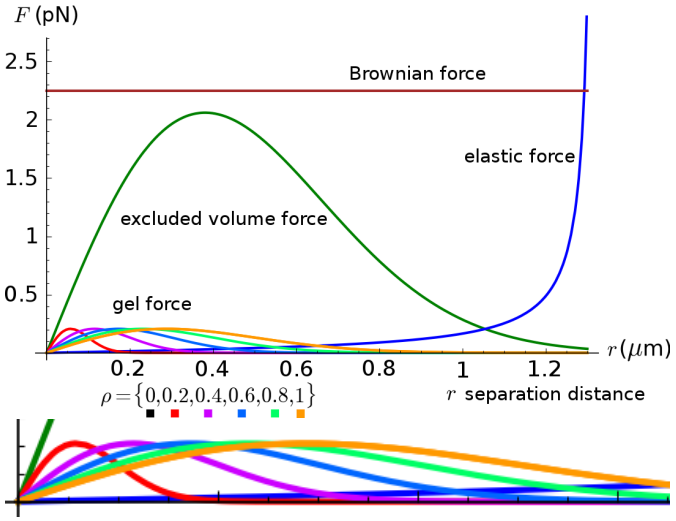

Figure 3.1: Graph of the forces applied to the beads, included (in various colours) the force due to the medium. Parameter $h = 1$ (representing the firmness) is fixed (soft perturbation), while the density ρ is tuned to simulate media of different densities.

As we can see in Fig. 3.2 top left which shows the motion in the absence of an electric field, the mobility of the chains depends on the presence of the suspension. In this case the motion of the polymers is due simply to the diffusion through the medium and we expect the Mean Squared Displacement (MSD) of the centre of mass of the chain to be linear with time. This is confirmed by my analysis as described in Section 3.3.1. As we are considering the time-averaged value of the MSD of a Brownian motion, the statistics are only good for a short time span, while becoming very noisy after a few seconds. For this reason, and only in the case of $E = 0$, we consider the value of the MSD after only 1 second, as opposed to 10 seconds in the presence of an electric field. We can see that in the absence of a suspension ($\rho = 0$, black points) or when the density is very low ($\rho = 0.2$, red points), all the knot types move at approximately the same speed and, unsurprisingly, faster than for higher densities. In particular, it is important to notice that no particular trend emerges and the mobility is independent of the knot type. In fact, the differences in the mobilities can be ascribed to random noise. This behaviour is as expected, as we are neglecting hydrodynamic interactions and in this case, according to the Rouse model (Section 2.4.1), the diffusion should only depend on the number of beads, which is common to all the chains. On the contrary, we can see that as the density of the suspension increases ($\rho = \{0.6, 0.8, 1.0\}$, green, blue and magenta points), the overall speed decreases accordingly and, most interestingly, a clear trend emerges: more complex knots tend to move more slowly than simpler knots.

In Fig. 3.2 top right, we can see what happens when we switch on a small electric field $E = 0.25$ V/cm. In this case the motion is no longer due simply to random motion and we have a linear displacement with time. In addition, the statistics are good for a longer period of time, so we consider the value of the RMS after 10 seconds, instead of just 1 s as we did in the previous case. For $E = 0.25$ V/cm the overall velocity increases, but when the density of the suspension is zero ($\rho = 0$, black points) or when it is very low ($\rho = 0.2$, red points), we still have that all the knot types move at approximately the same speed. Similarly to what happened for the diffusion in the absence of a field, as the density increases all the knots tend to move more slowly and the more complex types tend to lag behind the simpler ones.

In Fig. 3.2 bottom left, we increase the electric field to $E = 0.75$ V/cm. The electric field is three times as strong as the previous case, so, in general, as we

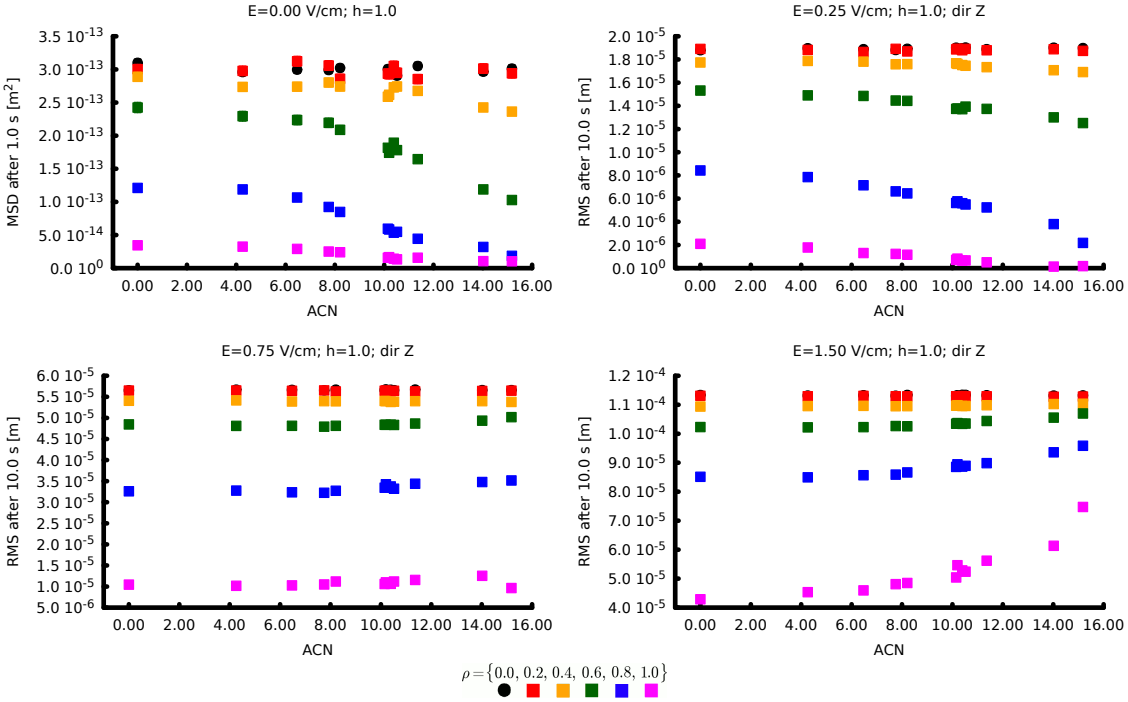

Figure 3.2: MSD or RMS displacement after 1 or 10 seconds for different knot types in gels of increasing densities at a fixed value of the firmness $h = 1$. Top left: no external electric field. For sufficiently dense suspensions the MSD decreases with the ACN. Top right: $E = 0.25$ V/cm. The trend is similar to that in the absence of a field. Bottom left: $E = 0.75$ V/cm. The different knot types move approximately at the same speed. Bottom right: $E = 1.5$ V/cm. More complex knots move faster than simpler knots.

expected, the chains move three times as fast. We notice, though, that the trend associated with the knot type has disappeared, and now all chains in the same suspension move approximately at the same speed, regardless of the topology.

Finally, in Fig. 3.2 bottom right, the electric field is further increased to $E = 1.5$ V/cm. Again, the electric field is twice as strong as the previous case so, unremarkably, when no suspension is present, all knot types move at approximately the same speed and twice as fast as the previous case. However, as the suspension gets thicker, we can observe a new trend emerging: more complex knots move faster than simpler ones. This is unexpected, as we have an inversion with respect to the behaviour we saw for low electric field or no field at all. This new trend is particularly noticeable for the higher values of the density, $\rho = \{0.8, 1.0\}$ (blue and magenta points in the picture).

As a note on the errorbars in the graphs of the mobility presented in this chapter, we saw in Section 2.9 that these data are the result of time-averaging

over a single trajectory. That is, I have one data point per each combination of the parameters (E, h, ρ and type of knot). In order to assess the error, in one case per each value of E I repeated the simulation 10 times with the same parameters (medium-thickness gel, six-crossing knot) and the value of the standard deviation has been used, as percent error, to calculate the errorbars. In practically all cases, the resulting errorbars are smaller than the size of the squares used in the graphs. This choice is certainly not perfect, and for example does not reflect the higher variability in the case of very thin gel or no gel at all.

3.2.2 Mobility for all considered values of the electric field and the firmness h

Before speculating about the reasons for this unexpected behaviour. I review the results for other parameter combinations. That is, I now show my results for $E = \{0, 0.12, 0.25, 0.50, 0.75, 1.00, 1.50\}$ V/cm and all the values of the firmness h that have been used in the simulations: $h = \{1, 2.5, 5, 10\}$. On the whole, we can see that in all cases the trends are compatible with the discussion for $h = 1$.

Mobility without electric field ($E = 0$ V/cm)

By comparing the outcome of our simulations for different values of the firmness h, as shown in Fig. 3.3, we can see that in all cases the effect of a small perturbation ($\rho = 0.2$, red points) is negligible and the motion is approximately the same for all knot types. As we increase the density, we can see that the value of the firmness h starts to be important as well. For the same value of the density ρ, higher values of the firmness h cause the polymers to move more slowly, and this is particularly visible in the cases $\rho = \{0.6, 0.8, 1.0\}$ (green, blue and magenta). In particular, for high values of both h and ρ (e.g. $h = 10$ and $\rho = 1.0$), the motion is impeded to a great extent and the polymers hardly move at all.

In all cases, however, the trend is compatible with what we saw in the previous section for $h = 1$; that is, for sufficiently dense suspensions, more complex knots move more slowly than simpler knots.

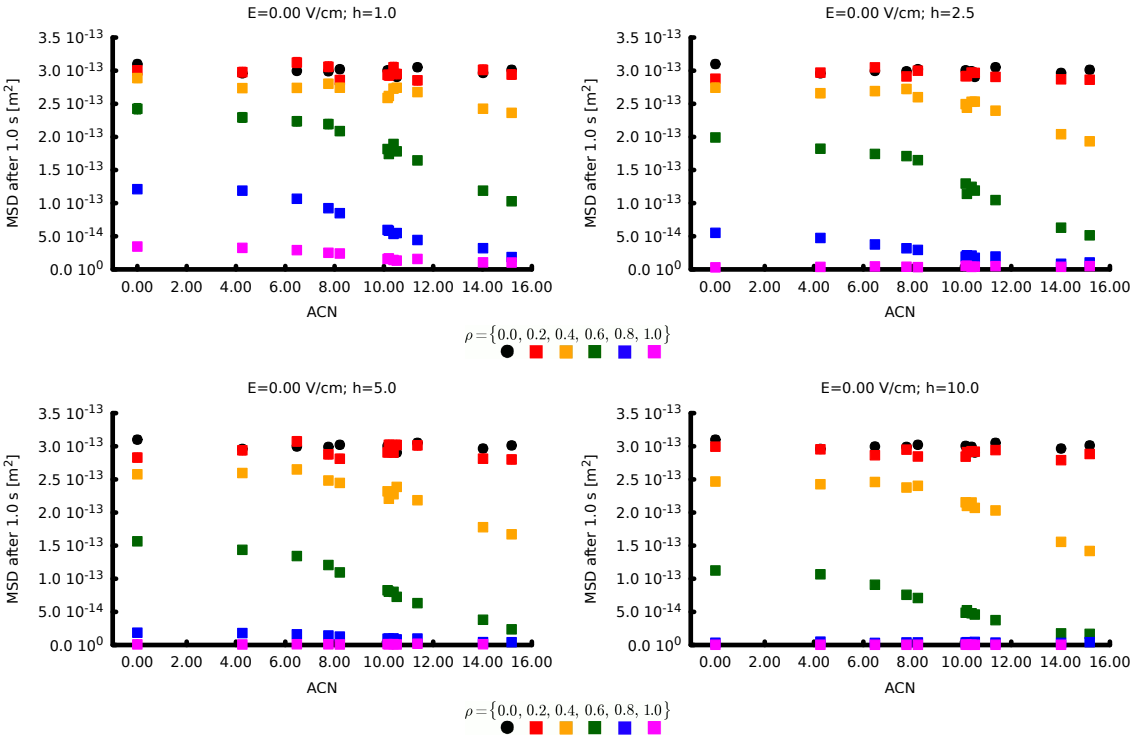

Figure 3.3: Mobility of the knotted chains as a function of the ACN for $E = 0$ V/cm and all values of the firmness h. More complex knots travel more slowly than simpler knots, and the effect is greater for larger values of the density ρ.

Mobility with low electric field ($E = 0.12$ and $E = 0.25$ V/cm)

If we apply a low electric field, we can see that all the chains start to move in the same direction as the field. The values of the time averaged RMS are shown in Fig. 3.4 for $E = 0.12$ V/cm and in Fig. 3.5 for $E = 0.25$ V/cm.

The trend is still the same as the case without electric field, that is, more complex knots travel more slowly than simpler knots, and the effect is greater for larger values of the density ρ.

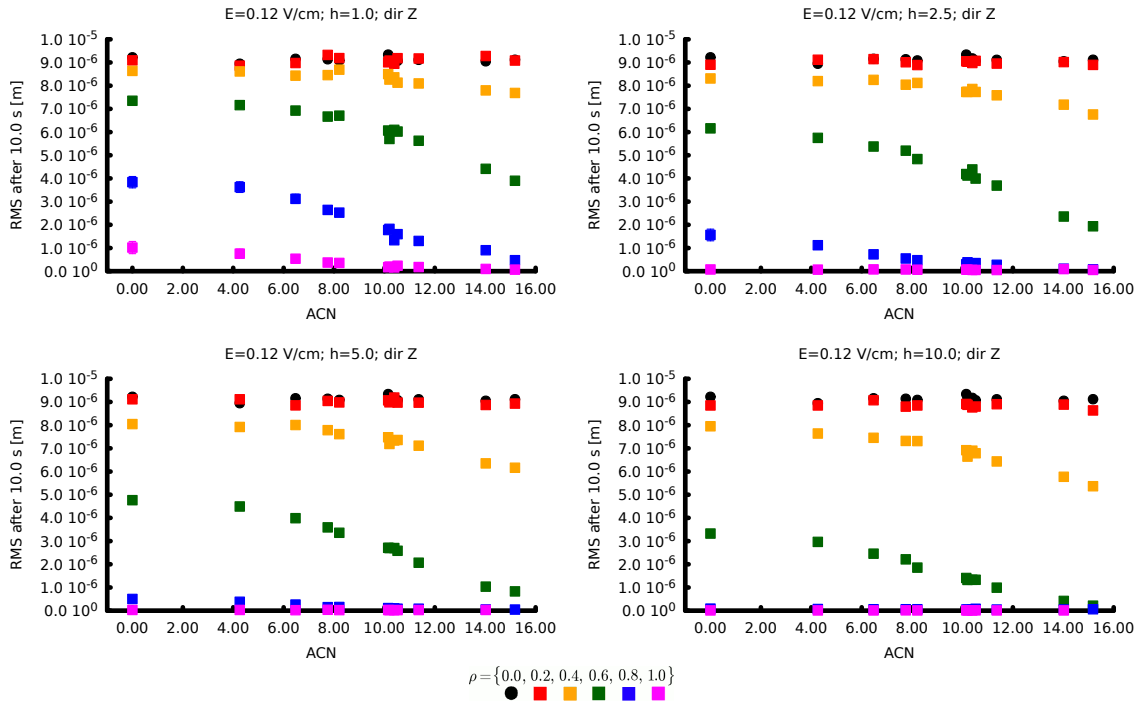

Figure 3.4: Mobility of the knotted chains as a function of the ACN for $E = 0.12$ V/cm and all values of the firmness h. Like for $E = 0$ V/cm, more complex knots travel more slowly than simpler knots, and the effect is greater for larger values of the density ρ.

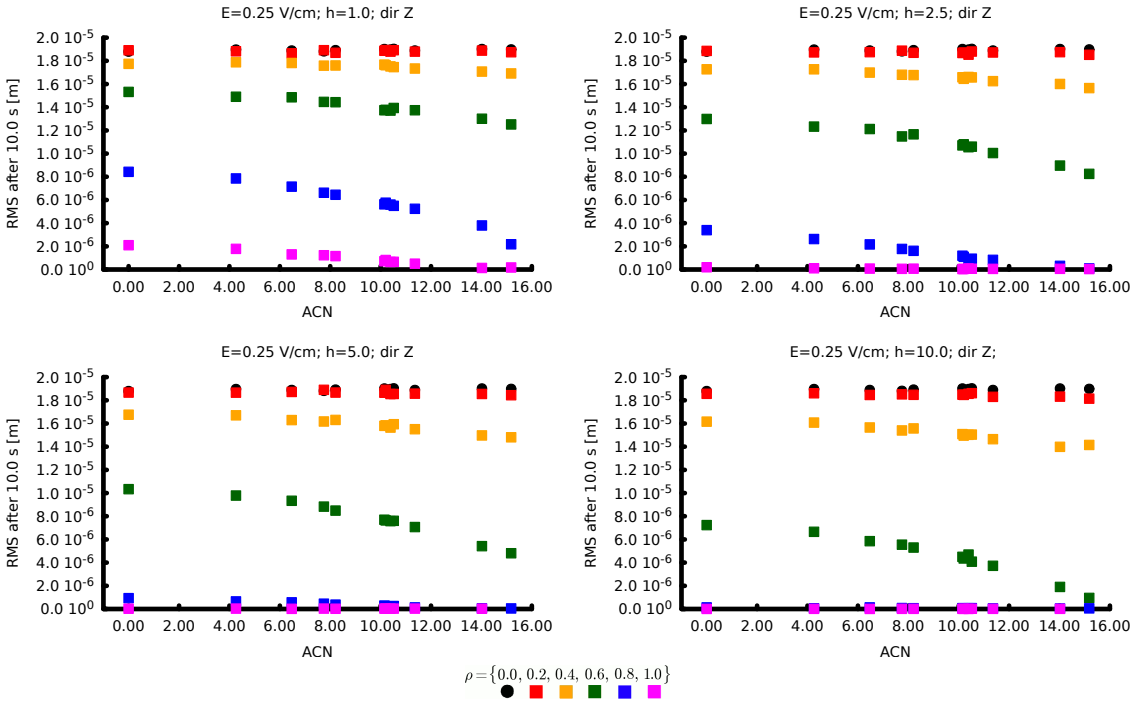

Figure 3.5: Mobility of the knotted chains as a function of the ACN for $E = 0.25$ V/cm and all values of the firmness h. Like for $E = 0$ and $E = 0.12$ V/cm, more complex knots travel more slowly than simpler knots, and the effect is greater for larger values of the density ρ.

Mobility with moderate electric field ($E = 0.50$ and $E = 0.75$ V/cm)

As we can see in Figures 3.6 and 3.7, for a moderate value of the electric field ($E = 0.50$ and $E = 0.75$ V/cm) all the chains move faster as expected. The effect of increasing the firmness h becomes even more evident. In fact, for sufficiently large density ρ the polymers are more and more delayed as the firmness h increases, to the point that for $\rho = 1.0$ (magenta points) they are essentially stuck for any value of $h > 1$. The effect is increasingly important also for $\rho = 0.6$ and $\rho = 0.8$ (green and blue), as the chains manage to travel shorter distances for higher values of the firmness h. As we have seen in Section 3.2.1 for $h = 1$, the trend with respect to the Average Crossing Number (ACN), that is, the complexity of the knot, at these values of E seems to have been lost.

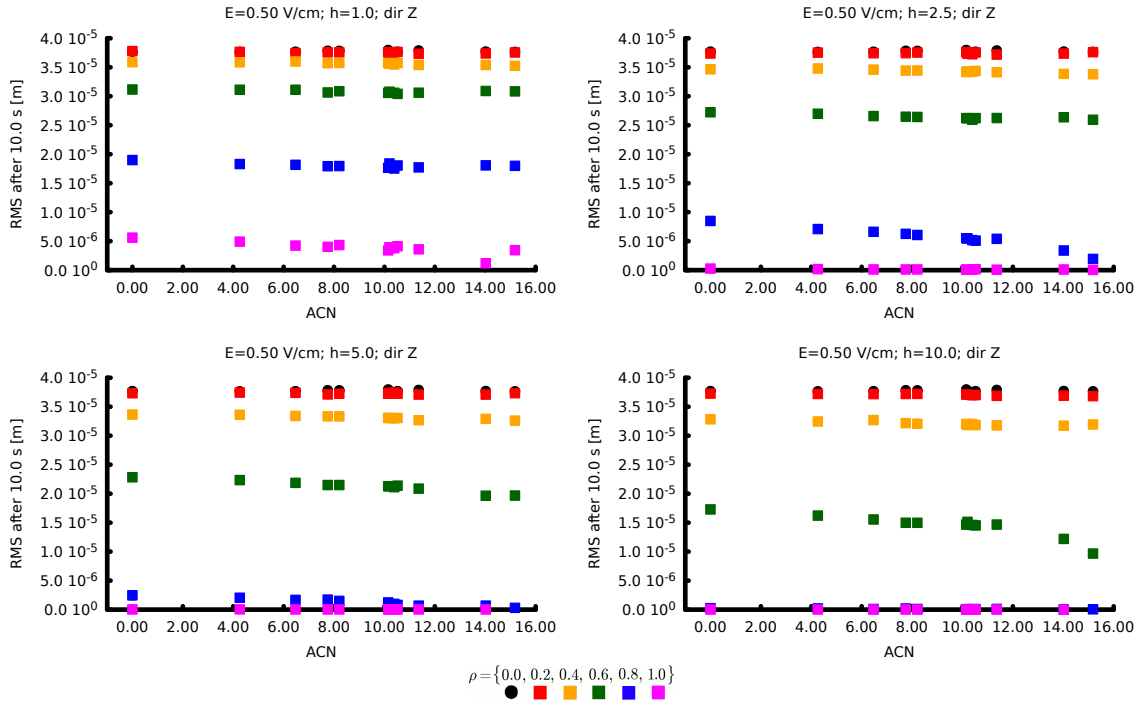

Figure 3.6: Mobility of the knotted chains as a function of the ACN for $E = 0.50$ V/cm and all values of the firmness h. Like for less strong electric fields, more complex knots seem to travel more slowly than simpler knots. However, this trend is very small.

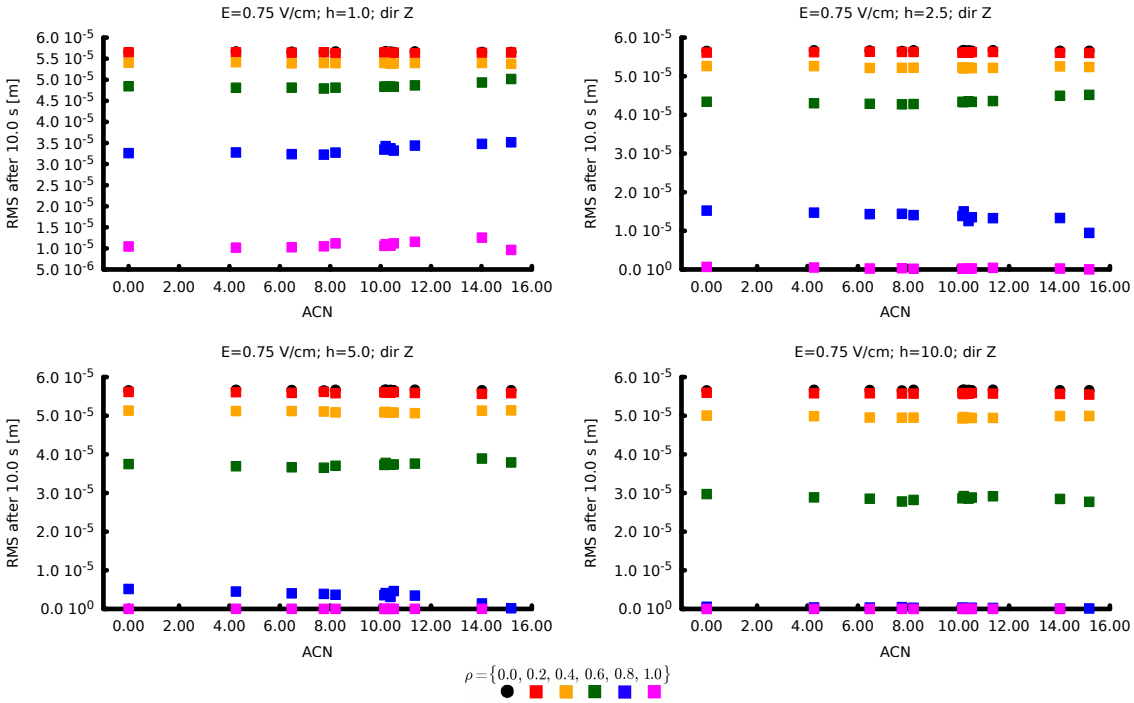

Figure 3.7: Mobility of the knotted chains as a function of the ACN for $E = 0.75$ V/cm and all values of the firmness h. At this value of the field, there does not seem to be a recognisable trend with respect to the type of knot.

Mobility with strong electric field ($E = 1.00$ and $E = 1.5$ V/cm)

The results for higher values of the electric field ($E = 1.0$ and $E = 1.5$ V/cm) are shown in Fig. 3.8 and Fig. 3.9. In these cases, the polymers travel considerably longer distances in general, and for this reason it is more difficult to see a small difference in the various speeds. However, when a trend is recognisable (e.g. for $h = 5$ and $\rho = 0.6$), it is compatible with the examined case of $h = 1$, that is, more complex knots move faster than simpler ones.

As before, the effect of having higher values of the firmness h is to delay the motion of the chains, especially for higher values of the density ρ, to the point that at the highest value of ρ, the polymers are hardly moving at all.

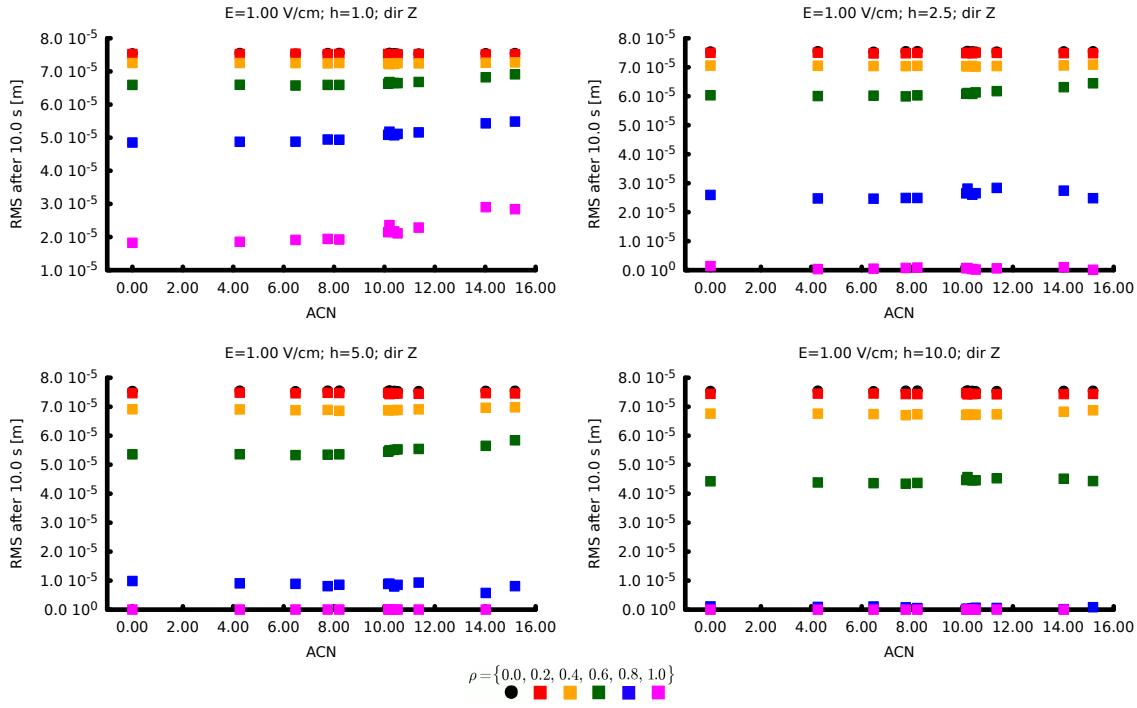

Figure 3.8: Mobility of the knotted chains as a function of the ACN for $E = 1.00$ V/cm and all values of the firmness h. When a trend is recognisable, more complex knots move faster than simpler ones.

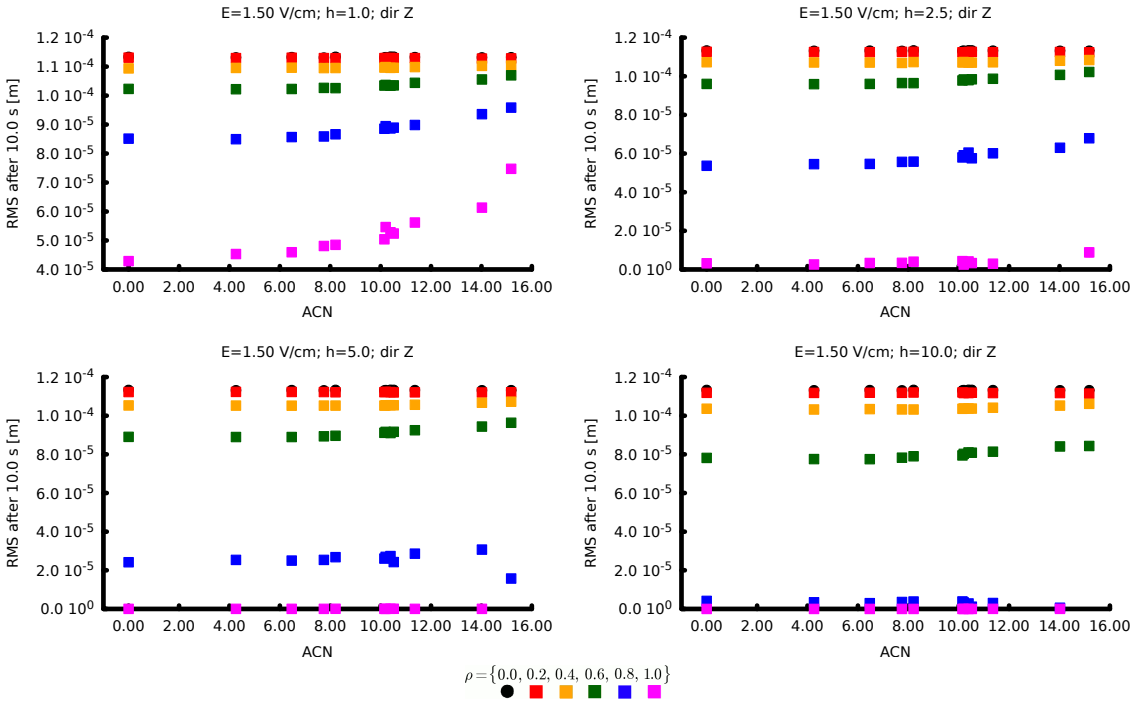

Figure 3.9: Mobility of the knotted chains as a function of the ACN for $E = 1.50$ V/cm and all values of the firmness h. Like for $E = 1.00$ V/cm, when a trend is recognisable, more complex knots move faster than simpler ones.

3.3 Analysis of the diffusion process

In order to understand the reasons for this change of trend, we can look into the plots of the mean squared displacement (MSD, for E=0) or the root mean squared displacement (RMS, for E>0). The reason why I considered these two different quantities is due to the different characteristics of the motion with or without a driving force acting on the beads.

For E=0, the motion of the chain is due to the Brownian force acting on the beads, so we expect the Mean Squared Displacement (MSD) to be linear with time. For this reason, I calculate and analyse the MSD of the center of mass of the chains.

For all $E > 0$ considered, the field-driven motion dominates over the Brownian motion, and we expect a linear displacement (RMS) with time (Fig. 3.12, left). For this reason, in this case, I calculate and analyse the RMS of the center of mass instead of the MSD.

3.3.1 Normal and anomalous diffusion

As mentioned, in the absence of an electric force we expect the Mean Squared Displacement (MSD) to be linear with time. This is what happens without gel or with thin gels (e.g. $\rho \leq$0.6 with h=1, Fig. 3.10, left). However, for thick gels the chains display a subdiffusive behaviour (see Section 1.3.3), as they are trapped in the medium (Fig. 3.10, right, and Fig. 3.11).

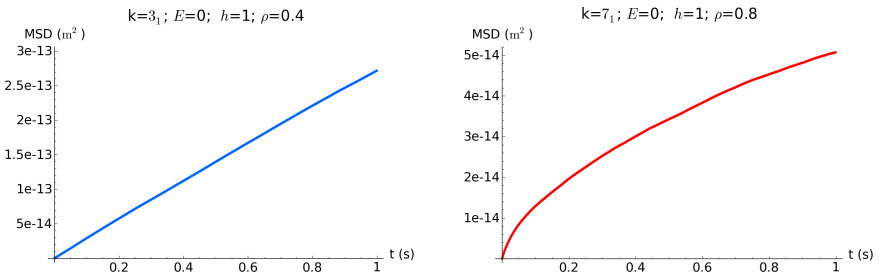

Figure 3.10: Example of mobility for a thin and for a thick gel without an electric field. Left: example of MSD for a thin gel. The MSD is linear with time. Right: example of MSD for a thick gel. The MSD is no longer linear.

In the presence of an electric force we find indeed that the RMS is linear with time. However, though to a lesser extent, also in this regime for very thick gels (e.g. $\rho \geq$0.8 with h=5) the behaviour is non-linear (Fig. 3.12, right and 3.13).

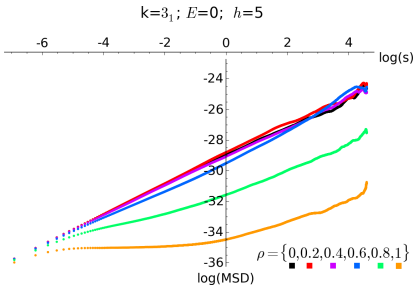

Figure 3.11: Example of logarithmic plot of the MSD for all values of ρ, showing the subdiffusive behaviour for thicker gels. $E = 0$.

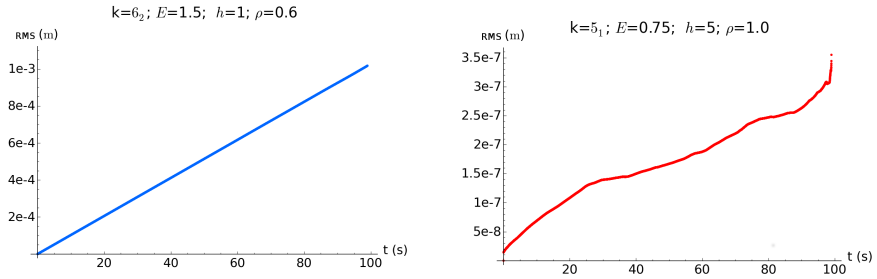

Figure 3.12: Example of mobility for a thin and for a thick gel in the presence of an electric field. Left: example of mobility for a thin gel. The mobility is linear with time. Right: example of mobility for a thick gel. The mobility is no longer linear. It has to be noted that, as it is a time-averaged quantity, the data are only significant within the first seconds. In relation to the graph on the right, after about 20 s the data become very noisy and not at all meaningful. In this case the only useful information is the shape of the curve near zero and the values of the RMS, which show that in fact the molecule hardly moves at all. Also, it has to be noted that this particular graph is only shown to illustrate the process and was obtained from preliminary shorter simulations of 100 s, instead of 1000 s, therefore it is noisier than the actual data presented in this chapter.

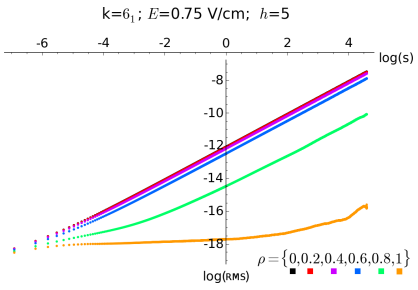

Figure 3.13: Example of logarithmic plot of the mobility for all values of the density ρ, showing the subdiffusive behaviour for thicker gels. $E > 0$.

3.3.2 Examples of diffusion with different suspensions

I will now discuss in more detail the diffusion with three different values of the electric field: no electric field (E=0 V/cm), intermediate electric field (E=0.50 V/cm) and strong electric field (E=1.5 V/cm).

Four types of gel are considered, of increasing strength depending on the firmness h and the density ρ:

- gel A : $h = 1, \rho = 0.2$;
- gel B : $h = 5, \rho = 0.6$;
- gel C : $h = 5, \rho = 0.8$;
- gel D : $h = 10, \rho = 0.8$.

For every combinations of parameters, we consider two knots of different complexity. The graphs show the first 10 s of the time-averaged mobility (MSD or RMS).

Gel A

If we look at the graphs in Fig. 3.14, we can see that, whatever the strength of the field, no anomalous diffusion is noticeable. The gel is weak and there is no trapping.

Gel B

The graphs in Fig. 3.15 show that in the absence of an electric field, the less complex knot (0_1) does not experience anomalous diffusion, but the more complex knot (8_1) does. This shows that more complex knots are trapped more easily than simpler ones.

With the introduction of an electric field, small or big, neither chain experiences anomalous diffusion, as the driving force is sufficient to set them free.

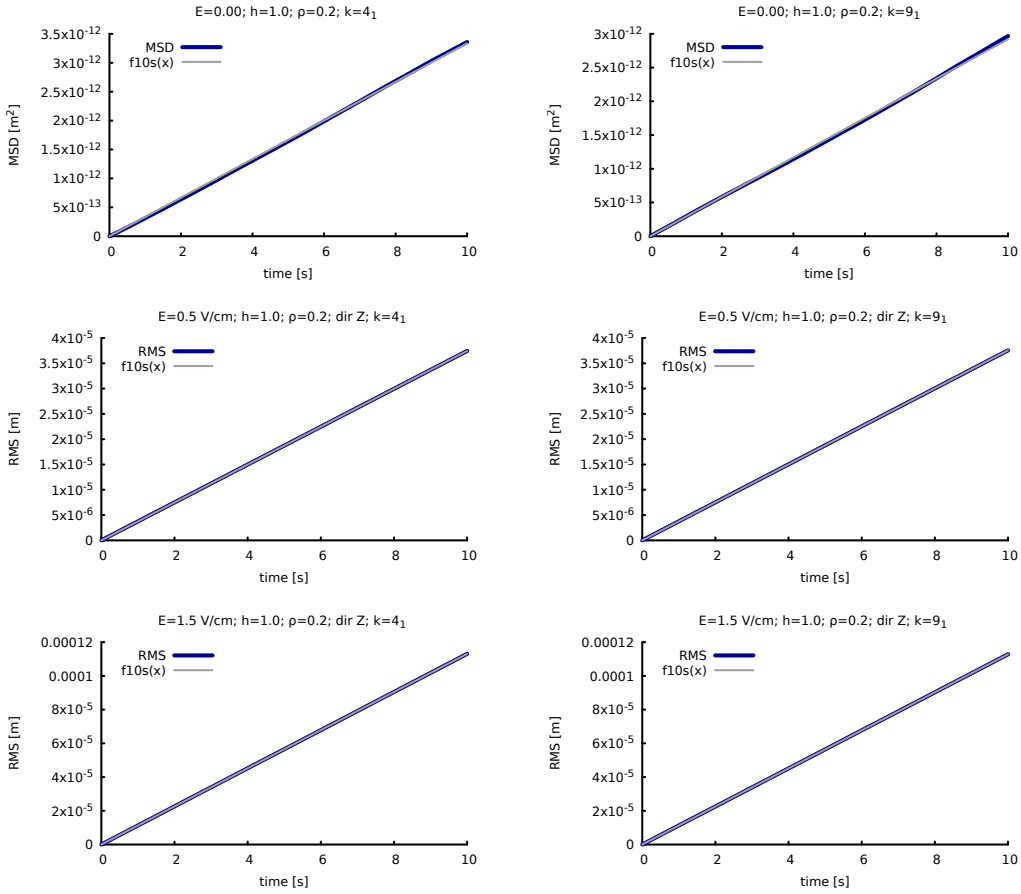

Figure 3.14: Mobility in a sample "thin" suspension: gel A ($h = 1$, $\rho = 0.2$).

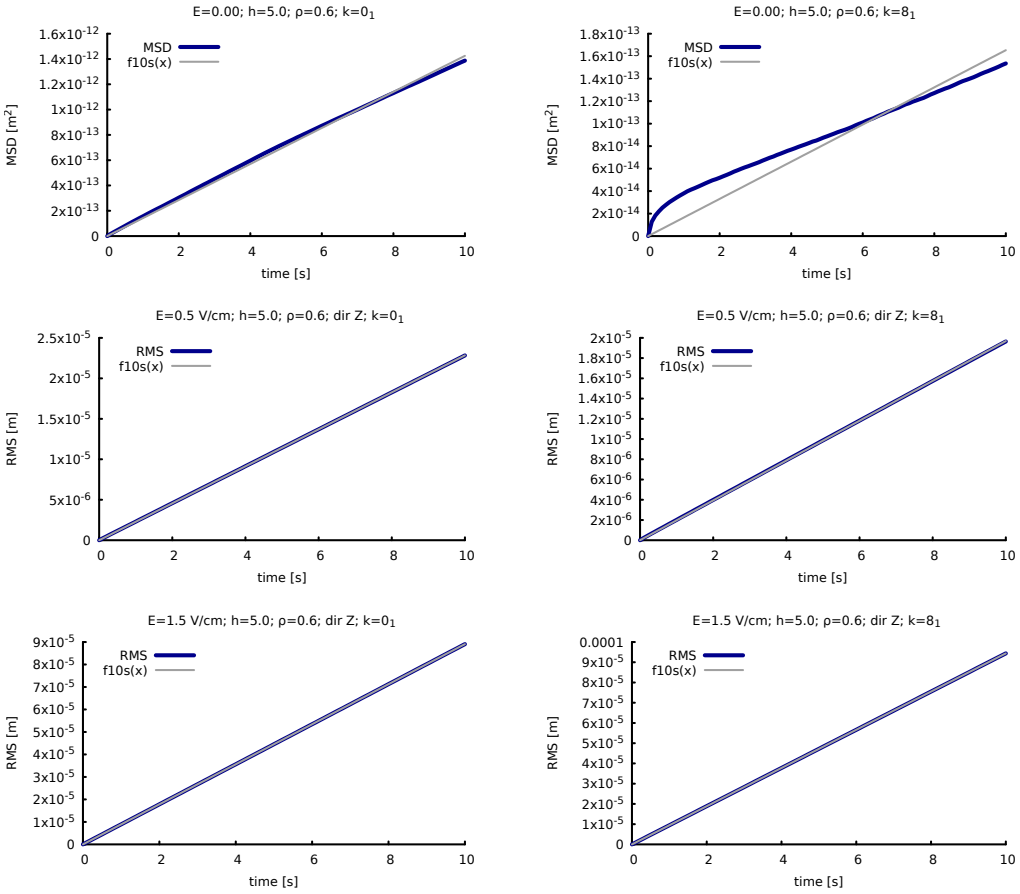

Figure 3.15: Mobility in a sample "medium-thin" suspension: gel B ($h = 5$, $\rho = 0.6$).

Gel C

The graphs in Fig. 3.16 show that in the absence of an electric field, with this gel the less complex knot (0_1) is starting to experience anomalous diffusion. However, for the more complex knot (8_1) this is much more accentuated.

With an intermediate electric field, the simpler knot is moving freely, while the more complex knot is showing some signs of anomalous diffusion.

With a stronger field both graphs are linear.

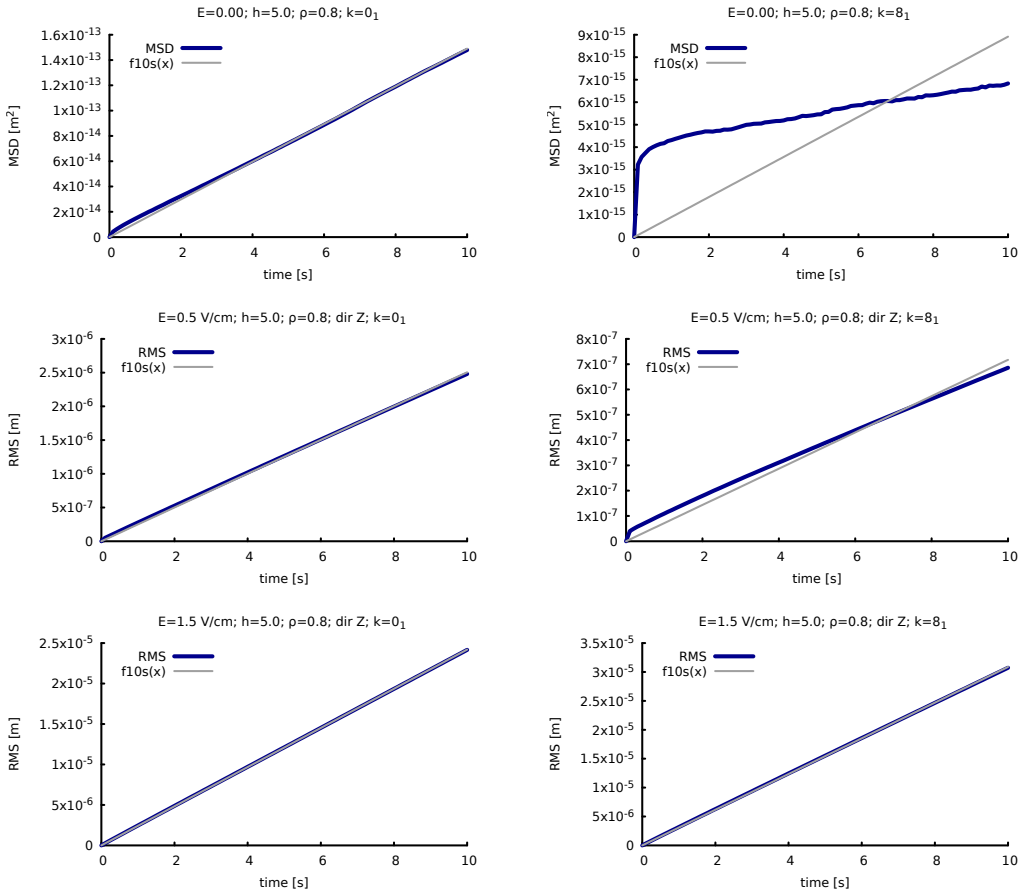

Figure 3.16: Mobility in a sample "medium-thick" suspension: gel C ($h = 5$, $\rho = 0.8$).

Gel D

With gel D (Fig. 3.17), the suspension is so thick that in all cases the motion shows signs of anomalous diffusion. However, in the case of a strong electric field, while the trapping is evident for the more complex knot (8_1), it is very small in the case of the simpler knot (4_1).

These graphs show that the effect of the gel is stronger on more tightly knotted molecules, as they are more easily trapped. This is clearly visible as the systems exhibit anomalous diffusion in the case of more complex knots first, while only for thicker gels also in the case of simpler knots.

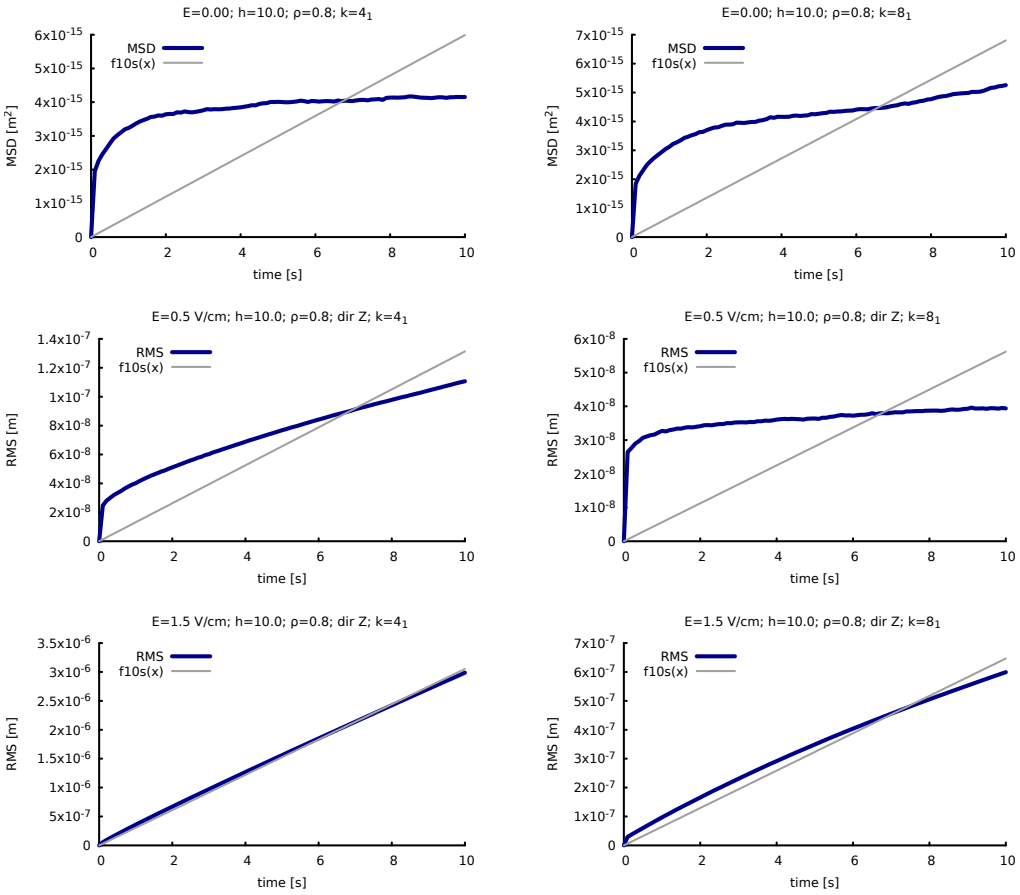

Figure 3.17: Mobility in a sample "very thick" suspension: gel D ($h = 10$, $\rho = 0.8$).

3.3.3 Analysis of the anomalous-diffusion exponent

As seen in Section 1.3.3, the type of diffusion (normal, subdiffusion or superdiffusion) can be characterised by the value of the anomalous-diffusion exponent α in the equation:

$$\text{MSD} = \langle x^2(t) \rangle \simeq D_\alpha t^\alpha, \tag{3.1}$$

This value can be visualised as the slope of the curve in a double logarithmic graph of the mobility versus time. These graphs are shown for all the values of the density ρ, in order of increasing firmness h and electric field E. Every combination is shown for two knots of different complexity.

No electric field

In Fig. 3.18, the mobilities of the 3_1 and the 9_1 are shown in the case of suspensions of firmness $h = 1$. We can notice that at low densities ρ, the diffusion is normal for both knots, while as ρ increases the slopes tend to decrease more for the more complex knot, confirming that in this case trapping is more pronounced.

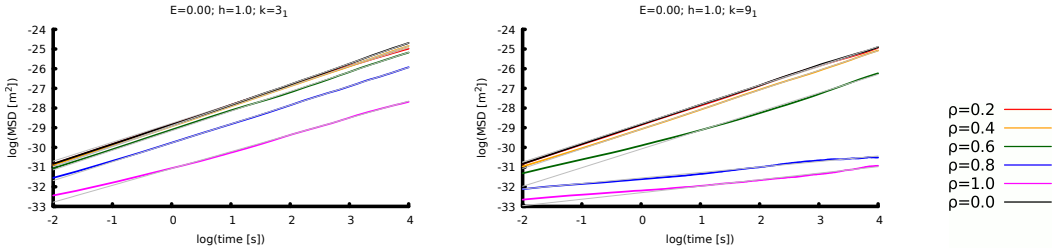

Figure 3.18: Mobility of the knots 3_1 and 9_1 in a suspension of firmness $h = 1$ at $E = 0$ V/cm. At low densities ρ, the diffusion is normal for both knots, while as ρ increases the slopes tend to decrease more for the more complex knot, confirming that in this case trapping is more pronounced.

In Fig. 3.19, the mobilities of the 4_1 and the 8_1 are shown in the case of suspensions of firmness $h = 5$. Again, at low densities ρ, the diffusion is normal for both knots, while as ρ increases the slopes tend to decrease more for the more complex knot.

Strong electric field, E=1.5 V/cm

In Fig. 3.20, the mobilities of the 3_1 and the 9_1 are shown in the case of suspensions of firmness $h = 1$. With a strong electric field, the slopes are all very similar and we cannot see any sign of subdiffusion.

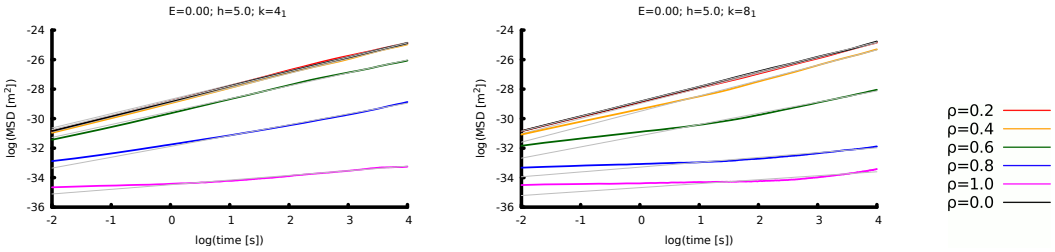

Figure 3.19: Mobility of the knots 4_1 and 8_1 in a suspension of firmness $h = 5$ at $E = 0$ V/cm. At low densities ρ, the diffusion is normal for both knots, while as ρ increases the slopes tend to decrease more for the more complex knot. Again, in this case trapping is more pronounced.

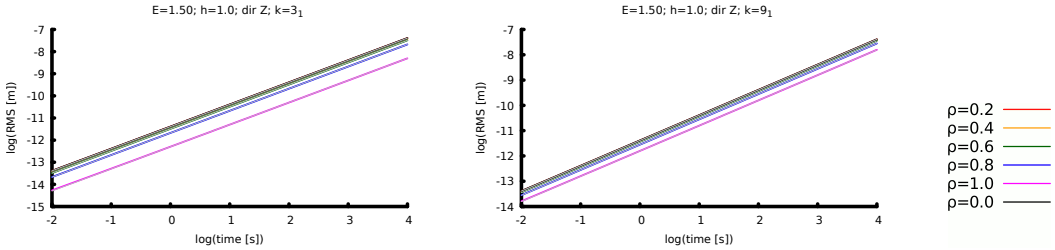

Figure 3.20: Mobility of the knots 3_1 and 9_1 in a suspension of firmness $h = 1$ at $E = 1.5$ V/cm. With a strong electric field, the diffusion is normal in all cases, as there is no trapping.

In Fig. 3.21, the mobilities of the 0_1 and the 8_1 are shown in the case of suspensions of firmness $h = 10$. With a strong electric field, the slopes are all very similar for small and medium densities, while we can see that there is subdiffusion for $\rho \geq 0.8$ and the slope is lower for the more complex knot.

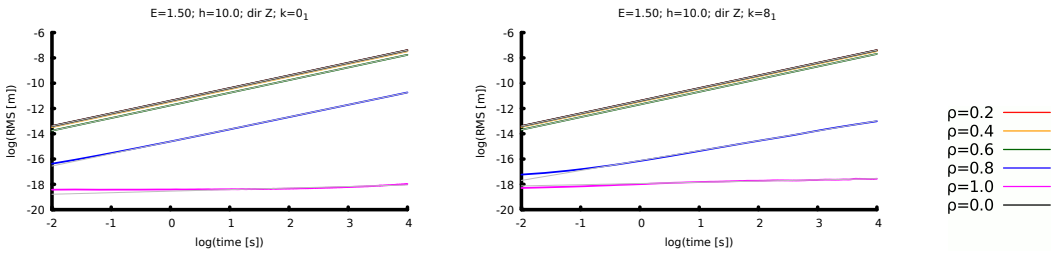

Figure 3.21: Mobility of the knots 0_1 and 8_1 in a suspension of firmness $h = 10$ at $E = 1.5$ V/cm. With a strong electric field, the diffusion is normal unless the density is very high, $\rho \geq 0.8$, and in this case the slope is lower for the 8_1.

Values of the anomalous-diffusion exponent as a function of the other parameters

The graphs shown in the previous paragraphs are a sample of the trend of behaviour of the anomalous-diffusion exponent α. In order to have a quantitative analysis, it is possible to plot the values of the slope for all the possible combinations of ACN, firmness h and densities ρ for a fixed electric field E in a three-dimensional plot where the colour of the points gives a measure of the value of α. In this "anomality" scale, lighter colours mean values close to 1 (normal diffusion) while increasingly darker colours indicate increasingly lower α's.

Figures 3.22, 3.23 and 3.24 show these 3D plots for $E = 0$ V/cm, $E = 0.75$ V/cm and $E = 1.50$ V/cm, respectively.

In all cases, the value of α decreases as any of the parameters increases, therefore confirming that the complexity of the knot, as well as the firmness and the density of the suspension, plays a role in making the motion subdiffusive.

We can also notice that, as the electric field is increased, the instances of anomalous diffusion become fewer, and lighter colours increasingly dominate.

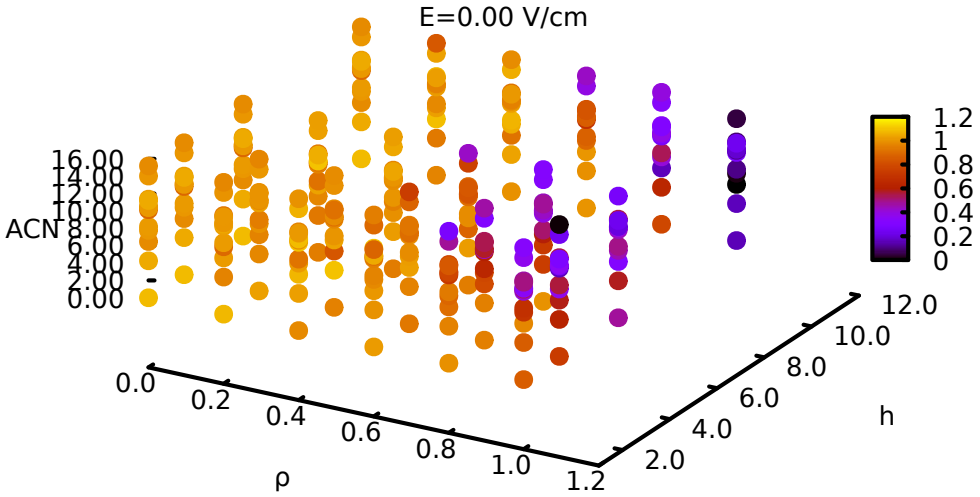

Figure 3.22: Value of the anomalous-diffusion exponent as a function of ACN, firmness h and density ρ for $E = 0.00$ V/cm. The colours become darker as either the ACN, the firmness h or density ρ increase, meaning lower values of the anomalous-diffusion exponent α.

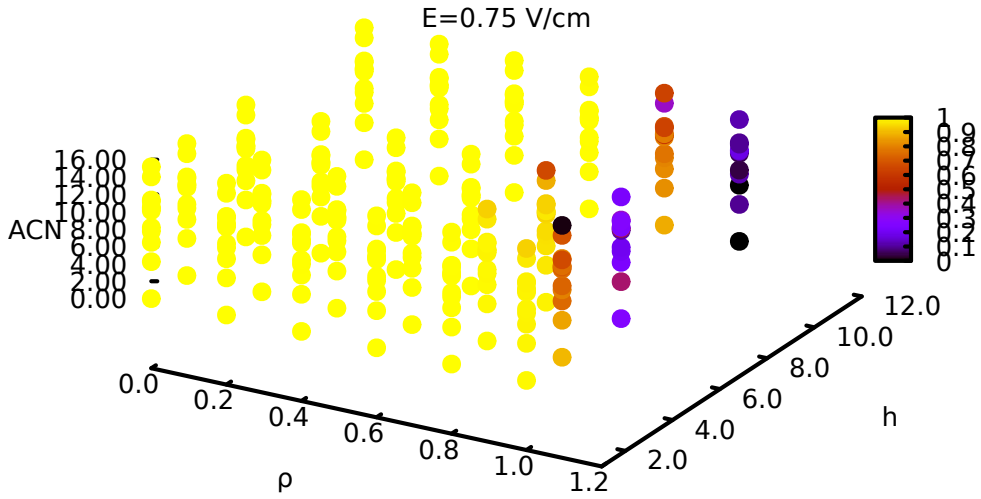

Figure 3.23: Value of the anomalous-diffusion exponent as a function of ACN, firmness h and density ρ for $E = 0.75$ V/cm. Again, the colours become darker as either the ACN, the firmness h or density ρ increase, meaning lower values of the anomalous-diffusion exponent α, however colours are overall lighter, as α is in general higher for stronger electric fields, as the driving force tends to free the molecules from trapping.

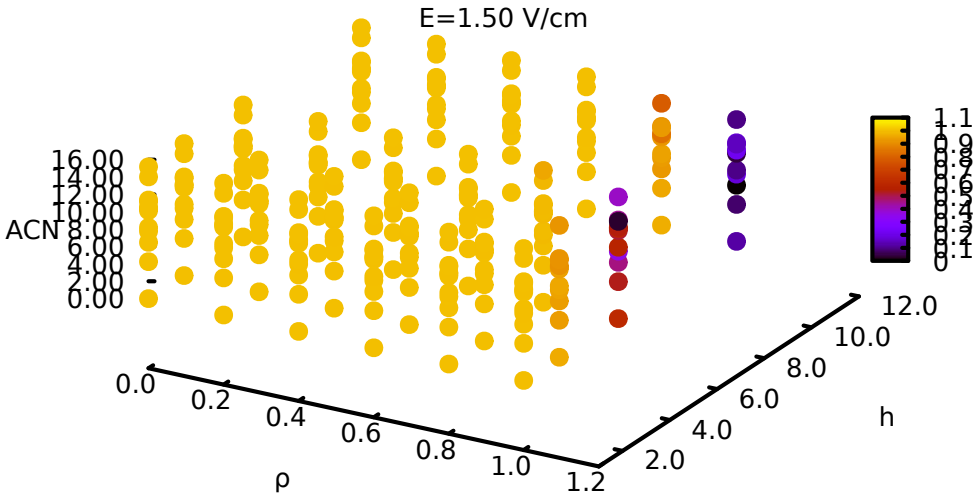

Figure 3.24: Value of the anomalous-diffusion exponent as a function of ACN, firmness h and density ρ for $E = 1.50$ V/cm. As before, the colours become darker as either the ACN, the firmness h or density ρ increase, meaning lower values of the anomalous-diffusion exponent α. Overall colours are lighter than in both the previous cases, as the driving force tends to free the molecules from trapping and therefore α is in general higher for stronger electric fields.

3.4 Further considerations: rigidity and compactness of the molecules

A characteristic that depends on the knot type and may affect the mobility of the chains is its rigidity. I chose to consider 40 beads as the minimal number that would allow the chains to be tied in knots up to 9 crossings and still ensure they would be able to change conformation. I noticed, however, that, in spite of not having any bending rigidity, more complex knots tend to be more rigid simply due to excluded volume reasons (see Fig. 2.11 for an example), and this may play a role in the dynamics of the system. As a quantity related to stiffness, we looked at the total curvature of the chains, defined as the sum of all the angles between adjacent beads, for different numbers of beads N (see Fig. 2.12).

If we compare these values with the values computed on tight knots available on the Ridgerunner website (Cantarella, 2012), we can see that for tight knots (black in Fig. 3.25) the total curvature tends to increase linearly with the ACN of the knots. On the contrary, the curvature of our chains tends to decrease with the crossing number, and for $N < 50$ and high enough ACN it tends to become the same as the corresponding tight knot. I think that, as the crossing number increases, the freedom of motion of the chains tends to become more restricted and they are forced to assume a specific conformation. Since the restriction is due to the excluded-volume force between the beads, this has a comparable effect to fixing the diameter of a tube of already fixed length: as a result, as the knots become more complex, their conformations will be more and more similar to those of ideal knots.

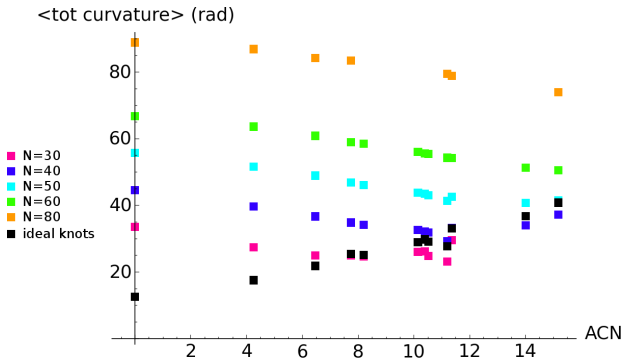

Figure 3.25: Total curvature of the chains as a function of the average crossing number of the ideal representations of the knots for different numbers of beads.

In the simulations presented in this chapter, the number of beads is $N = 40$, and the results shown in the graphs (Figures 3.2 to 3.9) reflect this choice. To test if the trend we observe for $N = 40$ is still present for a larger number of beads, I performed some sample simulations with $N = 80$, all other parameters unchanged.

We can see that also in this case the same trend as for $N = 40$ is present, although less pronounced, in all three cases $E = 0$ (Fig. 3.26), $E = 0.75$ V/cm (Fig. 3.27), $E = 1.5$ V/cm (Fig. 3.28).

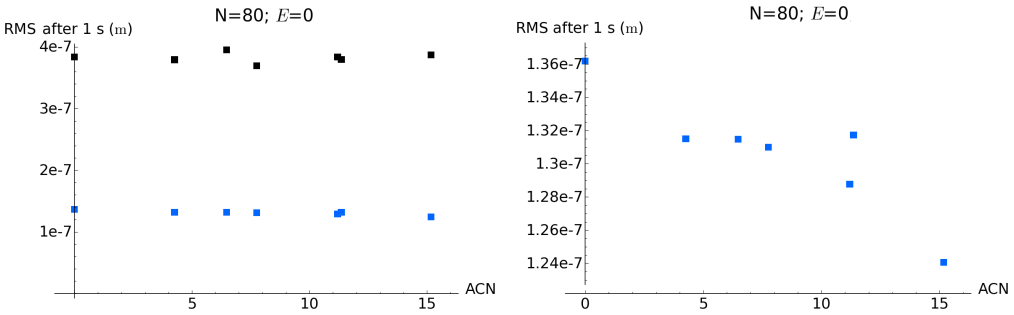

Figure 3.26: Mobility for longer molecules: RMS after 1 s for $N = 80$, $E = 0$, $h = 1$. Black: $\rho = 0$, blue: $\rho = 1$. On the right, we show $\rho = 1$ only, to highlight the trend. We can see the same trend as with $N = 40$ (i.e. more complex knots move more slowly than simpler knots), but less pronounced.

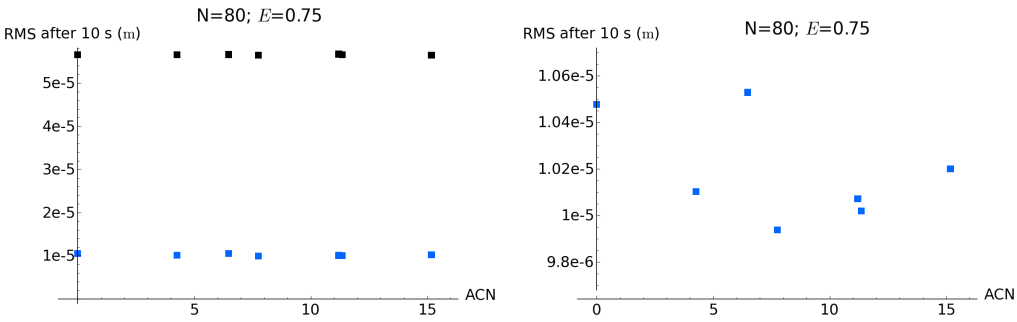

Figure 3.27: Mobility for longer molecules: RMS after 10 s for $N = 80$, $E = 0.75$ V/cm, $h = 1$. Black: $\rho = 0$, blue: $\rho = 1$. On the right, we show $\rho = 1$ only, to highlight the trend. As with $N = 40$, no particular trend is observed.

3.4.1 Radius of gyration

Radius of gyration as a function of the suspension and electric field

A measure of the compactness of the molecules is the radius of gyration. Therefore its relationship with the parameters external to the chains themselves, that

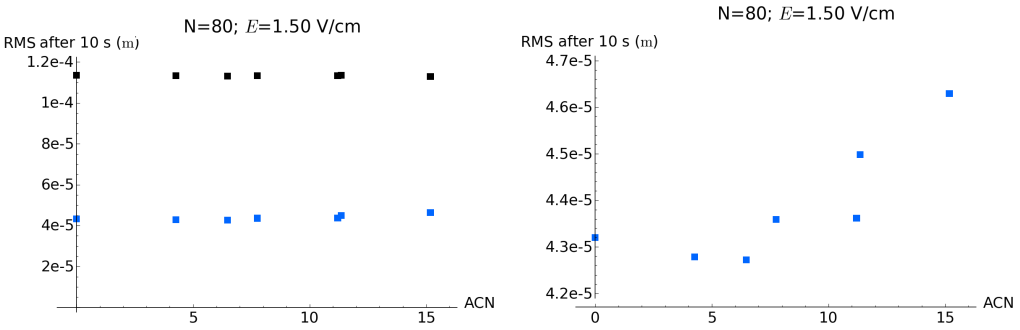

Figure 3.28: Mobility for longer molecules: RMS after 10 s for $N = 80$, $E = 1.5$ V/cm, $h = 1$. Black: $\rho = 0$, blue: $\rho = 1$. On the right, we show $\rho = 1$ only, to highlight the trend. We can see the same trend as with $N = 40$ (i.e. more complex knots move faster than simpler knots), but less pronounced.

is, with the suspension and the electric field, were examined. In Figs 3.29 and 3.30, the dependence on the values of the firmness h and the density ρ are shown at the lowest and highest values of E under consideration, $E = 0$ and $E = 1.5$ V/cm.

In all cases it is possible to notice two main features. The first is that, if we overlook some spurious behaviour for very thick suspensions, the radius of gyration for a fixed knot does not vary particularly with these parameters. The second is that for the more complex knots, with ACN around 10 or higher, the radius of gyration does not decrease with the ACN as much as for simpler knots. This can be seen as further proof that these molecules are reaching a very compact state which highly limits the available configurations.

Radius of gyration as a measure of trapping

As seen in Section 2.9.2, if the radius of gyration is defined as

$$R_G^2 = \frac{1}{N_{\text{beads}}} \sum_{m=1}^{N_{\text{beads}}} \langle (x_m - x_{CM})^2 + (y_m - y_{CM})^2 + (z_m - z_{CM})^2 \rangle, \tag{3.2}$$

the contributions due to the three orthogonal directions can be isolated by calculating:

$$\begin{aligned} (R_G^2)_X &= \tfrac{1}{N_{\text{beads}}} \textstyle\sum_{m=1}^{N_{\text{beads}}} \langle (x_m - x_{CM})^2 \rangle, \\ (R_G^2)_Y &= \tfrac{1}{N_{\text{beads}}} \textstyle\sum_{m=1}^{N_{\text{beads}}} \langle (y_m - y_{CM})^2 \rangle, \\ (R_G^2)_Z &= \tfrac{1}{N_{\text{beads}}} \textstyle\sum_{m=1}^{N_{\text{beads}}} \langle (z_m - z_{CM})^2 \rangle. \end{aligned} \tag{3.3}$$

Therefore, in the second set of data, the contributions to the radius of gyration from the three Cartesian directions x, y and z are examined.

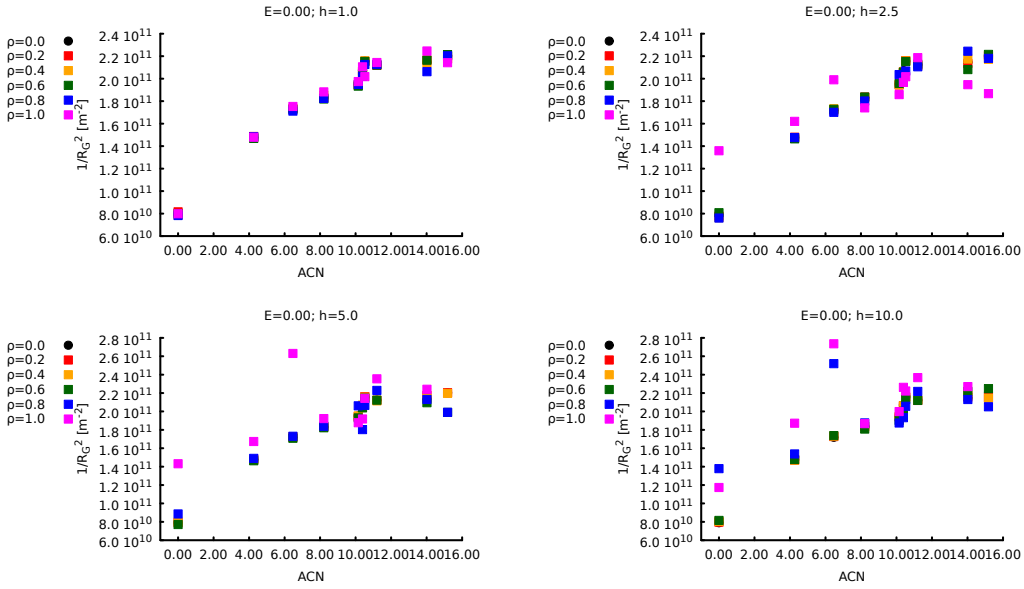

Figure 3.29: Radius of gyration for all the values of the firmness, $h = \{1, 2.5, 5, 10\}$, and the density, $\rho = \{0, 0.2, 0.4, 0.6, 0.8, 1\}$, at $E = 0$ V/cm.

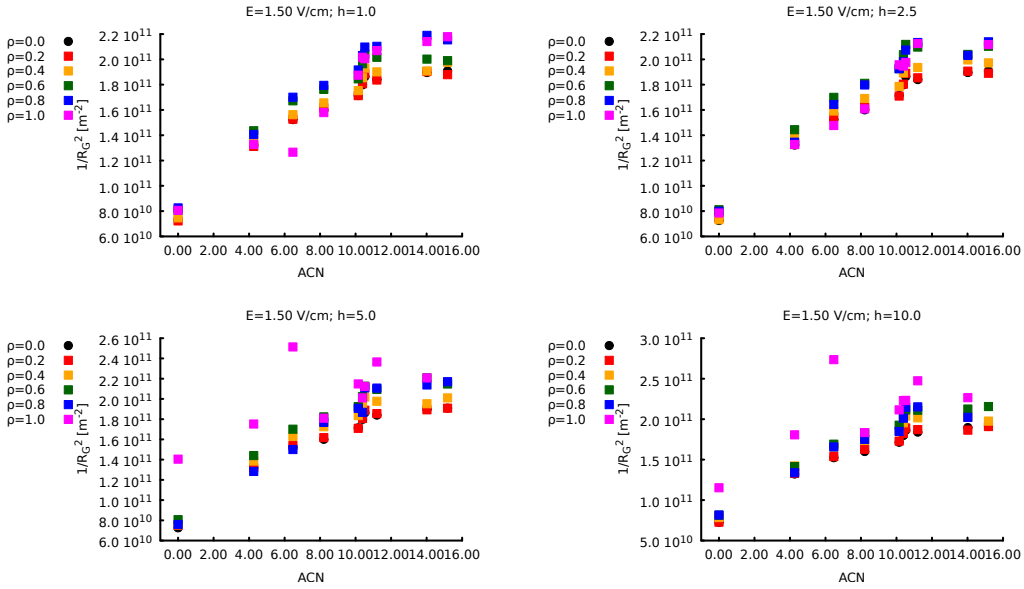

Figure 3.30: Radius of gyration for all the values of the firmness, $h = \{1, 2.5, 5, 10\}$, and the density, $\rho = \{0, 0.2, 0.4, 0.6, 0.8, 1\}$, at $E = 1.5$ V/cm.

For simplicity, these values can be normalised as $(R_G^2)_X/R_G^2$, $(R_G^2)_Y/R_G^2$ and $(R_G^2)_Z/R_G^2$, which in Figures 3.31, 3.32 and 3.33 are indicated as x^2/R_G^2, y^2/R_G^2 and z^2/R_G^2.

These are shown at the beginning of the simulation (left in the pictures),

averaged over the first 100 s (middle) and averaged over the last 100 s (right).

Data for different values of the firmness h and the density ρ are shown with the electric field being $E = 0$ in Fig. 3.31, $E = 0.5$ V/cm in Fig. 3.32 and $E = 1.5$ V/cm in Fig. 3.33.

Due to the way they are created, the knotted molecules are quite oblate on the (x, y) plane at the beginning of each simulation (see Section 2.6.1 and e.g. Fig. 2.7). For this reason the contribution to the radius of gyration from the z component of the beads is noticeably smaller at the beginning of the simulation in all cases.

As was expected, for no suspension or thin suspensions, during the run the molecules are able to move freely enough that by the end of the simulation their shape is no longer associated with any particular direction. However, for very thick suspensions, we can see that the z contribution is still low, which confirms that not only do the centres of mass of the molecules hardly move at all, but the individual beads remain in approximately the same position and configuration as they are trapped by the suspension. As seen with the analysis of the mobility, the presence of an electric field in thick suspensions tends to free the beads, especially for simpler knots. This is confirmed by the increased contribution of the z direction to the radius of gyration as the electric field increases, in particular at low ACN's.

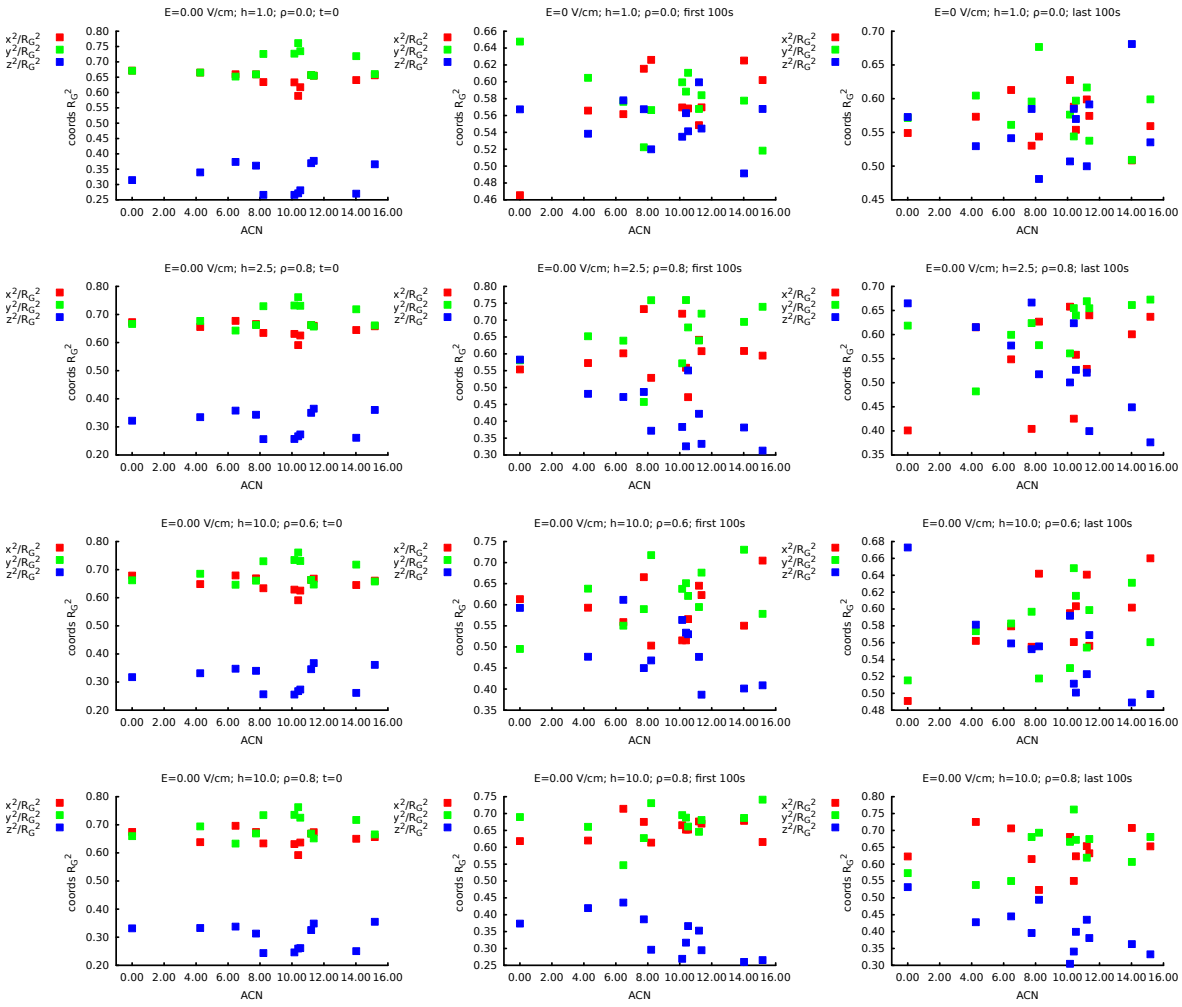

Figure 3.31: Contribution to the radius of gyration from the Cartesian coordinates of the beads as a function of the ACN for $E = 0$ V/cm. Each row is taken from a simulation with a suspension of different characteristics, as indicated in the pictures. The three columns show the values at three different times of the normalised contributions to the square radius of gyration due to the three Cartesian directions, as explained in Eq. 3.3 and following text. In particular, blue represents the contribution due to the z coordinate. The first column represents the values at the beginning of the simulation, the second column shows the average values over the first 100 s, and the last column shows the average values over the last 100 s (over a total simulation length of 1000 s). As explained in the text, the way the chains are initially created implies low values of this contribution with respect to the other two. This is reflected in the fact that the values for the blue dots at the very beginning of the simulations are always low. As the simulations proceed, we can see that for thin or medium suspensions the various contributions become randomly distributed within the first 100 s, or, in the case of the second row, at least by the end of the simulation. With the thickest suspension, that is, the last row, we can see that the distribution of the colours remains qualitatively the same until the end, so showing that not only does the centre of mass not move, but also the individual beads are trapped, as the conformation of the molecule does not essentially change.

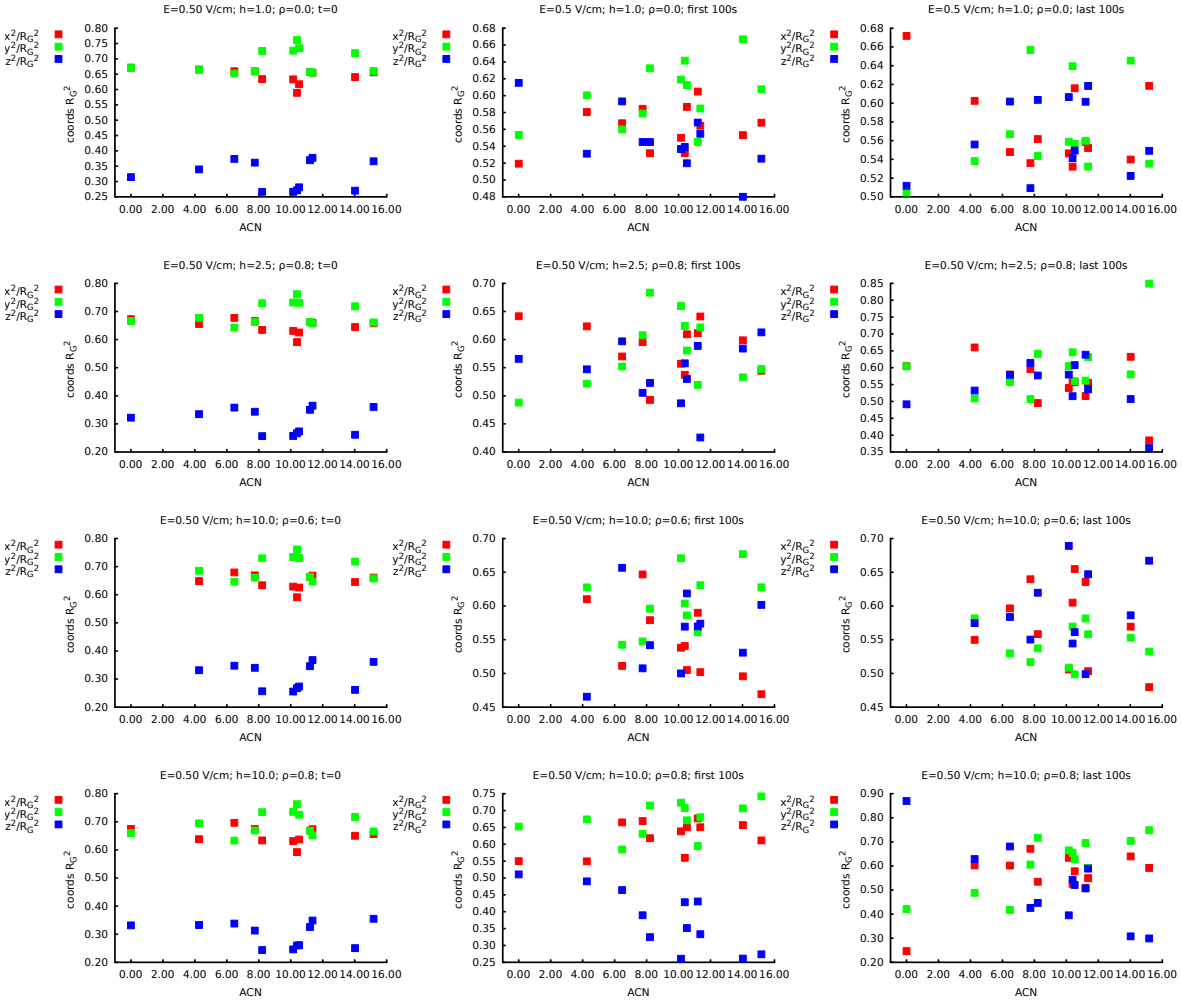

Figure 3.32: Contribution to the radius of gyration from the Cartesian coordinates of the beads as a function of the ACN for $E = 0.5$ V/cm. Like before, each row is taken from a simulation with a suspension of different characteristics, as indicated in the pictures. The three columns show the values at three different times of the normalised contributions to the square radius of gyration due to the three Cartesian directions, as explained in Eq. 3.3 and following text. In particular, blue represents the contribution due to the z coordinate. The first column represents the values at the beginning of the simulation, the second column shows the average values over the first 100 s, and the last column shows the average values over the last 100 s (over a total simulation length of 1000 s). As explained in the text, the values for the blue dots at the very beginning of the simulations are always low due to the initial configurations of the chains. Like in the previous case ($E = 0$ V/cm), the various contributions become randomly distributed as the simulation progresses. With respect to the previous case, we can see that this "mixing" happens sooner in the presence of an intermediate electric field and by the end the "memory" of the initial configuration is lost. However, we can notice that with the thickest suspension (last row), this requires more time, as the graph corresponding to the first 100 s is still similar to that at the beginning. We can also notice that the two most complex knots (8_1 and 9_1) are essentially still in the same configuration even at the end of the simulation.

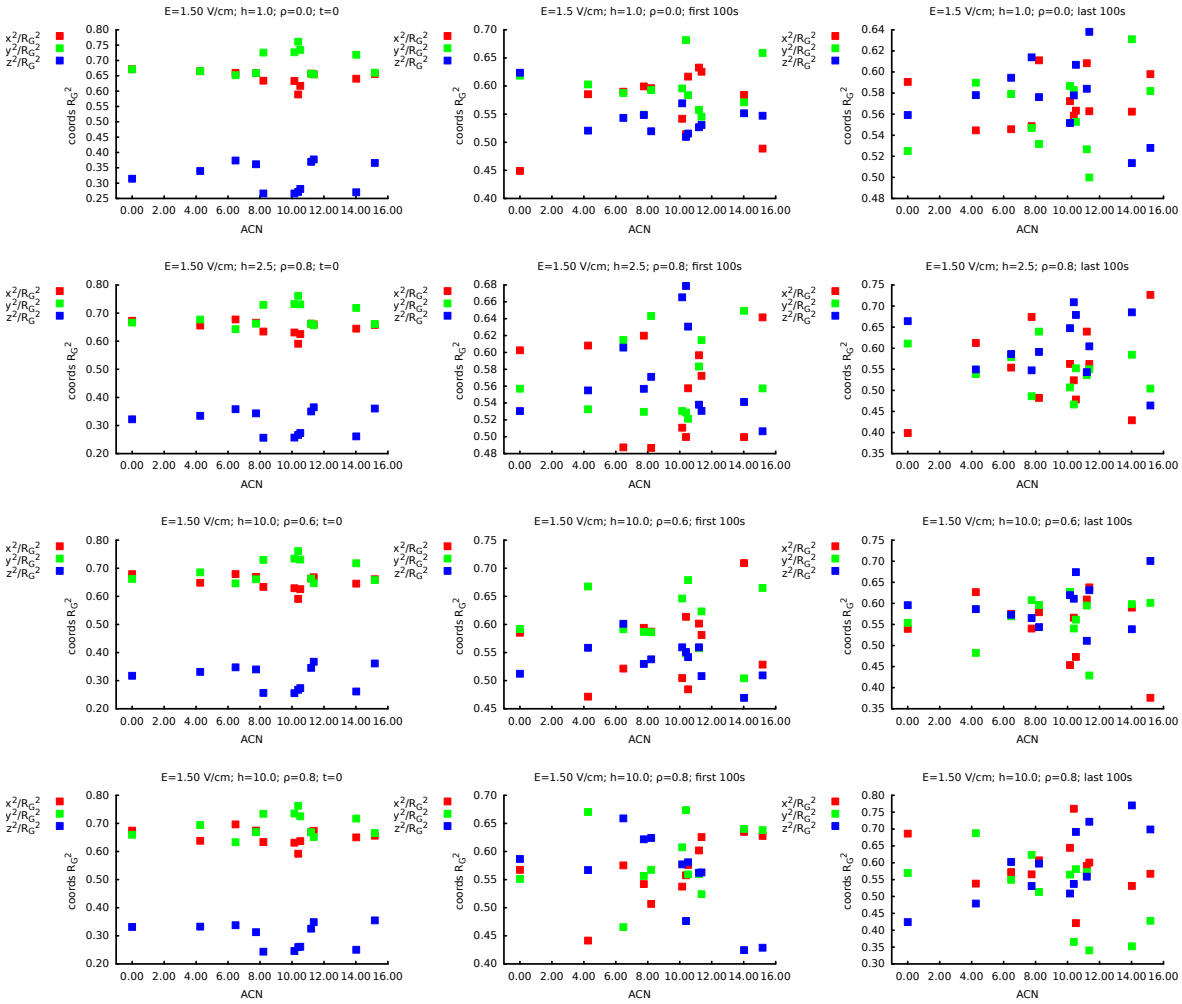

Figure 3.33: Contribution to the radius of gyration from the Cartesian coordinates of the beads as a function of the ACN for $E = 1.5$ V/cm. Like before, each row is taken from a simulation with a suspension of different characteristics, as indicated in the pictures. The three columns show the values at three different times of the normalised contributions to the square radius of gyration due to the three Cartesian directions, as explained in Eq. 3.3 and following text. In particular, blue represents the contribution due to the z coordinate. The first column represents the values at the beginning of the simulation, the second column shows the average values over the first 100 s, and the last column shows the average values over the last 100 s (over a total simulation length of 1000 s). As explained in the text, the values for the blue dots at the very beginning of the simulations are always low due to the initial configurations of the chains. Like in the previous cases, the various contributions become randomly distributed as the simulation progresses, but with respect to the previous cases, we can see that this "mixing" happens within the first 100 s in the presence of a strong electric field and the "memory" of the initial configuration is lost. Only in the case of the two most complex knots (8_1 and 9_1) this process seems to take longer, as we can see that in the first 100 s the molecules are still essentially flat on the (x, y) plane.

3.5 Discussion

For a real polymer, diffusion would depend on the radius of gyration, so we would expect a different behaviour for molecules with different shapes. In this model, though, we are not considering hydrodynamic interactions, so we expect the diffusion rates to depend only on the number of beads, which is constant in our simulations. The behaviour we would expect should be, therefore, independent of knot type. This is the case, as expected, in the absence of a suspension. On the contrary, when a suspension is present we find that this is not true: for $E = 0$ more complex knots move more slowly than simpler knots, while they move faster for a strong enough field.

Since for a given combination of the density ρ, the firmness h and the electric field E (that is, same colour in the same graph), all other parameters being kept constant, the knot type is the only element that changes, these results show a relationship between the topology and the speed of motion of the chains.

To explain why more complex knots travel more slowly in the suspension when no external force is applied, we can hypothesise that the suspension spheres may get trapped inside the polymers when the latter are more knotted (and subsequently more compact) so impeding the motion. In addition to this, the reduced flexibility of the chain may be a further hindrance to finding a way around the obstacles or, even more likely, a spatial conformation that would allow the molecule to minimize contact with the spheres of the suspension.

This is confirmed by the analysis of the diffusion. In fact, we can see that in all cases, and especially with no or very weak elecric field, a subdiffusive behaviour starts sooner (that is, for thinner suspensions) when the knots are more complex. This explains the trend for low or no electric field, as in these cases what counts for the speed of motion is the point at which subdiffusion starts to show and how dominant it is.

When we add a constant driving force, the trend is still the same as long as the force is small, while for higher fields, the behaviour is inverted: more complex knots move faster than simpler knots. We suppose that in this case the field is strong enough to “free” the trapped chain, and the motion is then mainly determined by the compactness of the molecule.

This is, too, confirmed by the analysis of the diffusion graphs. Indeed, we can see that the presence of an electric field delays the onset of a subdiffusive behaviour caused by the entrapping of the molecules in the suspension.

In addition to this, we notice that when no anomalous diffusion is present, more complex knots tend to move faster than simpler ones. We can suppose that, once a molecule is free from entrapment, its speed is determined by its compactness. In fact, in that case, the more compact a molecule, the fewer spheres of the suspension it will come into contact with.

Although our model is simplified as much as possible, we are interested in potential similarities with biologically-relevant systems. As we saw in Section 1.3.3, in a biological system, we can have one of three types of behaviour: normal diffusion, subdiffusion or superdiffusion. Even though a superdiffusive behaviour would have been possible due to the presence of an external driving force, we did not see any case of it. This is not surprising considering that, as we saw, superdiffusion is usually linked to, for example, actively-facilitated diffusion in the living cell, the presence of channels or capillary action, and nothing similar is present in our model.

3.6 Comparison with experiments and previous models

As we saw in Section 1.7.1, in previous theories and models, the linear relation between mobility and ACN in standard, one-dimensional agarose-gel electrophoresis is often explained through hydrodynamic interactions (Malevanets and Kapral, 1999; Gonzalez et al., 2004) or through the effect of a regular or thin gel, where the system does not exhibit evidence of trapping of the molecules (Michieletto et al., 2015).

Trapping plays an important factor, instead, in the models which aim at explaining non-standard behaviour in two-dimensional electrophoresis, like the inversion of the trend in the mobility (such as Weber et al. (2006) modelling experiments by Sogo et al. (1999)) or the arc pattern (such as Michieletto et al. (2015) modelling systems like Trigueros et al. (2001)).

Experimentally, in two-dimensional agarose-gel electrophoresis, higher electric fields seem to favour the mobility of simpler knots over more complex ones, at least up to 4–6 crossings depending on the experimental setup (Sogo et al., 1999; Trigueros et al., 2001; Cebrián et al., 2015). This supports the interpretation that, within these limits, more complex knots get trapped more easily than simpler ones in high fields, rather than the opposite.

Accordingly, in the previous models mentioned, trapping increases with the driving force, while in the model presented here the electric field plays the

opposite role, by freeing the chains rather than favouring trapping. Therefore, if we consider the two regimes of weak and strong electric fields, both in a thick gel, the trend exhibited in the simulations presented in this chapter is, if anything, the opposite of the trend found in, for example, Sogo et al. (1999) and Weber et al. (2006).

In spite of this, the trend exhibited by the system described in this chapter seems to agree with experimental one-dimensional agarose-gel electrophoresis as long as the driving force in the simulations is sufficiently strong to overcome any trapping by the medium, as indicated by the outset of anomalous-diffusion behaviour.

I think that these are interesting results, as they show that even with a very simple suspension of small spheres arranged in a regular cubic lattice with small lattice spacing compared to the size of the molecules, the type of knot present in the molecules has an effect on the mobility.

3.7 Conclusions

In this chapter, I have proposed a minimal model for the diffusion of a generic, short polymer in a regular suspension. We have seen that even with such a simple system, if the only difference between the closed chains is the type of knot they contain, all the other parameters being kept the same, the mobility shows a trend depending on the type of knot. This trend varies depending on other parameters, such as the density and firmness of the spheres or the applied electric field, but when present depends regularly (linearly or inversely linearly) on the average crossing number of the molecules. In the case of thick suspensions and strong electric field, this trend is similar to that observed in standard, one-dimensional agarose-gel electrophoresis.

The interest in this model lies in its simplicity. In order to have a system that is more similar to real polymers, it is necessary to make the molecules longer and use more complex parameters. This is what I will do in the next chapter, with the help of the simulation program LAMMPS.

4 Simulations of knotted DNA molecules in a suspension of random spheres

4.1 Introduction

While the previous chapter focused on a minimal system of generic knotted polymers in a regular lattice of spheres, this chapter will deal with a more physically-oriented system. To this end, as seen in Chap. 2, the molecular dynamics program LAMMPS was used for the simulations, and the parameters chosen to represent the molecules correspond to double-stranded DNA of total length 1.25 μm. The persistence length is also chosen to be 50 nm like in DNA and, as DNA molecules in these kind of experiments are usually nicked to remove any torsional strain (Cebrián et al., 2015), no torsional energy term has been considered.

As in the previous model, the obstacles are kept simple and are still represented by spheres. However, in this case the spheres are impenetrable, of comparable size to the radius of gyration of the molecules, and are randomly distributed in the simulation box with the specific purpose of delaying the motion of the knotted chains without stopping it altogether. In fact, as opposed to the previous system, here the aim is not to trap the molecules, but simply to partly interfere with the motion by means of obstacles distributed in the medium. Like in the previous chapter, a constant force is added to simulate the electric field present in gel electrophoresis.

The objective of these simulations is to test whether it is possible to obtain a relationship between the mobility of the chains and the kind of knots only due to this uncomplicated interference, without the introduction of complex hydrodynamic interactions. In fact these, like in the previous model, have not been considered.

This system has been studied in two similar configurations. In the first

configuration, the spheres are generated randomly in the box and, after a period of relaxation, are kept fixed in their position for the whole duration of the simulation. After analysing the results, it was found that in some instances the chains would become caught in the spheres and would stop travelling altogether. As this was not the aim of the simulations, a second configuration of the system was devised in which the spheres could move as they were subjected to Brownian motion. In this way, the knotted molecules could quickly free themselves from any obstructions.

The analysis of the motion and the results that will follow will show that with the fixed-sphere configuration the knotted molecules get trapped and, as a result, the mobility does not display any particular trend in connection with the type of knot. On the contrary, with moving spheres it is possible to see a linear relationship between the complexity of the knot, as expressed by the average knotting number, and the mobility of the chains. This is in line with traditional experiments of agarose-gel electrophoresis (Vologodskii et al., 1998) and with some previous models, like Gonzalez et al. (2004), and simulation results, like Piili et al. (2013), which, however, were based on hydrodynamic considerations and calculations (see Sections 1.6 and 1.7.1). The current model does not display an arc pattern like the simulations with an irregular mesh by Michieletto et al. (2015), but it shows a similar trend to their simulations with a weak electric field, or a strong field and a regular mesh.

4.2 Radius of gyration of the molecules

As a preliminary test, the square radius of gyration of the molecules was calculated as an average over all the simulations for the same knot (Fig. 4.1).

The square radius of gyration is calculated as follows (also see Section 1.3.1):

$$R_G^2 = \frac{1}{N_{\text{beads}}} \sum_{m=1}^{N_{\text{beads}}} \langle (x_m - x_{CM})^2 + (y_m - y_{CM})^2 + (z_m - z_{CM})^2 \rangle \tag{4.1}$$

In addition, the part of the radius of gyration due to the component in the direction of the electric field has been analysed as a quantitative measure of how the shape of a molecule is distorted during the simulation:

$$(R_G^2)_Z = \frac{1}{N_{\text{beads}}} \sum_{m=1}^{N_{\text{beads}}} \langle (z_m - z_{CM})^2 \rangle \tag{4.2}$$

This second quantity will be examined later throughout the chapter.

As expected, the radius of gyration decreases with the increasing complexity of the knot, with the square radius varying between around $5 \cdot 10^2\ \sigma$ for the 9_1 and around $1.5 \cdot 10^3\ \sigma$ for the unknot. There is a small difference in the value for the unknotted and the linear molecules in the case of fixed or moving spheres, due to the different probability of trapping in these cases (see Section 4.3). Otherwise the values are consistent regardless of the suspension.

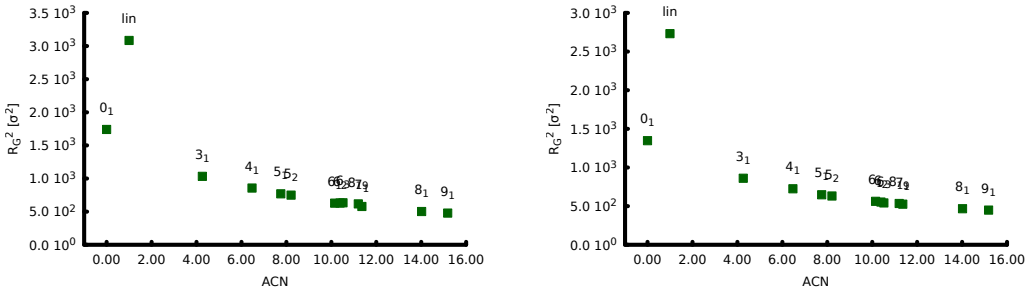

Figure 4.1: Square of the radius of gyration of the molecules made of 500 beads as a function of the ACN in the simulations with fixed (left) and moving (right) spheres. The label "lin" indicates the linear (open) chain.

The displacement of the centre of mass versus time was then calculated and the results are shown in the following Section 4.3 for fixed spheres and Section 4.4 for moving spheres.

4.3 Mobility with fixed spheres

For fixed spheres, first of all we notice (Fig. 4.2) that, in the direction perpendicular to the applied force, the motion is purely random and no particular direction is favoured. The distribution of the displacement versus time of ten randomly-selected 3_1 chains is compatible with a Wiener process centred around zero and the velocities of all the 112 chains simulated for the trefoil are randomly distributed around zero. This is confirmed by the plot of the average of these velocities over all the simulations against the average knotting number, which does not show any particular trend (Fig. 4.3).

On the contrary, in the direction parallel to the electric field we can observe that, although most of the displacement graphs show a linear trend centred around an average value, some of them show a clear delay in the motion. For example, Fig. 4.4 on the left shows the displacement versus time of ten randomly-selected 3_1 chains. We can see that the black curve clearly displays a long initial trapping, before being released and proceeding with its motion, while the red

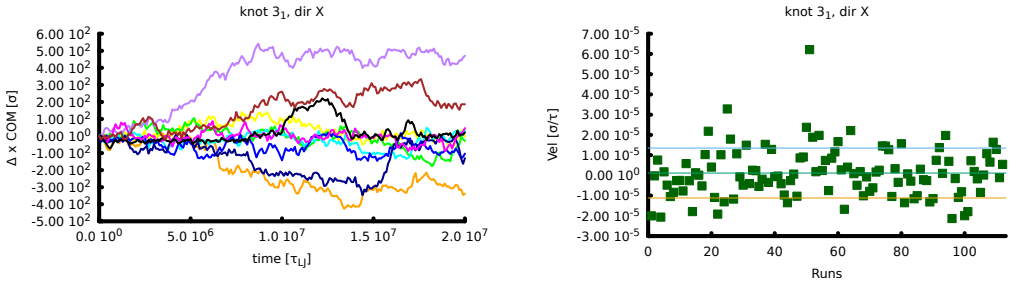

Figure 4.2: Mobility of a sample knot (3_1) with fixed spheres in a direction perpendicular to the electric field. Left: displacement of the centre of mass versus time of ten randomly-selected chains. We can see that in all cases the motion is similar to a random walk. Right: velocities of all the 112 chains simulated for a sample knot (3_1) with fixed spheres in a direction perpendicular to the electric field. The horizontal lines represent the mean value and the mean plus or minus the standard deviation. The velocities are randomly distributed around zero and do not show any particular trend.

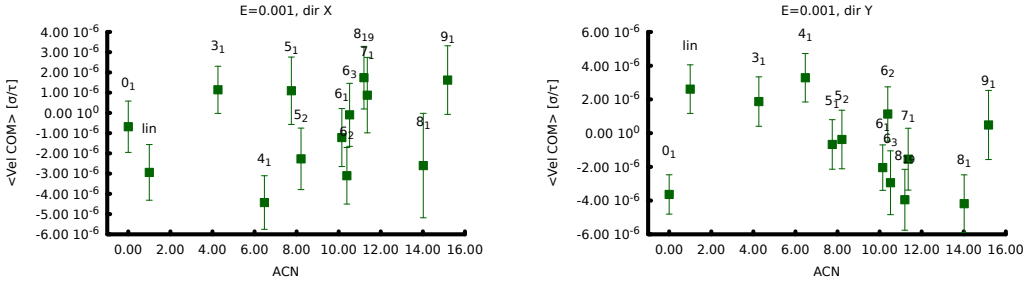

Figure 4.3: Average velocity with fixed spheres of all knot types in the directions perpendicular to the electric field, as a function of the ACN. Left: x direction; right: y direction. No particular trend depending on the type of knot emerges.

curve shows two smaller, but still noticeable, instances of trapping. Fig. 4.4 on the right shows the velocities in the direction parallel to the electric field of all the chains tied in a 3_1 knot simulated with fixed spheres. Again, we can see that many molecules have been delayed in their motion and their velocities are well below the average.

If we compare these graphs with the value of the radius of gyration of some molecules (Fig. 4.5), we can see that a proportion of the molecules get trapped in the suspension, due to one or more spheres being in close contact and not allowing the chains to proceed. Snapshots from the VMD videos of some simulations that show an examples of such trapping are also shown in the relative figures.

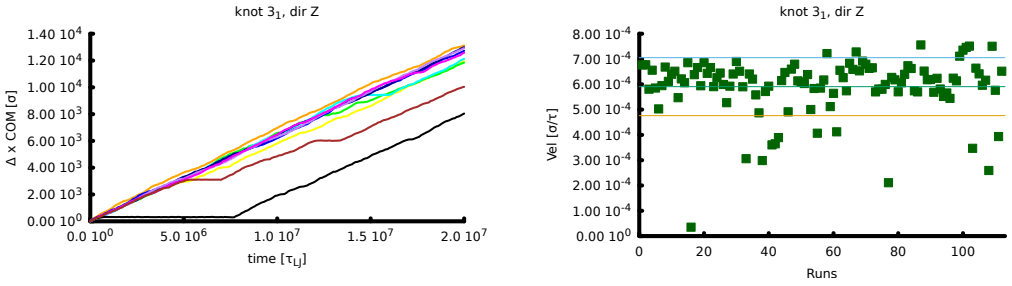

Figure 4.4: Left: displacement of the centre of mass versus time in the direction parallel to the electric field of ten randomly-selected chains. We can see that the black and the red curves clearly display evidence of trapping. Right: velocities of all the chains simulated for a sample knot (3_1) with fixed spheres in the direction parallel to the electric field. The horizontal lines represent the mean value and the mean plus or minus the standard deviation. Many molecules have been delayed in their motion and their velocities are below the average.

By plotting the resulting velocities against the average crossing number, we do not notice a clear trend in the mobility of the chains in connection with the topology (Fig. 4.6). With this system, it is not possible to separate the knotted molecules by the type of knot.

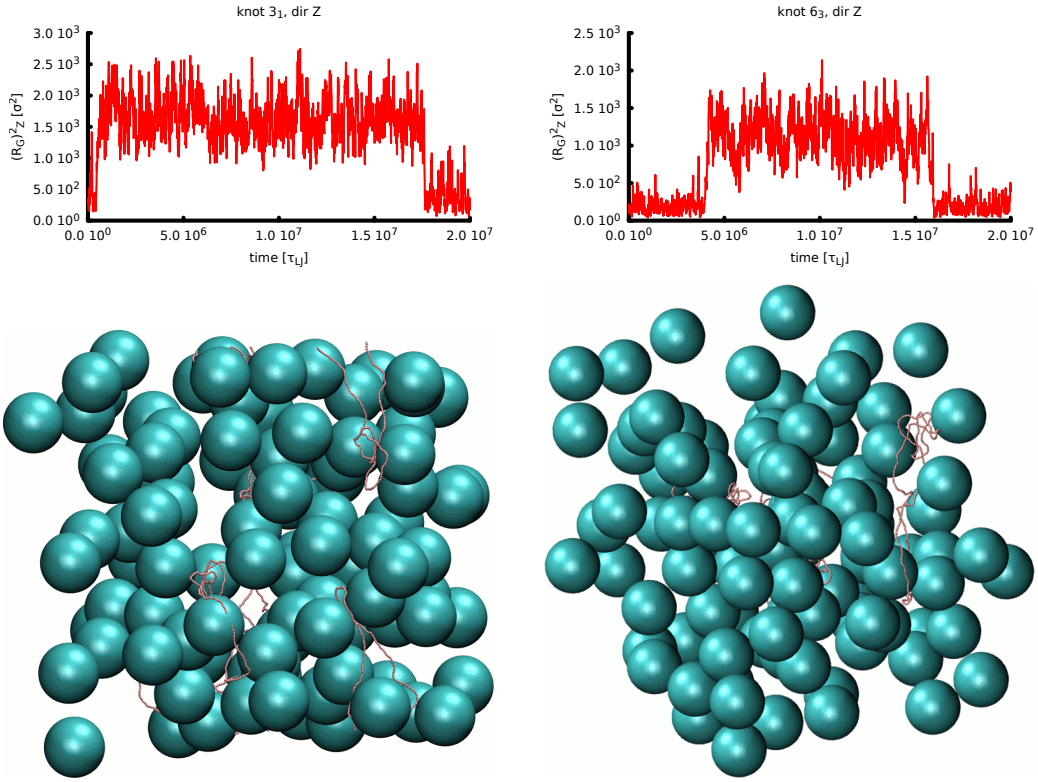

Figure 4.5: Square radius of gyration (Z component as defined in Eq. 4.2) of sample knots (left: 3_1, right: 6_3) with fixed spheres. Top: in some cases, the radius of gyrations suggests an elongated molecule in the direction of the driving force. Bottom: this corresponds to trapped configurations as shown in the snapshot from the relative simulation. If we observe the molecules on the right in both pictures, we can see that in both cases trapping results in an elongated configuration. The 3_1 in the image on the left appears in two parts due to the periodic boundary conditions.

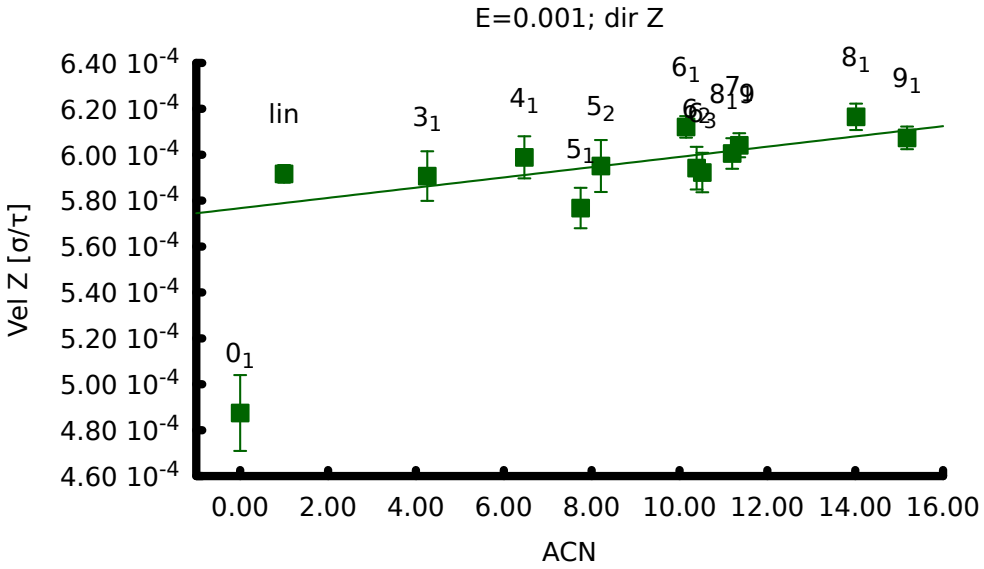

Figure 4.6: Average velocity in the direction parallel to the electric field of the knotted molecules versus the average crossing number of the ideal configurations of the corresponding knots with fixed spheres. No particular trend is noticeable. As the ACN for the linear chain is not defined, in this graph and in the following it is indicated as 1 for illustration purposes only and its value is not used in the computation of the fit parameters. In this graph only, also the mobility for the 0_1 has been ignored in the computation of the fit line, as the point is an outlier. The errorbars have been calculated as the standard error of the mean over 112 chains per knot type that were performed (4 chains per simulation, 28 simulations per knot type). As the values are not distributed according to a Poisson law, the error bars shown effectively underestimate the actual fluctuations.

4.4 Mobility with moving spheres

With moving spheres, we can notice the same overall behaviour as with fixed spheres in the directions perpendicular to the electric field, that is, random motion centred on zero (Fig. 4.7). This is reflected in the plot of the average velocities as a function of the ACN: as Fig. 4.8 shows, all the values are small and centred around zero.

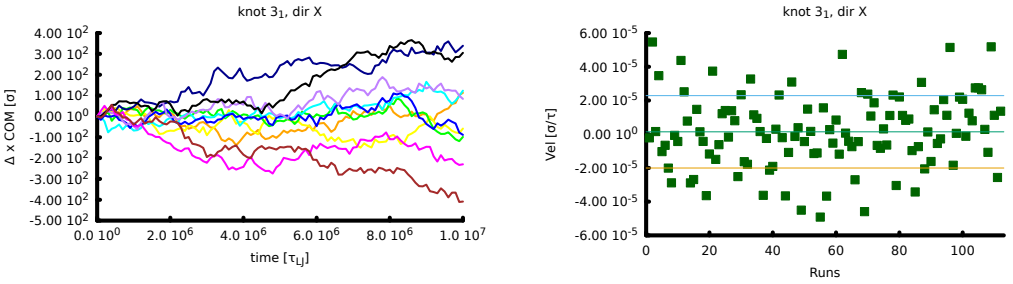

Figure 4.7: Mobility of a sample knot (3_1) with moving spheres in a direction perpendicular to the electric field. Left: displacement of the centre of mass versus time of ten randomly-selected chains. In all cases the motion is similar to a random walk. Right: velocities of all the chains simulated for a sample knot (3_1) with fixed spheres in a direction perpendicular to the electric field. The horizontal lines represent the mean value and the mean plus or minus the standard deviation. The velocities are randomly distributed around zero and do not show any particular trend.

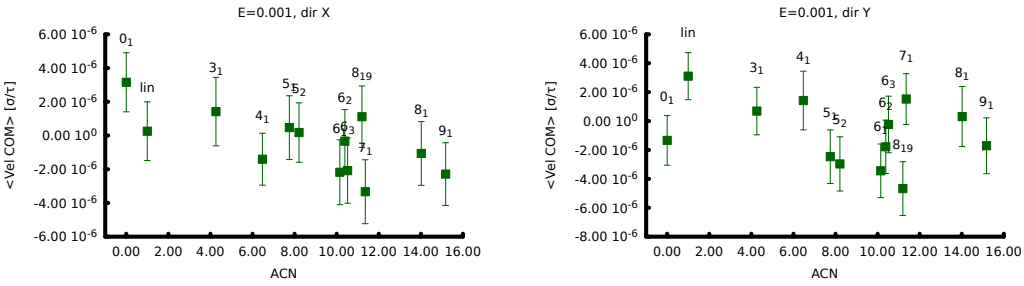

Figure 4.8: Average velocity with moving spheres of all knot types in the directions perpendicular to the electric field, as a function of the ACN. Left: x direction; right: y direction. No particular trend depending on the type of knot emerges.

In the direction parallel to the electric field, we can see that all the graphs show a linear trend centred around an average value and there are no cases of trapping (Fig. 4.9). Fig. 4.10 shows some examples of the radius of gyration of the molecules in this case. All of the simulations were examined and no

instances of trapping were noticed. Looking at Fig. 4.10, it appears the more open 0_1 has more significant stretches than the more compact 8_1.

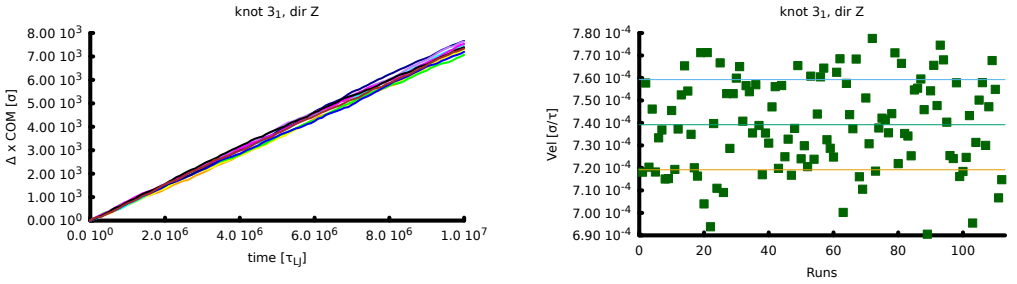

Figure 4.9: Mobility of a sample knot (3_1) with moving spheres in the direction parallel to the electric field. Left: displacement of the centre of mass versus time in the direction parallel to the electric field of ten randomly-selected chains. Right: velocities of all the chains simulated for a sample knot (3_1) with moving spheres in the direction parallel to the electric field. The horizontal lines represent the mean value and the mean plus or minus the standard deviation. The displacement and the velocities are distributed symmetrically around the mean as there is non trapping.

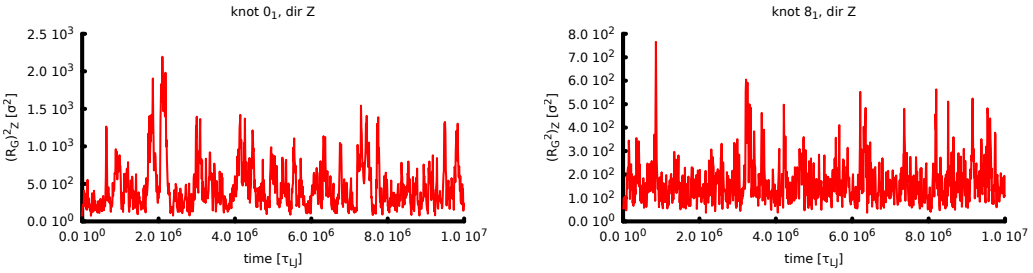

Figure 4.10: Square radius of gyration (Z component as defined in Eq. 4.2) of sample knots (left: 0_1, right: 8_1) with moving spheres. The radius of gyration suggests a molecule with shape varying randomly with time. However the excursins in $(R_G^2)_Z$ that we can see in the graph on the left suggest that the 0_1 is occasionally stretching quite significantly compared to the more compact knot types, such as the 8_1 (on the right).

By plotting the average velocities against the ACN (Fig. 4.11), we can see a clear trend in the mobility: more complex knots move faster than simpler knots and the relationship is close to linear. In all these plots, the ACN for the linear molecule has been arbitrarily set to 1 as in this case the value of the ACN is not defined, and the corresponding data has not been considered in the calculation of the line of best fit.

In addition, we can notice that all the molecules move faster than in the fixed-sphere case, which confirms that the hindrance due to moving spheres is

less important than that due to fixed spheres, even though the density of space occupied is the same.

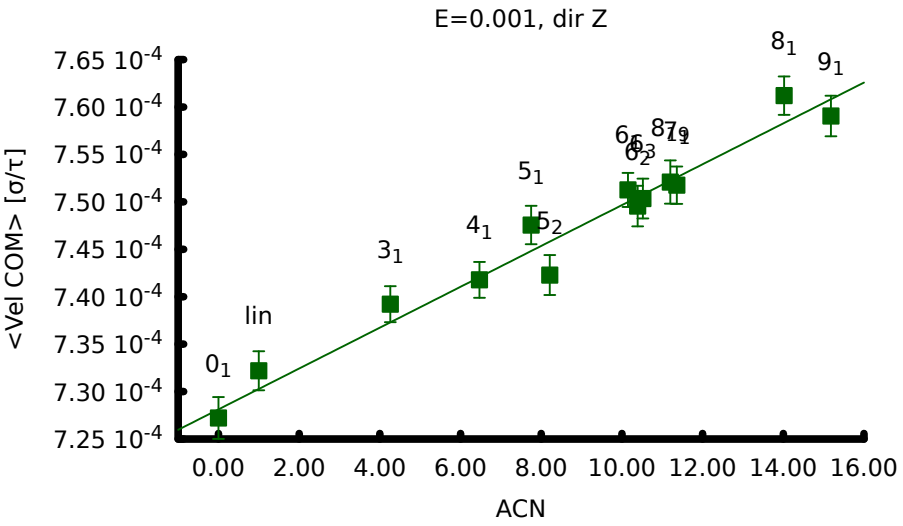

Figure 4.11: Average velocity in the direction parallel to the electric field of the knotted molecules versus the average crossing number of the ideal configurations of the corresponding knots with moving spheres. There is a small, but clear trend: the velocity increases linearly with the ACN.

4.4.1 Check for possible changes in the gel

In the case of moving spheres, the fact that the components of the gel are able to move poses the question of whether the spheres may evolve into a non-uniform configuration, so changing the characteristics of the suspension. This would be a similar problem to the well-known issue of ageing in real experiments with gels (Russell, 1987; Scherer, 1988).

To this end, the motion of 10 spheres randomly selected from a simulation was analysed and the MSD versus time measured. A sample of the results for two of them is shown in Fig. 4.12. This shows that the motion of the spheres is indeed random as wanted, and the fact that they move away from the initial position and then back many times indicates that they often bounce against each other, so inverting the direction of motion. Therefore the motion of the spheres changes the configuration of the suspension during the simulations, but not its inherent characteristics of spatial uniformity and randomness.

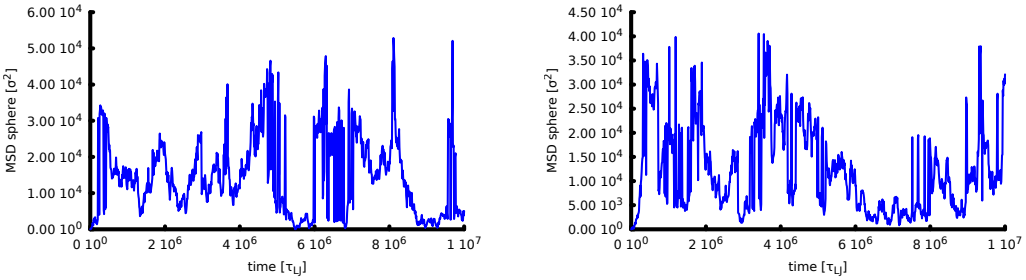

Figure 4.12: MSD of two sample moving spheres (out of 100) from the same simulation. The motion is random and shows evidence that the spheres bounce against each other many times.

4.5 Comparison with the case of free solution

In order to understand whether the trend in the mobility of the molecules is due to the presence of the suspension of spheres, rather than simply by the motion through the solution, a set of simulations was performed with the same knotted chains but in the absence of any spheres.

As shown in Fig. 4.13, in the absence of spheres the knotted chains move at approximately the same speed in the direction of the driving force regardless of the topology, and no particular trend emerges.

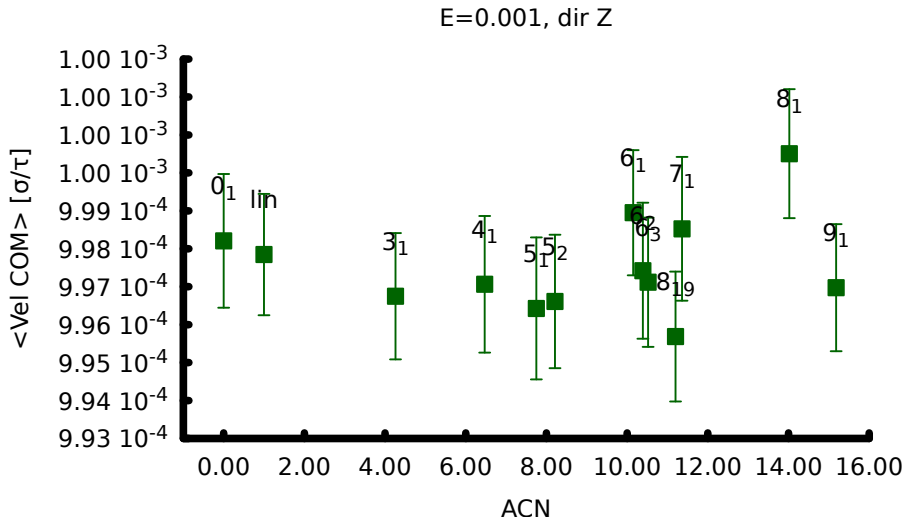

Figure 4.13: Average velocity with moving spheres of all knots in the direction parallel to the electric field without a suspension. In accordance with the Rouse model, the velocities have all very similar values and do not show any particular trend as all the chains are composed of the same number of beads.

As hydrodynamic interactions are not considered in this model, this is the expected behaviour. In fact, as seen in Section 2.4.1, the sedimentation speed according to the Rouse model depends inversely on the number of beads, not on the shape of the molecules, and the number of beads is the same for all the molecules considered. As a result, this confirms that the trend seen in the case of moving spheres is indeed due to the suspension and not simply to the viscosity of the medium.

If we compare the three cases in Fig. 4.14, we can see that, regardless of the kind of knot, the overall mobility is maximum for a free solution, while it is minimum for a suspension of fixed spheres. This confirms again that fixed spheres generate a higher level of hindrance to the motion, sufficient to disrupt the the trend in the mobility with respect to the ACN that we can see with moving spheres.

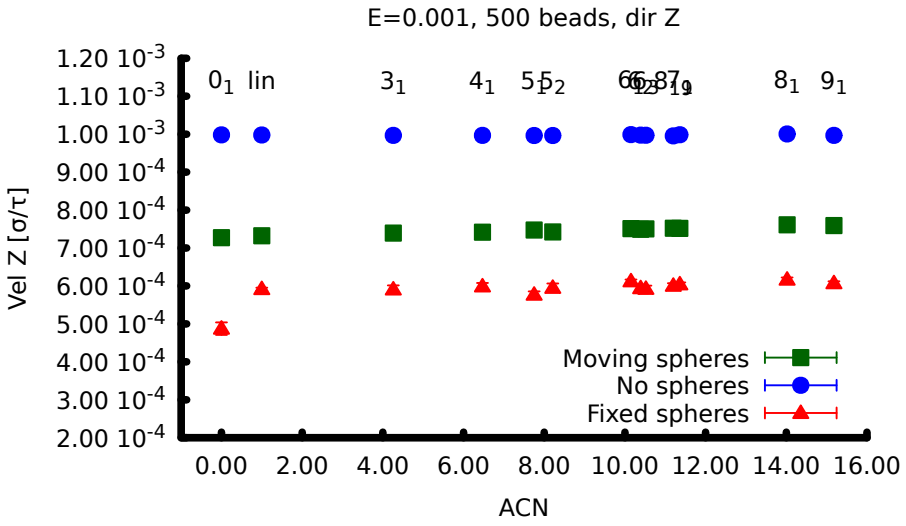

Figure 4.14: Comparison of the average velocities of all knots in the direction parallel to the electric field in the case of no suspension and for fixed or moving spheres. The motion is fastest in the absence of spheres and slowest when these are fixed. At this scale, it is not possible to appreciate the small trend that emerges in the case of moving spheres.

4.6 Comparison with molecules of different length

As explained in Section 4.1, the value of 500 beads has been chosen in order to represent a typical length of DNA in agarose-gel electrophoresis experiment of 1.25 micron, as for example in Cebrián et al. (2015). However, it is interesting to determine if these results hold in the same conditions for longer or shorter molecules. To this end, simulations were performed with molecules half and twice the length considered so far, that is to say, 250 and 1000 beads.

It has to be noted that due to time constraints in the length of the simulations, a considerably shorter total time has been simulated in these cases and therefore the results are statistically less meaningful, especially in the case of longer molecules.

4.6.1 Comparison of the average radius of gyration

Figures 4.15 and 4.16 show the value of the radius of gyration in the case of 250 beads and 1000 beads, with either fixed spheres (left) or moving spheres (right). In Fig. 4.17, a plot of the radius of gyration in the case of moving spheres of a sample knot (the 0_1 in all cases) is shown against the square root of the numbers of beads. The graph shows that the dependence is approximately linear, as we saw it would be for an ideal chain (Section 1.3.1).

Apart from this expected dissimilarity due to the different linear length of the molecules, we can observe that the radius of gyration behaves in a different way in the two cases of shorter and longer molecules. In fact, in the case of 250 beads the radius of gyration does not change whether the spheres of the suspension are fixed or moving. On the contrary, we can see that in the case of 1000 beads the type of suspension has an effect and the average square radius of gyration is approximately double when the spheres are fixed. This suggests a much higher amount of trapping, with subsequent distortion of the shape of the molecules. As it will be shown below (see Fig. 4.36 later in the chapter), the trapping of the molecule results in an elongated shape in the direction of the electric field rather than a globular configuration.

4.6.2 Mobility with shorter molecules

The graphs of the mobility for 250-bead-long molecules show a very similar behaviour to the 500-bead case, as the following graphs will show.

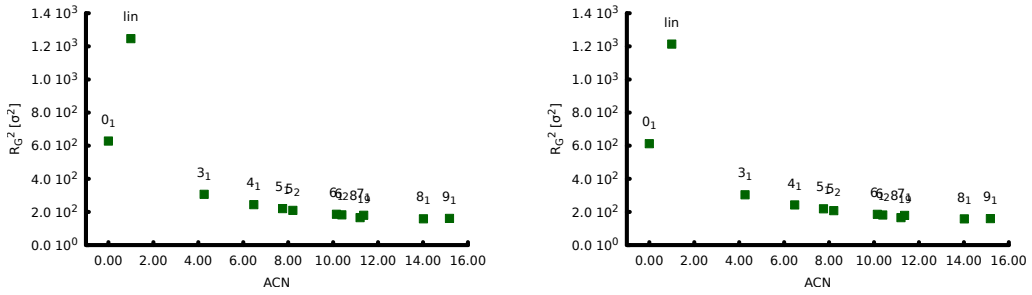

Figure 4.15: Square of the radius of gyration of the 250-bead molecules in the simulations with fixed (left) and moving (right) spheres. We can see that for molecules of this length, the radius of gyration is not noticeably affected by the different suspensions.

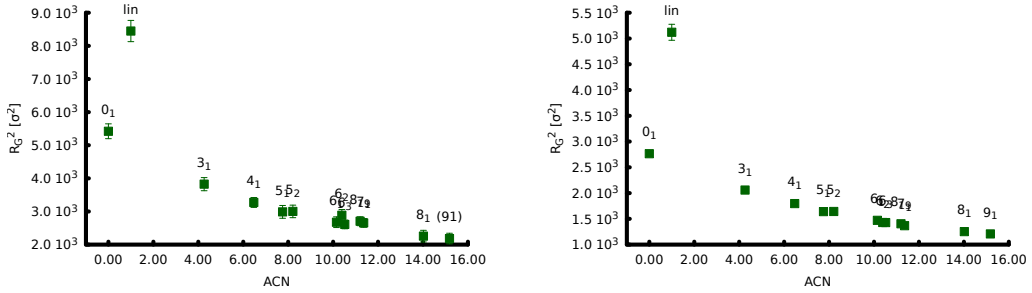

Figure 4.16: Square radius of gyration of the 1000-bead molecules in the simulations with fixed (left) and moving (right) spheres. We can see that for molecules of this length, the radius of gyration is affected by the different suspensions and it is noticeably longer in the case of fixed spheres, suggesting a more elongated, less globular, configuration.

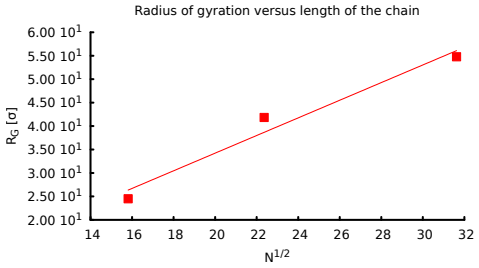

Figure 4.17: Radius of gyration of a sample knot, the 0_1 in all cases, as a function of the square root of the number of beads. With moving spheres, $R_G \propto \sqrt{N}$ like for an ideal chain.

Mobility in the directions perpendicular to the electric field

In the direction perpendicular to the electric field, the displacement simply corresponds to a random walk due to thermal motion. Therefore for a sample

knot the velocities are randomly distributed around zero. This is valid both in the case of fixed spheres, as shown in Fig. 4.18, and in the case of moving spheres, as shown in Fig. 4.19.

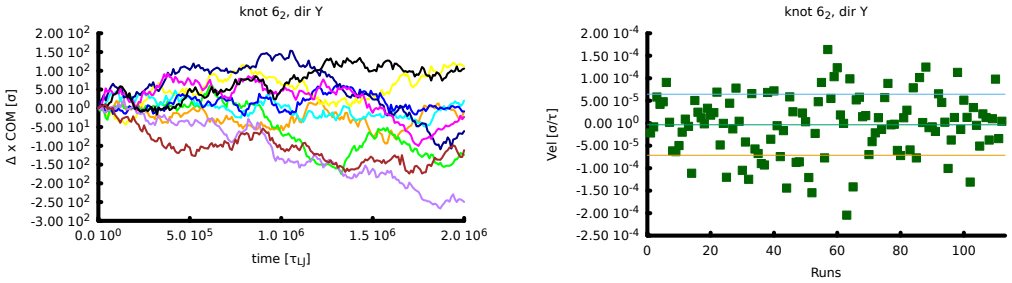

Figure 4.18: Mobility of a sample knot (6_2) with fixed spheres in the direction perpendicular to the electric field. Left: displacement of the centre of mass versus time in the direction perpendicular to the electric field of ten randomly-selected chains. Right: velocities of all the chains simulated for the sample knot. The horizontal lines represent the mean value and the mean plus or minus the standard deviation. The velocities are randomly distributed around zero and do not show any particular trend. Length of the molecules: 250 beads.

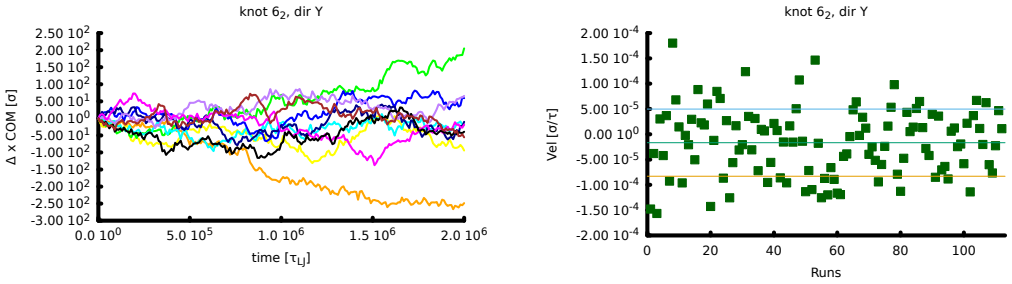

Figure 4.19: Mobility of a sample knot (6_2) with moving spheres in the direction perpendicular to the electric field. Left: displacement of the centre of mass versus time in the direction perpendicular to the electric field of ten randomly-selected chains. Right: velocities of all the chains simulated for the sample knot. The horizontal lines represent the mean value and the mean plus or minus the standard deviation. The velocities are randomly distributed around zero and do not show any particular trend. Length of the molecules: 250 beads.

As expected, we do not observe a specific trend of the mobility with respect to the knot complexity in the direction perpendicular to the electric field either for fixed (Fig. 4.20) or moving spheres (Fig. 4.21).

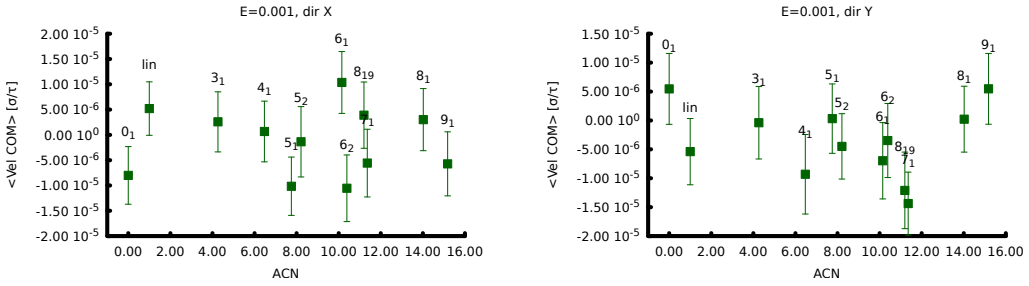

Figure 4.20: Average velocity with fixed spheres of all knot types in the directions perpendicular to the electric field, as a function of the ACN. Left: x direction; right: y direction. Length of the molecules: 250 beads. No particular trend depending on the type of knot emerges.

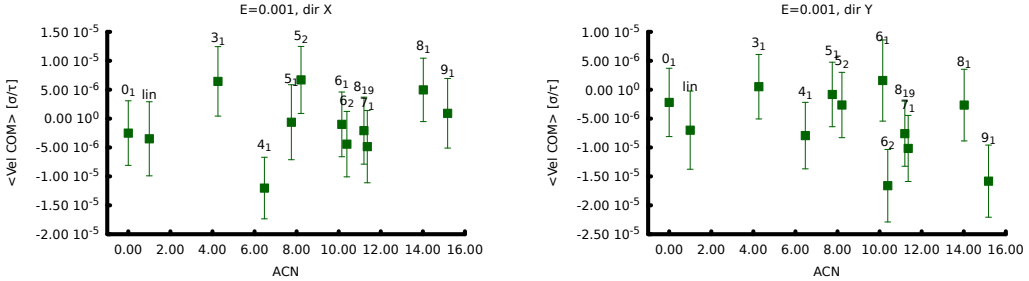

Figure 4.21: Average velocity with moving spheres of all knot types in the directions perpendicular to the electric field, as a function of the ACN. Left: x direction; right: y direction. Length of the molecules: 250 beads. No particular trend depending on the type of knot emerges.

Mobility in the direction parallel to the electric field

In the direction parallel to the electric field we can see an approximately linear displacement with time in all cases, as we would expect.

As for the molecules of 500 beads, we can see that in the case of fixed spheres, the motion seems to be delayed in many places. However, these delays never last for a long time, as is shown in Fig. 4.22.

Again, we can see (Fig. 4.23) that when the spheres are moving, the molecules do not get trapped in the suspension and the displacement with time is more regularly linear.

Similarly to the case of 500 beads, we do not observe a specific trend in the direction parallel to the electric field in the case of fixed spheres (Fig. 4.24), while we can see a clear linear relationship between average crossing number and mobility in the case of moving spheres (Fig. 4.25). With these shorter molecules the trend seems to be more pronounced (see also below Section 4.6.4).

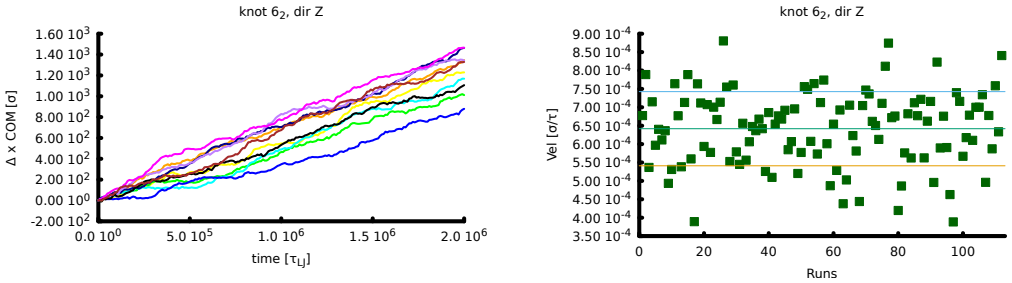

Figure 4.22: Mobility of a sample knot (6_2) with fixed spheres in the direction parallel to the electric field. Left: displacement of the centre of mass versus time in the direction parallel to the electric field of ten randomly-selected chains. Right: velocities of all the chains simulated for the sample knot. The horizontal lines represent the mean value and the mean plus or minus the standard deviation. Length of the molecules: 250 beads.

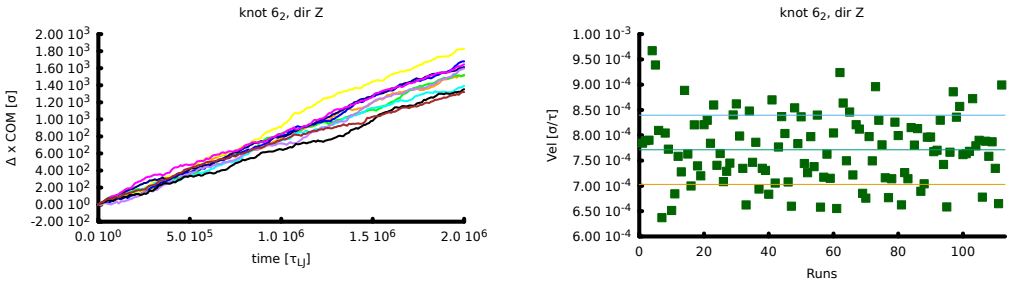

Figure 4.23: Mobility of a sample knot (6_2) with moving spheres in the direction parallel to the electric field. Left: displacement of the centre of mass versus time in the direction parallel to the electric field of ten randomly-selected chains. Right: velocities of all the chains simulated for the sample knot. The horizontal lines represent the mean value and the mean plus or minus the standard deviation. Length of the molecules: 250 beads.

Trapping

As noted above for the displacement of the center of mass (Fig. 4.22), in the case of fixed spheres the analysis of the radius of gyration of the molecules (Fig. 4.26) seems to suggest a slightly higher probability of trapping with respect to the case of moving spheres (Fig. 4.27), but the effect is quite small. This definitely lasts for shorter periods of time with respect to the molecules made of 500 beads, which is understandable, as shorter molecules are more difficult to trap than longer ones.

Even though the molecules are forced by the electric field to squeeze through fixed spheres by changing shape, these smaller molecules keep approximately a globular configuration at all times (Fig. 4.26, bottom).

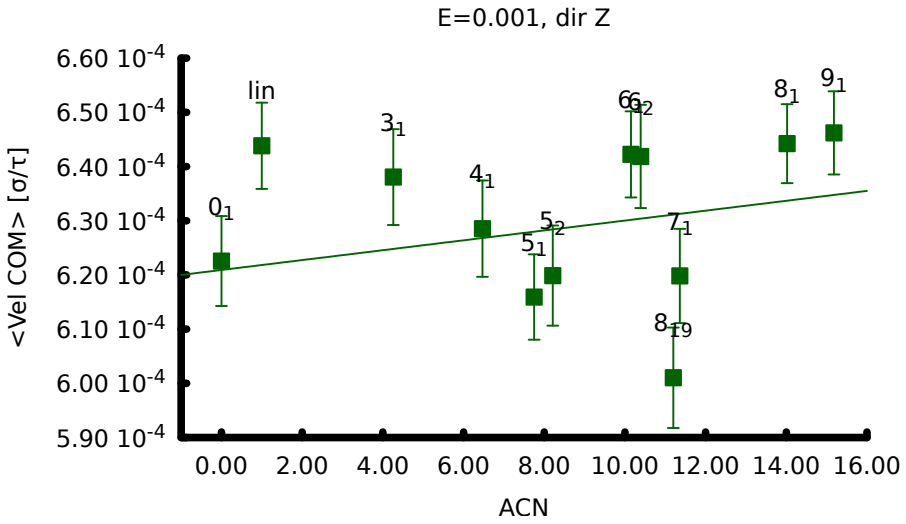

Figure 4.24: Average velocity in the direction parallel to the electric field of the knotted molecules versus the average crossing number with fixed spheres. Length of the molecules: 250 beads. No particular trend is noticeable.

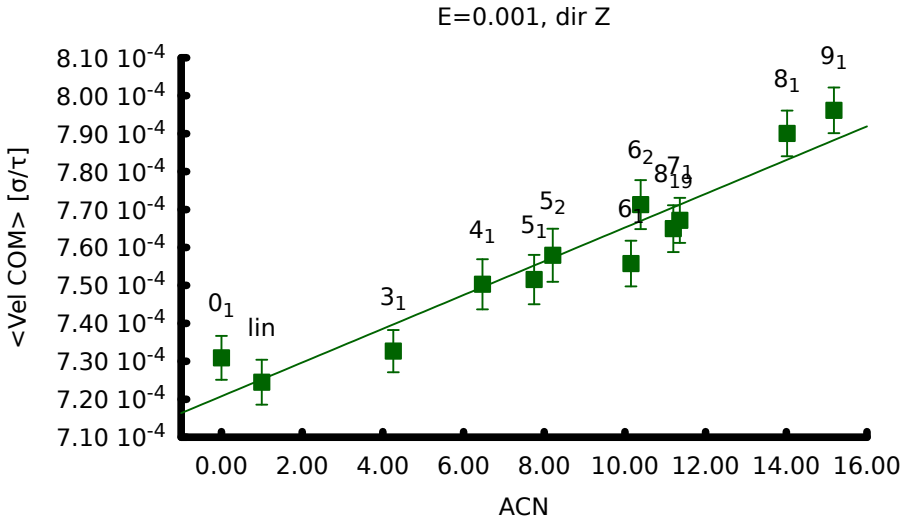

Figure 4.25: Average velocity in the direction parallel to the electric field of the knotted molecules versus the average crossing number with moving spheres. Length of the molecules: 250 beads. Like in the case of 500 beads, the mobility shows a clear trend: the molecules travel linearly faster as their ACN increases.

Although smaller than for longer molecules, the hindrance due to the fixed spheres is still present and sufficient to disrupt the linear dependence of the mobility on the ACN.

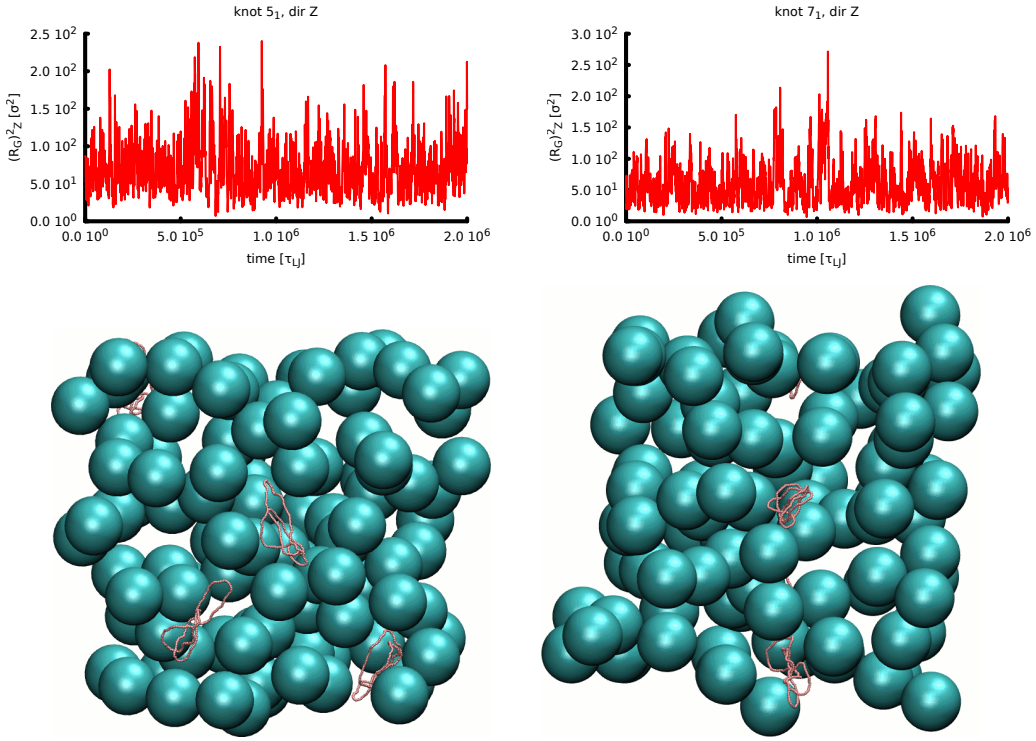

Figure 4.26: Square radius of gyration (Z component as defined in Eq. 4.2) of sample knots (left: 5_1, right: 7_1) with fixed spheres. Top: the radius of gyrations suggests an elongated molecule in the direction of the driving force for very short periods of time. Bottom: snapshots from the corresponding simulations. With molecules of 250 beads, the shape may temporarily become more elongated in the direction of the field (left), but it is typically more compact than in the case of longer molecules.

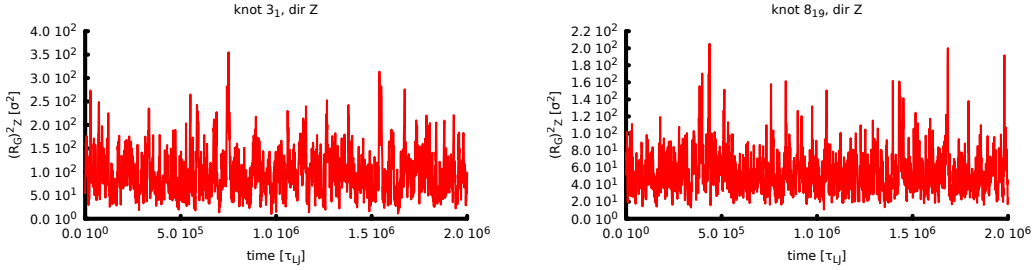

Figure 4.27: Square radius of gyration (Z component as defined in Eq. 4.2) of sample knots (left: 3_1, right: 8_{19}) with moving spheres. In this case, the molecules never seem to get trapped by the suspension.

4.6.3 Mobility with longer molecules

Again, the graphs of the mobility for 1000-bead-long molecules show a similar behaviour to the 500-bead and the 250-bead cases. However the simulations for these molecules were not performed for a long simulation time and the data are therefore much more noisy.

Mobility in the directions perpendicular to the electric field

Also in the case of 1000 beads, the results are in line with the 500-bead case. That is, we can see random motion of the centre of mass in the direction perpendicular to the electric field both in the case of fixed spheres (Fig. 4.28) and moving spheres (Fig. 4.29).

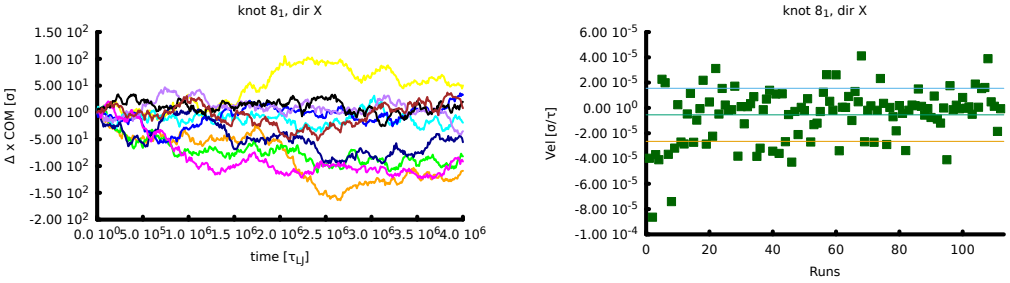

Figure 4.28: Mobility of a sample knot (8_1) with fixed spheres in a direction perpendicular to the electric field. Left: displacement of the centre of mass versus time of ten randomly-selected chains. Again, in all cases the motion is similar to a random walk. Right: velocities of all the chains simulated for the sample knot. The horizontal lines, as before, represent the mean value and the mean plus or minus the standard deviation. The velocities are randomly distributed around zero and do not show any particular trend. Length of the molecules: 1000 beads.

This is once more reflected in the distribution of the average velocities as a function of the type of knot, which are randomly distributed around zero both with fixed spheres (Fig. 4.30) and with moving spheres (Fig. 4.31). This is again as expected, as the motion in the direction perpendicular to the electric field is only due to Brownian motion.

Mobility in the direction parallel to the electric field

If we now consider the motion in the direction parallel to the electric field with a suspension of fixed spheres, as shown in Fig. 4.32, we still have linear displacement with respect to time, but the instances of trapping appear to be

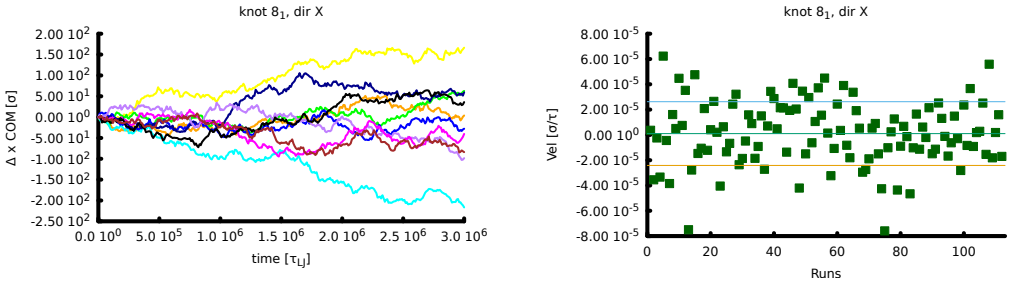

Figure 4.29: Mobility of a sample knot (8_1) with moving spheres in a direction perpendicular to the electric field. Left: displacement of the centre of mass versus time of ten randomly-selected chains. Again, in all cases the motion is similar to a random walk. Right: velocities of all the chains simulated for the sample knot. The horizontal lines, as usual, represent the mean value and the mean plus or minus the standard deviation. The velocities are randomly distributed around zero and do not show any particular trend. Length of the molecules: 1000 beads.

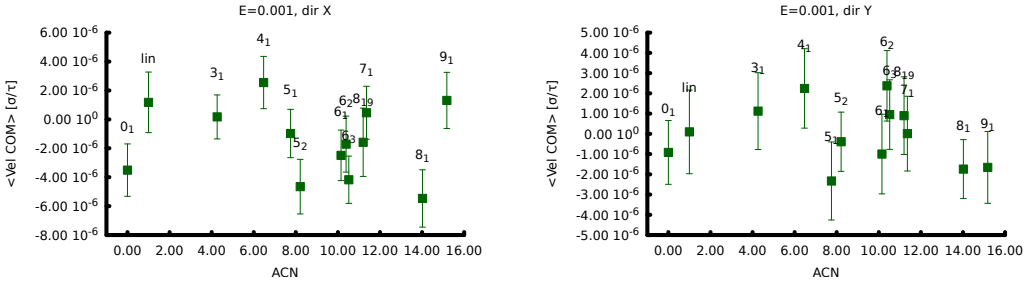

Figure 4.30: Average velocity with fixed spheres of all knot types in the directions perpendicular to the electric field, as a function of the ACN. Left: x direction; right: y direction. This is a random motion and no particular trend depending on the type of knot emerges. Length of the molecules: 1000 beads.

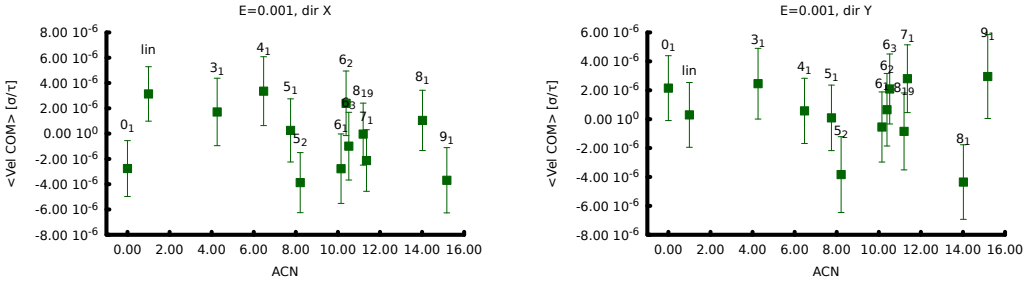

Figure 4.31: Average velocity with moving spheres of all knot types in the directions perpendicular to the electric field, as a function of the ACN. Left: x direction; right: y direction. This is a random motion and no particular trend depending on the type of knot emerges. Length of the molecules: 1000 beads.

more numerous and to last for longer periods of time. In fact, most of the chains show signs of trapping at some time, and in the case of the purple, blue and magenta lines in the graph depicting the displacements (on the left), this lasts for most of the simulation time. The average velocities shown on the right indicate that, in the sample, many more cases appear to be significantly delayed, than the ones able to move significantly faster than the average.

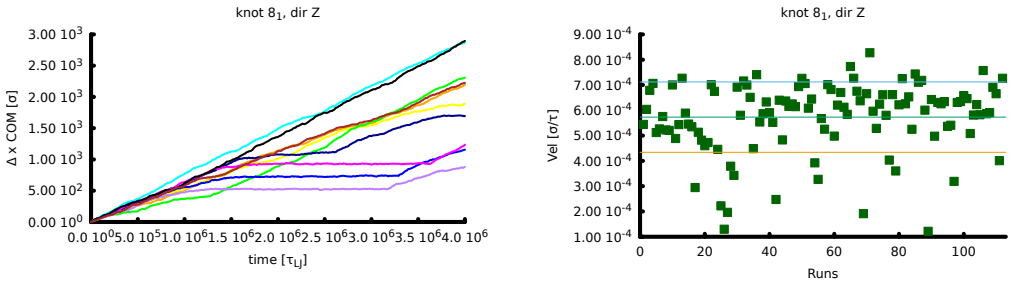

Figure 4.32: Mobility of a sample knot (8_1) with fixed spheres in the direction parallel to the electric field. Left: displacement of the centre of mass versus time of ten randomly-selected chains. Right: velocities of all the chains simulated for the sample knot. The horizontal lines, as before, represent the mean value and the mean plus or minus the standard deviation. The graphs show many instances of long delays in the motion. Length of the molecules: 1000 beads.

If we now switch to the system with moving spheres (Fig. 4.33), we can see that, like in the case of 250 and 500 beads, molecules never get trapped for long periods of time, as any obstruction from the spheres is quickly cleared as these move quickly away.

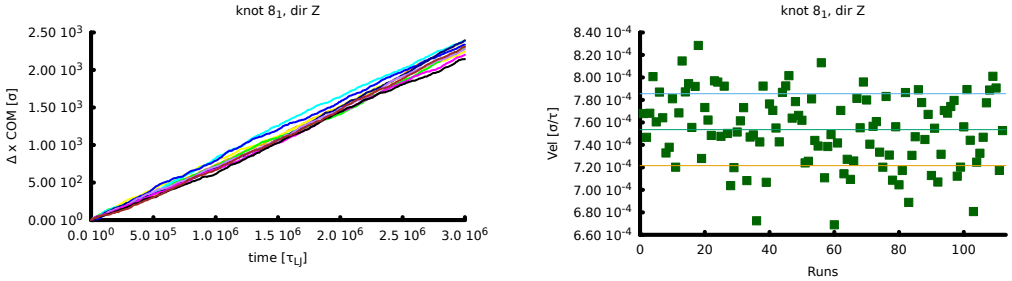

Figure 4.33: Mobility of a sample knot (8_1) with moving spheres in the direction parallel to the electric field. Left: displacement of the centre of mass versus time of ten randomly-selected chains. Right: velocities of all the chains simulated for the sample knot. The horizontal lines, as before, represent the mean value and the mean plus or minus the standard deviation. If trapping occurs, it is short lived. Length of the molecules: 1000 beads.

In the same way as for 250 and 500 beads, we do not seem to see a particular trend of the mobility in relation to the type of knot in the case of fixed spheres (Fig. 4.34). The data are too noisy to be able to tell with certainty, but it seems that the fixed spheres are able also in this case to disrupt any trend due to the type of knot. Better statistics are necessary in order to be able to say this with any certainty.

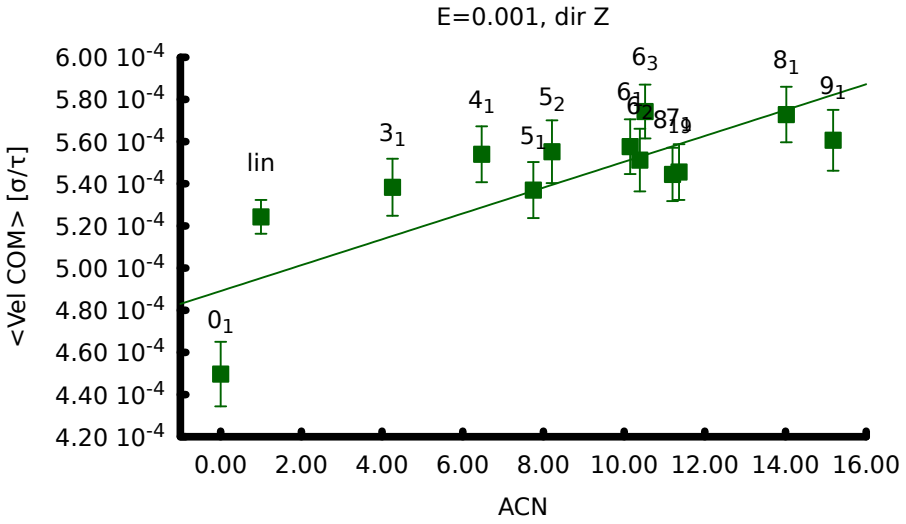

Figure 4.34: Average velocity in the direction parallel to the electric field of the 1000-bead knotted molecules versus the average crossing number with fixed spheres. It is difficult to say whether these data show a trend or not.

In the case of moving spheres (Fig. 4.35), there may be a small linear trend with the ACN, although it seems less pronounced and the statistics in this case are not good enough to state this with confidence.

Trapping

If we look at the square radius of gyration in the direction of the field (as defined in Eq. 4.2), we can confirm that when a long molecule gets trapped in the suspension of fixed spheres, it tends to stay trapped for a long period of time (Fig. 4.36, top), while its conformation tends to become very elongated in the direction of the force (Fig. 4.36, bottom).

As opposed to the case of 250 or 500 beads, however, we can notice that in some instances the molecules happen to get trapped even when the spheres of the suspension are moving. Nonetheless, when this happens, it is for much shorter periods of time than in the case of fixed spheres. Two examples of the

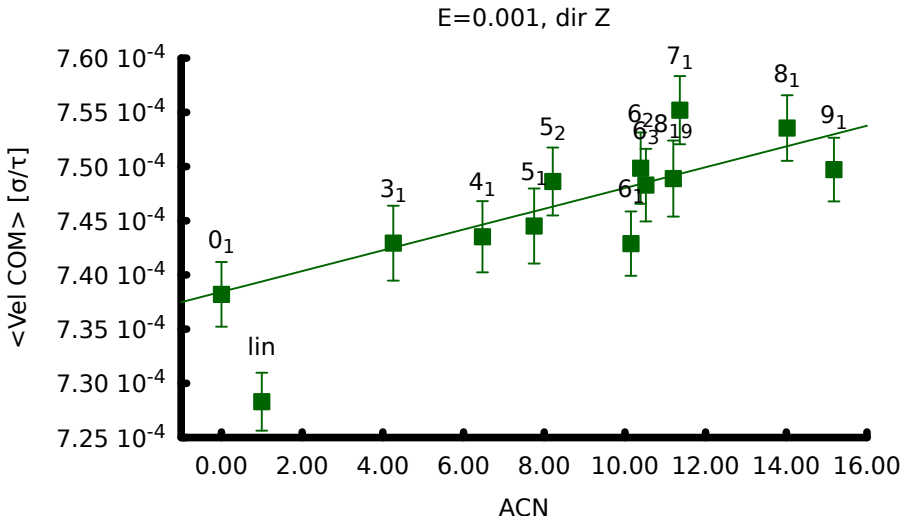

Figure 4.35: Average velocity in the direction parallel to the electric field of the 1000-bead knotted molecules versus the average crossing number with moving spheres. Although less pronounced than with shorter molecules and with noisier data, there may be a linear dependence of the mobility on the ACN, but this is not very clear.

square radius of gyration in the direction of the field for 1000-bead molecules in a moving-sphere suspension are shown in Fig. 4.37.

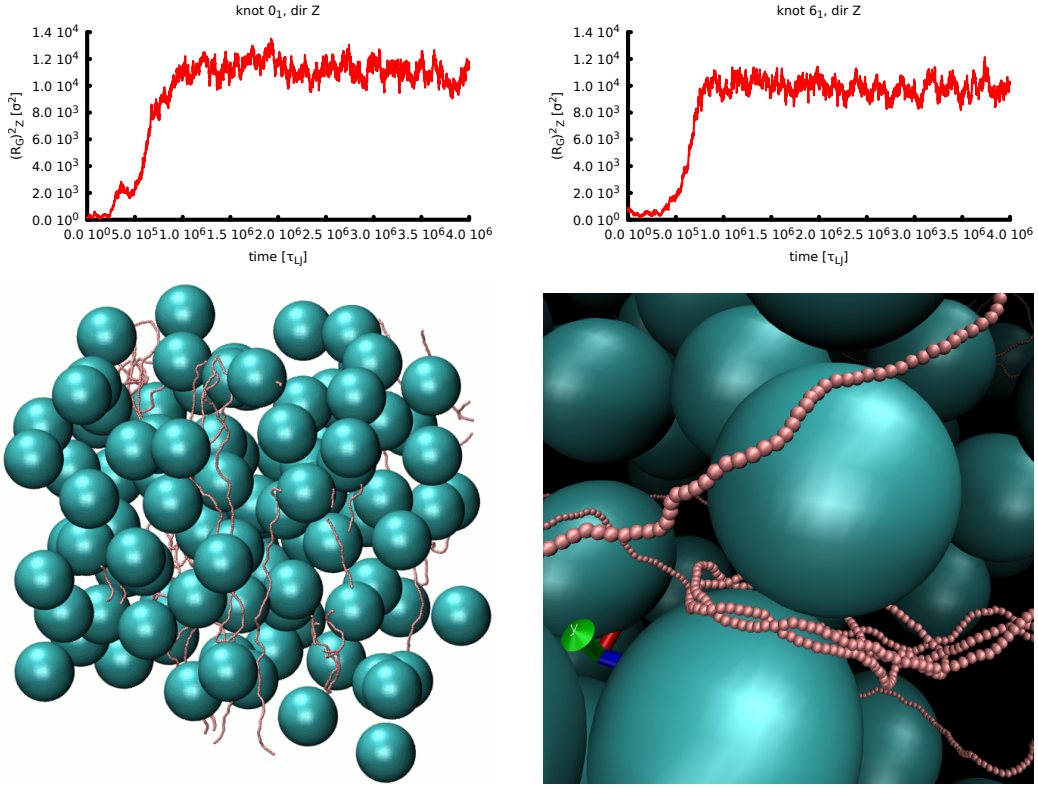

Figure 4.36: Square radius of gyration (Z component as defined in Eq. 4.2) of sample knots (left: 0_1, right: 6_1) of 1000 beads with fixed spheres. Often the radius of gyrations suggests an elongated molecule in the direction of the driving force, as confirmed by snapshots of the simulation for the 6_1 at the bottom.

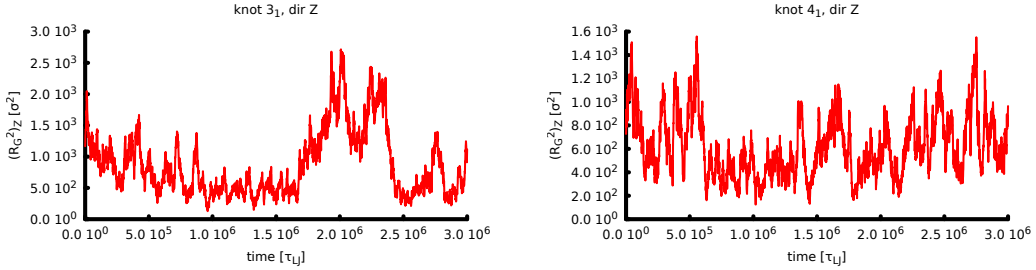

Figure 4.37: Square radius of gyration (Z component as defined in Eq. 4.2) of sample knots of 1000 beads (3_1 and 4_1) with moving spheres.

4.6.4 Comparison of the mobility for molecules of different lengths

Fig. 4.38 shows together the graphs of the average velocities in the direction of the electric field for a suspension of moving spheres as a function of the ACN for the three cases examined, that is, molecules consisting of 250, 500 and 1000 beads.

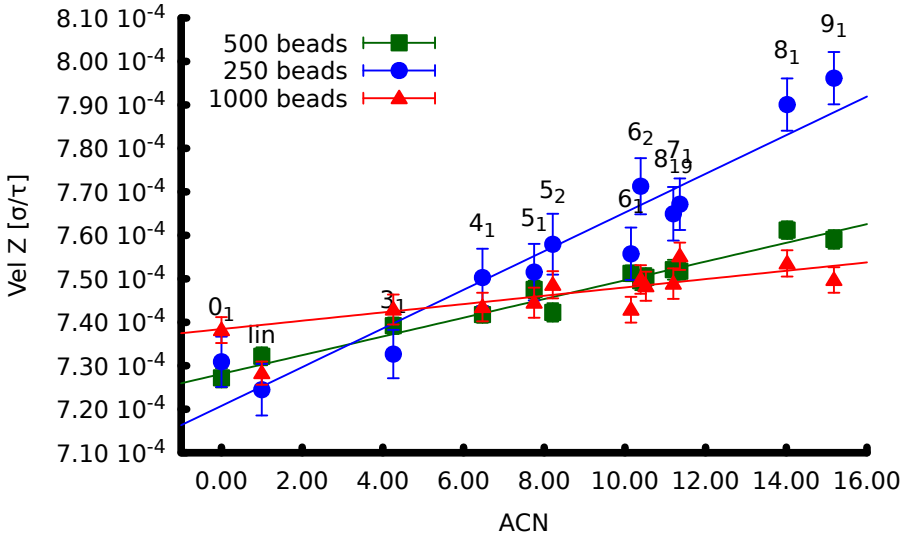

Figure 4.38: Average velocity with moving spheres of all knots in the direction parallel to the electric field in the case of 250 beads (blue), 500 beads (green) and 1000 beads (red). Overall, the magnitude of the velocities does not change much with the length of the chains. However, the effect of the type of knot on the slope of the curve increases significantly as the molecules are made shorter.

We can notice that, in general, the velocity of the molecules in the three sets are very similar. However, the three slopes are different and decrease significantly for increasing length of the molecules. A visual examination of the simulations seems to suggest that in longer molecules the knot tends to be more localised (see, for example, previous Figures 4.5, 4.26 and 4.36). This would mean that, with respect to the overall shape, the knotted area would be confined, and a large section of the molecule would behave as if it was unknotted, making the difference between the shapes of differently-knotted molecules less pronounced.

If we consider the least and the most knotted molecules in the simulations performed, that is, the unknot 0_1 and the knot 9_1, and we plot their mobility against the number of beads in all the cases considered, we can compare these trends with the two theoretical trends predicted by the Rouse model and the

Zimm model. This is done in Fig. 4.39. Here the simulation results with fixed spheres are identified with square points and the results with moving spheres with triangles, while the two theoretical trends are indicated by round points. In both cases, the theoretical points have to be read as a trend, and not as specific values, as the height of the first point in each set is arbitrary.

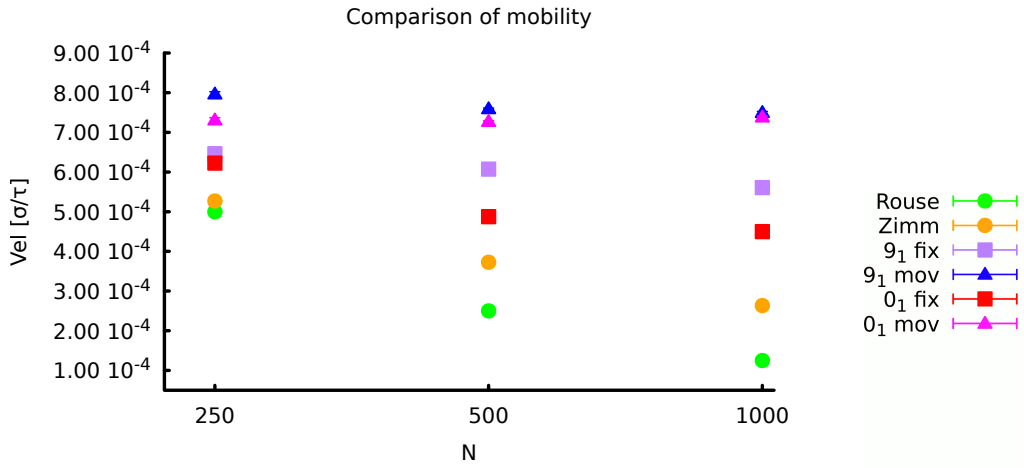

Figure 4.39: Mobility versus number of beads for the knots 0_1 and 9_1 with fixed and moving spheres. The scale is double logarithmic. The trends calculated according to the models by Rouse and Zimm are shown for comparison.

As seen in Section 2.4, the Rouse model does not take into consideration hydrodynamic interactions and predicts a diffusion constant associated with the centre of mass of a molecule inversely proportional to the number of beads, that is, $D_{CM} = \propto \frac{1}{N}$ (see Eq. 2.22). On the contrary, the Zimm model takes hydrodynamics into account and predicts a diffusion constant inversely proportional to the square root of the number of beads, that is, $D_{CM} \propto \frac{1}{\sqrt{N}}$ (see Eq. 2.24).

The results obtained with the simulations presented in this chapter do not correspond to either of these models. The closer trend is, though, the one associated with the Zimm model, and this is interesting because it means that the spheres introduce an effect somehow comparable to hydrodynamic interactions.

4.7 Discussion and conclusions

In this chapter we have seen how a simple suspension consisting of spheres of fixed size randomly distributed in space can affect the mobility of knotted chains.

The simulations analysed show a linear relationship between the complexity of the knots and their mobility in the suspension as long as the suspension is not fixed and cannot trap the chains. This is in agreement with traditional experiments of agarose-gel electrophoresis in which gel concentration and electric field are limited.

This is also in agreement with some previous mathematical models and simulations as seen in Section 1.7, with two critical differences. The first is that the model presented in this chapter does not take into consideration hydrodynamic interactions, while these were crucial in some of the previous systems reviewed, like Piili et al. (2013), who simulated the sedimentation of knotted polymers, and Gonzalez et al. (2004), who examined the dynamics of rigid filaments in the shape of ideal knots in a viscous fluid under a uniform external force. Secondly, this model relies on the interference of the suspension, which has been shown to determine the particular trend observed, while in the previous models just mentioned, the chains were moving in a viscous solution, but no attempt had been made at modelling a gel. If we consider the fact that the mobility of DNA molecules in free solution (no gel) during electrophoresis is independent of molecular length (see Section 1.6), it seems reasonable to assume that the effect of the gel in traditional, one-dimensional, agarose-gel electrophoresis should be due to more than simple hydrodynamic effects, and therefore some modelling of the gel seems essential.

As seen in the first chapter of this thesis (Section 1.7.3), the gel modelled by Michieletto et al. (2015) succeeded in reproducing the arc pattern sometimes observed in two-dimensional agarose-gel electrophoresis. In addition, as part of their simulations, they obtained a linear relationship between mobility and ACN either in the case of weak electric field or when they removed the irregularities and dangling ends from the gel they modelled. In this sense, the results obtained in this chapter are in line with those obtained with their model in those specific cases. With respect to their model, on the one hand the system presented in this chapter is much simpler and easier to reproduce, on the other hand it fails to show evidence of an arc pattern, at least with the parameters used so

far. Further simulations with higher electric field may in the future show more interesting types of behaviour.

In this model the absence of trapping proves to be important. In fact, when the suspension is immobile in a fixed configuration and the molecules can not easily free themselves, the resulting trend is no longer linear and all dependence of the mobility from the topology is lost, while trapping dominates.

The results were obtained for a typical DNA length of 1.25 micron, but additional tests with molecules half and twice as long have proven to be in agreement with the general trend. In addition, as the molecules were made longer the trend observed with moving spheres seemed to become less important, so suggesting a greater importance of the type of knot for shorter molecules than for larger ones. Ideally, better statistics are required to confirm these results for the longer molecules.

Blends of knotted DNA molecules

5

5.1 Introduction

When the concentration of polymers in a solution is such that the molecules start to overlap, entanglement and interactions start to arise, which can cause a more complex, collective behaviour. Typically, this starts at a critical concentration called the *overlap concentration* such that the volume occupied by the polymers is of the same order as the available volume:

$$N_{Tot} \cdot R_G^3 \approx V, \tag{5.1}$$

where R_G is the radius of gyration of the molecule.

When more than one type of polymer is present in a solution we have a polymer blend. These solutions are in general non-uniform mixtures of the different types. In fact, if we consider the Flory-Huggins theory applied to a mixture of two different polymers, the free energy of mixing can be expressed as (Doi, 1996):

$$f_m = \frac{1}{N_A}\phi_A \ln \phi_A + \frac{1}{N_B}\phi_B \ln \phi_B + \chi \phi_A \phi_B, \tag{5.2}$$

where A and B represent the two types of polymers, N_A and N_B their respective numbers of monomers, and ϕ_A and ϕ_B their respective volume fractions.

The first two terms of Eq. 5.2, represents the configurational free energy, and always tends to promote the mixing of molecules of different types, while the third term is the contact interaction term. As $\chi = \chi(T)$ is usually positive, this term determines phase separation as the temperature is varied.

In fact, if we have two types of molecules in a solution, and the interactions between molecules of different types is the same or very similar to the interactions between molecules of the same species, entropy favours the mixing of the two. On the contrary, if the interactions between different species are

considerably different from those between the same species, the two become partially miscible or immiscible. This property changes with other parameters like temperature or pressure because these affect molecular interactions. In many systems, decreasing the temperature favours phase separation, and in this case the process can be illustrated by the graph in Fig. 5.1.

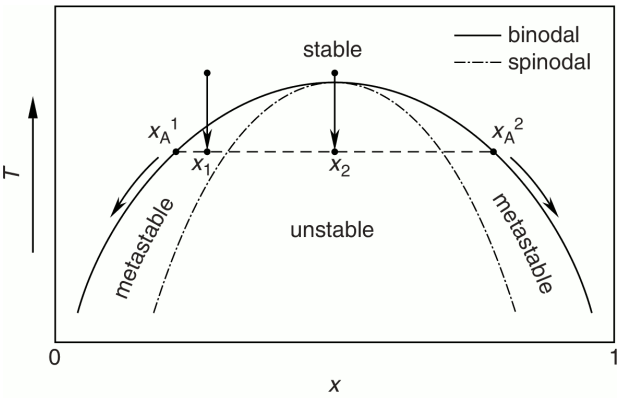

Figure 5.1: Phase separation at different concentrations x in an upper critical solution temperature system, that is a system where a decrease in temperature favours phase separation. The solid line represents the binodal curve, while the dashed line represents the spinodal curve. For simplicity, the figure shows the case of two simple, small molecule types of equal size. Otherwise the binodal and spinodal curves would not necessarily be symmetric. Image from Cheng (2008).

With reference to the graph, at a certain concentration x, the two species are mixed for any temperature T over the binodal line. As the temperature is lowered, say at concentration x_1 in the picture, and the binodal line is crossed, the mixture will separate into two phases with concentrations x_A^1 and x_A^2, which depend on the temperature and the position of the binodal. In the region between the binodal and the spinodal lines, the system is metastable and it is still possible to observe only one phase for a certain time, while below the spinodal line the mixture will exhibit spontaneous separation. After phase separation, one of the compositions will be more rich in one species and the other composition will be more rich in the other. This may not be straightforward to see, but by lowering the temperature further, the driving force of the separation becomes greater and the concentrations purer and easier to identify.

In a real system, χ in Eq. 5.2 and therefore the shape of the binodal line, will depend, as well as on the temperature and the pressure, on the shape of the molecules and the ways they come into contact with each other. In fact, many instances have been observed in experiments and simulations where

the shape was the driving force for a characteristic behaviour. Arguably the most famous case, due to its applications to modern display screens, is that of liquid crystals (Onsager, 1949). These are usually rod-like particles which exhibit phase transitions from a disordered (isotropic) phase where the particles are randomly oriented, to various different ordered phases if the temperature is decreased or the concentration increased (thermotropic or lyotropic liquid crystals, respectively). In the nematic phase, the particles tend to align with each other in such a way as to occupy a smaller fraction of volume, while in the smectic phase, in addition to the alignment, the particles separate themselves into layers. This effect is exclusively entropy driven, as the rotational entropy lost due to the alignment is more than balanced by the gain in the excluded-volume entropy due to the larger volume available to translational entropy. This increased translational entropy allows the particles in the "crystal" to move freely like in a "liquid". An even more remarkable effect of shape emerges in the cholesteric phase of liquid crystals, where the chirality of the molecules is directly reflected in the spiral twist from one layer to the next of the crystal.

In a similar way, when colloidal rods are mixed with molecules of different shapes, the two types tend to separate into different phases. In particular, mixtures of rod-like colloids and spheres have been studied, with different characteristics of the phase separation depending on the geometry and relative concentrations of the particles involved (Adams et al., 1998; Antypov and Cleaver, 2003), while the separation or otherwise of blends of rods and flexible coils (Lekkerkerker et al., 1992; Liu and Fredrickson, 1996) is decisive in industrial applications of new materials, in particular for self-reinforced materials or nano-composites.

The attraction between colloidal particles can also be promoted by the presence of smaller particles or globular macromolecules such as polymers, in what is known to physicists as the osmotic *depletion effect* (Asakura and Oosawa, 1954, 1958; Vrij, 1976) and to biologists as *macromolecular crowding*. This effect can be summarised as follows: when the distance between the surfaces of two of the larger particles becomes shorter than the diameter of the smaller ones, the volume between those large particles is depleted of smaller particles and this causes a difference in the osmotic pressure with respect to the rest of the surface around the two large particles. This results in a net attraction between the large particles which favours a phase separation between the two types of sizes. In the case of hard spheres, for example, phase separation still remains a topic of

research (see, e.g., Roth et al. (2002); Dijkstra et al. (1999)), and different models suggest that either this separation never occurs for any size ratio (Lebowitz and Rowlinson, 1964), or it is predicted to happen when this ratio is significantly less than one, namely less than 0.2 (Biben and Hansen, 1991).

Along the same lines, it would be interesting to determine if a blend of knotted polymers can be phase separated according to the topology. As we have seen in the previous chapters of this thesis, molecules that are knotted in different ways have different radii of gyration, with the presence of more complex knots making the molecules more compact. This situation can be comparable to that of spheres with different radii, yet it is not possible to expect the same results as with hard spheres, as the knotted molecules considered are flexible and the strands can overlap and intertwine with each other. In addition, the shape of different knots is also different, unlike hard spheres. Nevertheless, there is a possibility that the combination of different compactness and different shape may give rise to a phase separation, and this chapter will focus on testing different systems of knotted polymers and checking for any such separations.

In order to have the largest possible effect, the knots considered in this chapter will be the unknot 0_1 and the 9-crossing torus knot 9_1. In fact, these two types of knots are the ones with the biggest difference in shape and size among those already considered in the previous chapters of this thesis.

5.2 Simulation setup

The simulations are set up as described in Section 2.8.3. The systems contain a blend of unknots and 9_1 knots in equal proportions. In order to compare results and be sure that any potential findings are due to the topology rather than other spurious effects, systems of either unknots or 9_1's exclusively are also generated and run in simulations.

Different values of the persistence length are considered. The persistence length of double-stranded DNA corresponds to $\lambda = 20$ in Lennard-Jones units, however, shorter persistence lengths have been tested to verify if it is possible to see a difference of behaviour in the case of less rigid and more globular molecules. In addition to that, three different sets of simulations have been performed: lowering the temperature, increasing the pressure and reducing the simulation box while keeping the number of molecules fixed.

In order to compare these results with a situation known to lead to phase

separation, two additional settings were considered at the beginning, where the Lennard-Jones potentials have been modified so as to be attractive for particles of the same kind. In these cases, the cut off of the potential was set at 2σ, which means the attractive part of the potential is included, and the energy coefficient ε was set to $\varepsilon = 1.5$ between beads of the same kind and $\varepsilon = 1.0$ between beads of different kinds.

This corresponds to having a positive interaction-energy term in Eq. 5.2, so causing a phase separation between the two species of molecules, and gives a sense of what we could expect to see, both in the snapshots and in the analysis graphs, if phase separation should occur in the subsequent systems.

5.3 Simulations and analysis

It is intended that snapshots of all the simulations at the beginning and at the end of the run should make any phase separation apparent.

However, if there should be less obvious effects, graphs of the average distance separations between the centres of mass of different types of molecules are shown, as well as histograms of the same separation distance. The average separation distances considered are between the centres of mass of the three possible pairs of species, that is, 1–1, 2–2 and 1–2. The histograms detail the partial pair distribution functions of the three possible pairs, again 1–1, 2–2 and 1–2. The bin width considered is 2.5 σ, with the first bin, labelled as zero, representing distances between zero and 2.5 σ.

Where two different types of knots are present, type 1 (red in the pictures) will be the 9_1 and type 2 (blue) the 0_1.

5.3.1 Different attraction energies between the types

As explained above, in the first simulations presented, the cut off of the potential was set to 2 σ, while the energy coefficient ε is set to $\varepsilon = 1.5$ between beads of the same kind and $\varepsilon = 1.0$ between beads of different kinds.

The system is composed of 256 molecules with a length of 250 beads each. The persistence length is set to be $\lambda = 1$, so that the shape is allowed to be more globular, and the temperature is fixed at $T = 1$ in Lennard-Jones units. Half the molecules are of type 1 and half of type 2.

In this case, the figures show the simulations at different times. These simulations run for 10^8 timesteps, or 10^6 τ_{LJ}. Most of the change happens

within the first tenth of the simulation. The topology of the knots does not have a perceptible impact in the dynamics due to the overwhelming effect of the added attraction energy. For this reason, only one combination of knots per system is shown.

Medium-sized box

The first system shown has been simulated in a cubic box with sides of 60 σ. As shown below in Section 5.3.4, a box of this size corresponds to a pressure of about 0.1 in Lennard-Jones units. The Brownian dynamics are performed in an NVE ensemble, as explained in Section 2.5.2.

A few snapshots of the simulation are shown in Fig. 5.2. The snapshots on the top were all taken within the first tenth of the simulation, when most of the change in the distribution of the molecules happens. We can see that separation starts immediately and reaches a configuration similar to the final one within a short time. As we can see from the snapshots at the bottom, only small adjustments happen for most of the rest of the simulation. This means that even a small difference in the attraction energies between the two types of molecules has a powerful effects on the phase separation between them.

As we can see in Fig. 5.3, the phase separation shows clearly both in the graph of the average distances between different types of pairs and in the corresponding histogram. In fact, within very few timesteps, the average distance between pairs of different types (in red) increases considerably, while the average distances between pairs of the same kind (in green and blue) both decrease to a very small quantity. The small difference between the two final distances can be attributed to a random asymmetry in the final configuration: as this does not change with time, any random unevenness in the distribution will maintain indefinitely. It is also possible that the more complex knots, such as the 9_1 in this case, might experience a slightly higher configurational rigidity, due to the many crossings, which may prevent two molecules from getting too close to each other. As far as the histogram is concerned, we can see that when the molecules are of the same type, a high proportion of the pairs are close to each other and fewer and fewer are at increasing distances. On the contrary, when the molecules are of different types, a small number are in proximity of each other, while the numbers increase as the distance increases. The two curves relative to the distances between 0_1's with each other and the distances between 9_1's with each other show a different distribution in the first few bins. Again, this

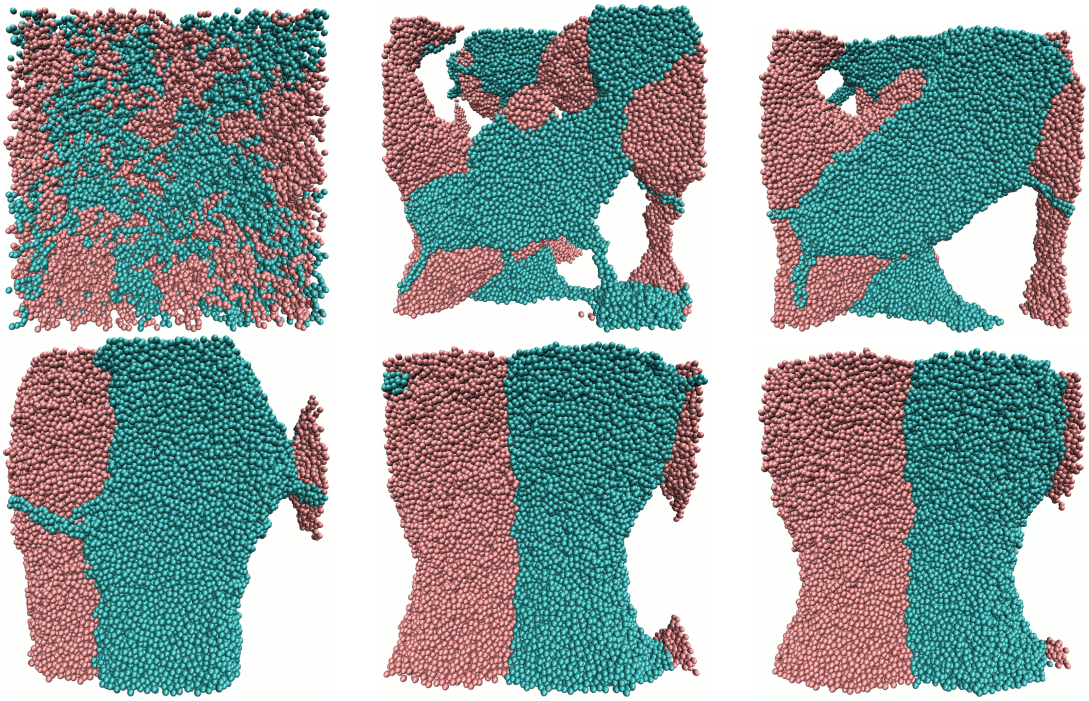

Figure 5.2: Screenshots of knotted blends with different interaction energies at various stages of the simulation. Parameters: the system is composed of 256 molecules, 250 beads per molecule; the box is $60 \times 60 \times 60$; the persistence length is λ=1; the ensemble is NVE at T=1. Simulation length: $6.8 \cdot 10^7$ timesteps $= 6.8 \cdot 10^5\ \tau_{LJ}$. Types of knots – red: 9_1, blue: 0_1.

suggests that the two types pack together differently because of the different configurational rigidity due to the different number of crossings.

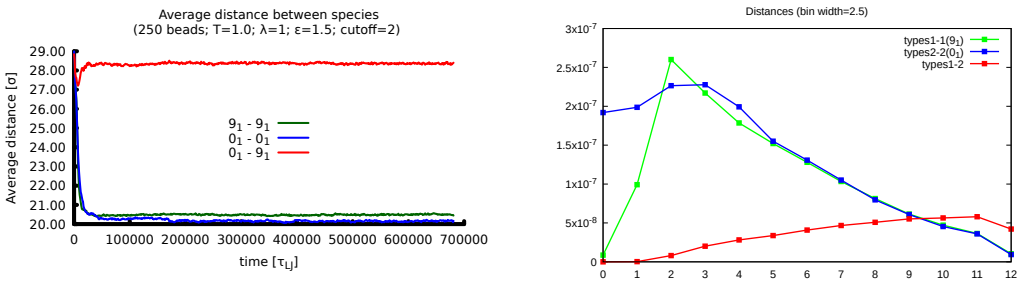

Figure 5.3: Analysis of the distance between species. Left: average distances over time. Right: histogram of the values every 10^3 timesteps over the last 10^5 timesteps. Two different types of knots (0_1 and 9_1) are considered in this system. As in Fig. 5.2, the system is composed of 256 molecules, 250 beads per molecule; the box is $60 \times 60 \times 60$; the persistence length is λ=1; the ensemble is NVE at T=1.

Smaller box

The second system shown has been simulated in a smaller cubic box with sides of 48 σ. Again, as shown below in Section 5.3.4, a box of this size corresponds to a pressure of about $P \approx 1.0$ in Lennard-Jones units. Also in this case, the Brownian dynamics are performed in an NVE ensemble (Section 2.5.2).

A few snapshots are shown in Fig. 5.4. This is a very similar system to the previous one. The main difference, apart from the size of the simulation box, is that in this case the two type of molecules are topologically the same, that is, they are both the unknot. This shows that the phase separation is not due to the topology, but it only depends on the different interaction energies. Again, a small difference between them has a very strong effect, and a dramatic change happens within the first part of the simulation, while in the rest of the time there are only small variations.

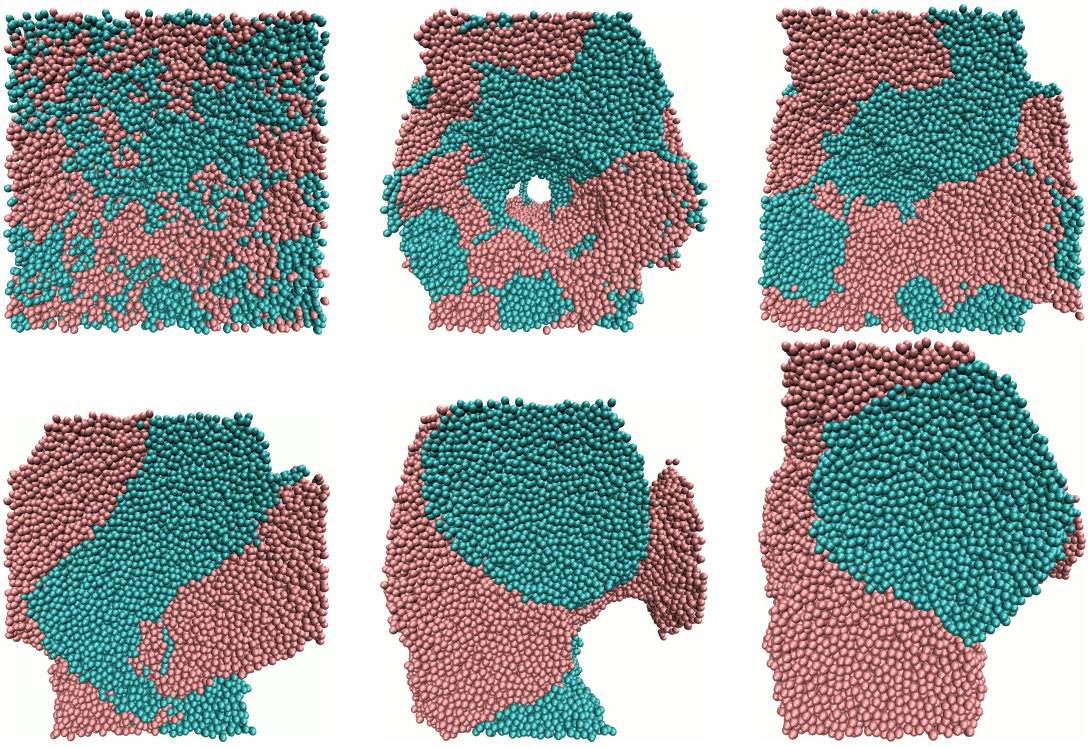

Figure 5.4: Screenshots of knotted blends with different interaction energies at various stages of the simulation. The system is composed of 256 molecules, 250 beads per molecule; the box is $48 \times 48 \times 48$; the persistence length is λ=1; the ensemble is NVE at T=1. Simulation length: $1 \cdot 10^8$ timesteps = $1 \cdot 10^6$ τ_{LJ}. Types of knots – both red and blue: 0_1.

The analysis in Fig. 5.5 shows a very similar trend as in the previous case.

Now, again, the average distances between the centres of mass of molecules of the same kind decrease quickly to a very small value, while the average distance between molecules of different types increases. The final values are reached within a short time and stay approximately constant for the rest of the simulation. Like before, a small difference in the final values may be attributed to small anisotropies in the configuration which cannot be resolved once it stabilises.

Similar considerations as in the previous case can be made also regarding the histograms: more molecules of the same type are found in the vicinity of each molecule, while the distribution of the number of molecules of different type increases with the distance. The green and the blue lines in the histogram correspond almost exactly, as we would expect from the fact that in this case all the molecules are topologically identical.

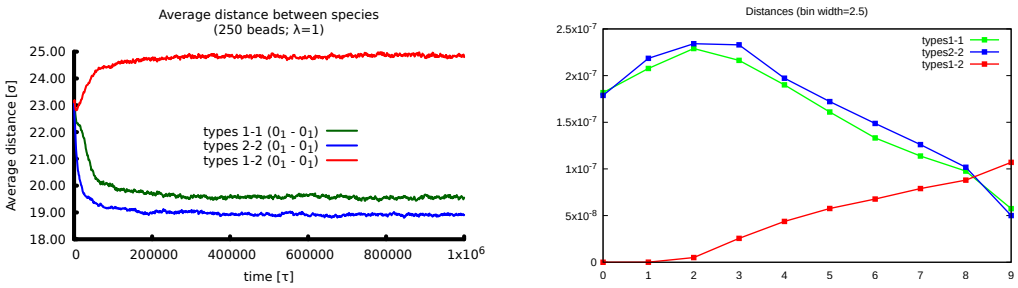

Figure 5.5: Analysis of the distance between species. Left: average distances over time. Right: histogram of the values every 10^3 timesteps over the last 10^5 timesteps. The different species are actually the same type of knot (0_1). As in Fig. 5.4, the system is composed of 256 molecules, 250 beads per molecule; the box is $48 \times 48 \times 48$; the persistence length is λ=1; the ensemble is NVE at T=1.

Through the addition of an extra energy term, it has been possible to see a phase separation between the two kinds of molecules considered and appreciate the kind of distribution of the distances between the centres of mass of molecules of the same or different types when separation occurs.

In the following systems, the excluded-volume potential is kept purely repulsive as the beads will interact with each other as hard spheres regardless of the type of molecule they belong to. Different parameters are changed in the following simulations, but in all cases the only difference between the two types of molecules will be the topology, so that any separation, if present, will be due exclusively to this characteristic.

5.3.2 Time evolution at constant temperature

The simplest test that is possible to perform is to just create the molecules and let them move undisturbed at constant temperature for a determined amount of time. In this simulation, there are 128 molecules in total, as usual half of type 1 and half of type 2, all composed of 500 beads. Their persistence length is set to $\lambda = 5$, that is, less rigid and more globular than DNA, and the temperature is $T = 1$ in Lennard-Jones units. The Brownian dynamics are simulated in an NVE system for a duration of $2 \cdot 10^8$ timesteps = $2 \cdot 10^6$ τ_{LJ}. Snapshots of the system at the beginning and at the end of the simulation are shown in Fig. 5.6. No appreciable difference is present between the two distributions of the molecules and a visual observation of the trajectories during the simulation only shows random motions. The same qualitative behaviour manifests itself regardless of the composition of the system (two knot types or only one).

The absence of a phase separation is confirmed by the analysis of the average distances between the centres of mass of different species, as shown in Fig. 5.7. The various distances are all of the same general magnitude, with values changing randomly with time. No particular trend suggesting any phase separation is observed. This means that for this system at a constant temperature of $T = 1$ the different topologies are not sufficient to cause a phase separation.

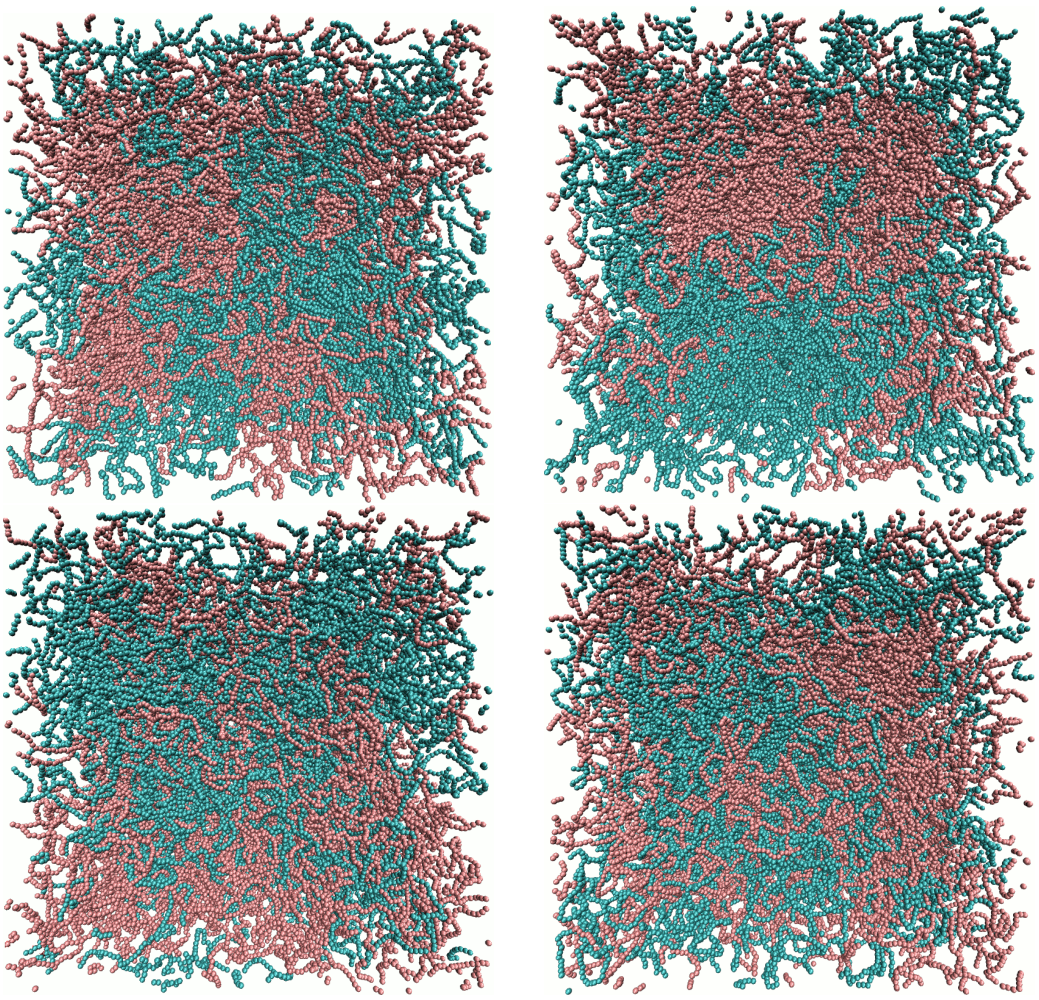

Figure 5.6: Screenshots of start and end of a simulation of a blend of knotted molecules at constant temperature $T = 1$. Parameters: 500 beads per molecule; 128 molecules in total; box: $100 \times 100 \times 100$; λ=5; ensemble: NVE; $T = 1$. Simulation length: $2 \cdot 10^8$ timesteps = $2 \cdot 10^6\ \tau_{LJ}$. Top: two different types of knots – red: 9_1, blue: 0_1. Bottom: both colours are the same species (0_1). In either case it is not possible to see any indication of phase separation.

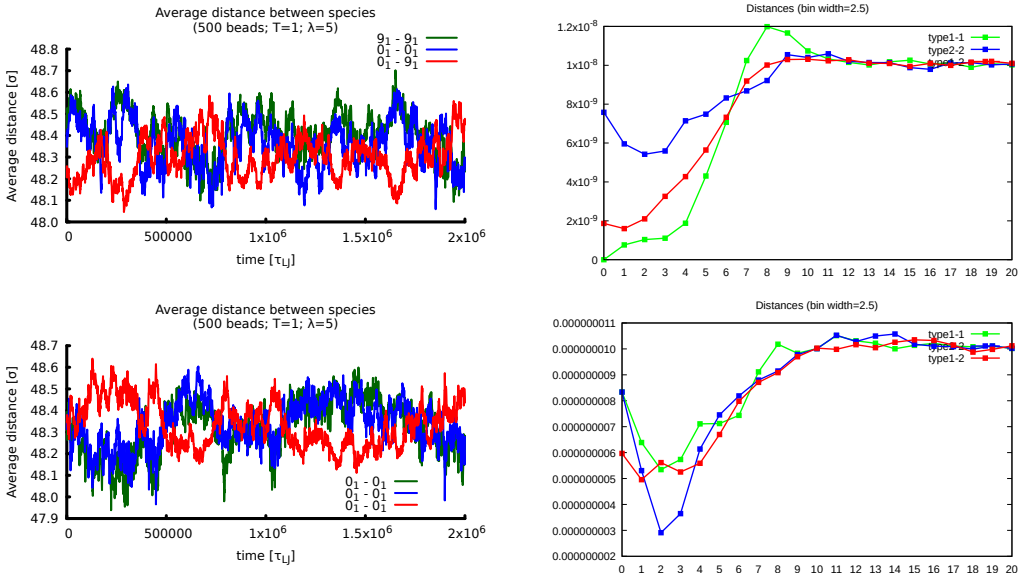

Figure 5.7: Analysis of the average distances between the centres of mass of pairs of molecules of different species. Left: average distances over time. Right: histogram of the values every 10^3 timesteps over the last 10^5 timesteps. Top: two different types of knots (type 1 is the 9_1 and type 2 is the 0_1). Bottom: both species are the same knot (0_1). As in Fig. 5.6, 500 beads per molecule; 128 molecules; box: $100 \times 100 \times 100$; λ=5; ensemble: NVE; T=1. In either case it is not possible to see any indication of phase separation.

5.3.3 Time evolution at decreasing temperature

As seen in the introduction to this chapter (Section 5.1), lowering the temperature of a binary mixture may promote phase separation. With that in mind, in the next set of simulations, the evolution of the system is shown as the temperature is decreased in various steps from $T = 1$ to $T = 0.5$, with the statistical ensemble set to NVE. The molecules considered in these simulations are, again, made of 500 beads, but the persistence length considered is $\lambda = 20$, the same as double-stranded DNA.

The first step is to lower the temperature from $T = 1$ down to $T = 0.75$. As shown in Fig. 5.8, the snapshot of the system at the end of the simulation does not seem qualitatively different from the snapshot at the beginning.

This absence of a trend is confirmed by the analysis of the average distances between the centres of mass of the different types of pairs as shown in Fig. 5.9. The average distances do not seem to change appreciably, regardless of the types of molecules involved, except for random variations. We can note again that the two curves relative to the distances between 0_1's with each other and the distances between 9_1's with each other show a different distribution, and different still from pairs of different types. This confirms the idea that the different types pack in different ways, with the centre of mass of the 9_1's kept at a distance from other molecules by its own strands winding around each other.

The following step is to allow the system to evolve at this lower temperature and verify if any particular behaviour emerges. Fig. 5.10 shows the snapshot at the beginning and at the end of this simulation. Like in the previous case, the molecules of the two kinds stay well mixed and do not show any sign of phase separation.

This is again confirmed by the analysis of the average distances between pairs of centres of mass of molecules of different types (Fig. 5.11). No matter whether the types of molecules are different or all the same kind of knot, only random variations occur and it is not possible to observe any difference in the behaviour. In this case, we can observe an anomalous behaviour of the first few bins of the histograms with respect to the previous case, and the previous considerations about the different distances between types of pairs depending on the respective knots do not seem to hold any more.

The next and final step in this set of simulations is to further lower the temperature, from $T = 0.75$ to $T = 0.5$, all the other parameters kept constant.

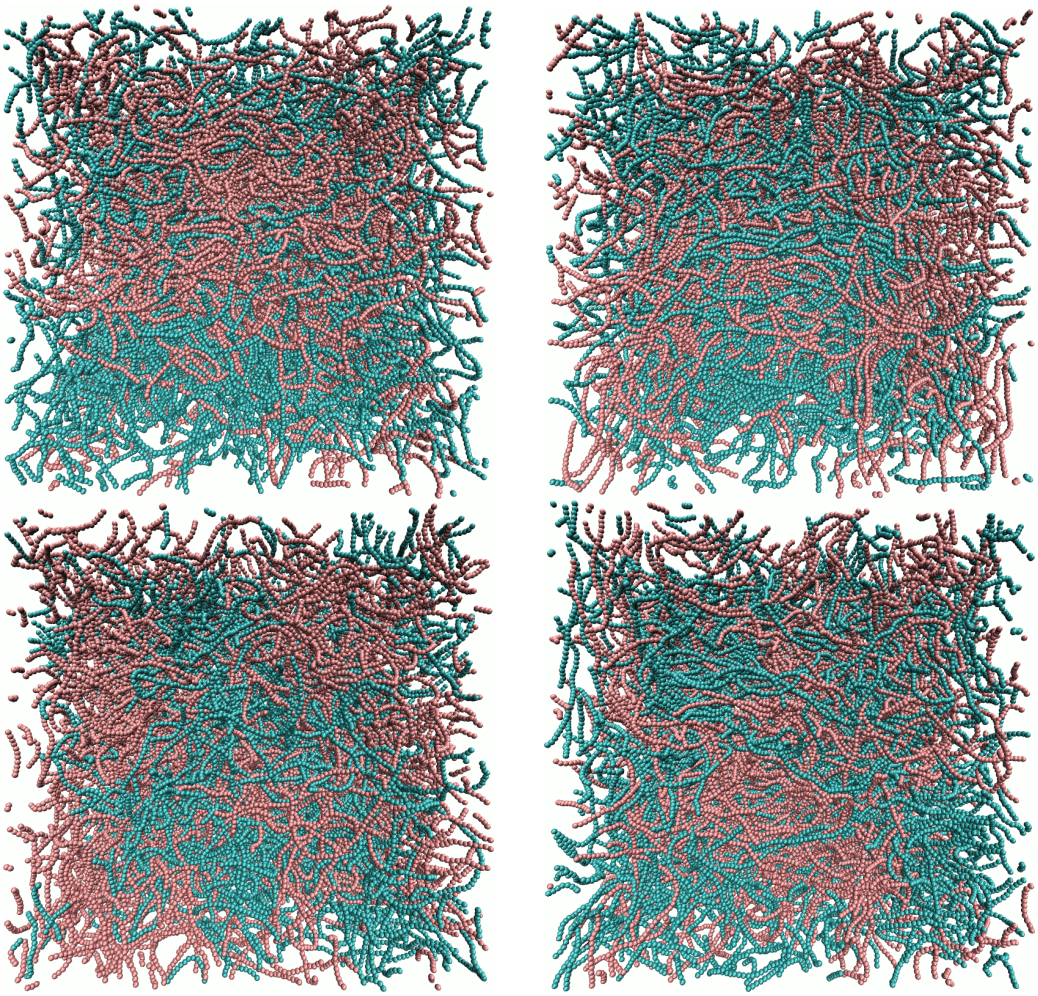

Figure 5.8: Screenshots of start and end of a simulation of a blend of knotted molecules at decreasing temperature, $T = 1 \rightarrow 0.75$. Parameters: 500 beads per molecule; 128 molecules; box: $100 \times 100 \times 100$; λ=20; ensemble: NVE; $T = 1 \rightarrow 0.75$; Simulation length: $2 \cdot 10^8$ timesteps = $2 \cdot 10^6\ \tau_{LJ}$. Top: two different types of knots – red: 9_1, blue: 0_1. Bottom: both colours are the same species (9_1). In either case it is not possible to see any indication of phase separation.

Snapshots at the beginning and at the end of these simulations, as usual for knots of different or the same type, are shown in Fig. 5.12. Even at a temperature half the initial one, it is not possible to see any qualitative difference in the system. The different shapes and sizes of the two kinds of molecules are not sufficient to determine a phase separation only by lowering the temperature to this value.

The absence of a trend is confirmed by the analysis of the average distances between pairs of centres of mass shown in Fig. 5.13. Once again, the values are

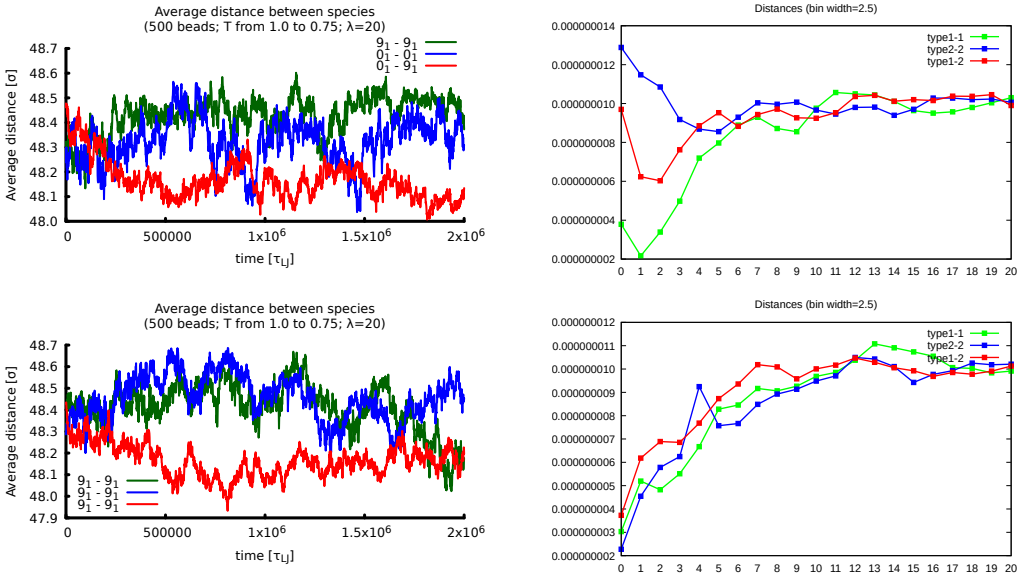

Figure 5.9: Analysis of the average distances between the centres of mass of pairs of molecules of different species at decreasing temperature, $T = 1 \rightarrow 0.75$. Left: average distances over time. Right: histogram of the values every 10^3 timesteps over the last 10^5 timesteps. Top: two different types of knots (type 1 is the 9_1 and type 2 is the 0_1). Bottom: both species are the same knot (9_1). In either case it is not possible to see any indication of phase separation. As in Fig. 5.8, 500 beads per molecule; 128 molecules; box: $100 \times 100 \times 100$; λ=20; ensemble: NVE; T=1 $\rightarrow$ 0.75.

entirely comparable and only show random variations with time, regardless of the species involved. Like in the previous case, the distribution of the distances shown in the histogram appears anomalous. It may be possible that the system is not fully equilibrated, perhaps also due to the lower temperature, or maybe the model is too small to average effectively over enough configurations. Further analysis is necessary to find a clear explanation.

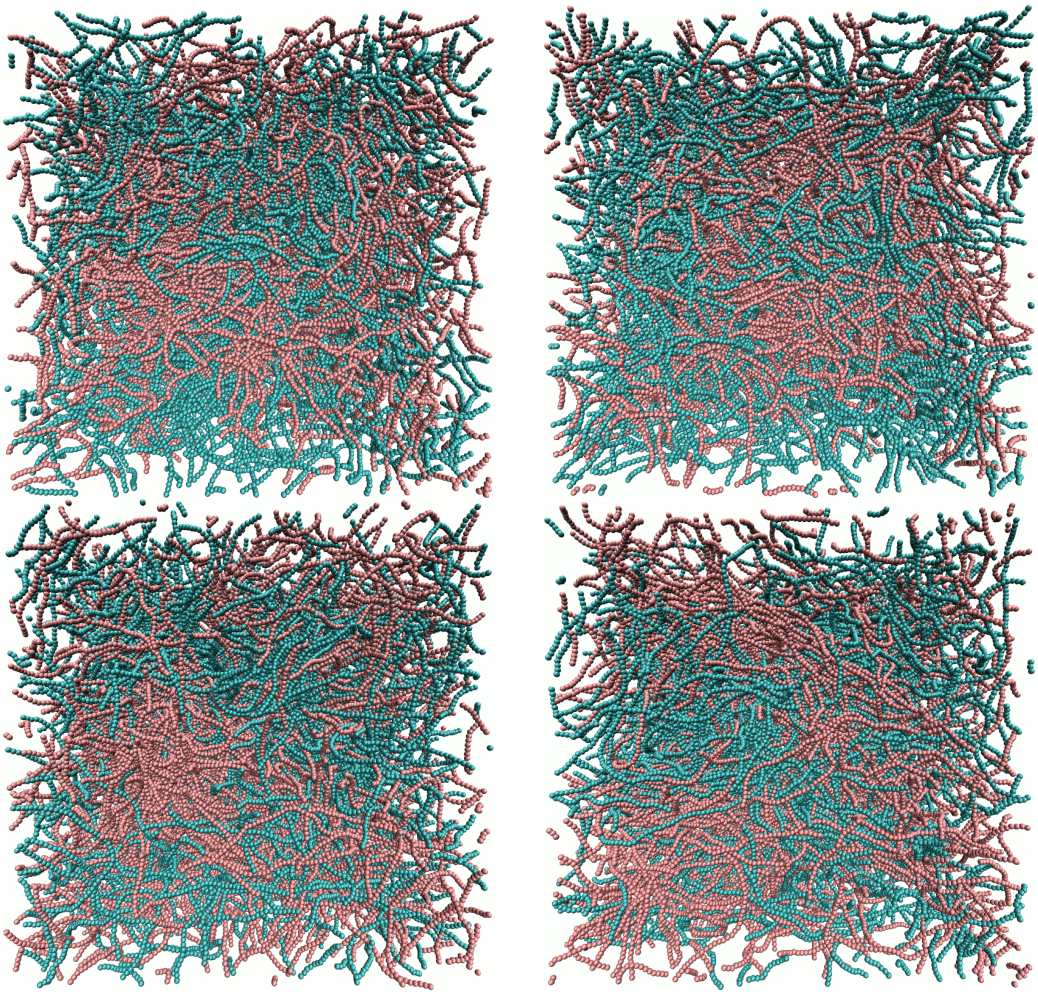

Figure 5.10: Screenshots of start and end of a simulation of a blend of knotted molecules at constant temperature $T = 0.75$. Parameters: 500 beads per molecule; 128 molecules; box: $100 \times 100 \times 100$; λ=20; ensemble: NVE; $T = 0.75$; Simulation length: $6 \cdot 10^8$ timesteps = $6 \cdot 10^6$ τ_{LJ}. Top: two different types of knots – red: 9_1, blue: 0_1. Bottom: both colours are the same species (0_1). In either case it is not possible to see any indication of phase separation.

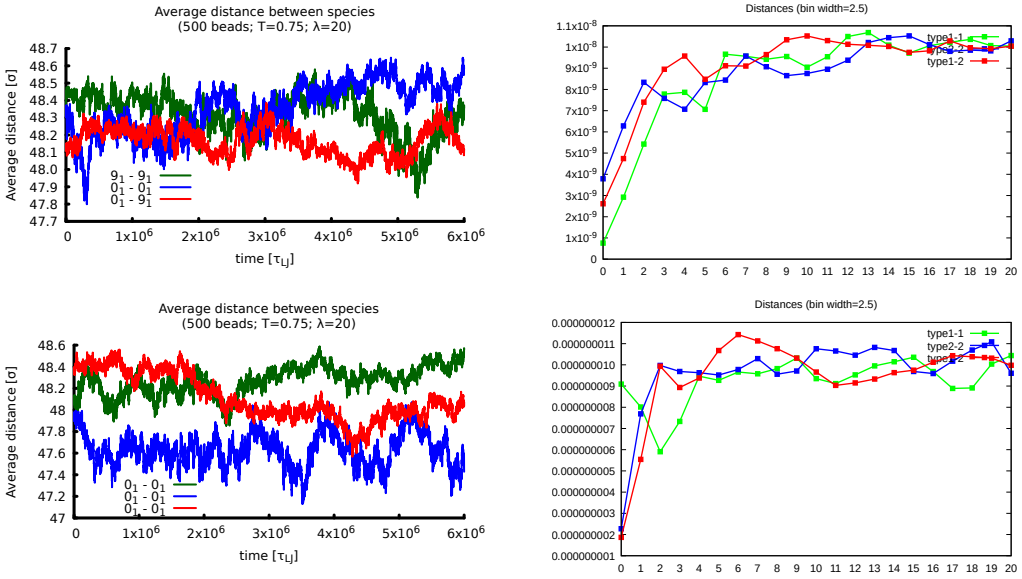

Figure 5.11: Analysis of the average distances between the centres of mass of pairs of molecules of different species at constant temperature $T = 0.75$. Left: average distances over time. Right: histogram of the values every 10^3 timesteps over the last 10^5 timesteps. Top: two different types of knots (type 1 is the 9_1 and type 2 is the 0_1). Bottom: both species are the same knot (0_1). In either case it is not possible to see any indication of phase separation. As in Fig. 5.10, 500 beads per molecule; 128 molecules; box: $100 \times 100 \times 100$; λ=20; ensemble: NVE; T=0.75.

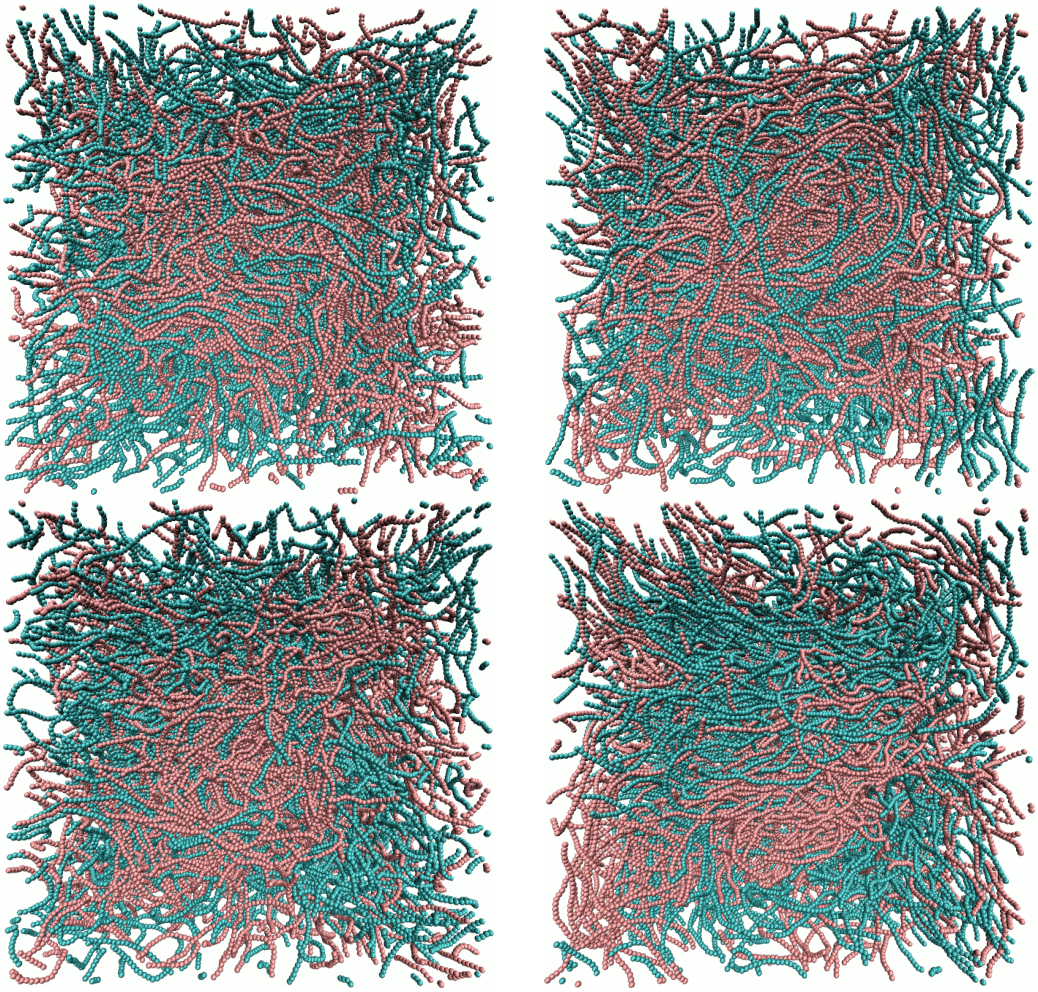

Figure 5.12: Screenshots of start and end of a simulation of a blend of knotted molecules at decreasing temperature, $T = 1 \rightarrow 0.75$. Parameters: 500 beads per molecule; 128 molecules; box: $100 \times 100 \times 100$; λ=20; ensemble: NVE; $T = 0.75 \rightarrow 0.5$; Simulation length: $2 \cdot 10^8$ timesteps = $2 \cdot 10^6$ τ_{LJ}. Top: two different types of knots – red: 9_1, blue: 0_1. Bottom: both colours are the same species (9_1). In either case it is not possible to see any indication of phase separation.

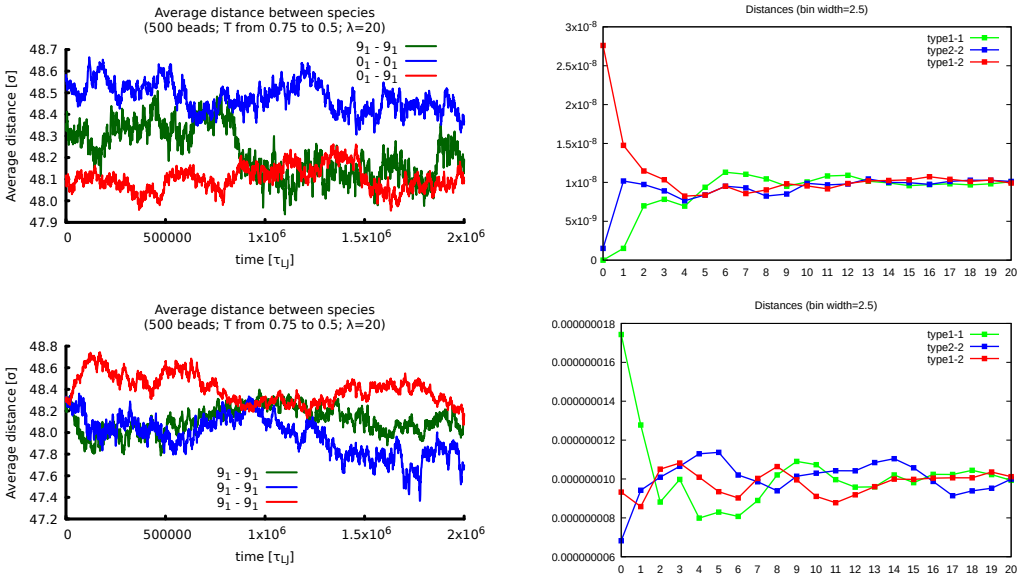

Figure 5.13: Analysis of the average distances between the centres of mass of pairs of molecules of different species at decreasing temperature, $T = 0.75 \rightarrow 0.5$. Left: average distances over time. Right: histogram of the values every 10^3 timesteps over the last 10^5 timesteps. Top: two different types of knots (type 1 is the 9_1 and type 2 is the 0_1). Bottom: both species are the same knot (9_1). In either case it is not possible to see any indication of phase separation. As in Fig. 5.12, 500 beads per molecule; 128 molecules; box: $100 \times 100 \times 100$; λ=20; ensemble: NVE; $T = 0.75 \rightarrow 0.5$.

5.3.4 Time evolution at increased pressure

As lowering the temperature in the previous simulations did not lead to any interesting behaviour, a higher density of the sample was tested. This was achieved by increasing the pressure of the system to different values up to $P = 1$ in Lennard-Jones system units. In this case, the statistical-mechanics ensemble during the simulation is NPT (fixed number of molecules, pressure and temperature), with $T = 1$.

The molecules are composed of 250 beads, for a total number of 256 molecules, and the persistence lengths tested are $\lambda = 20$ at $P = 0.1$ and $\lambda = 1$ at $P = 0.1, 0.5$ and 1.0.

Due to the fact that the simulation box in this case does not have fixed dimensions, a quantitative analysis of the distances would have required further development of the analysis code which the lack of separation did not justify, and for this reason it is deferred to the following sets of simulations (Section 5.3.5) which have similar characteristics but are performed at fixed volume. In this section, only the snapshots at the beginning and at the end of the simulations are shown.

Increased pressure, persistence length $\lambda = 20$

Fig. 5.14 shows snapshots at the start and at the end of simulations for two kinds of knots (red: 9_1, blue: 0_1), or the same knot type (0_1). There are 256 molecules in total, each composed of 250 beads. The persistence length is $\lambda = 20$, the temperature is $T = 1$ and the system is NPT. The pressure is set to $P = 0.1$.

Due to the smaller volume available, the strands of molecules acquire texture similar to a nematic liquid-crystal phase, with clear evidence of alignment and the presence of disinclinations. In spite of this, no phase separation is observed in this system, and the two types of molecules appear to be distributed randomly. This shows that the shape of the molecules in this system is not sufficient to induce a phase separation even when we change from a constant-volume state, where the system is not fully occupying the box, to a constant-pressure condition, where the density is higher.

Increased pressure, persistence length $\lambda = 1$

More globular molecules are considered now, as the persistence length is decreased to $\lambda = 1$. Otherwise, the number and type of molecules is the same as

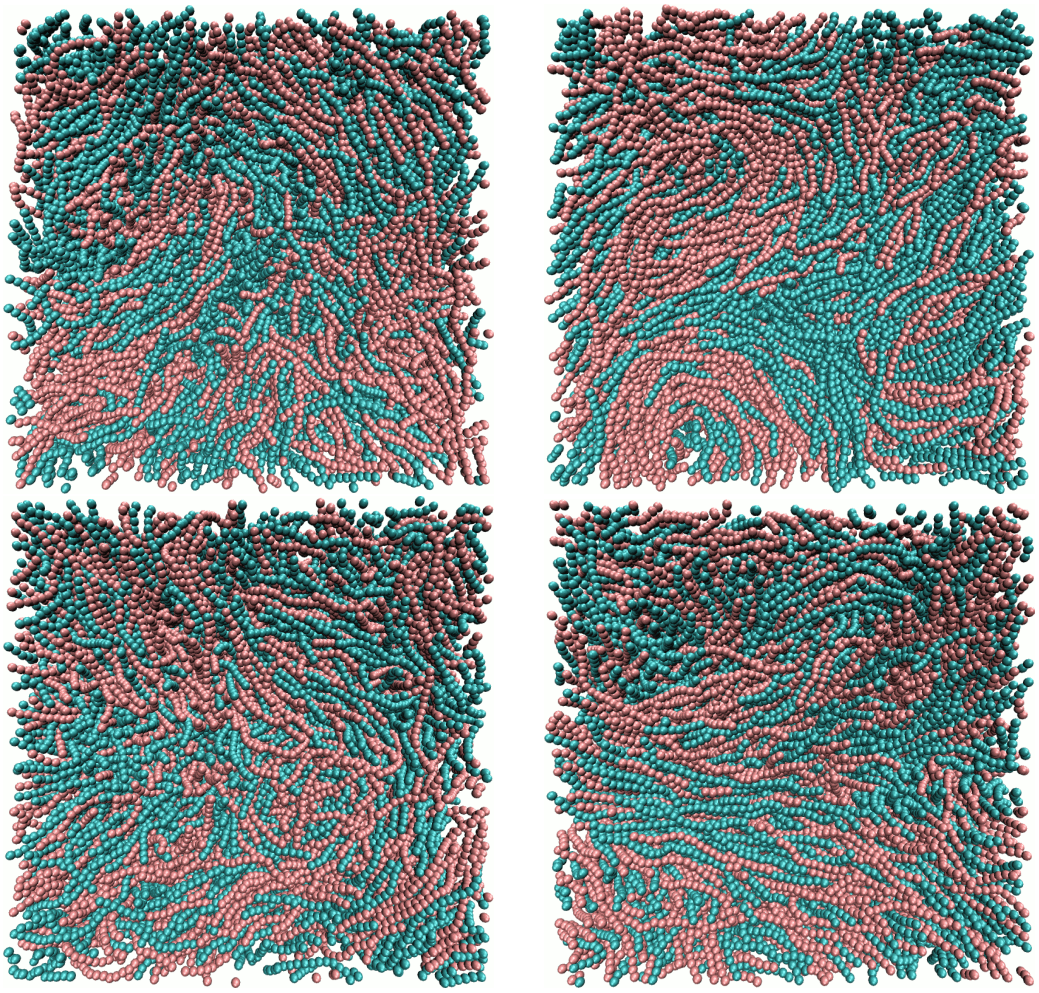

Figure 5.14: Screenshots of start and end of a simulation of a blend of knotted molecules at increased pressure: $P = 0.1$. Parameters: 250 beads per molecule; 256 molecules; λ=20; ensemble: NPT; T=1; P=0.1 Simulation length: $1.8 \cdot 10^8$ timesteps = $1.8 \cdot 10^6\ \tau_{LJ}$. The size of the simulation box is not fixed, but $L \approx 61$. Top: two different types of knots – red: 9_1, blue: 0_1. Bottom: both colours are the same species (0_1). In either case it is not possible to see any indication of phase separation.

in the previous paragraph, that is, 256 molecules, each 250 beads long. Three sets of simulations have been performed at different values of the pressure: P = 0.1, 0.5 and 1.0. As noted, in these simulations the size of the box is not fixed. However, it does not vary greatly at a definite pressure, which enables us to establish a reasonable volume for the subsequent simulations performed in the NVE system, that is, in a fixed box. In fact, the resulting simulation boxes vary around values approximately as follows: $L \approx 61.2\ \sigma$ at $P = 0.1$, $L \approx 51.7\ \sigma$ at $P = 0.5$ and $L \approx 48.4\ \sigma$ at $P = 1.0$. The box size settles within the first few

timesteps and fluctuates by about 1–2% during the simulation.

Snapshots at the beginning and at the end of the simulations are shown in Fig. 5.15 for $P = 0.1$, Fig. 5.16 for $P = 0.5$ and Fig. 5.17 for $P = 1$. The difference in the persistence length with respect to the previous case is apparent, as the chains are much more globular and there is non sign of stiffness.

Also in these cases, there is no visible sign of phase separation. Therefore it is clear that forcing the molecules into a smaller space is not sufficient to give rise to a dissociation, even when the pressure is increased by ten times.

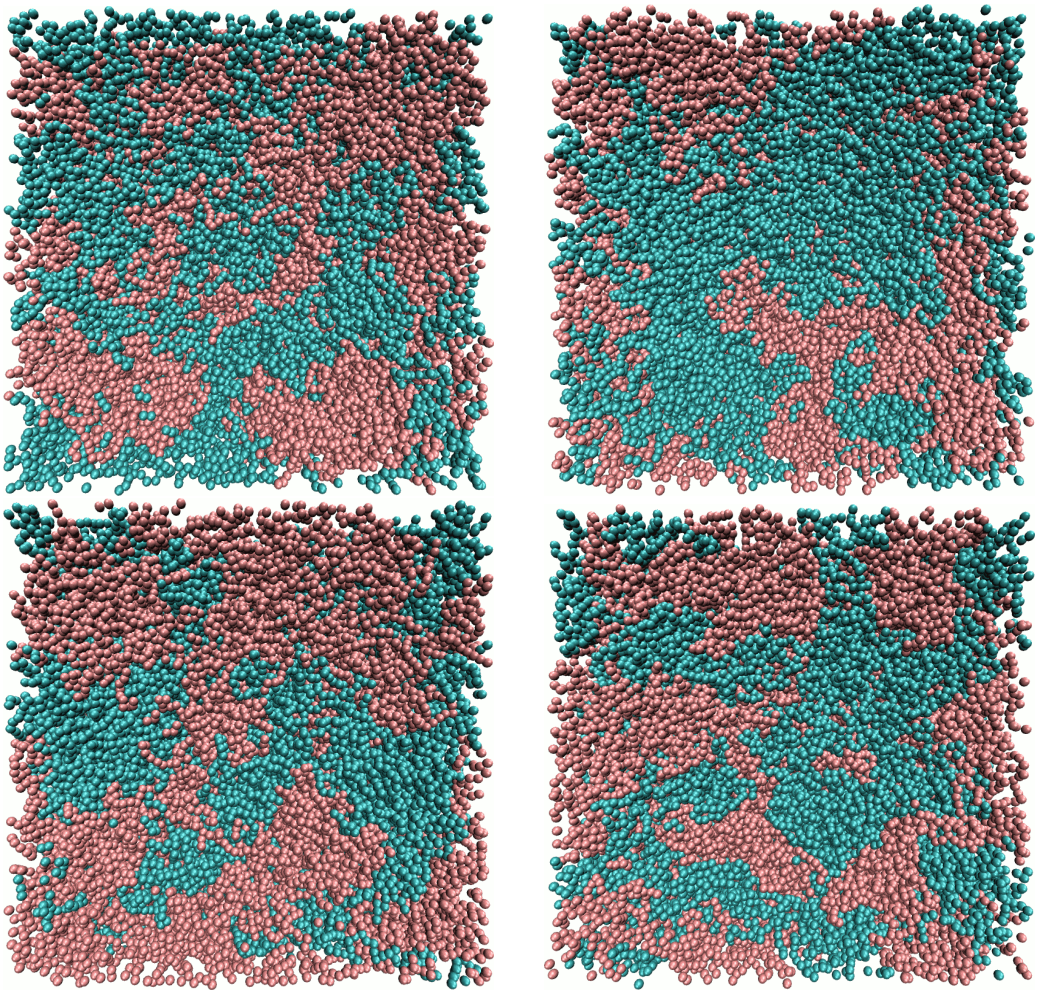

Figure 5.15: Screenshots of start and end of a simulation of a blend of knotted molecules at increased pressure: $P = 0.1$. Parameters: 250 beads per molecule; 256 molecules; λ=1; ensemble: NPT; T=1; P=0.1 Simulation length: $1 \cdot 10^8$ timesteps = $1 \cdot 10^6\ \tau_{LJ}$. The size of the simulation box is not fixed, but $L \approx 61$. Top: two different types of knots – red: 9_1, blue: 0_1. Bottom: both colours are the same species (9_1). In either case it is not possible to see any indication of phase separation.

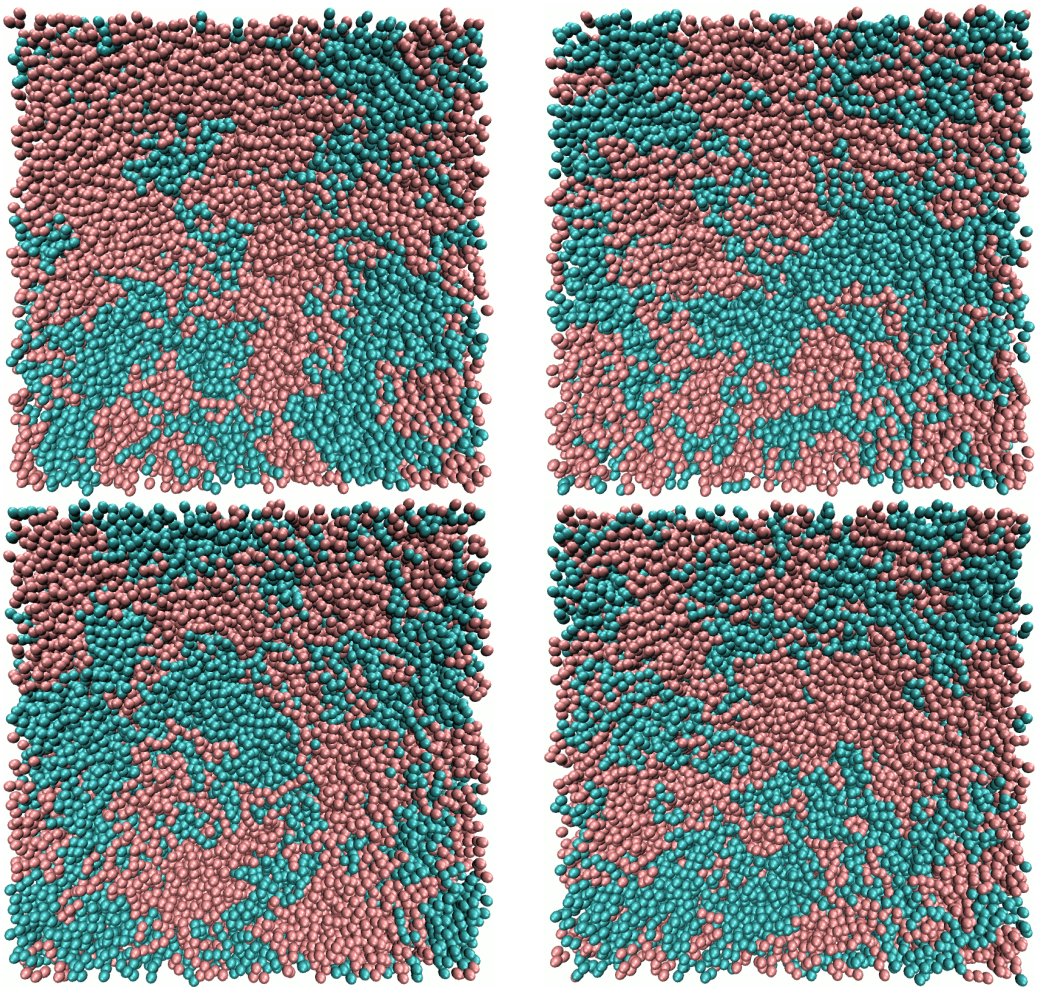

Figure 5.16: Screenshots of start and end of a simulation of a blend of knotted molecules at increased pressure: $P = 0.5$. Parameters: 250 beads per molecule; 256 molecules; λ=1; ensemble: NPT; T=1; P=0.5 Simulation length: $8.65 \cdot 10^7$ timesteps = $8.65 \cdot 10^5\ \tau_{LJ}$. The size of the simulation box is not fixed, but $L \approx 52$. Top: two different types of knots – red: 9_1, blue: 0_1. Bottom: both colours are the same species (0_1). In either case it is not possible to see any indication of phase separation.

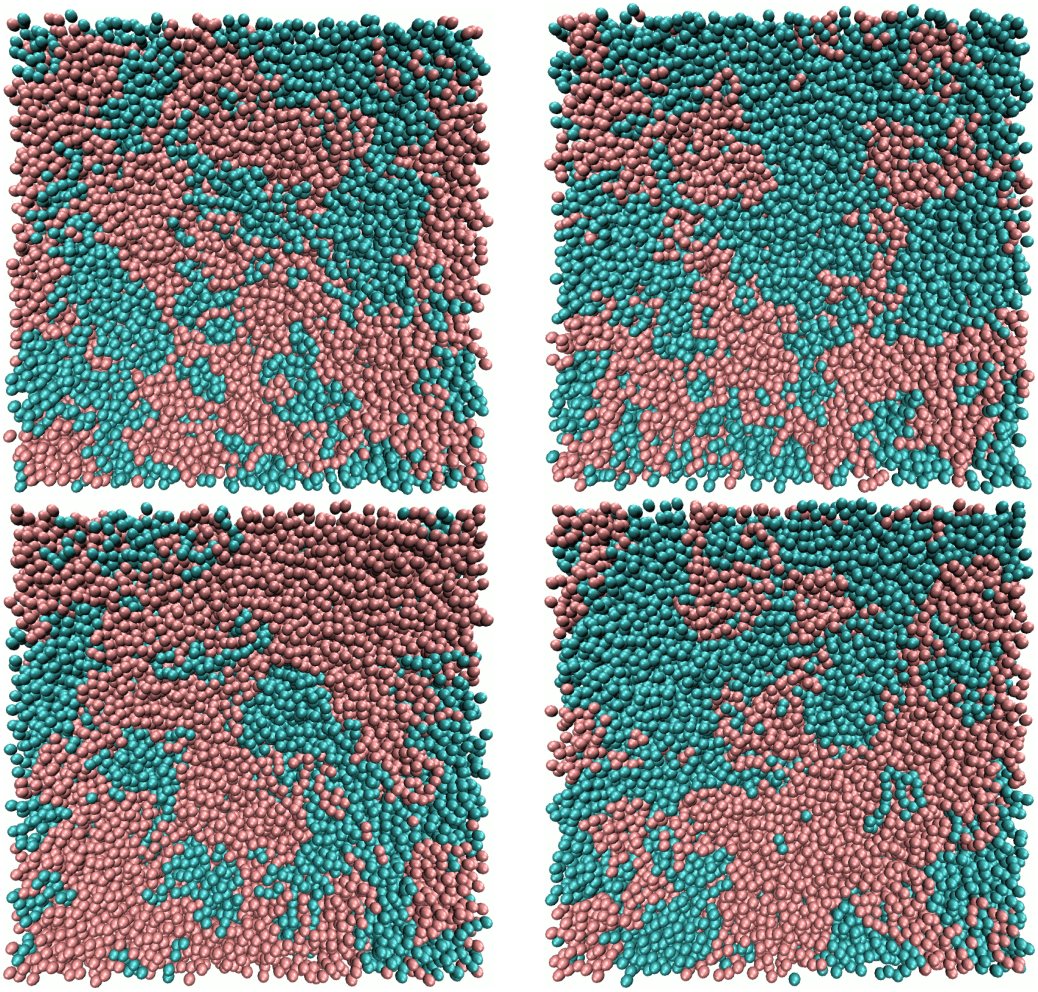

Figure 5.17: Screenshots of start and end of a simulation of a blend of knotted molecules at increased pressure: $P = 1$. Parameters: 250 beads per molecule; 256 molecules; λ=1; ensemble: NPT; $T = 1.0$; $P = 1.0$ Simulation length: $1 \cdot 10^8$ timesteps = $1 \cdot 10^6\ \tau_{LJ}$. The size of the simulation box is not fixed, but $L \approx 48$. Top: two different types of knots – red: 9_1, blue: 0_1. Bottom: both colours are the same species (9_1). In either case it is not possible to see any indication of phase separation.

5.3.5 Time evolution at a smaller volume

In order to be able to quantify the results of the previous section, a final set of simulations have been performed in a cubic box with a side length of $L = 48\,\sigma$, which approximately corresponds to having a pressure of $P = 1.0$ as seen in the previous set of simulations. The system however is an NVE ensemble, therefore is kept at constant volume, while the pressure can technically vary. Like in the previous section, the number of molecules is 256, half for each type, and every chain is made of 250 beads. This means that this system is very similar to the last one presented in the previous section and, like that one, it is not possible to see evidence of phase separation between the two types, as shown in Fig. 5.18.

In this case it is straightforward, however, to calculate the average distances between the centres of mass of the different types, which are presented in Fig. 5.19. In the histogram on the right, the distance distributions between centres of mass seem to suggest a difference in the minimum proximity with respect to the type of knot, like in some of the previous simulations. In fact, also here the 9_1's seem to be more distant from each other and, to a lesser extent, from the 0_1's. This again seems to suggest that the 9_1 knot may be, on average, more globular, due to the higher number of convolutions needed to accommodate the number of crossings. This would prevent its centre of mass from being too close to the centre of mass of any other molecules.

Like in the previous case, there is no indication of separation between the two species. Restricting the molecules to a smaller volume does not seem to be sufficient to force them into a more ordered state where the two knot types aggregate with each other.

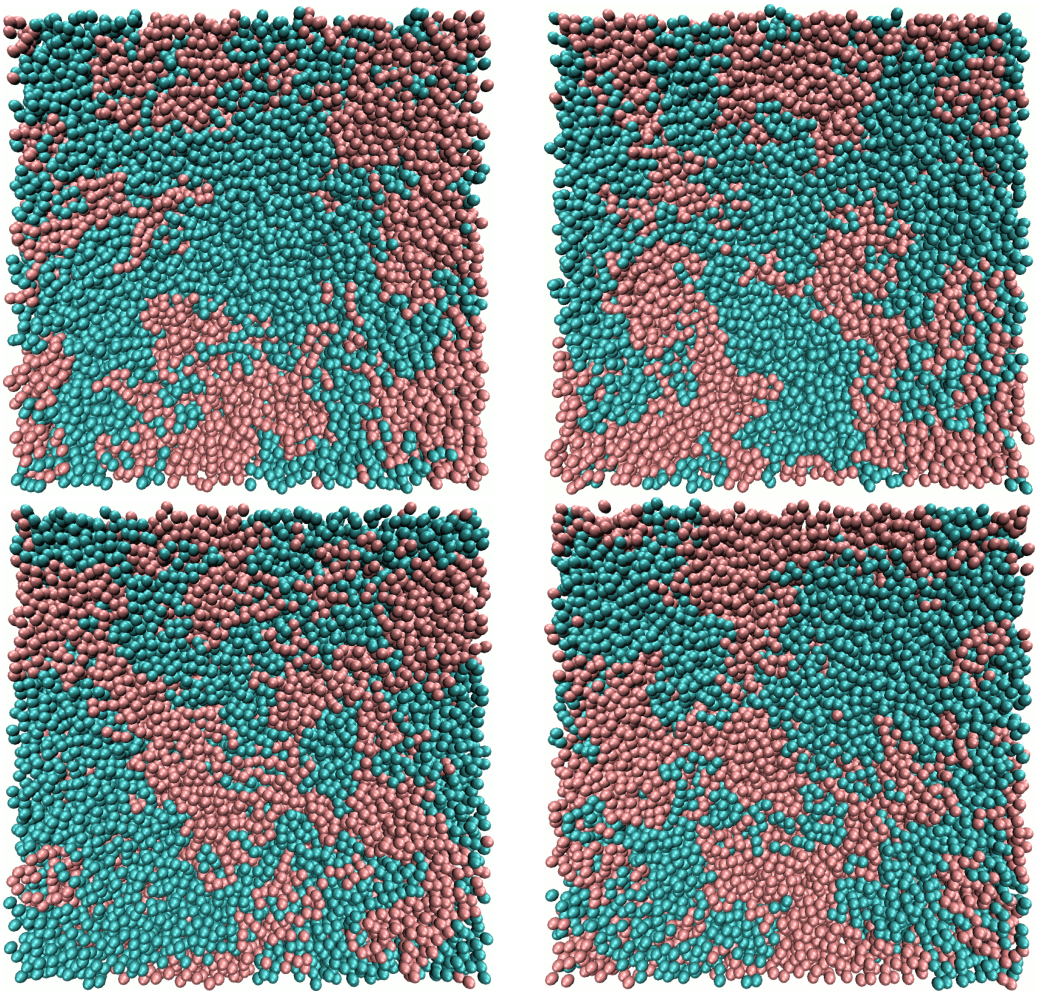

Figure 5.18: Screenshots of start and end of a simulation of a blend of knotted molecules in a smaller volume. Parameters: 250 beads per molecule; 256 molecules; box: $48 \times 48 \times 48$; λ=1; ensemble: NVE; $T = 1$. Simulation length: $1 \cdot 10^9$ timesteps = $1 \cdot 10^7\ \tau_{LJ}$. Top: two different types of knots – red: 9_1, blue: 0_1. Bottom: both colours are the same species (9_1). In either case it is not possible to see any indication of phase separation.

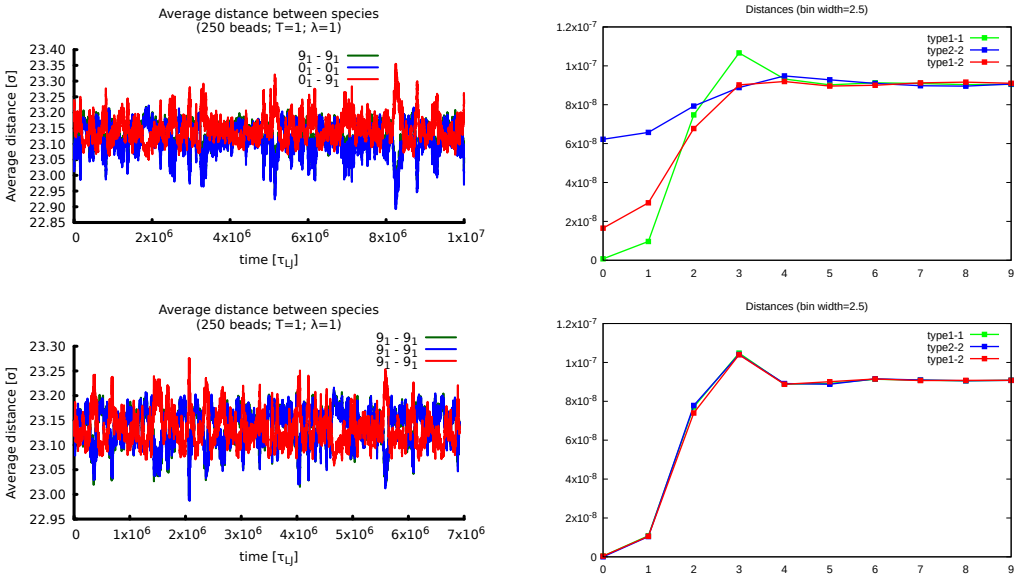

Figure 5.19: Analysis of the average distances between the centres of mass of pairs of molecules of different species in a smaller volume, $L = 48\sigma$. Left: average distances over time. Right: histogram of the values every 10^3 timesteps over the last 10^5 timesteps. Top: two different types of knots (type 1 is the 9_1 and type 2 is the 0_1). Bottom: both species are the same knot (9_1). In either case it is not possible to see any indication of phase separation. As explained in the text, the distance distributions between centres of mass shown in the histograms seem to suggest a difference in the minimum proximity with respect to the type of knot. As in Fig. 5.18, 250 beads per molecule; 256 molecules; box: $48 \times 48 \times 48$; λ=1; ensemble: NVE; T=1.

5.4 Visualisation of single molecules

For completeness of the description of the systems studied in this chapter, two pictures are presented to show the size and shape of the individual molecules in two typical settings among the ones seen above.

As an example of longer molecules of 500 beads with long persistence length λ=20, in a cubic box with $L = 100$, Fig. 5.20 shows a snapshot of a simulation presented in Section 5.3.3, where the different colours highlight different molecules, rather than the molecule type as in the previous cases. Two of them, a 0_1 and a 9_1, are shown separately on the right.

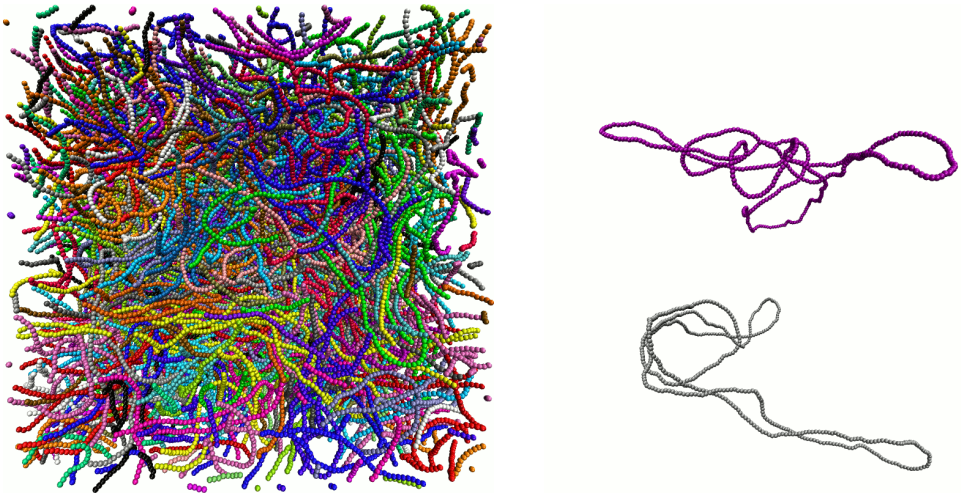

Figure 5.20: Screenshots at the end of a simulation with longer and more rigid molecules, where all the molecules are in different colours. On the right, two molecules of different types are shown separately (top: 9_1; bottom: 0_1). Parameters: 500 beads per molecule; 128 molecules; box: $100 \times 100 \times 100$; λ=20; ensemble: NVE; T=0.75.

Similarly, as an example of shorter molecules with persistence length λ=1 in a smaller cubic box with $L = 48$, a snapshot from a simulation described in Section 5.3.5 is shown in Fig. 5.21, with the different chains shown in different colours. An unknot and a 9_1 are shown separately on the right.

It has to be noted that the molecule size is large compared with any apparent separated regions, therefore some systems in the pictures shown in this chapter may appear separated or near the critical point by eye, when in reality they are not.

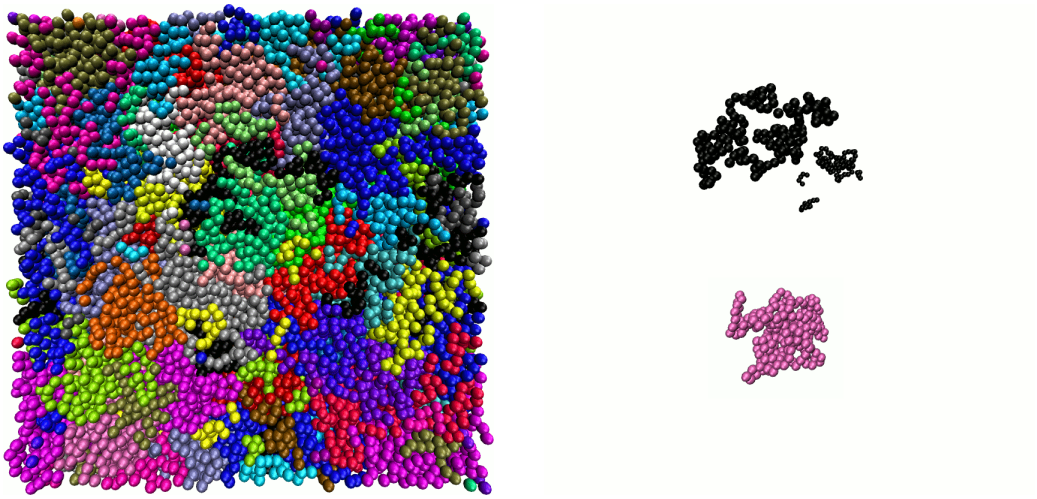

Figure 5.21: Screenshots at the end of a simulation with shorter and flexible molecules, where all the molecules are in different colours. On the right, two molecules of different types are shown separately (top: 0_1; bottom: 9_1). It is to be noted that the molecule in black appears as if it was separated into pieces as a result of the periodic boundary conditions of the system. Parameters: 250 beads per molecule; 256 molecules; box: $48 \times 48 \times 48$; λ=1; ensemble: NVE; T=1.

5.5 Discussion, conclusions and outlook

The aim of the simulations in this chapter was to test whether is was possible to encourage a phase transition in a blend of two types of ring polymers whose only difference was the type of knot. The two knots considered, the unknot and the 9_1, differ both in size, as measured in terms of radius of gyration, and shape. Therefore the possibility exists that, in the same way as in the case of mixtures of rods and polymers or rods and spheres (as seen in the introduction to this chapter), the geometry of the molecules might drive a separation between the two types. In order to have this, the loss in entropy due to demixing needs to be balanced in other ways, like by the increased translational entropy typical of liquid crystals or by some kind of osmotic depletion effect.

Due to the complexity of these types of molecules, and the number of different geometric shapes they are allowed to have because of their flexibility, an exact mathematical solution to the question whether this separation is possible or not is not easy to calculate, therefore computer simulations of these kind of systems are essential.

In the simulations performed so far, it was not possible to show any evidence of phase separation due to the type of knot only. Neither lowering the

temperature nor increasing the density of the system was sufficient to trigger any behaviour in that sense. As a negative result, this does not mean that such a phase separation is not possible, but it does establish some limits on the characteristics of the systems in which such a separation can be looked for in future simulations. Temperature, concentration, persistence length and length of the polymers are all parameters that can be tuned and there may be a combination that will lead to phase separation. In particular, shortening the molecules while keeping the persistence length significant, like it is in DNA, may render the molecules quite rigid, and this stiffness may both promote alignment of the strands and make the difference in shape between the 0_1's and the 9_1's more pronounced. This may, in turn, favour the phase separation between the two types.

Alternatively, a different type of simulations that might be interesting to try would be to keep a small interaction energy to promote phase separation, and test whether different combinations of knot types separate at different values of this energy or at different temperatures.

In summary, some of the possibilities of obtaining phase separation in a binary mixture of differently-knotted molecules have been explored here. In spite of the absence of clear positive results in this sense, it may still be possible to have phase separation in such a system, as it has been shown that only a small energy term between the two types is sufficient to trigger the process. Some limits to the parameters have been set, but more work is necessary to establish the answer to this question.

6 Conclusions

Knots have fascinated humans for millennia. They can be inconvenient, they can be useful, they can be just beautiful. Undoubtedly, they are part of our lives in many ways.

In addition, we now also know that they play an important part in the very fabric of our biology: they are in every and each one of our cells, and they play a role in the basic mechanisms of functioning and replicating.

As we saw in Chapter 1 of this thesis, being able to control these mechanisms is increasingly becoming part of the standard practice in medicine, and being able to recognise the presence, type and function of the knots present in a biological polymer has been the focus of much research for many decades, with many important results.

As is frequently the case in science, the more we know about this subject, the more questions arise. One of them is how we can separate molecules that are knotted in different ways, when they are equivalent in every other respect. We have seen that one of the most common tools in biology laboratories is agarose-gel electrophoresis, that is, forcing the molecules through a gel by means of an electric field and have them separated in bands of differently-knotted types in the process.

Although the basic concepts at the basis of this process are straightforward, the subtler mechanisms underlying it are still not perfectly clear, as is highlighted for example by the puzzling issue of the appearance of an arc pattern in some instances of two-dimensional electrophoresis.

Many previous theoretical and computational models have tried to give an answer to this question; however, a complete and totally satisfactory understanding is still lacking. With this in mind, in this thesis I have tried to devise some models for the separation of molecules, and in particular biological poly-

mers, according to the type of knot they are tied into, with the fundamental stipulation that these models be as simple as possible.

After an explanation, in Chapter 2, of the methods used in the rest of the thesis, in Chapter 3 I proposed a minimal model for the mobility of knotted polymers in a suspension and presented the results of simulations performed with an *ad hoc* program I developed in the C programming language. The chains were as short as possible, and the suspension was represented by a set of spheres arranged on the vertices of a regular cubic lattice, with lattice spacing small in relation to the size of the polymers. By changing the firmness and size of the spheres, I have explored the effects of this suspension, with and without the addition of a driving force, on the motion of the chains. I have shown that even with this simple model it is possible to separate the chains according to the type of knot.

In Chapter 4, I have explored a more biologically-oriented model, with longer polymers specifically aimed at representing double-stranded DNA molecules in the shape of closed rings tied in knots of different types. Due to the greater complexity of this system, the simulations were performed by means of the molecular-dynamics software program LAMMPS. I have introduced disorder in the suspension, while keeping it simple, as in this case the gel is represented by spheres of comparable size to the knotted chains, randomly distributed in the simulation box. I have shown that if the spheres are in random motion, the interference introduced by this suspension is sufficient to separate the molecules according to the type of knot, as more complex knots are found to travel faster than simpler ones. If the spheres are fixed in space, the hindrance is such that no particular trend emerges. These findings have been confirmed for molecules of different lengths.

Finally, in Chapter 5, I have explored the possibility of phase separating a binary mixture of differently-knotted molecules according to the type of knot. This was prompted by the well-known effects of different shapes on the separation of mixtures of various components, such as for example rods and polymers or rods and spheres. I have generated a blend of two types of polymers and changed the parameters of the system, for example by reducing the temperature or the size of the simulation box, or by changing the persistence length of the molecules, and I have presented the results of these simulations. So far, it was not possible to show any evidence of phase separation due to the type of knot only, but the results are still preliminary, and as well as establishing

some limits on the parameters of the problem, I have made some suggestions about possible changes it may be worth trying in future simulations. This would include looking for example at further changes in temperature, concentration, persistence length and length of the polymers. In particular, I think that making the chains shorter while keeping them stiff like DNA is, may make the difference in shape more pronounced and therefore promote separation.

With this work, I hope I have given my small input to the study of the effect of knotting on the mobility and separation on polymers, with a particular focus on DNA molecules. This contribution is certainly modest, and necessarily incomplete, but I hope that, as part of the bigger picture, it can be of some value and benefit to future research in this field.

Bibliography

Adams C C (1994). *The Knot Book*. American Mathematical Society, Providence, Rhode Island, 2004 edition.

Adams M, Dogic Z, Keller S L and Fraden S (1998). Entropically driven microphase transitions in mixtures of colloidal rods and spheres. *Nature* **393**(6683), 349–352.

Alberts B, Johnson A, Lewis J, Raff M, Roberts K and Walter P (2002). *Molecular Biology of the Cell, Fifth Edition*. Garland Science, 2008 edition.

Antypov D and Cleaver D J (2003). Orientational and phase-coexistence behaviour of hard rod–sphere mixtures. *Chemical Physics Letters* **377**(3-4), 311–316.

Aragão De Carvalho C, Caracciolo S and Fröhlich J (1983). Polymers and $g|\varphi|^4$ theory in four dimensions. *Nuclear Physics B* **215**(2), 209–248.

Arnott S, Fulmer A, Scott W, Dea I, Moorhouse R and Rees D (1974). The agarose double helix and its function in agarose gel structure. *Journal of Molecular Biology* **90**(2), 269–284.

Asakura S and Oosawa F (1954). On interaction between two bodies immersed in a solution of macromolecules. *The Journal of Chemical Physics* **22**(7), 1255–1256.

Asakura S and Oosawa F (1958). Interaction between particles suspended in solutions of macromolecules. *Journal of Polymer Science* **33**(126), 183–192.

Barron A E, Soane D S and Blanch H W (1993). Capillary electrophoresis of DNA in uncross-linked polymer solutions. *Journal of Chromatography A* **652**(1), 3–16.

Berezhkovskii A M, Dagdug L and Bezrukov S M (2014). Discriminating between anomalous diffusion and transient behavior in microheterogeneous environments. *Biophysical Journal* **106**(2), L09–L11.

Berg B and Foester D (1981). Random paths and random surfaces on a digital computer. *Physics Letters B* **106**, 323.

Biben T and Hansen J P (1991). Phase separation of asymmetric binary hard-sphere fluids. *Physical Review Letters* **66**(17), 2215.

Buck D (2009). DNA topology. In D Buck and E Flapan, editors, *Applications*

of Knot Theory: American Mathematical Society, Short Course, January 4-5, 2008, San Diego, California, volume 66 of *Proceedings of Symposia in Applied Mathematics*, page 47. American Mathematical Society, Providence.

Buck D and Flapan E (2007). A topological characterization of knots and links arising from site-specific recombination. *Journal of Physics A: Mathematical and Theoretical* **40**(41), 12377.

Bühler W K (2012). *Gauss: a biographical study*. Springer Science & Business Media.

Călugăreanu G (1961). Sur les classes d'isotopie des noeuds tridimensionnels et leurs invariants. *Czechoslovak Mathematical Journal* **11**(4), 588–625.

Campagnola G, Nepal K, Schroder B W, Peersen O B and Krapf D (2015). Superdiffusive motion of membrane-targeting C2 domains. *Scientific Reports* **5**(1), 1–10.

Cantarella J (2012). Ridgerunner: Knot tightening software. `http://www.jasoncantarella.com/wordpress/software/ridgerunner/`. Accessed: 2016-12-13.

Castiglione F, Casalegno M, Ferro M, Rossi F, Raos G and Mele A (2019). Evidence of superdiffusive nanoscale motion in anionic polymeric hydrogels: Analysis of PGSE-NMR data and comparison with drug release properties. *Journal of Controlled Release* **305**, 110–119.

Cebrián J, Kadomatsu-Hermosa M J, Castán A, Martínez V, Parra C, Fernández-Nestosa M J, Schaerer C, Martínez-Robles M L, Hernández P, Krimer D B et al. (2015). Electrophoretic mobility of supercoiled, catenated and knotted DNA molecules. *Nucleic Acids Research* **43**(4), e24–e24.

Cheng S Z (2008). *Phase transitions in polymers: the role of metastable states*. Elsevier.

Cole K D and Åkerman B (2003). The influence of agarose concentration in gels on the electrophoretic trapping of circular DNA. *Separation Science and Technology* **38**(10), 2121–2136.

Cozzarelli N, Boles T and White J (1990). Primer on the topology and geometry of DNA supercoiling. *DNA Topology and its Biological Effects* pages 139–184.

Crisona N J, Kanaar R, Gonzalez T N, Zechiedrich E L, Klippel A and Cozzarelli N R (1994). Processive recombination by wild-type Gin and an enhancer-independent mutant: insight into the mechanisms of recombination selectivity and strand exchange. *Journal of Molecular Biology* **243**(3), 437–457.

Das C, Hoang Q Q, Kreinbring C A, Luchansky S J, Meray R K, Ray S S, Lansbury

P T, Ringe D and Petsko G A (2006). Structural basis for conformational plasticity of the Parkinson's disease-associated ubiquitin hydrolase UCH-L1. *Proceedings of the National Academy of Sciences of the United States of America* **103**(12), 4675–4680.

De Gennes P G (1979). *Scaling concepts in polymer physics*. Cornell University Press.

Dean F B, Stasiak A, Koller T and Cozzarelli N R (1985). Duplex DNA knots produced by Escherichia coli topoisomerase I. *Journal of Biological Chemistry* **260**(8), 4975–4983.

Deutsch J (1988). Theoretical studies of DNA during gel electrophoresis. *Science* **240**(4854), 922–924.

Deweese J E and Osheroff N (2009). The DNA cleavage reaction of topoisomerase II: wolf in sheep's clothing. *Nucleic Acids Research* **37**(3), 738–748.

Dijkstra M, van Roij R and Evans R (1999). Phase diagram of highly asymmetric binary hard-sphere mixtures. *Physical Review E* **59**(5), 5744.

Doi M (1996). *Introduction to polymer physics*. Oxford University Press.

Einstein A (1905). Über die von der molekularkinetischen Theorie der Wärme geforderte Bewegung von in ruhenden Flüssigkeiten suspendierten Teilchen. *Annalen der Physik* **322**(8), 549–560.

Ernst M, John T, Guenther M, Wagner C, Schaefer U F and Lehr C M (2017). A model for the transient subdiffusive behavior of particles in mucus. *Biophysical Journal* **112**(1), 172–179.

Euler L (1768-1770). *Institutionum calculi integralis*. Impensis Academiae Imperialis Scientiarum.

Flory P J (1953). *Principles of polymer chemistry*. Cornell University Press.

Froelich-Ammon S J and Osheroff N (1995). Topoisomerase poisons: harnessing the dark side of enzyme mechanism. *Journal of Biological Chemistry* **270**(37), 21429–21432.

Fuller F B (1971). The writhing number of a space curve. *Proceedings of the National Academy of Sciences* **68**(4), 815–819.

Gonzalez O, Graf A and Maddocks J (2004). Dynamics of a rigid body in a Stokes fluid. *Journal of Fluid Mechanics* **519**, 133–160.

Hickford J, Jones R, Du Pont S C and Eggers J (2006). Knotting probability of a shaken ball-chain. *Physical Review E* **74**(5), 052101.

Humphrey W, Dalke A and Schulten K (1996). VMD: visual molecular dynamics. *Journal of Molecular Graphics* **14**(1), 33–38.

Ibáñez-García G O and Hanna S (2009). Relaxation of an initially-stretched, tethered polymer under shear flow: a Brownian dynamics simulation. *Soft Matter* **5**(22), 4464–4476.

Jendrejack R M, de Pablo J J and Graham M D (2002). Stochastic simulations of DNA in flow: Dynamics and the effects of hydrodynamic interactions. *The Journal of Chemical Physics* **116**(17), 7752–7759.

Kanaar R, Klippel A, Shekhtman E, Dungan J M, Kahmann R and Cozzarelli N R (1990). Processive recombination by the phage Mu Gin system: implications for the mechanisms of DNA strand exchange, DNA site alignment, and enhancer action. *Cell* **62**(2), 353–366.

Katritch V, Bednar J, Michoud D, Scharein R G, Dubochet J and Stasiak A (1996). Geometry and physics of knots. *Nature* **384**, 142–145.

LAMMPS documentation (2019a). angle_style cosine command. `https://lammps.sandia.gov/doc/angle_cosine.html`. Accessed: 2019-12-10.

LAMMPS documentation (2019b). fix langevin command. `https://lammps.sandia.gov/doc/fix_langevin.html`. Accessed: 2019-12-20.

Larson R G (2005). The rheology of dilute solutions of flexible polymers: Progress and problems. *Journal of Rheology (1978-present)* **49**(1), 1–70.

Lebowitz J and Rowlinson J (1964). Thermodynamic properties of mixtures of hard spheres. *The Journal of Chemical Physics* **41**(1), 133–138.

Lekkerkerker H N, Poon W K, Pusey P N, Stroobants A and Warren P (1992). Phase behaviour of colloid+ polymer mixtures. *EPL (Europhysics Letters)* **20**(6), 559.

Lennard-Jones J E (1924). On the determination of molecular fields.–II From the equation of state of a gas. *Proceedings of the Royal Society of London. Series A, Containing Papers of a Mathematical and Physical Character* **106**(738), 463–477.

Levene S D and Zimm B H (1987). Separations of open-circular DNA using pulsed-field electrophoresis. *Proceedings of the National Academy of Sciences* **84**(12), 4054–4057.

Levine C, Hiasa H and Marians K J (1998). DNA gyrase and topoisomerase IV: biochemical activities, physiological roles during chromosome replication, and drug sensitivities. *Biochimica et Biophysica Acta (BBA)-Gene Structure and Expression* **1400**(1), 29–43.

Liu A J and Fredrickson G H (1996). Phase separation kinetics of rod/coil mixtures. *Macromolecules* **29**(24), 8000–8009.

Liu L F, Davis J L and Calendar R (1981a). Novel topologically knotted DNA from bacteriophage P4 capsids: studies with DNA topoisomerases. *Nucleic Acids Research* **9**(16), 3979–3989.

Liu L F, Perkocha L, Calendar R and Wang J C (1981b). Knotted DNA from bacteriophage capsids. *Proceedings of the National Academy of Sciences* **78**(9), 5498–5502.

Lumpkin O J, Déjardin P and Zimm B H (1985). Theory of gel electrophoresis of DNA. *Biopolymers* **24**(8), 1573–1593.

Lumpkin O J and Zimm B H (1982). Mobility of DNA in gel electrophoresis. *Biopolymers* **21**(11), 2315–2316.

Maaloum M, Pernodet N and Tinland B (1998). Agarose gel structure using atomic force microscopy: gel concentration and ionic strength effects. *Electrophoresis* **19**(10), 1606–1610.

Malevanets A and Kapral R (1999). Mesoscopic model for solvent dynamics. *The Journal of Chemical Physics* **110**(17), 8605–8613.

Marenduzzo D, Micheletti C, Orlandini E et al. (2013). Topological friction strongly affects viral DNA ejection. *Proceedings of the National Academy of Sciences* **110**(50), 20081–20086.

Marenduzzo D, Orlandini E, Stasiak A, Tubiana L, Micheletti C et al. (2009). DNA–DNA interactions in bacteriophage capsids are responsible for the observed DNA knotting. *Proceedings of the National Academy of Sciences* **106**(52), 22269–22274.

Marsaglia G (1972). Choosing a point from the surface of a sphere. *The Annals of Mathematical Statistics* **43**(2), 645–646.

Matsumoto M and Nishimura T (1998). Mersenne twister: a 623-dimensionally equidistributed uniform pseudo-random number generator. *ACM Transactions on Modeling and Computer Simulation (TOMACS)* **8**(1), 3–30.

Michieletto D (2016). *Topological interactions in ring polymers*. Springer.

Michieletto D, Marenduzzo D and Orlandini E (2015). Topological patterns in two-dimensional gel electrophoresis of DNA knots. *Proceedings of the National Academy of Sciences* **112**(40), E5471–E5477.

Noolandi J, Rousseau J, Slater G W, Turmel C and Lalande M (1987). Self-trapping and anomalous dispersion of DNA in electrophoresis. *Physical Review Letters* **58**(23), 2428.

Nordlund I (1914). A new determination of Avogadro's number from Brownian motion of small mercury spherules. *Zeitschrift für Physikalische Chemie* **87**,

40–62.

Olivera B M, Baine P and Davidson N (1964). Electrophoresis of the nucleic acids. *Biopolymers: Original Research on Biomolecules* **2**(3), 245–257.

Onsager L (1949). The effects of shape on the interaction of colloidal particles. *Annals of the New York Academy of Sciences* **51**(4), 627–659.

Orlandini E and Whittington S G (2007). Statistical topology of closed curves: Some applications in polymer physics. *Reviews of Modern Physics* **79**(2), 611–642.

Pernodet N, Maaloum M and Tinland B (1997). Pore size of agarose gels by atomic force microscopy. *Electrophoresis* **18**(1), 55–58.

Perrin J (1908). L'agitation moléculaire et le mouvement brownien. *Comptes Rendus Hebdomadaires des Séances de l'Académie des Sciences* **146**, 967–970.

Pierański P (1998). In search of ideal knots. In A Stasiak, V Katritch and L H Kauffman, editors, *Ideal knots*, volume 19, chapter 2, pages 20–41. World Scientific.

Piili J, Marenduzzo D, Kaski K and Linna R (2013). Sedimentation of knotted polymers. *Physical Review E* **87**(1), 012728.

Reverey J F, Jeon J H, Bao H, Leippe M, Metzler R and Selhuber-Unkel C (2015). Superdiffusion dominates intracellular particle motion in the supercrowded cytoplasm of pathogenic Acanthamoeba castellanii. *Scientific Reports* **5**(1), 1–14.

Richardson L F (1926). Atmospheric diffusion shown on a distance-neighbour graph. *Proceedings of the Royal Society of London. Series A, Containing Papers of a Mathematical and Physical Character* **110**(756), 709–737.

Rollins G C, Petrov A S and Harvey S C (2008). The role of DNA twist in the packaging of viral genomes. *Biophysical Journal* **94**(5), L38–L40.

Roth R, Evans R, Lang A and Kahl G (2002). Fundamental measure theory for hard-sphere mixtures revisited: the White Bear version. *Journal of Physics: Condensed Matter* **14**(46), 12063.

Rouse Jr P E (1953). A theory of the linear viscoelastic properties of dilute solutions of coiling polymers. *The Journal of Chemical Physics* **21**(7), 1272–1280.

Russell P L (1987). The ageing of gels from starches of different amylose/amylopectin content studied by differential scanning calorimetry. *Journal of Cereal Science* **6**(2), 147–158.

Rybenkov V V, Cozzarelli N R and Vologodskii A V (1993). Probability of DNA

knotting and the effective diameter of the DNA double helix. *Proceedings of the National Academy of Sciences* **90**(11), 5307–5311.

Samanta H S and Thirumalai D (2019). Origin of superdiffusive behavior in a class of nonequilibrium systems. *Physical Review E* **99**(3), 032401.

Sandia National Laboratories (2004 – present). Large-scale Atomic/Molecular Massively Parallel Simulator (LAMMPS). `https://lammps.sandia.gov/`.

Sayre T C, Lee T M, King N P and Yeates T O (2011). Protein stabilization in a highly knotted protein polymer. *Protein Engineering Design and Selection* **24**(8), 627–630.

Scherer G W (1988). Aging and drying of gels. *Journal of Non-Crystalline Solids* **100**(1-3), 77–92.

Serwer P (1983). Agarose gels: properties and use for electrophoresis. *Electrophoresis* **4**(6), 375–382.

Shure M and Vinograd J (1976). The number of superhelical turns in native virion SV40 DNA and minicol DNA determined by the band counting method. *Cell* **8**(2), 215–226.

Smithies O (1955). Zone electrophoresis in starch gels: group variations in the serum proteins of normal human adults. *Biochemical Journal* **61**(4), 629.

Sogo J M, Stasiak A, Martínez-Robles M L, Krimer D B, Hernández P and Schvartzman J B (1999). Formation of knots in partially replicated DNA molecules. *Journal of Molecular Biology* **286**(3), 637–643.

Sokolov I M (2012). Models of anomalous diffusion in crowded environments. *Soft Matter* **8**(35), 9043–9052.

Sommerfeld A (1909). *Ein beitrag zur hydrodynamischen erklaerung der turbulenten fluessigkeitsbewegungen*.

Soret M and Ville M (2015). Lissajous and Fourier knots. *arXiv preprint arXiv:1507.00880* .

Sossinsky A B (2002). *Knots: mathematics with a twist*. Harvard University Press, Cambridge, Massachussetts. London, England.

Spakowitz A J and Wang Z G (2005). DNA packaging in bacteriophage: is twist important? *Biophysical Journal* **88**(6), 3912–3923.

Stasiak A, Dubochet J, Katritch V and Pierański P (1998). Ideal Knots and Their Relation to the Physics of Real Knots. In A Stasiak, V Katritch and L H Kauffman, editors, *Ideal knots*, volume 19, chapter 1, pages 1–19. World Scientific.

Stasiak A, Katritch V, Bednar J, Michoud D and Dubochet J (1996). Electrophoretic mobility of DNA knots. *Nature* **384**(6605), 122.

Stellwagen N C and Stellwagen E (2009). Effect of the matrix on DNA electrophoretic mobility. *Journal of Chromatography A* **1216**(10), 1917–1929.

Sułkowska J I, Rawdon E J, Millett K C, Onuchic J N and Stasiak A (2012). Conservation of complex knotting and slipknotting patterns in proteins. *Proceedings of the National Academy of Sciences* **109**(26), E1715–E1723.

Sułkowska J I, Sułkowski P, Szymczak P and Cieplak M (2008). Stabilizing effect of knots on proteins. *Proceedings of the National Academy of Sciences* **105**(50), 19714–19719.

Swope W C, Andersen H C, Berens P H and Wilson K R (1982). A computer simulation method for the calculation of equilibrium constants for the formation of physical clusters of molecules: Application to small water clusters. *The Journal of Chemical Physics* **76**(1), 637–649.

Taylor A J and other SPOCK contributors (2017). pyknotid knot identification toolkit v0.5.3. `https://github.com/SPOCKnots/pyknotid`.

The Knot Server (2003). Knot data. `http://www.colab.sfu.ca/KnotPlot/KnotServer/`. Accessed: 2016-12-13.

Treloar L R G (1975). *The physics of rubber elasticity*. Oxford University Press, USA.

Trigueros S, Arsuaga J, Vazquez M E, Roca J et al. (2001). Novel display of knotted DNA molecules by two-dimensional gel electrophoresis. *Nucleic Acids Research* **29**(13), e67–e67.

Trigueros S and Roca J (2007). Production of highly knotted DNA by means of cosmid circularization inside phage capsids. *BMC Biotechnology* **7**(1), 94.

Tse-Dinh Y C (2007). Exploring DNA topoisomerases as targets of novel therapeutic agents in the treatment of infectious diseases. *Infectious Disorders-Drug Targets (Formerly Current Drug Targets-Infectious Disorders)* **7**(1), 3–9.

Tubiana L, Orlandini E and Micheletti C (2011a). Multiscale entanglement in ring polymers under spherical confinement. *Physical Review Letters* **107**(18), 188302.

Tubiana L, Orlandini E and Micheletti C (2011b). Probing the entanglement and locating knots in ring polymers: a comparative study of different arc closure schemes. *Progress of Theoretical Physics Supplement* **191**, 192–204.

Tubiana L, Polles G, Orlandini E and Micheletti C (2018). Kymoknot: A web server and software package to identify and locate knots in trajectories of linear or circular polymers. *The European Physical Journal E* **41**(6), 72.

Turmel C, Brassard E, Slater G W and Noolandi J (1990). Molecular detrap-

ping and band narrowing with high frequency modulation of pulsed field electrophoresis. *Nucleic Acids Research* **18**(3), 569–575.

Urbach A R and Waring M J (2005). Visualising DNA: footprinting and 1-2D gels. *Molecular BioSystems* **1**(4), 287–293.

Valle F, Favre M, Roca J and Dietler G (2005). Atomic force microscopy of complex DNA knots. In *Physical And Numerical Models In Knot Theory: Including Applications to the Life Sciences*, pages 161–170. World Scientific.

Vandermonde A T (1771). Remarques sur les problèmes de situation. *Mémoires de l'Académie Royale des Sciences (Paris)* **2**, 566–574.

Verlet L (1967). Computer "experiments" on classical fluids. I. Thermodynamical properties of Lennard-Jones molecules. *Physical Review* **159**(1), 98.

Virnau P, Mirny L A and Kardar M (2006). Intricate knots in proteins: Function and evolution. *PLOS Computational Biology* **2**(9), e122.

Volkmuth W and Austin R H (1992). DNA electrophoresis in microlithographic arrays. *Nature* **358**(6387), 600–602.

Volkmuth W, Duke T, Wu M, Austin R H and Szabo A (1994). DNA electrodiffusion in a 2D array of posts. *Physical Review Letters* **72**(13), 2117.

Vologodskii A V, Crisona N J, Laurie B, Pieranski P, Katritch V, Dubochet J and Stasiak A (1998). Sedimentation and electrophoretic migration of DNA knots and catenanes. *Journal of Molecular Biology* **278**(1), 1–3.

Vrij A (1976). Polymers at interfaces and the interactions in colloidal dispersions. *Pure and Applied Chemistry* **48**(4), 471–483.

Wang X, Egan C E, Zhou M, Prince K, Mitchell D R and Caruso R A (2007). Effective gel for gold nanoparticle formation, support and metal oxide templating. *Chemical Communications* (29), 3060–3062.

Warner Jr H R (1972). Kinetic theory and rheology of dilute suspensions of finitely extendible dumbbells. *Industrial & Engineering Chemistry Fundamentals* **11**(3), 379–387.

Wasserman S A, Dungan J M and Cozzarelli N R (1985). Discovery of a predicted DNA knot substantiates a model for site-specific recombination. *Science* **229**(4709), 171–174.

Weber C (1995). Questions de topologie en biologie moléculaire. *Gazette des Mathématiciens* **64**, 29–42. ID: unige:12754.

Weber C, Carlen M, Dietler G, Rawdon E J and Stasiak A (2013). Sedimentation of macroscopic rigid knots and its relation to gel electrophoretic mobility of DNA knots. *Scientific Reports* **3**, 1091.

Weber C, Stasiak A, De Los Rios P and Dietler G (2006). Numerical simulation of gel electrophoresis of DNA knots in weak and strong electric fields. *Biophysical Journal* **90**(9), 3100–3105.

Weeks J D, Chandler D and Andersen H C (1971). Role of repulsive forces in determining the equilibrium structure of simple liquids. *The Journal of Chemical Physics* **54**(12), 5237–5247.

Weiss M, Elsner M, Kartberg F and Nilsson T (2004). Anomalous subdiffusion is a measure for cytoplasmic crowding in living cells. *Biophysical Journal* **87**(5), 3518–3524.

White J H (1969). Self-linking and the Gauss integral in higher dimensions. *American Journal of Mathematics* **91**(3), 693–728.

Williams T, Kelley C, Lang R, Kotz D, Campbell J, Elber G, Woo A et al. (1986 – present). gnuplot 5.2. `http://www.gnuplot.info`.